INVESTIGATING NOVEL THERAPIES FOR FRIEDREICH'S ATAXIA

Thesis submitted for the degree of Doctor of Philosophy by

Mursal Sherzai

April 2018

College of Health and Life Sciences
Department of Life Sciences
Division of Biosciences

Abstract

Friedreich's ataxia (FRDA) is a progressive neurodegenerative disorder caused by a homozygous GAA repeat expansion mutation in intron 1 of the frataxin gene (*FXN*), which instigates transcriptional issues. As a consequence, reduced levels of frataxin protein lead to mitochondrial iron accumulation, oxidative stress and ultimately cell death; particularly in dorsal root ganglia (DRG) sensory neurons and the dentate nucleus of the cerebellum. In addition to neurological disability, FRDA is associated with cardiomyopathy, diabetes mellitus and skeletal deformities. Currently there is no effective treatment for FRDA and patients die prematurely.

Recent findings suggest that abnormal GAA expansion plays a role in histone modification, subjecting the *FXN* gene to heterochromatin silencing. Therefore, as an epigenetic-based therapy, I investigated the efficacy and tolerability of two histone methyltransferase (HMTase) inhibitor compounds, BIX0194 (G9a-inhibitor) and GSK126 (EZH2-inhibitor), to specifically target and reduce H3K9me2/3 and H3K27me3 levels, respectively, in FRDA human and mouse primary fibroblasts. We show that a combination treatment of BIX0194 and GSK126, significantly increased *FXN* gene expression levels and reduced the repressive histone marks. However, no increase in frataxin expression was seen. Nevertheless, our results are still promising and may encourage to investigate HMTase inhibitors with other synergistic epigenetic-based therapies for further preliminary studies.

Additionally, it has been reported that ubiquitin-proteasome pathway (UPP) controls frataxin stability, thus leading to the development of new therapeutic approaches aimed at preventing the degradation of frataxin. Here we investigated the efficacy of various proteasome inhibitors (MG132, Bortezomib, Salinosporamide A and Ixazomib) using human primary fibroblasts. Only treatments using ixazomib indicated a small increase in frataxin protein;

however, an increase in the cell cycle stress modulator, $p27^{Kip1}$, was also observed. Therefore, at this stage the use of proteasome inhibitor compounds cannot be advocated for FRDA therapy.

Moreover, a study has proposed that increased degradation of D-serine by D-amino acid oxidase (DAO), may lead to low NMDA functioning and impair neural signalling, causing ataxia. Therefore, we investigated a DAO inhibitor, TAK-831, on the YG8sR FRDA mouse model, and detected a significant improvement in ataxia motor coordination deficits. TAK-831 is now proposed for further studies and is currently undergoing randomized Phase 2 clinical trials for FRDA in USA.

Acknowledgements

First and foremost, I would like to express my sincere gratitude to my supervisor, Dr. Mark Pook, for his encouragement, guidance and patience, and most importantly his incredible support throughout my PhD.

I would like to extend my appreciation to Dr. Sahar Al-Mahdawi for all her insightful comments and encouragement, and invaluable guidance in designing my experiments and in the writing of this thesis. I am very grateful for Dr. Sara Anjomani-Virmouni for being the first person to believe in me and for providing the essential training that I needed before I even commenced my PhD.

My experience in Brunel would not have been the same without my wonderful colleagues within the 'Ataxia Research Group', Dr. Aurélien Bayot, Dr. Saba Saqlain, Dr. Hajar Mikaeili, and Anastasia Gketsopoulou. I immensely appreciate their constant support and advice, throughout the last three years.

I must sincerely thank my dear friends Dr. Sheba Adam-Zahir and Dr. Marianne Henry, for their continual support, especially during stressful times. I am forever indebted to Dr. Layal Hakim, for always being so kind and generous in supporting me whenever I needed her, for as long as I can remember.

I am eternally grateful for my loving family, especially my mother Dr. Sharifa Sherzai, my sister Mariam Nazari and my husband Amal Hashemi for believing in me and constantly encouraging me.

Lastly, I would like to acknowledge Takeda Pharmaceutical Limited Cambridge for providing financial support for this PhD.

This research and all my future successes are dedicated to my loving husband, Amal Hashemi.

You are my inspiration in life. Thank you for being there with me every step of the way.

Declaration

I hereby declare that the research presented in this thesis is my own work, except where otherwise specified, and has not been submitted for any other degree.

Mursal Sherzai

Abbreviations

5-aza-CdR	5-Aza-2'-deoxycytidine
AMV RT	avian myeloblastosis virus reverse transciptase
ANOVA	analysis of variance
ATP	adenosine triphosphate
BAC	bacterial artificial chromosome
BCA	bicinchoninic acid
CBP	CREB binding protein
cDNA	complementary DNA
ChIP	chromatin immunoprecipitation
cm	centimetre
CNS	central nervous system
DAO	D-amino acid oxidase
DEPC	diethyl pyrocarbonate
DMEM	Dulbecco's Modified Eagle Medium
DMSO	dimethyl sulfoxide
DNA	deoxyribonucleic acid
DNMT	DNA methyltransferase
dNTP	deoxyribonucleotide triphosphate
DRG	dorsal root ganglion
DTT	Dithiothreitol
DUB	deubiquitinating enzymes
ECL	enhanced chemiluminescent
EDTA	ethylene diamine-tetra acetic acid
EPO	erythropoietin
EtOH	ethanol
EZH2	enhancer of zeste homologue 2
FBS	fetal bovine serum
FDA	food and drug administration
FRDA	Friedreich ataxia
GAA	guanine-adenine-adenine
GAPDH	glyceraldehyde-3-phosphate dehydrogenase
gDNA	genomic DNA
GLP	G9a-like protein
HAT	histone acetyl transferase
HDAC	histone deacetylase
HDM	histone demethylases
HMTase	histone methyltransferase
HP1	heterochromatin protein 1
HRP	horseradish peroxidase
IgG	immunoglobulin G
IMS	industrial methylated spirit

IP	immunoprecipitation
iPS	induced pluripotent stem cells
iPSCs	induced pluripotent stem cells
kb	kilo base
Kg	kilogram
kPa	kilopascal
LMW	low molecular weight
mg	milligram
ml	millilitre
mm	millimetre
MRC	mitochondrial respiratory chain
mRNA	messenger RNA
mt-DNA	mitochondrial DNA
NaAc	sodium acetate
NaCl	sodium chloride
NaHCO3	sodium bicarbonate
NMDAR	*N*-methyl D-aspartate receptor
PAGE	polyacrylamide gel electrophoresis
PBS	phosphate-buffered saline
PCP	1-phenylcyclohexyl piperidine
PCR	polymerase chain reaction
PEV	position-effect variegation
PIC	protease inhibitor cocktail
pmol	picomole
PRC2	polycomb repressive complex 2
PVDF	polyvinylidene difluoride
qRT-PCR	quantitative real-time RT-PCR
rhuEPO	recombinant human erythropoietin
RIPA	Radio-Immunoprecipitation Assay
RNA	ribonucleic acid
ROS	reactive oxygen species
rpm	revolutions per minute
RT	room temperature
SAM	S-adenosyl methionine
SDS	sodium dodecyl sufate
SRR	serine racemase
TAE	tris-acetic acid EDTA
TBE	tris-borate-EDTA
TEMED	tetramethylethylenediamine
TNR	trinucleotide repeat
Tris	tris(hydroxymethyl)aminomethane
UCM	ubiquitin competing molecules
UPP	ubiquitin-proteasome pathway
UV	ultra violet
V	voltage
W	Watts
WT	wild-type
YAC	yeast artificial chromosome
µl	microliter
µM	micro molar

Table of contents

List of figures

List of tables

CHAPTER I - GENERAL INTRODUCTION

1.1 Friedreich's ataxia (FRDA)

FRDA is a form of neuropathy that was discovered in 1863 by the German pathologist, Nikolaus Friedreich (Figure 1.1). He first described the disorder in a series of 5 papers published from 1863 to 1877, defining a characteristic type of progressive spinal degeneration and atrophy in nine members of three families, distinguishable from tabes dorsalis (Friedreich, 1863a, 1863b, 1863c, 1876, 1877, Koeppen and Mazurkiewicz, 2013). Friedreich recognised the main clinical and pathological features of the disorder, including the remarkable description of fatty degeneration in the cardiac muscle, which is now identified as hypertrophic cardiomyopathy, a prominent cause of death in FRDA. Although Friedreich articulated the familial element of the condition, he was unable to identify the exact mode of inheritance. It was not until 120 years later that our knowledge on the genetic defect(s) underlying FRDA, and its pattern of autosomal recessive inheritance was discovered (Campuzano *et al.*, 1996). The discovery of the pathogenic mutation, an intronic trinucleotide (GAA) repeat expansion in the causative gene that encodes frataxin (*FXN*), has served as a catalyst for rapidly advancing research on FRDA (Koeppen and Mazurkiewicz, 2013). Being the most common autosomally recessive neurodegenerative disorder, FRDA now exemplifies a fascinating model of the so-called 'triplet-repeat' diseases.

Figure 1. 1 - Nikolaus Friedreich (1825–1882)

1.1.1 Prevalence

FRDA most commonly occurs in Caucasian populations with an estimated prevalence of 1:20,000 to 1: 50,000 with no gender preference (Harding, 1981, Cossee *et al.*, 1997, Vankan, 2013). Epidemiological studies have provided evidence of a west to east incidence gradient in Europe, with highest levels in the south of France, north of Spain and Ireland and lowest levels in Scandinavia and Russia (Vankan, 2013). The carrier frequency varies from 1:60 to 1:110. FRDA is almost non-existent amongst far eastern populations and sub-Saharan Africans (Labuda *et al.*, 2000, Pandolfo and Montermini, 1998, Vankan, 2013).

1.1.2 Clinical features

The cardinal clinical feature of FRDA is progressive gait ataxia, which usually appears around puberty, but the age of symptom onset can vary from infancy (2-3 years) to adulthood (25 years old) (De Michele *et al.*, 1994, Moschner *et al.*, 1994). Scoliosis and foot deformities are also early signs that present when neurological symptoms appear. With disease progression, other clinical features become prominent due to degenerative atrophy of the spinal cord, including sensory loss and muscle weakness, dysphagia, dysarthria, visual and hearing loss, and presence of spasticity. Additionally, following neurological symptoms, asymptomatic hypertrophic cardiomyopathy usually develops, contributing to the disability, causing premature death. At a later stage, diabetes mellitus is often observed in up to 30% of cases. Patients with late onset FRDA show a slower disease progression, where tendon reflexes are often retained. Nearly all patients gradually lose their ability to walk at approximately 15 years after disease onset, and become wheelchair bound in their early teens. This is followed by premature death at the end of their third decade (Harding, 1981, Alper and Narayanan, 2003, Tsou *et al.*, 2011). Although cognitive ability seems unaffected, FRDA has a substantial effect on patient's daily activity, and also on their personal and professional development (Pandolfo, 2008).

1.1.3 Pathophysiological features

In FRDA, the primary site of pathology is the dorsal root ganglion (DRG), accompanied by early loss of large sensory neurons in the peripheral nerves, and degeneration of posterior columns in the spinal cord, spinocerebellar and pyramidal tracts, and the dentate nucleus of the cerebellum (Harding *et al.*, 1984, Koeppen, 2011). The process appears to progressively demyelinate the longest and largest fibres arising from the posterior columns which carry proprioceptive information (Hughes *et al.*, 1968, Rizzuto *et al.*, 1981, Said *et al.*, 1986, Murayama *et al.*, 1992). In early stages of the disease, the cerebellum is minimally affected, but with disease prominence, atrophy occurs in the superior vermis and medulla oblongata (Koeppen *et al.*, 2007). As a typical secondary effect, FRDA is also associated with non-neuronal tissue pathologies such as cardiac muscle and pancreatic β-cell dysfunction (Schulz *et al.*, 2009). This triggers hypertrophic cardiomyopathy, which is observed in the majority of patients, due to thickening of the ventricular septum walls (Lamarche *et al.*, 1980, Sanchez-Casis *et al.*, 1976). Additionally, FRDA patients have an increased risk to diabetes mellitus, due to the decrease in pancreatic β-cells with a combination of insulin resistance and insufficient insulin response (Schoenle *et al.*, 1989, Cnop *et al.*, 2012).

1.2 Frataxin gene: structure and expression

In 1988, Chamberlain *et al.* mapped the human FRDA gene (*FXN*) to chromosome 9 by linkage analysis (Chamberlain *et al.*, 1988), and subsequently localised the gene in the long proximal arm at position 9q13-21.1 (Figure 1.2 A). Using complementary DNA (cDNA) selection and sequence analysis, the FRDA gene (initially referred as *X25*) was identified as one of the expressed genes. Further studies detected a mutation in *X25* in some FRDA patients, which resulted in the identification of an expanded GAA (guanine-adenine-adenine) trinucleotide repeat within the first intron of the FRDA gene. The *FXN* gene covers 95kb of genomic DNA and is comprised of seven exons: 1-5a, 5b and 6 (Campuzano *et al.*, 1996)

(Figure 1.2 B). The main functionally-relevant mRNA is 1.3kb in size and is transcribed from the first five exons, 1-5a, in the centromere to telomere direction. This encodes a 220 amino acid protein named *frataxin*. Exon 6 is non-coding; however, exon 5b can be transcribed by alternative splicing to synthesise a potential 171 amino acid protein (Campuzano *et al.*, 1996, Cossee *et al.*, 1997).

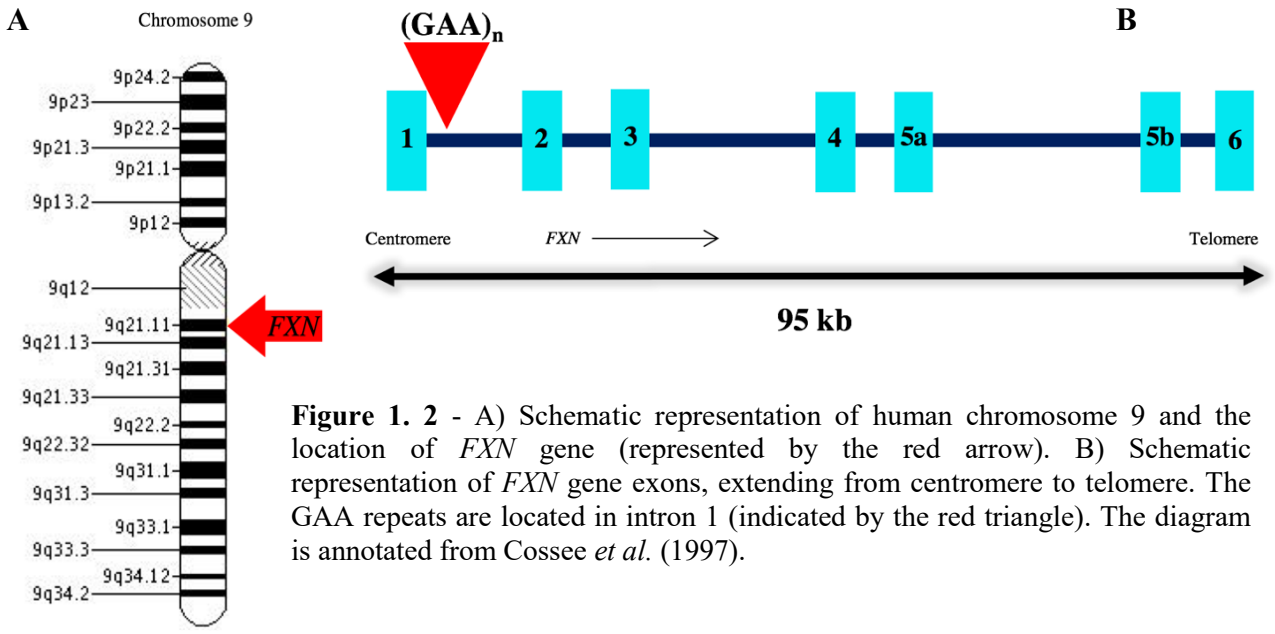

Figure 1. 2 - A) Schematic representation of human chromosome 9 and the location of *FXN* gene (represented by the red arrow). B) Schematic representation of *FXN* gene exons, extending from centromere to telomere. The GAA repeats are located in intron 1 (indicated by the red triangle). The diagram is annotated from Cossee *et al.* (1997).

The *FXN* gene is ubiquitously expressed in all cells, but at variable levels in different tissues and during development (Campuzano *et al.*, 1996, Koutnikova *et al.*, 1997). In adult humans, frataxin mRNA is most abundant in mitochondria-rich cells, such as cardiomyocytes and neurons. Tissues such as the DRG, cerebellum, cerebral cortex and heart display the highest level of frataxin. In mouse embryos, frataxin mRNA is highly expressed in the developing brain, spinal cord and in the DRG. However, frataxin mRNA expression drastically reduces in the adult mouse brain but remains high in the spinal cord and DRG (Koutnikova *et al.*, 1997). Moreover, minute frataxin levels have also been detected in the liver, skeletal muscle, kidney, pancreas and brown fat (Koutnikova *et al.*, 1997, Campuzano *et al.*, 1997).

1.2.1 The GAA trinucleotide repeat mutation

Molecular analysis has revealed that a biallelic GAA triple repeat hyperexpansion is the leading (98% of cases) cause of FRDA. This GAA triplet repeat is found within an Alu sequence in intron 1, at 1.4kb downstream from the end of exon 1. Normal alleles contain less than 40 triplets, whereas alleles in FRDA contain 70 to 1700 triplet repeats (Cossee *et al.*, 1997, Montermini *et al.*, 1997a). Consequently, this GAA expansion has shown to influence the disruption of *FXN* gene transcription, and subsequently reduce the level of frataxin protein as verified by ribonuclease (RNase) protection assays and western blot analysis, respectively (Figure 1.3) (Cossee *et al.*, 1997, Campuzano *et al.*, 1997, De Biase *et al.*, 2007a, Punga and Buhler, 2010, Silva *et al.*, 2015). In fact, a study by Punga and Buhler (2010) demonstrated an inverse correlation between the GAA repeat length and frataxin gene and protein expression levels in FRDA patient-derived lymphoblastoid cell lines.

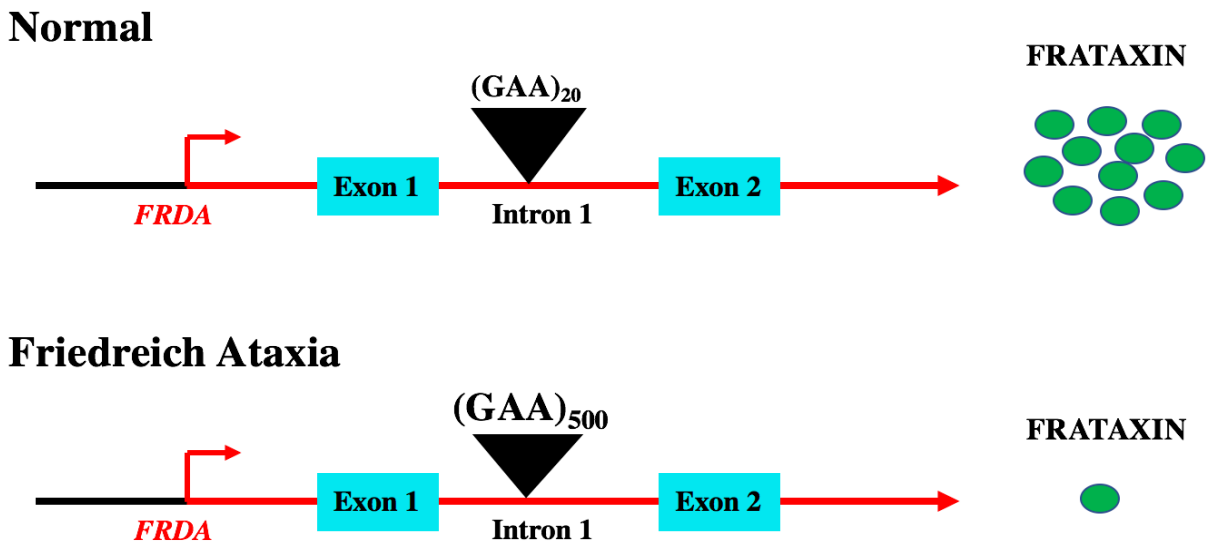

Figure 1. 3 - Schematic presentation of the frataxin expression. In FRDA, the hyperexpansion of GAA repeats within intron 1 of *FXN* gene instigates reduced expression of frataxin.

Due to the recessive nature of the disease, the majority of the patients are homozygous for GAA expansion, whereas heterozygous carriers show no disease phenotype and appear

clinically normal (Bidichandani *et al.*, 2000, Grabczyk and Usdin, 2000). Rarely (4%) patients are compound heterozygous for a GAA expansion in one allele and a missense or nonsense point mutation, disrupting the coding sequence in *FXN* gene (Campuzano *et al.*, 1996). To date, the most frequent point mutations are I154F, M1I and G130V (Alper and Narayanan, 2003). So far, no FRDA patient has been found to carry a homozygous point mutation, suggesting that this mutation may be associated with lethality (or incompatible with survival).

1.2.2 Genotype-phenotype correlation

Since smaller GAA repeat expansions permit higher residual *FXN* gene expression, expansion sizes can influence the severity of the FRDA disease phenotype and age of onset, a feature also observed in other repeat disorders (Pandolfo, 2002). With increased repeat expansion, the age of onset reduces, disease progression becomes more rapid, and the presence of additional disease manifestations, such as cardiomyopathy and diabetes, appear more prominent, suggestive of a more widespread degeneration (Montermini *et al.*, 1997c). Nevertheless, the size of the GAA repeat expansions only accounts for about 50% of the age of onset variability. This indicates that there is still substantial variability in the FRDA phenotype, which is influenced by other factors. The molecular mechanisms underlying such clinical variability are unknown, but it has been proposed that somatic mosaicism for the expansion size, variation and interruption in the repeat sequence, modifier genes and environmental factors may all contribute to clinical variability (Filla *et al.*, 1996, Durr *et al.*, 1996, Montermini *et al.*, 1997c). Therefore, it is not possible to accurately predict disease severity or rate of progression, based on GAA repeat size only.

1.2.3 GAA repeat instability

Along with FRDA, trinucleotide repeat (TNR) expansions have also been the underlying mechanism for other inherited human disorders. This includes expansion of CAG repeats in Huntington disease (HD), and CTG repeats in myotonic dystrophy type 1 (MD1) (Cossee *et al.*, 1997, Cummings and Zoghbi, 2000, Savouret *et al.*, 2003). Generally, these expansions occur in either the coding or the non-coding regions of genes. Non-coding TNR expansion disorders typically result in loss of gene function, while coding trinucleotide repeat expansions instigate either a polyglutamine or polyalanine tract in the protein products, thus resulting in protein dysfunction (Pizzi *et al.*, 2007). Moreover, a significant molecular phenomenon is observed, which is a TNR expansion instability, where the repeats increase in size across generations (meiotic instability) and within tissues (somatic instability). Such instability has also been identified in FRDA with GAA repeat expansions (La Spada, 1997).

1.2.3.1 Intergenerational instability

In FRDA, the GAA repeat expansion is unstable when transmitted from parent to child, where both expansion and contraction are observed. Thus, non-pathogenic parental pre-mutations can be transmitted to offspring as expanded pathogenic GAA repeats (Montermini *et al.*, 1997a). During maternal transmission the pathological GAA repeat is equally prone to either contract or to further expand, whereas during paternal transmission only contraction is identified (Campuzano *et al.*, 1996, Durr *et al.*, 1996, Pianese *et al.*, 1997, Monros *et al.*, 1997). This sex bias in the intergenerational GAA instability has been confirmed by sperm analysis, although the underlying molecular mechanism instigating this is still unknown (De Michele *et al.*, 1998, Pearson *et al.*, 2005, Delatycki *et al.*, 1998, Monros *et al.*, 1997). Moreover, parental age and the intergenerational change in expansion are directly correlated in maternal transmission and inversely correlated in paternal transmission (Kaytor *et al.*, 1997, De Michele *et al.*, 1998).

1.2.3.2 Somatic instability is tissue and age dependant

In FRDA, progressive somatic instability has been observed, where different lengths of repeats are identified in various tissues from the same patient (Sharma *et al.*, 2002). This was detected by small pool PCR studies in the particular disease-relevant tissues, cerebellum and DRG, which displayed a preference to a higher rate of expansion as compared to other tissues (Figure 1.4). Additionally, an age-depended significant increase in repeat expansion was also observed in DRG, which ranged from 0.5% at 17 years to 13.9% at 47 years (De Biase *et al.*, 2007a). Similarly, analysis from tissues of an 18-week foetus homozygous for expanded GAA alleles revealed very low instability levels as compared to adult-derived tissues (4.2% versus 30.6%). The mutation load in blood samples from multiple patients and carriers increased significantly with age, ranging from 7.5% at 18-week gestation to 78.7% at 49 years of age (Figure 1.5). This suggests that somatic instability is a crucial element in FRDA and commonly arises after embryonic development and it progresses throughout life (De Biase *et al.*, 2007b). Moreover, an inconsistent heterogeneity in expansion sizes is detected amongst cells from different tissues, whereby fibroblasts show less heterogeneity and lymphocytes show more heterogeneity. Extensive cellular heterogeneity in repeat size is also observed in different brain regions (Montermini *et al.*, 1997b), indicating a manifestation of extreme mitotic instability. These findings support the role of postnatal somatic instability in disease pathogenesis (De Biase *et al.*, 2007b), possibly involving DNA repair and replication mechanisms.

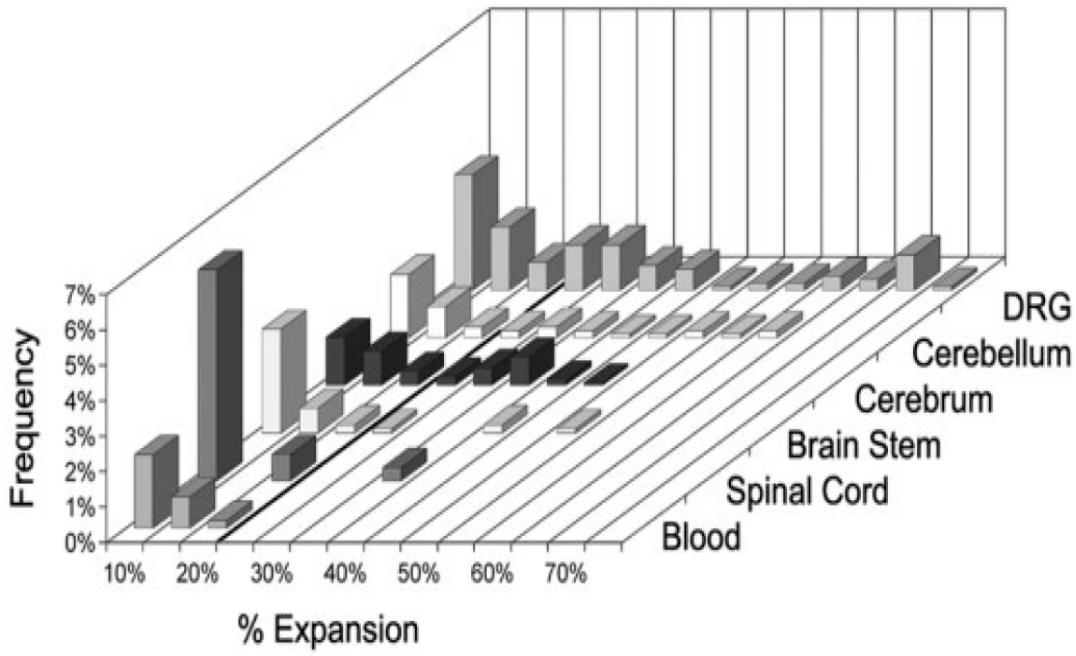

Figure 1. 4 - Small pool-PCR analysis detected a higher prevalence of large expansions in DRG. Frequency distribution (plotted on the Y-axis) of expansion (magnitude plotted on the X-axis as increase in size (%) over constitutional allele) seen in various tissues derived from FRDA patient. All data points to the right of the bold line, plotted at 20% represent large expansions (De Biase *et al.*, 2007a).

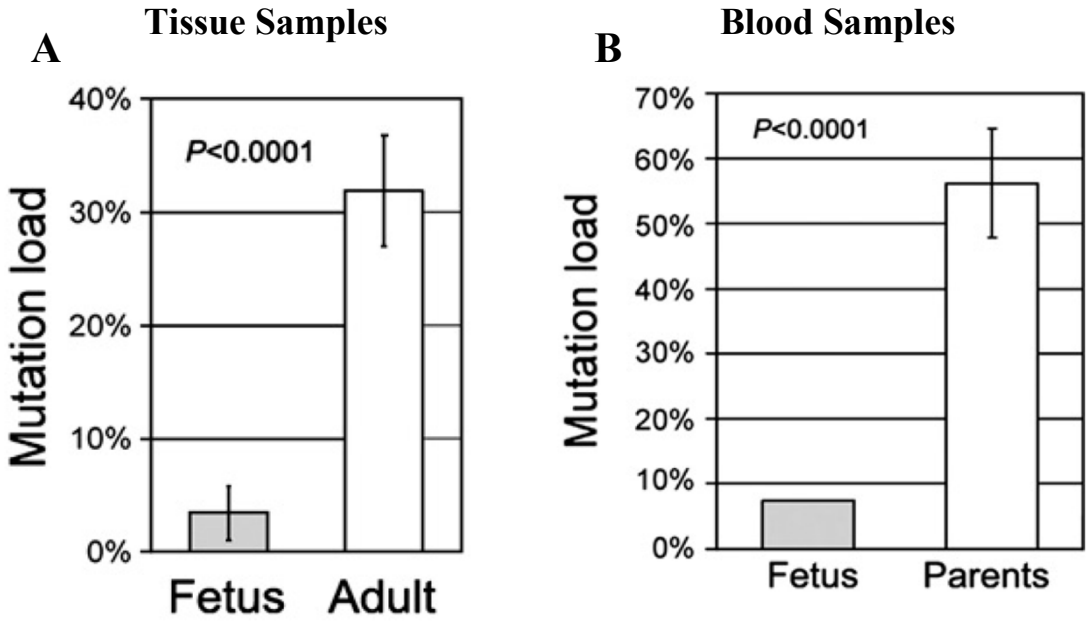

Figure 1. 5 - Small-pool PCR analysis indicating different GAA mutation load in foetus versus adults. A) Tissues analysis showing a highly significant 7.3 fold lower levels of somatic instability in foetal tissues compared with adult tissues. B) Mutational load in blood of foetus versus both parents combined showing a highly significant, 7 fold lower levels of somatic instability in foetal blood compared with adult blood. Error bar -/+ 2 SEM (De Biase *et al.*, 2007b).

In FRDA, studies have revealed that the decrease in *FXN* mRNA molecules is essentially due to a dysfunction at the pre-transcriptional level, instigated by the mutational GAA repeat expansion, and not at the post-transcriptional RNA processing level (Delatycki *et al.*, 2000, Sakamoto *et al.*, 2001). Although, the exact mechanism of transcriptional reduction remains controversial, there are several hypotheses presently under debate. Recent evidence has proposed that the transcriptional silencing caused by pathologic GAA repeat expansions may be due to the formation of non-B DNA structures, such as DNA triplexes, RNA-DNA hybrids and sticky DNA structures (Mariappan *et al.*, 1999, Sakamoto *et al.*, 1999, Sakamoto *et al.*, 2001), and/or cause epigenetic changes, such as heterochromatin formation (Figure 1.6) (Herman *et al.*, 2006, Al-Mahdawi *et al.*, 2008). Therefore, a better understanding of the mutational mechanisms involved in GAA-induced inhibition of *FXN* gene transcription associated with FRDA could lead to the development of several effective therapeutic approaches.

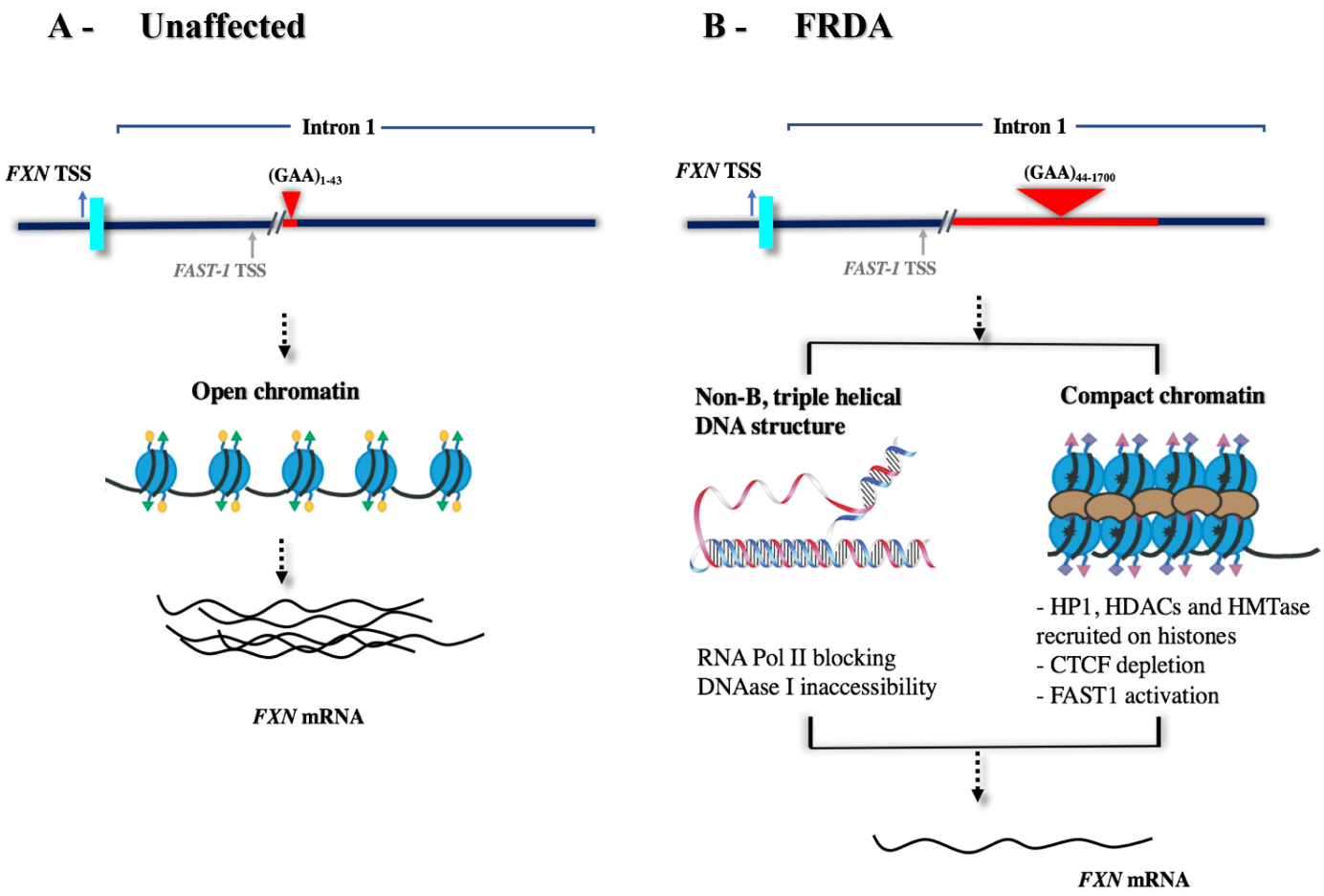

Figure 1. 6 - Schematic illustration of *FXN* gene silencing in FRDA. A) Unaffected individuals carrying 1-40 GAA repeats contain functional histone marks at the *FXN* promoter involved in gene transcription initiation and elongation. B) Individual with FRDA carry an expanded GAA repeat (≤1700) which leads to *FXN* gene silencing by two potential mechanisms: 1) the GAA repeat may adopt abnormal non-B DNA structures (triplexes) which triggers RNA Polymerase II arrest, 2) heterochromatin formation at the *FXN* gene triggers increased DNA methylation and HP1 levels, which subsequently causes a significant enrichment of repressive histone marks (Image annotated from Sandi *et al.* (2014)).

1.2.4 DNA triplex formation

DNA triple helix structures are formed upon binding of a single strand, generally containing pyrimidine (Y) or purine (R), to the major-groove of a DNA double helix pairs through the Hoogsteen or reverse-Hoogsteen type of hydrogen bonding (Jain *et al*, 2002). Triplexes in general may take the form R.R.Y or Y.R.Y and depending whether the third strand is purine rich or pyrimidine rich it can be formed as either intermolecular structures or as folded intramolecular structures (Figure 1.7) (Frank-Kamenetskii and Mirkin, 1995, Usdin and Grabczyk, 2000, Mirkin, 2007). In FRDA, the GAA•TTC tract is a purine•pyrimidine (R•Y) polymer, containing only purines (R) in one strand and pyrimidine (Y) in the complementary strand and thus it may adopt the unusual triple helix DNA structure. Recent evidence suggests, that during transcription of a long GAA•TTC tract a transient intramolecular R•R–Y triplex is formed behind the RNA polymerase II (RNAPII), entrapping the RNAPII at the distal end of the repeat. At the transcription bubble, the polymerase covers the Y (TTC) template strand, allowing the available non-template (GAA) strand to fold back which initiates the formation of R•R–Y triplex structure and creating a loop. The spread of triplex formation is propelled by the wave of negative superhelical energy released with the movement of RNAPII along the GAA•TTC tract. This unusual conformation pushes the RNAPII to the distal (3') triplex-duplex junction, pausing its activity and consequently resulting in significant truncation and obstruction in transcription elongation (Mariappan *et al.*, 1999, Usdin and Grabczyk, 2000, Grabczyk and Usdin, 2000, Jain *et al.*, 2002).

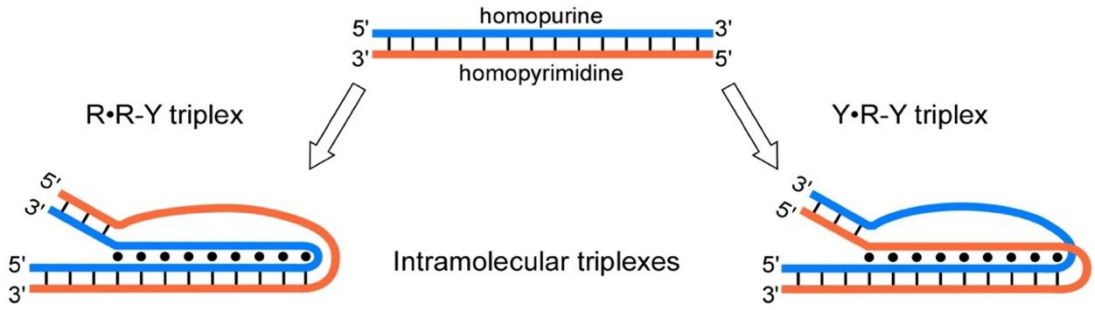

Figure 1. 7 - Schematic diagram of intramolecular R•R–Y and Y•R–Y triplexes. R•R–Y type triplex (left) is formed when the single-stranded purine-rich folds back and interacts with the purine-rich strand of the remaining duplex in an antiparallel orientation. Y•R–Y type triplex (right) is formed when the single-stranded pyrimidine-rich folds back and interacts with the purine-rich strand of the remaining duplex in a parallel orientation (image annotated from Bacolla *et al.* (2015)).

1.2.5 RNA-DNA hybrid formation

Further studies by Grabczyk *et al.* (2007) reported an extensive RNA-DNA hybrid (R-loops) formation on the GAA•TTC template in *E.coli* by using T7 polymerase. During *in vitro* transcription of longer repeat, T7 RNAPII paused at the distal end of the repeat which was tightly linked to a persistent RNA-DNA hybrid formation (Figure 1.8) (Grabczyk and Usdin, 2000, Grabczyk *et al.*, 2007). Additionally, lesser extents of RNA-DNA hybrids were also detected with smaller GAA•TTC repeats (pre-mutation size), that do not cause the disease but are prone to expansion. Furthermore, a recent study revealed in patient cells that RNA/DNA hybrid (R-loops) forms on expanded GAA repeats, impede RNAPII transcription and co-localises with H3K9me2, a characteristic repressive chromatin mark of the disease. Moreover, the study also reported that a decrease in H3K9me2 levels has no effect on R-loop levels. However, increasing R-loop levels by treatment with DNA topoisomerase inhibitor camptothecin leads to up-regulation of H3K9me2, resulting in *FXN* transcriptional silencing. This provides a direct molecular link between R-loops and FRDA pathology, suggesting that R-loops may act as an initial trigger to promote *FXN* silencing. Therefore, R-loops now provide a new therapeutic target for FRDA (Grabczyk *et al.*, 2007, Groh *et al.*, 2014).

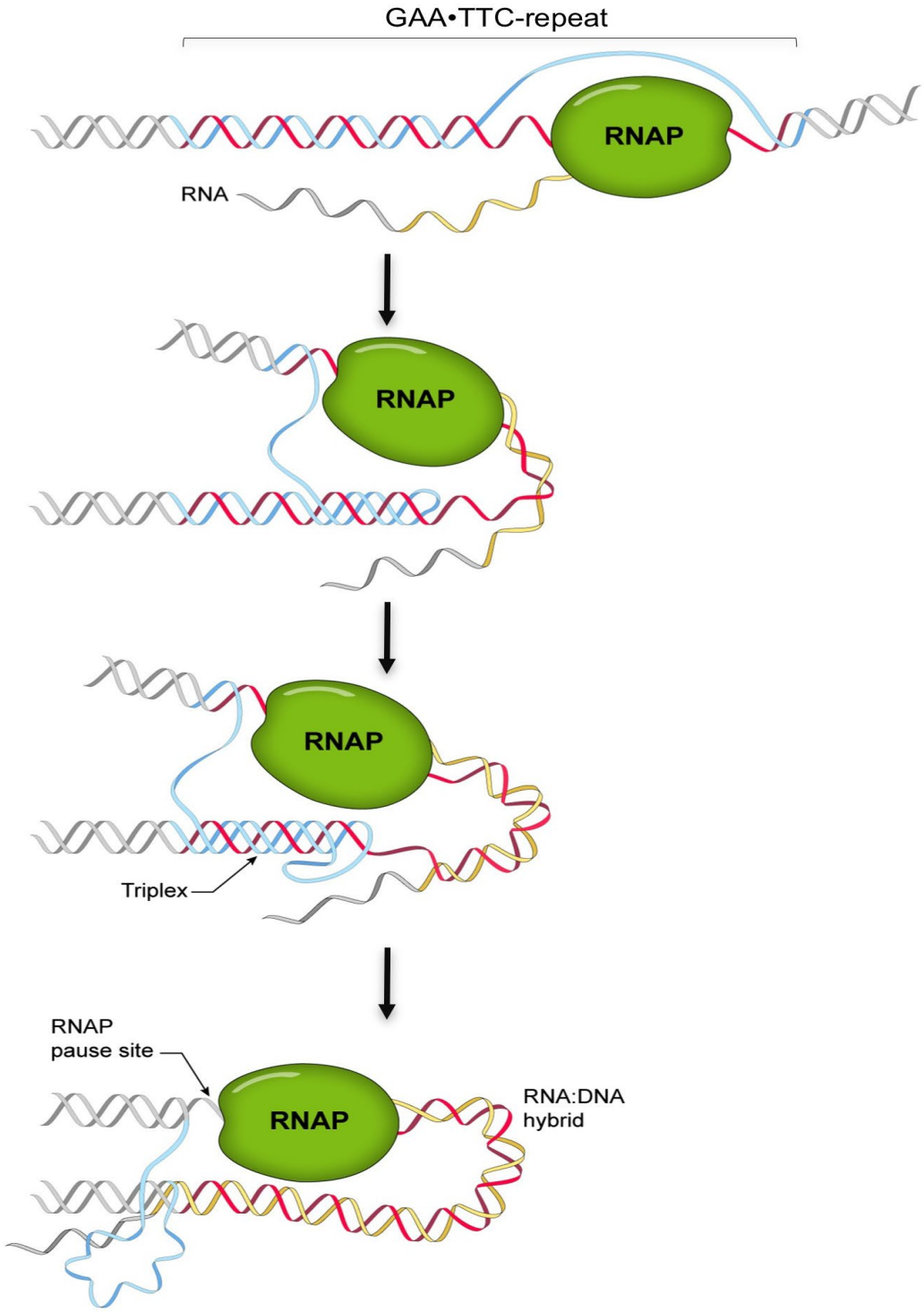

Figure 1. 8 - Schematic illustration of a triplex and RNA-DNA hybrid formation in FRDA. Transcription through the repeat leaves the non-template purine-rich strand transiently unpaired. This strand can then fold back and interact with the duplex that has already reannealed behind the RNAPII, thereby forming a triplex. Triplex formation, in turn, leaves the pyrimidine-rich strand in the second half of the repeat free to form a hybrid with the nascent purine-rich RNA strand, forming a highly stable RNA-DNA hybrid (R-loop) construction. The net result is the formation of a stable R-loop in which the pyrimidine strand of the repeat is hybridized to the nascent transcript leaving the purine-rich strand unpaired. This subsequently traps the RNAPII on the template at the 3' end of the repeat (Diagram annotated from Kumari and Usdin (2012).

1.2.6 Sticky DNA formation

Further investigation demonstrates the stable triplex formation, adopted by the long GAA•TTC tract, to form a higher-order conformation known as sticky DNA (Gacy *et al.*, 1998, Sakamoto *et al.*, 1999). Sticky DNA structures are formed intramolecularly by two interacting R•R–Y triplexes that are distal to each other and is highly dependent on negative supercoiling and divalent metal ions (Figure 1.9) (Vetcher *et al.*, 2002). This in turn severely impairs transcription by sequestrating the progression of RNAPII complex to unwind the DNA template and move forward, and possibly providing a direct mechanism for *FXN* silencing. A direct correlation was also documented between the length of GAA repeat and sticky DNA formation, which confers its pathogenicity in FRDA. However, the length threshold to encourage sticky DNA structure formation is about 60 repeats, and lower repeats have failed to demonstrate these non-B DNA structure conformations (Sakamoto *et al.*, 2001, Pandolfo, 2008). Furthermore, agents used to interrupt GAA•TTC repeat sequence have been shown to destabilise the sticky DNA structure and encourage normal *FXN* gene transcription *in vitro* and *in vivo* (Ohshima *et al.*, 1999, Burnett *et al.*, 2006).

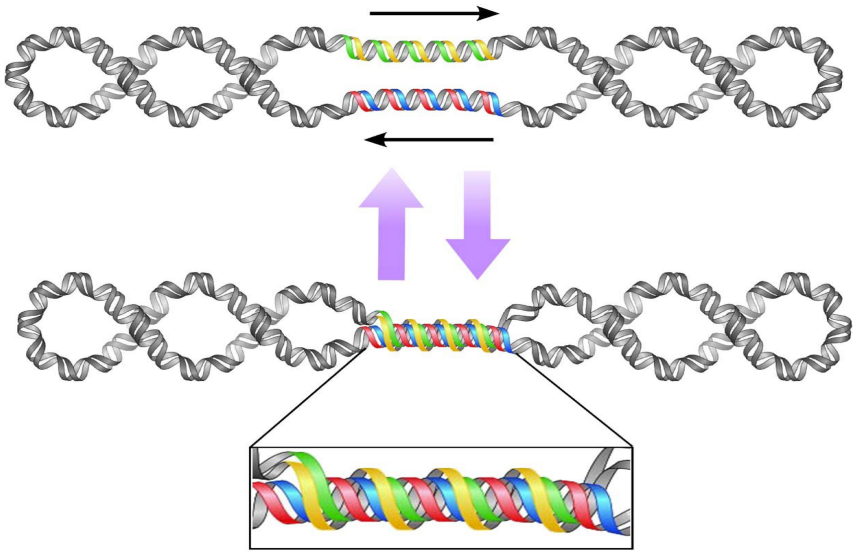

Figure 1. 9 - Schematic diagram for sticky DNA structure in a closed circular plasmid. The green and yellow strands represent one GAA•TTC duplex and the red and blue strands represent the other duplex. Sticky DNA is the structure formed by the association of two long GAA•TTC repeat sequences in one DNA molecule. The interaction of these two tracts is dynamic and is facilitated by negative supercoiling and divalent cations (Son *et al.*, 2006).

1.2.7 Epigenetic changes in FRDA

In contrast to the abnormal DNA structure-based mechanism for gene silencing, the expanded GAA repeat is also consistent to behaving like pericentromeric heterochromatin and inducing chromatin condensation. This renders the gene inaccessible to the transcriptional machinery, thereby leading to *FXN* gene silencing (Saveliev *et al.*, 2003). To understand whether the mutational GAA repeat exerts this heterochromatin gene silencing, Festenstein *et al.* (1996) generated an artificial transgene with a heterochromatin-sensitive lymphoid cell-surface marker protein (CD2). He demonstrated that the expanded repeats induce silencing of nearby genes via a phenomenon known as position-effect variegation (PEV). PEV is the hallmark of heterochromatin-mediated gene silencing, and is thought to occur when a gene is aberrantly positioned near regions of heterochromatin, characterized by various competing epigenetic marks. This includes increases in DNA methylation, histone modification, and antisense transcription, as well as sequence elements such as silencers, enhancers, insulators or locus control region and repetitive DNA (Figure 1.10) (Zuckerkandl, 1974, Tartof *et al.*, 1989, Tartof *et al.*, 1984, Locke *et al.*, 1988, Festenstein *et al.*, 1996, Festenstein *et al.*, 1999, Dillon and Festenstein, 2002). In FRDA, this hypothesis was further strengthened by the findings of a differential DNA methylation profile accompanied by histone acetylation and methylation changes. Additionally, the *FXN* gene silencing was found to be highly correlated with an essential constituent of heterochromatin and a powerful PEV modifier, known as heterochromatin protein 1 (HP1) (Saveliev *et al.*, 2003, Elgin and Reuter, 2013, Yandim *et al.*, 2013).

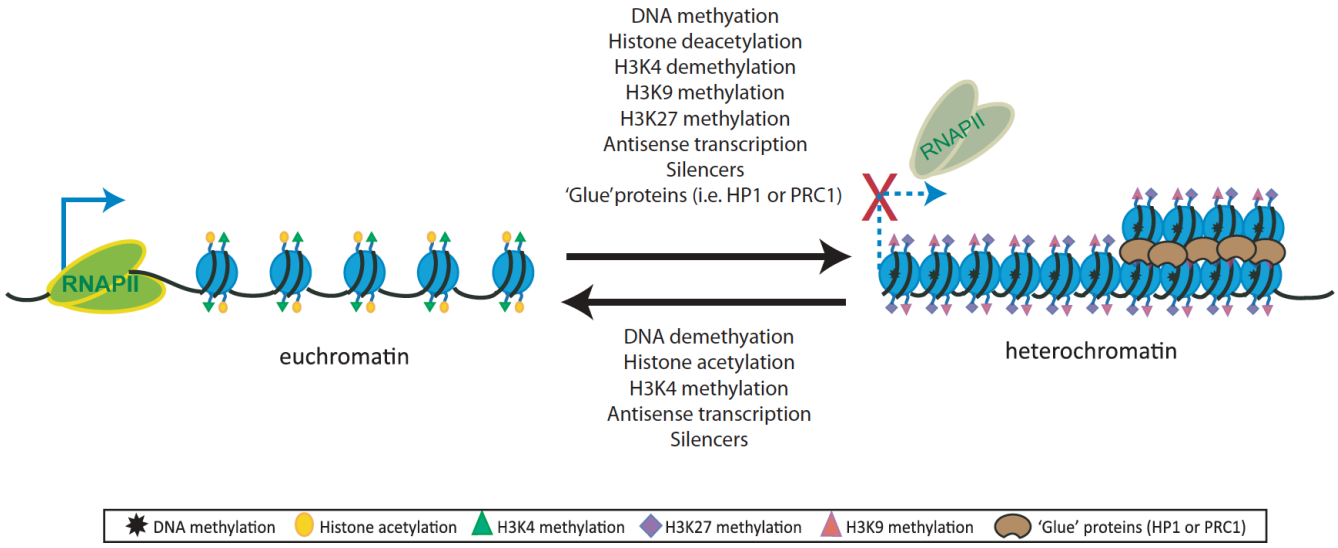

Figure 1. 10 - Histone modifications between euchromatin and heterochromatin. Euchromatin structure is associated with DNA methylation, histone acetylation and H3K4 methylation. On the other hand, the tightly packed heterochromatin is related to DNA methylation, histne deacetylation, H3K4 demethylation, H3K9 and H3K27 methylation. The 'glue proteins' such as HP1 or PRC1 components allows strong nucleosome interaction and create a higher order chromatin structure. The final status of transcription is determined by the concentration of these modifiers and the presence of the binding sites. It is hypothesised that if heterochromatin and euchromatin factors are in balance, stochastic expression of genes (PEV) takes place (Image annotated from Yandim *et al.* (2013)).

1.2.7.1 Histone modifications

Recent FRDA studies have identified various heterochromatin hallmarks associated with gene silencing. This includes hypoacetylation of histone H3 and H4, and increased H3K9me2/3, H3K27me3 and H3K20me3 levels, predominantly at upstream and downstream regions of the expanded GAA repeat tract compared to normal individuals. Furthermore, it has been shown that the promoter region of FRDA patients is associated with reduced levels of acetylated H3K5, H3K14, H4K5, H4K12 and H4K16 (Herman *et al.*, 2006, Al-Mahdawi *et al.*, 2008, Sandi *et al.*, 2014), indicating a less permissive region for transcription (Figure 1.11). Although several epigenetic changes have been identified in FRDA, it is still unclear of which histone modification is directly involved in *FXN* silencing. Nevertheless, considering these histone changes in future studies may perhaps give rise to more potential FRDA therapies.

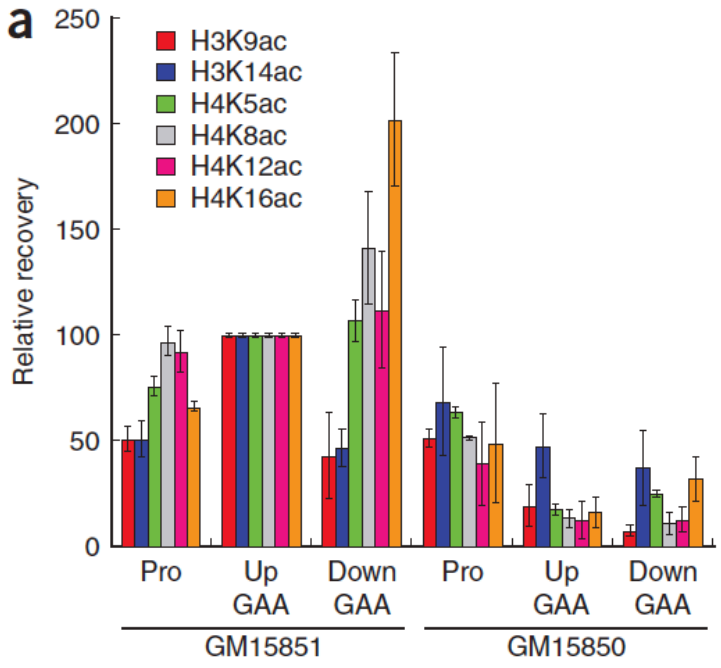

Figure 1. 11 - Investigation of histone modifications in the *FXN* gene by ChIP analysis on a FRDA (GM15850) versus a normal lymphoblastoid cell line (GM15851). In FRDA, histone acetylation levels at specific lysine residues are generally lower immediately upstream and downstream of the GAA repeat (Herman *et al.*, 2006).

1.2.7.2 DNA methylation changes

Al-Mahdawi and colleagues (2008) studied the DNA methylation changes of the *FXN* promoter and flanking GAA regions by performing bisulfite sequence analysis on FRDA patient brain, cerebellum and heart tissues. The results revealed a shift in the FRDA DNA methylation profile, with the GAA-upstream CpG sites being consistently hypermethylated and the GAA-downstream CpG sites being consistently hypomethylated (Figure 1.12). Only 4 selected CpG sites in the promoter region showed any degree of methylation, and the levels of methylation were not specifically and significantly increased in the FRDA samples. Comparable methylation patterns were also detected in tissues from two different strains of YAC transgenic FRDA mice, YG8 and YG22 (Al-Mahdawi *et al.*, 2008). Furthermore, a positive correlation has been seen with the degree of methylation and extent of GAA expansion (Evans-Galea *et al.*, 2012).

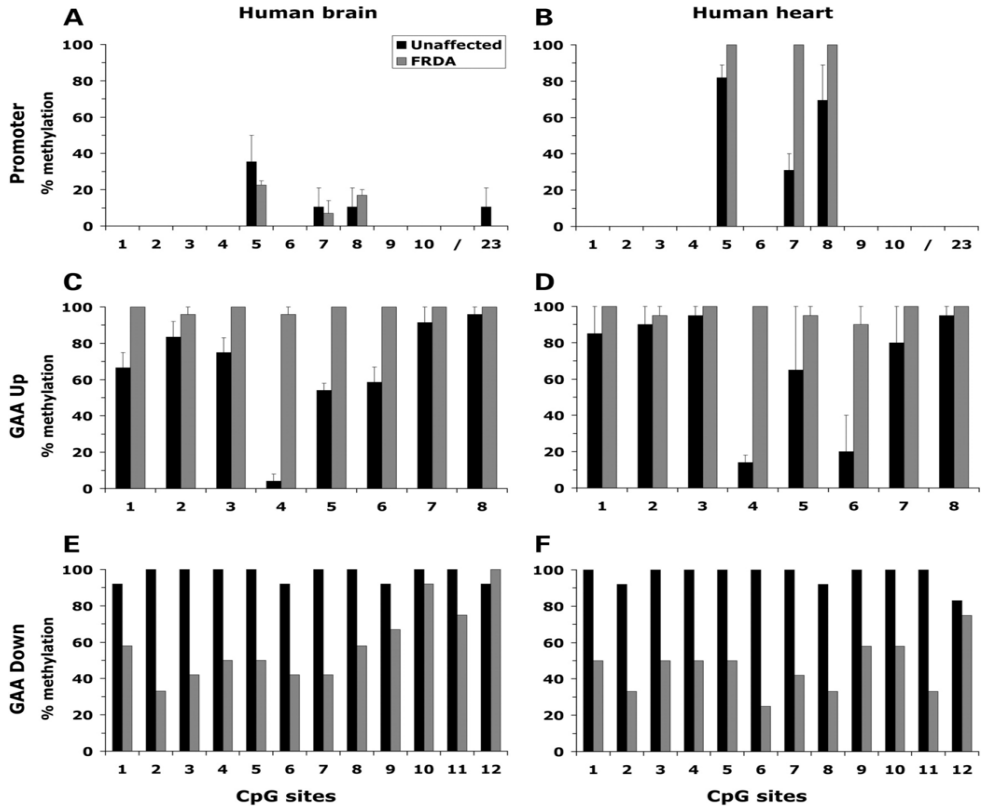

Figure 1. 12 - DNA methylation analysis of the FXN promoter (A and B), upstream GAA (C and D) and downstream GAA (E and F) regions of human brain and heart tissues. In each case the mean percentage of methylated CpG sites is shown, as determined by bisulfate sequencing (Al-Mahdawi *et al.*, 2008).

1.3 Frataxin protein: structure, localisation and maturation

Frataxin is an essential and highly conserved mitochondrial protein that is found ubiquitously in most eukaryotic and prokaryotic cells (Adinolfi *et al.*, 2002). In eukaryotes, frataxin is encoded in the nucleus, translated in the cytoplasm and then imported into mitochondria (Koutnikova *et al.*, 1997). Initially, a precursor form of frataxin is translated consisting of 210 amino acids, containing an N-terminal transit amino acid sequence, that allows its passage into the mitochondrial matrix (Gibson *et al.*, 1996). The precursor form was originally found to undergo two proteolytic cleavages that removed the transit sequence and converted it first to a 19kDa intermediate form and then to a final form of 17kDa. These cleavages were shown take place in the mitochondria by the mitochondrial processing peptidase (MPP), with the first cleavage occurring between G41 and L42, and the second between A55 and S56 (Koutnikova *et al.*, 1998). However, more recent studies have shown that frataxin processing in human cells actually produces an even smaller protein of 14kDa, by cleaving between K80 and S81 (Condo *et al.*, 2007, Schmucker *et al.*, 2008). The resulting 130 amino acid protein is recognised as the mature and fully functional form of frataxin, and is predominantly localised in the mitochondrial matrix as a free soluble protein (Campuzano *et al.*, 1997). Crystal structure analysis shows that mature frataxin consists of a globular and compact assembly in which two α-helices (α_1-α_2) are packed against seven β-sheets (β_1-β_5, β_6 and β_7). The two helices are N- and C-terminals to the β-sheets, forming a short and well-ordered structure. The C-terminal coil fills a groove between the two α-helices (Figure 1.13) (Dhe-Paganon *et al.*, 2000, Condo *et al.*, 2007). The extensive structure and biochemical analysis of human (hFXN), yeast (Yfh1), and bacterial frataxin orthologues (CyaY) show that they all share a very similar fold, which directly reflects the high degree of sequence conservation and strongly indicates a common function (Sazanov and Hinchliffe, 2006).

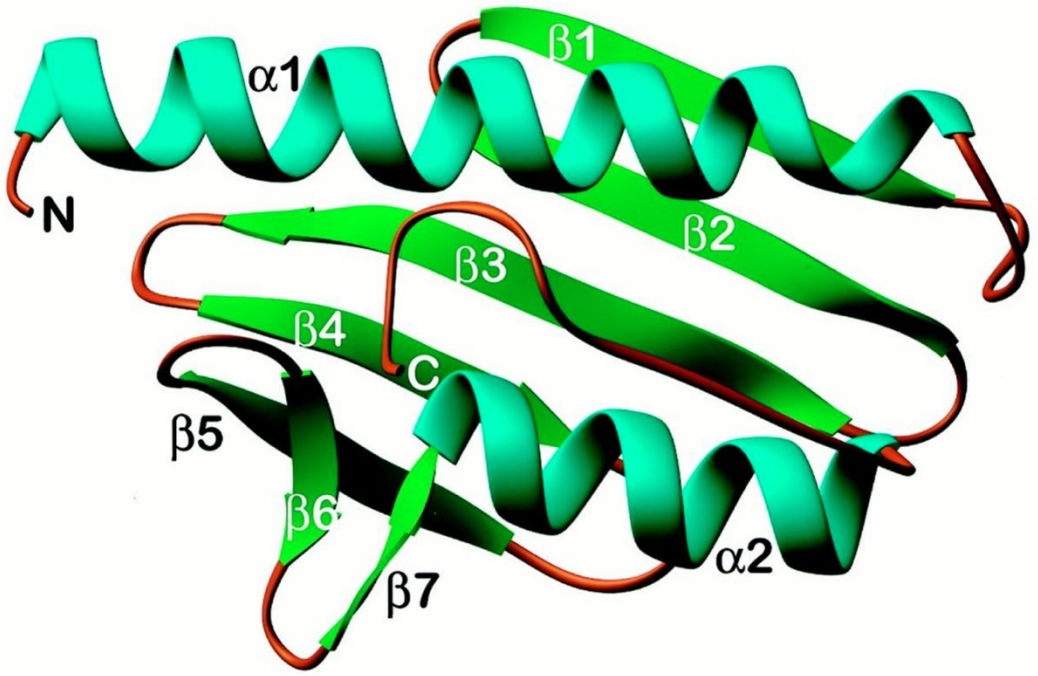

Figure 1. 13 - A ribbon illustration of frataxin protein structure, demonstrating a compact assembly of α-helices (turquoise) and β-sheets (green) sandwich. The β-sheets, β_1-β_5, form a flat antiparallel strand with the two α-helices, α_1-α_2. The two α-helices are nearly parallel to each other and to the plane of the large β-sheets. A second, smaller β-sheets, β_6 and β_7, are formed by the C-terminus of β_5 (Dhe-Paganon *et al.*, 2000).

1.3.1 Molecular function of frataxin

Although the exact function of frataxin has been a matter of debate since its discovery, lack of frataxin is known to result in mitochondrial dysfunction and ultimately cell death. Studies have emphasized a fundamental role of frataxin in cell survival by regulating mitochondrial iron homeostasis (Bradley *et al.*, 2000, Lodi *et al.*, 2001b), synthesizing Fe-S cluster (ISC) proteins (Koutnikova *et al.*, 1997, Cavadini *et al.*, 2000) and providing protection from oxidative stress (Schulz *et al.*, 2000, Wilson, 2003). In addition, studies in FRDA human tissues, yeast and mouse frataxin-depleted mutants with selective disruption of the *FXN* homologue, have provided further evidence on the role of frataxin and FRDA pathogenesis. For example, frataxin deficiency in a conditional KO mouse model has been shown to develop cardiomyopathy, a prominent cause of death seen in most FRDA patients (Cossee *et al.*, 2000, Calabrese *et al.*, 2005).

1.3.2 Frataxin and iron homeostasis

Studies carried out on the yeast frataxin homologue (Yfh1) led to the proposal that frataxin is involved in regulating iron efflux in mitochondria, because absence of Yfh1 resulted mitochondrial damage due to iron overload (Radisky *et al.*, 1999, Babcock *et al.*, 1997, Foury and Cazzalini, 1997). Furthermore, iron accumulation and deposits were consistently seen in the autopsy of heart muscles (Bradley *et al.*, 2000) and the dentate nucleus (Waldvogel *et al.*, 1999, Koeppen *et al.*, 2007) of FRDA patients. This led to the conclusion that frataxin was involved in mitochondrial iron homeostasis (Pandolfo, 1999).

In the absence of iron, CyaY, Yfh1 and hFXN frataxin homologues all exist as highly soluble monomers. However, early *in vitro* studies of CyaY and Yfh1 show that in aerobic conditions, frataxin protein form iron-rich oligomeric spheroidal structures with high ionic strength (Adamec *et al.*, 2000, Adinolfi *et al.*, 2002, Gakh *et al.*, 2002, Layer *et al.*, 2006, Adinolfi *et al.*, 2009). More recent studies have demonstrated that human frataxin can bind six to seven iron atoms, and depending on the type of frataxin homologue and oxidative state of iron, several iron binding sites have been identified. This indicates that frataxin may also play a role in mitochondrial iron storage. (Yoon and Cowan, 2003, Bou-Abdallah *et al.*, 2004, Yoon *et al.*, 2007, Huang *et al.*, 2008). Further biochemical investigations proposed that frataxin deficiency leads to a reduction of mitochondrial aconitase, ferrochelatase and proteins of the ISC machinery (Gerber *et al.*, 2003, Bulteau *et al.*, 2004, Yoon and Cowan, 2004, Bencze *et al.*, 2007). Additionally, studies of hFXN and Yfh1 frataxin homologues have reported an iron dependent interaction with Nfs1-Isu1 complex, suggesting that frataxin is required for ISC cluster biosynthesis, by acting as an iron donor (Yoon and Cowan, 2003). However, bacterial studies of CyaY have indicated that frataxin also serves as a molecular regulator to inhibit the formation of 2Fe-2S and store iron in a bio-available form for utilisation (Figure 1.14) (Layer *et al.*, 2006, Adinolfi *et al.*, 2009).

Furthermore, studies of a conditional knockout mouse model mimicking the FRDA cardiomyopathy showed that mitochondrial iron accumulation and changes in Fe-S dependent enzyme activity occur significantly later than the onset of pathology (Puccio *et al.*, 2001, Martelli *et al.*, 2007). This indicates that deregulation in ISC formation is a secondary consequence and cannot be the only causative pathological mechanism.

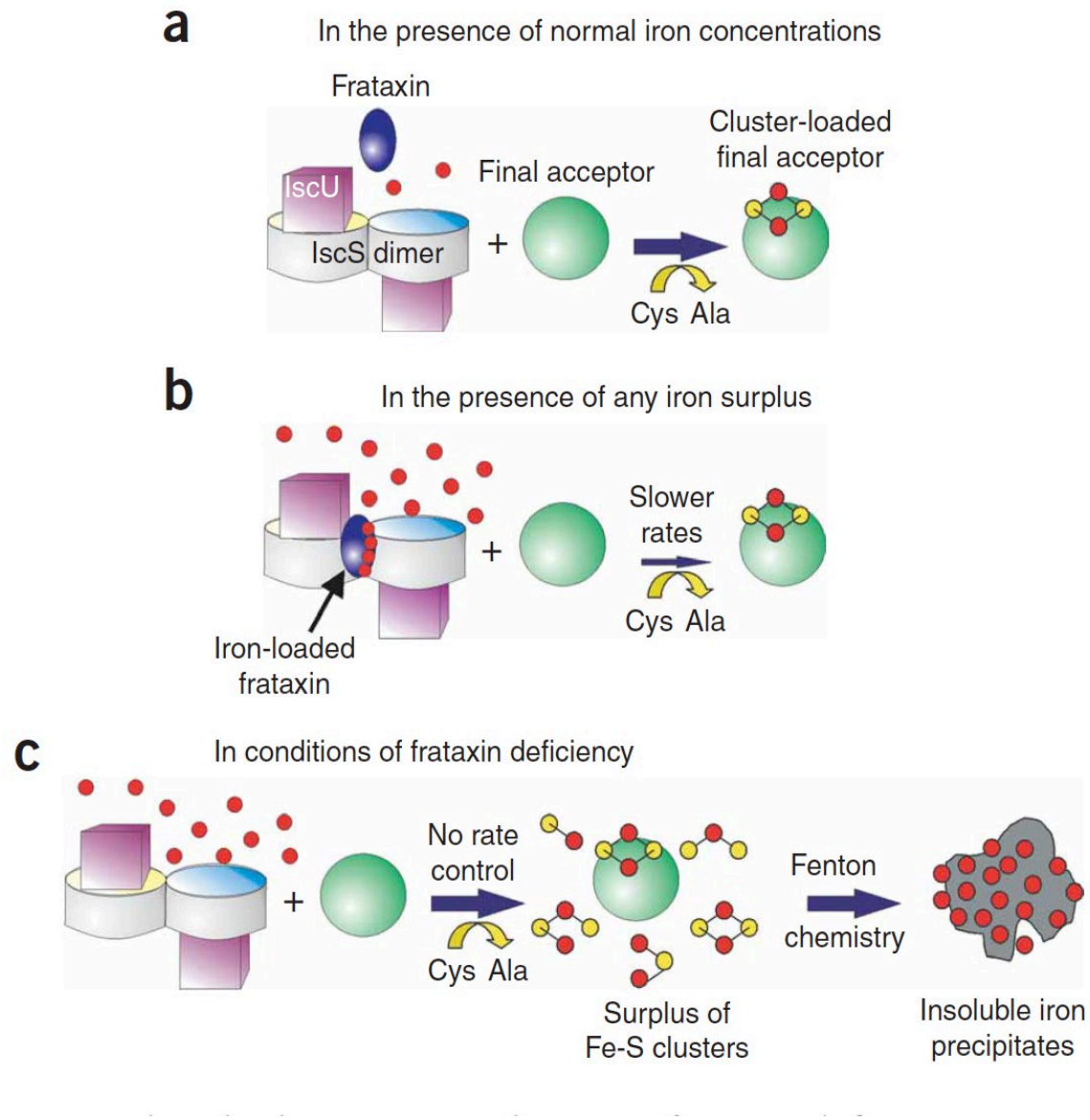

Figure 1. 14 - Schematic representation of the molecular mechanism of frataxin in the cell during a) normal iron concentration, b) excess of iron concentrations, and c) absent/ insufficient frataxin conditions (Adinolfi *et al.*, 2009).

1.3.3 Frataxin and oxidative stress

In frataxin-deficient cells, cellular oxidative stress has been observed as a secondary effect of impaired iron homeostasis and respiratory chain dysfunction, due to the increased production of reactive oxygen species (ROS). This was initially proposed when high levels of hydrogen peroxide (H_2O_2) were detected in frataxin-deficient cells (Babcock *et al.*, 1997, Wong *et al.*, 1999). The freely available Fe^{2+} can generate toxic reactive oxygen species by reducing oxygen and H_2O_2 to the extremely reactive superoxide and hydroxyl radical, respectively (Fenton chemistry) (Tozzi *et al.*, 2002). Free radicals are known to be lethal and cause severe damage to essential proteins, lipids, nucleic acids and ultimately result in cell death. As well as triggering an iron overload, inefficient ISC synthesis in FRDA impairs the ISC-containing subunits of mitochondrial electron transport chain (ETC) complexes I, II and III, which triggers a subsequent increase in H_2O_2 levels, particularly in the cardiac tissue (Rotig *et al.*, 1997, Bradley *et al.*, 2000, Tozzi *et al.*, 2002). Additionally, aconitase, an ISC protein involved in iron homeostasis, is also reported to be deficient in FRDA (Figure 1.15) (Rotig *et al.*, 1997). Furthermore, decreased levels of mitochondrial-DNA (mt-DNA) have been detected in patients with FRDA (Houshmand *et al.*, 2006, Heidari *et al.*, 2009). Naturally, mt-DNA lacks the protective histones, and therefore, it is easily susceptible to damage by ROS. As mt-DNA partially encodes the ETC complexes, its damage by ROS in FRDA can further aggravate mitochondrial dysfunction yielding further ROS (Orsucci *et al.*, 2011). Moreover, frataxin not only functions to protect against oxidative stress, but also determines antioxidant responses in the presence or absence of excess iron (O'Neill *et al.*, 2005). This ability to interact with antioxidant defences is reduced in frataxin-deficient cells following mild exposure to oxidants (Jiralerspong *et al.*, 2001, Chantrel-Groussard *et al.*, 2001). As evidence of oxidative stress in FRDA, elevated urinary 8-hydroxy-2'-deoxyguanosine (a marker of

oxidative DNA damage) (Schulz *et al.*, 2000) and raised plasma malondialdehyde (a lipid peroxidation product) (Emond *et al.*, 2000) levels, have been observed.

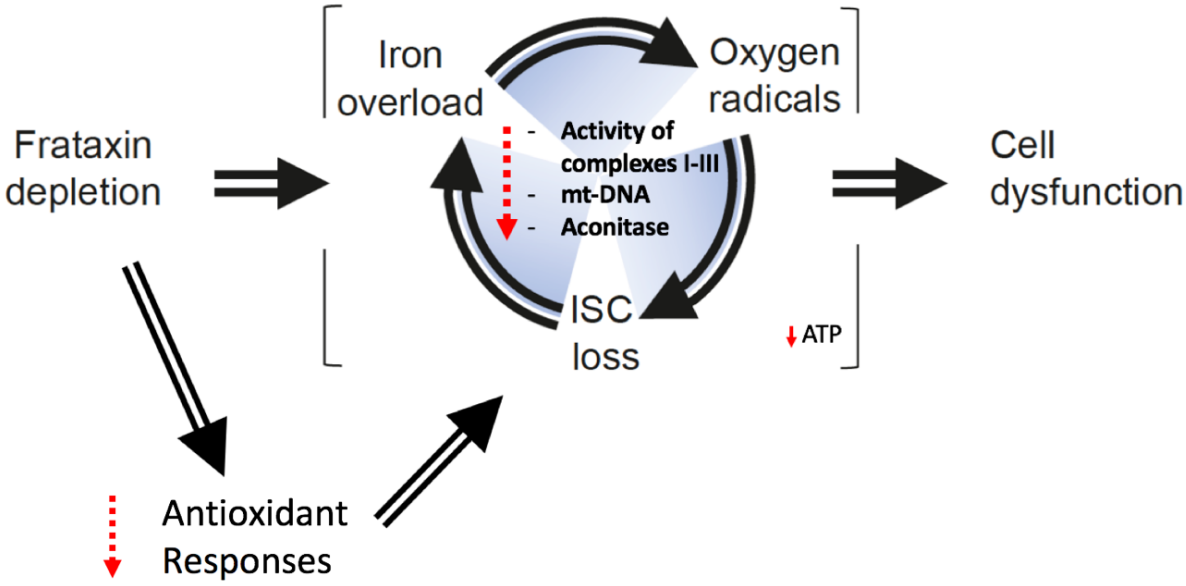

Figure 1. 15 - Schematic representation of events leading to cell dysfunction in FRDA. Although the precise sequence of events in FRDA pathogenesis is uncertain, it is proposed that frataxin depletion results in impaired ISC synthesis and/or stability with intramitochondrial accumulation of reactive iron. Reactive iron promotes Fenton chemistry, producing superoxide and hydroxyl radical, which in turn destroys more ISCs. Subsequently, this results in decrease in complexes I-III function, mitochondrial aconitase activity and mt-DNA. Impaired respiratory chain activity and decreased aconitase activity will impair ATP synthesis, which together with oxidative damage to cellular components, will compromise cell viability. Additionally, in frataxin-depleted cells, deficient signalling of antioxidant defences sensitises the frataxin-free ISCs to reactive oxygen species. This antioxidant sensitisation process results in intramitochondrial iron accumulation, mostly as amorphous nonreactive precipitates. Image annotated from Bradley *et al.* (2000); Bayot and Rustin (2013).

1.4 Therapeutic approaches

Currently, there are no therapeutic approaches that have proven effective for treating FRDA or slowing progression of symptoms. However, based on improved research and findings on the role of frataxin and disease pathogenesis, presently numerous new compounds are in various different phases of development and testing (Figure 1.16). This mainly consists of compounds which target to either improve mitochondrial function or enhancing frataxin expression. However, the mode of action for most of these compounds in up-regulating frataxin expression is still unclear.

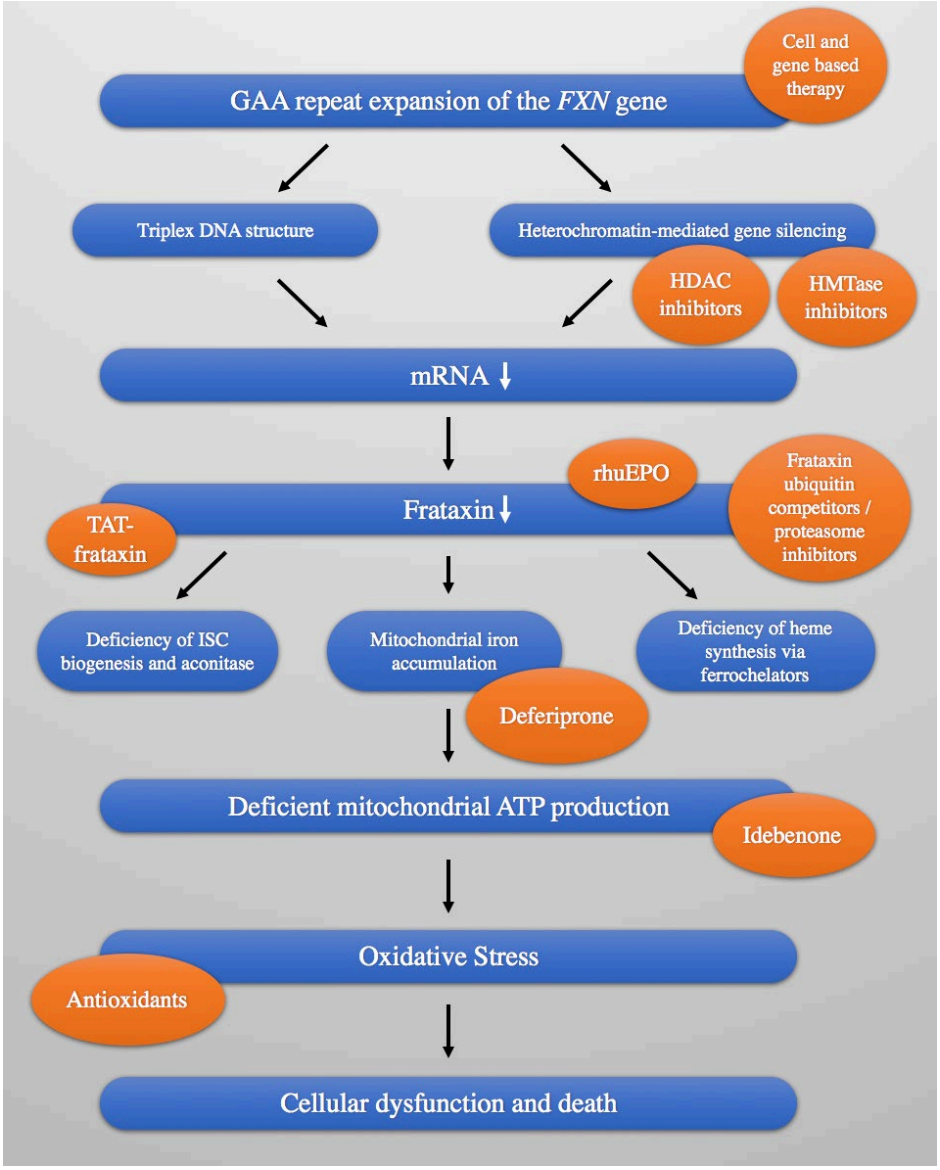

Figure 1. 16 - Schematic illustration of the pathophysiological mechanisms in FRDA and their associated relevant therapeutic point of application (Nachbauer *et al.*, 2011).

1.4.1 Antioxidant therapy

Recent studies have identified decreased mitochondrial respiratory chain function and increased oxidative stress in FRDA pathophysiology (Cooper and Schapira, 2007). Therefore, the possible use of energy enhancement and antioxidant agent to preserve aerobic respiration may be a useful treatment in preventing or delaying disease symptoms and cell death. After extensive preclinical studies, several clinical trials on the antioxidant drugs, idebenone and coenzyme Q10, were conducted. The majority of clinical therapeutic studies were carried out on idebenone, a synthetic short-chain quinine analogue of coenzyme Q10. It plays a role in both shuttling electrons between damaged ETC complex proteins and scavenges intracellular potent free radicals (Rustin *et al.*, 1999, Meier and Buyse, 2009). The initial clinical studies of idebenone revealed promising results, improving neurological symptoms (Di Prospero *et al.*, 2007a), decreasing oxidative stress and lipid peroxidation and slowing down the progression of heart disease (Rustin *et al.*, 1999, Schulz *et al.*, 2000). However, very recently idebenone failed its Phase III study as no clinical significant benefits of neurological symptoms or cardiac hypertrophy in patients were reported (Lagedrost *et al.*, 2011, Parkinson *et al.*, 2013). However, these inconsistent outcomes could be a result of several variabilities, such as disease stage and age of treatment initiation, which could have influenced these negative effects. Therefore, this failure does not rule out antioxidants as potential therapeutic agents (Di Prospero *et al.*, 2007a, Di Prospero *et al.*, 2007b, Schulz *et al.*, 2009). Moreover, several small trials have evaluated the effect of coenzyme Q10 and vitamin E in FRDA patients. Co-enzyme Q10 plays a role in mitochondrial ATP production, and vitamin E is a naturally occurring lipid-soluble antioxidant. A combination treatment of co-enzyme Q10 and vitamin E have shown an improvement of energy metabolism in cardiac- and skeletal muscle bioenergetics (Lodi *et al.*, 2001a, Hart *et al.*, 2005). However, more studies need to be carried out to make a conclusive evaluation.

1.4.2 Iron chelators

Frataxin deficiency in FRDA is known to result in mitochondrial iron accumulation, thus disturbing ISC assembly (Yoon and Cowan, 2003, Pandolfo and Hausmann, 2013). As such, much effort has been put in designing and testing drugs with iron chelating potential for use in FRDA (Lodi *et al.*, 2006, Santos *et al.*, 2010). So far, many potential iron chelators have been disadvantaged by poor permeability in biological membranes (Pandolfo and Hausmann, 2013). This includes deferoxamine and deferiprone, which have been investigated in both *in vitro* models (Goncalves *et al.*, 2008, Kakhlon *et al.*, 2008) and in clinical trials (Boddaert *et al.*, 2007). Deferoxamine has not performed well in FRDA, as it can chelate iron in cell culture, but simultaneously also decreased the mRNA levels of both aconitase and frataxin, making it unsuitable for use in FRDA (Li *et al.*, 2008). In contrast, deferiprone is an orally administered iron chelator with good permeability and is capable of crossing the blood brain-barrier and shuttle iron between subcellular compartments (Glickstein *et al.*, 2005, Pandolfo and Hausmann, 2013). Although deferiprone have been shown to successfully protect the mitochondria from ROS damage (Kakhlon *et al.*, 2008) and reduce iron build-up in the brain with a small improvement in neurological function (Boddaert *et al.*, 2007), it also reduced aconitase activity due to excessive iron chelation (Goncalves *et al.*, 2008). Therefore, due to the inconclusive results obtained, more investigation is required to understand the effectiveness of deferiprone as a treatment for FRDA.

1.4.3 Epigenetic based therapies

In FRDA, expanded GAA repeats have been shown to induce heterochromatin-mediated silencing of *FXN* gene, due to highly condensed DNA, in a manner reminiscent of PEV gene silencing (Saveliev *et al.*, 2003). Further studies have subsequently identified epigenetic changes, including DNA methylation, histone deacetylation and histone methylation which may be involved in the *FXN* gene silencing in FRDA (Gottesfeld *et al.*, 2013, Silva *et al.*, 2015). Thus, a promising therapeutic strategy is to directly target these epigenetic states with DNA demethylation agents, histone deacetylase (HDAC) inhibitors and the newly proposed histone methyltransferase (HMTase) inhibitors to restore frataxin levels.

DNA demethylation therapies

Numerous studies have indicated an increase of DNA methylation upstream of GAA repeat region of FRDA associated *FXN* alleles. Therefore, treatment with DNA demethylating agents, such as 5-Aza-2'-deoxycytidine (5-aza-CdR), is now suggested as a therapeutic option for FRDA (Figure 1.15). The nucleoside analogue DNA methyltransferase (DNMT) inhibitor, 5-aza-CdR, has previously been studied either alone or in combination with HDAC inhibitors in treating Fragile X syndrome (FXS) lymphoblasts, effectively restoring the *FMR1* promoter hypermethylation and reinstating mRNA and protein levels to normal (Chiurazzi *et al.*, 1999). Additionally, a recent study testing a combination treatment of 5-aza-CdR and HMTase, increased *FMR1* transcripts in FXS cells (Kumari and Usdin, 2016). Thus far, no reports have been published describing the effects of DNA demethylation agents in treating FRDA. However, promising results are obtained from using these agents to treat FXS, a disease similar to FRDA in having a non-translated nucleotide repeat inducing CpG hypermethylation and histone deacetylation. The FXS results further support the use of DNA demethylating agents as a potential therapeutic procedure for FRDA (Sandi *et al.*, 2014).

HDAC inhibitors

The use of small molecule inhibitor of chromatin modifying enzymes, such as HDAC inhibitors, have proven to be beneficial in reactivating *FXN* gene in FRDA, by reverting the silent heterochromatin to an active chromatin conformation (Gottesfeld, 2007, Soragni and Gottesfeld, 2016). Currently, HDAC inhibitors are the subject of intense research as a promising therapeutic strategy for FRDA (Figure 1.15). Treatment using HDAC inhibitors have produced a significant increase of frataxin mRNA and protein expression, and elevated levels of histone acetylation in cellular (Herman *et al.*, 2006) and animal models (Rai *et al.*, 2008, Rai *et al.*, 2010). This effect was supported by a five-month study on the mildly affected YG8R mice, where three 2-aminobenzamide (class I) HDAC inhibitors were investigated (Sandi *et al.*, 2011). One of the HDAC inhibitors, designated 109/RG2833, has recently completed a small phase Ib clinical trials and is currently being further engineered to improve brain distribution and metabolic stability (Soragni *et al.*, 2014, Shan *et al.*, 2014, Gottesfeld *et al.*, 2013). Another therapeutic testing with the class III HDAC inhibitor, nicotinamide (a form of vitamin B), decreased histone methylation marks, H3K9me3 and H3K27me3, at the *FXN* locus and increased *FXN* expression in FRDA cell lines and mouse models. Although nicotinamide was well tolerated by FRDA patients, it was observed, after entering the early stage of FRDA clinical trials (an open label pilot study), that it did not significantly improve or establish any clinical benefits (Chan *et al.*, 2013, Libri *et al.*, 2014, Aranca *et al.*, 2016). Therefore, further research is still required to understand the underlying mechanism of nicotinamide treatment. Currently, research is underway to develop new and more potent HDAC inhibitors specific to the frataxin locus in addition to more complete animal studies determining the bioavailability and efficacy (Puccio *et al.*, 2014).

HMTase inhibitors

Histone lysine methylation, which is regulated by HMTases and histone demethylases (HDMs), is also highly associated with gene transcriptional repression and activation (Kouzarides, 2007). Such histone lysine modifications, including H3K9me2/3 and H3K27me3, are seen in FRDA. Therefore, specific HMTase inhibitors are currently being explored to revert the silent heterochromatin by inhibiting repressive marks and restoring *FXN* gene function (Figure 1.17). Thus far, treatments with HMTase inhibitors have produced a significant reduction in histone methylation and activation of previously silenced genes (McCabe *et al.*, 2012, Sato *et al.*, 2013, Sandi *et al.*, 2013). Recently, treating FRDA lymphoblastoid cells with HMTase inhibitors caused significant reduction in H3K9me2/3 levels, but no substantial change in *FXN* mRNA levels was detected (Punga and Buhler, 2010). This may suggest a redundant role for the H3K9me2/3 alone in *FXN* gene silencing and perhaps targeting more than one methylation marks may be more effective. Therefore, to further explore the efficacy of HMTase inhibitors, we have carried out *in vitro* studies using human and mouse FRDA fibroblasts, which will be discussed in more detail in Chapter 3.

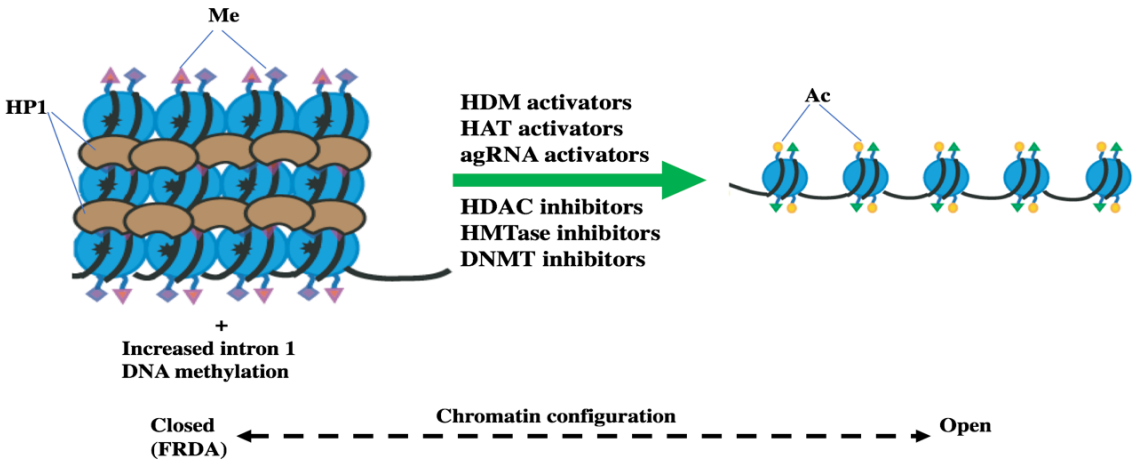

Figure 1. 17 - Potential epigenetic-based therapies for FRDA. Large GAA repeats in FRDA patients are associated with heterochromatin-mediated *FXN* gene silencing. Agents designed to increase histone acetylation by inhibiting HDAC activity, and to reduce DNA and histone methylation levels by inhibiting DNMT and HMTase activity, are expected to increase *FXN* gene expression by reversing the heterochromatin formation to more open chromatin structure. Other epigenetic-based therapies for FRDA include HDM activators, HAT activators and agRNA activation (Image annotated from Festenstein (2006) and Chan *et al.* (2013)).

1.4.4 Synthetic transcription elongation factors

In FRDA cells, the expanded GAA repeats are enriched in repressive histones and can also adopt abnormal DNA conformations that impede *FXN* transcription, by inducing a barrier to the productive elongation (Yandim *et al.*, 2013, Li *et al.*, 2015). A recent study reported the development of a sequence-specific synthetic transcription elongation factors (Syn-TEF1), capable of binding to the repressive GAA repeats and actively assisting productive elongation to restore *FXN* expression to normal levels (Erwin *et al.*, 2017). The study demonstrated that Syn-TEF1 treatment significantly stimulated *FXN* gene expression and restored biological functions in primary cells derived from more than 20 FRDA patients with broad range of GAA repeat expansions and diverse genetic background. Furthermore, Syn-TEF1 treatment in mice carrying cells with expanded GAA repeats was found to restore frataxin protein levels to almost normal values (Erwin *et al.*, 2017). This precision-tailored synthetic molecule may have the potential to treat FRDA and other diseases caused by transcriptional dysfunction; however, further research needs to be carried out before this molecule could be applied to humans.

1.4.5 Frataxin protein stabilising and enhancement therapies

Erythropoietin

In the past few years, erythropoietin (EPO) has received considerable attention as a therapeutic potential for FRDA, due to its neuroprotective capability. EPO is a glycoprotein that controls erythropoiesis, a process which regulates red blood cell production (Grasso *et al.*, 2007, Siren *et al.*, 2009). Initial *in vitro* treatments of recombinant human erythropoietin (rhuEPO) have been shown to significantly increase frataxin protein levels in FRDA patient lymphocytes and fibroblasts in a dose-dependent manner, without a concurrent rise in mRNA expression. This suggests that EPO acts at the post-transcriptional level (Sturm *et al.*, 2005, Acquaviva *et al.*, 2008). Subsequently, initial small open-label studies testing this drug indicated an improvement in FARS and SARA ratings and a decrease in oxidative-stress biomarkers, in the urine and blood of patients (Boesch *et al.*, 2007, Boesch *et al.*, 2008). However, the latest two open-label studies showed that regular high dose administration of rhuEPO resulted in a cumulative long lasting frataxin expression without any clinical improvements (Sacca *et al.*, 2011, Nachbauer *et al.*, 2011). Another latest phase II clinical trial study (double-blind and placebo-controlled), evaluated the safety and tolerability of carbamylated EPO (CEPO) in FRDA patients. The results indicated that while CEPO was safe and well tolerated, no significant change in frataxin levels or clinical outcomes were seen between the drug and placebo groups (Boesch *et al.*, 2014). Therefore, due to the inconsistent evidence on the efficacy of EPO, and lack of knowledge on the specific drug mechanism of action in neuroprotection, EPO is not a likely candidate to be further investigated as a potential drug in treating FRDA (Mariotti *et al.*, 2013).

Preventing frataxin ubiquitin-proteasome degradation

It has been reported that frataxin protein stability and degradation is regulated by the ubiquitin-proteasome pathway (UPP) before its functional mitochondrial maturation. Therefore, researchers have proposed the use of ubiquitin competing molecules (UCMs) may have therapeutic potential by inhibiting frataxin ubiquitination and subsequently rescuing intracellular frataxin deficiency (Rufini *et al.*, 2011, Rufini *et al.*, 2015, Benini *et al.*, 2017). Furthermore, other small molecules inhibitors designed to target different steps of the UPS pathway have been developed. These include proteasome inhibitors, some of which are now approved for cancer treatments and have shown to modulate frataxin turnover in FRDA cells (Richardson *et al.*, 2006, Rufini *et al.*, 2011, Kisselev *et al.*, 2012, Rentsch *et al.*, 2013, Rufini *et al.*, 2015). Therefore, with aims to prevent frataxin degradation *in vitro,* we have carried out an extensive investigation on the efficacy of various proteasome inhibitors using human and mouse FRDA fibroblast, which is discussed in detail in chapter 4.

1.4.6 Cell and gene therapy

Recently, there has been a lot of interest in the development of cell and/or gene based therapies as an alternative to classical drug-based treatment for FRDA. The success of these therapies in other genetic diseases has encouraged their use with different experimental approaches for FRDA treatment. This includes the proposed autologous transplantation of patient's own, genetically corrected, bone marrow (BM) derived cells or induced pluripotent stem cells (iPSCs) (Tajiri *et al.*, 2014, Qin *et al.*, 2015). Similar to other FRDA cellular models, FRDA iPSCs generated from FRDA patient fibroblasts retain the characteristics of unstable trinucleotide GAA expansions and decreased *FXN* mRNA expression (Ku *et al.*, 2010, Liu *et al.*, 2011, Hick *et al.*, 2013, Codazzi *et al.*, 2016) with impaired mitochondrial function (Hick *et al.*, 2013). This is also considered to be the same for FRDA BM-derived cells (Tajiri *et al.*, 2014). Additionally, both iPSCs and BM-derived cells have been shown to

successfully transdifferentiate to neurons and cardiomyocytes, the two cell types primarily affected in FRDA (Weimann *et al.*, 2003, Shetty *et al.*, 2009, Liu *et al.*, 2011, Hick *et al.*, 2013). Therefore, the genetically corrected stem cell transplantation can fuse with these damaged cells and eventually prevent FRDA-associated disease hallmarks and display normal phenotypes (Rocca *et al.*, 2015). Importantly, since FRDA patients produce frataxin at low levels, transplantation of patient's own stem cells expressing increased frataxin should not provoke an immune response (Evans-Galea *et al.*, 2014b). Moreover, gene therapy is being considered as a strategic system to correct the genetic abnormality in FRDA by offering permanent *FXN* gene delivery (Khonsari *et al.*, 2016). So far, several lines of evidence have indicated that FRDA is amenable to various gene therapy approaches. An initial attempt by Fleming *et al.* (2005) reported the functional recovery of frataxin and partially reversing the oxidative stress effect in primary FRDA patient fibroblasts by delivering human frataxin cDNA encoded in adeno-associated viral (AAV) and lentiviral (LV) vector constructs. This effect was also seen in a recent study using LV-*FXN* gene delivery to FRDA patient and YG8sR cells, which reported long-term overexpression of *FXN* mRNA and frataxin protein levels (Khonsari *et al.*, 2016). Furthermore, injection of AAV-*FXN* in a mouse model of FRDA with severe cardiomyopathy (caused by total cardiac knockout of frataxin), completely reverses the functional features of cardiomyopathy (Perdomini *et al.*, 2014). In addition, mice treated with the AAV9-FXN display an increase in frataxin protein expression, reduced cardiac hypertrophy, and a prolonged lifespan when compared to typical FRDA mouse models (Gerard *et al.*, 2014). These findings suggest that AAV-*FXN* gene therapy may be beneficial as effective therapy for FRDA. Therefore, FRDA can be highly responsive to cell and gene therapy, with multiple and potential cellular targets (Evans-Galea *et al.*, 2014a).

1.4.7 Pharmacotherapies for cerebellar ataxia

Increasing knowledge of cerebellar ataxia (CA) disease pathophysiology has led to the development of potential new treatments. In particular, neuromodulation therapies which aim to reinforce residual cerebellar function, could be appropriate when cerebellar function is impaired (Ilg *et al.*, 2014, Feil *et al.*, 2016). Currently, only treatments with aminopyridines [4-aminopyridine (4-AP), 3, 4-diaminopyridine (3, 4-DAP)] have been shown to compliment motor rehabilitation and significantly improve specific cerebellar symptoms (episodic ataxia type 2, downbeat nystagmus), as well as benefitting gait ataxia in patients (Strupp *et al.*, 2003, Schniepp *et al.*, 2011, Schniepp *et al.*, 2012, Ilg *et al.*, 2014). Aminopyridines act as K+ channel blockers and increase the excitability of neurons, especially of cerebellar Purkinje cells (PCs) and other cerebellar cells (Etzion and Grossman, 2001). Additionally, improved motor behaviour has been observed in ataxin-1 mutant mice treated with aminopyridines, which may be mediated by a neuroprotective effect due to an enhanced electrical activity of PCs (Hourez *et al.*, 2011). Other drugs which have displayed significant improvement in clinical ataxic scales include acetyl-DL-leucine and chlorzoxazone (Feil *et al.*, 2013, Strupp *et al.*, 2013). However, the efficacies of these drugs in CAs, especially in improving daily life activities, still needs to be confirmed (Mitoma and Manto, 2016). In addition to these therapeutic approaches in treating CAs symptoms, we have investigated the long-term efficacy of a new small molecule compound inhibitor of D-amino acid oxidase (DAO) in FRDA mice, which is discussed in detail in chapter 5.

1.5 FRDA Mouse models

To get a further insight into the physiological role of frataxin, the disease aetiology and progression, and to validate new therapeutic strategies, several FRDA mouse models have been developed.

1.5.1 Knock-out models

To study the disease mechanism Cossee *et al.* (2000) developed a mouse model by inactivating the *Fxn* gene by exon 4 deletion. However, while heterozygous deletion appeared normal, homozygous inactivation leads to early embryonic lethality, signifying an essential role for frataxin throughout early development. These results suggest that the weaker phenotype in humans is due to remaining frataxin expression associated with the expansion mutations. Subsequently, through a gene-targeting approach, Puccio *et al.* (2001) developed two conditional knockout mouse models in parallel. These are the striated muscle frataxin-deficient line and a neuron/cardiac muscle frataxin-deficient line. Both models displayed important progressive pathophysiological and biochemical features of FRDA.

1.5.2 Knock-in models

With the aim to generate an animal model closely mimicking the human FRDA disease, Miranda *et al.* (2002) inserted 230 GAA repeats into the mouse *Fxn* intron 1 region by homologous recombination to develop an FRDA knock-in mouse model. GAA repeat knock-in mice were crossed with frataxin knockout mice to obtain knock-in, knockout (KIKO) mice expressing 25-36% of wild-type frataxin levels. Although a decreased frataxin expression was observed in these mouse models, they failed to develop FRDA associated pathology such as GAA repeat instability, motor coordination abnormality, mitochondrial iron accumulation and premature death (Miranda *et al.*, 2002).

1.5.3 FRDA YAC transgenic mouse models

Human Frataxin is functional and rescues the FXN knockout mouse

In an initial attempt to overcome the embryonic lethality in a homozygous *Fxn* knockout mice and to generate an essential resource to study the human frataxin effect in a mouse cellular environment, Pook *et al.* (2001) developed a human WT FRDA yeast artificial chromosome (YAC) transgenic mouse line, designated Y47R. The FRDA YAC transgenes were crossbred twice with heterozygous *Fxn* exon 4 deletion knockout mice (Figure 1.18) (Cossee *et al.*, 2000, Pook *et al.*, 2001). The transgenic mice showed to contain the entire *FXN* gene within the YAC clone, and effectively substitute for the endogenous murine frataxin, preventing lethality and producing phenotypically normal offspring (Pook *et al.*, 2001). These findings confirmed that the generation of rescued mice through re-introduction of human frataxin onto a mouse null background was an effective method that paved the way for further FRDA therapeutic studies.

***Human FXN YAC* transgenic mouse containing a GAA repeat**

Subsequently, Al-Mahdawi *et al.* (2004) made further advances by delivering a GAA expansion mutation, derived from a FRDA patient's DNA, into this transgenic model, using a yeast pop-in/pop-out homologous recombination strategy (Cemal *et al.*, 1999). Two lines of human FRDA YAC transgenic mice, designated YG8R and YG22R, were generated (Figure 1.19). Both lines of transgenic mice contained 370kb of human YAC frataxin transgene sequence spanning the entire *FXN* gene with expanded GAA repeats. The main difference between the two lines is that YG8R mice contained two copies of GAA sequence with 190 and 90 repeats, whereas YG22R mice carried only one copy of 190 GAA repeats (Table 1.1) (Al-Mahdawi *et al.*, 2004). Interestingly, both FRDA transgenic mice showed intergenerational and age-related somatic instability, particularly in the cerebellum, as seen in FRDA patients.

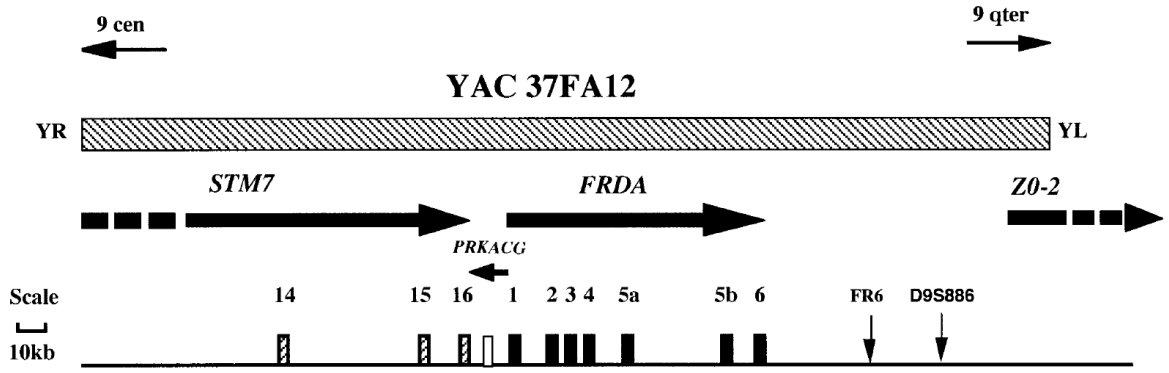

Figure 1. 18 - The position of YAC 37FA12 with respect to FRDA locus at 9q13. Genes are represented as solid arrows, which indicate the direction of transcription, and the broken lines represent incomplete gene sequence. Individual exons are numbered and are shown below the relevant gene. STS markers used in the analysis are shown as downward pointing arrows (Pook *et al.*, 2001).

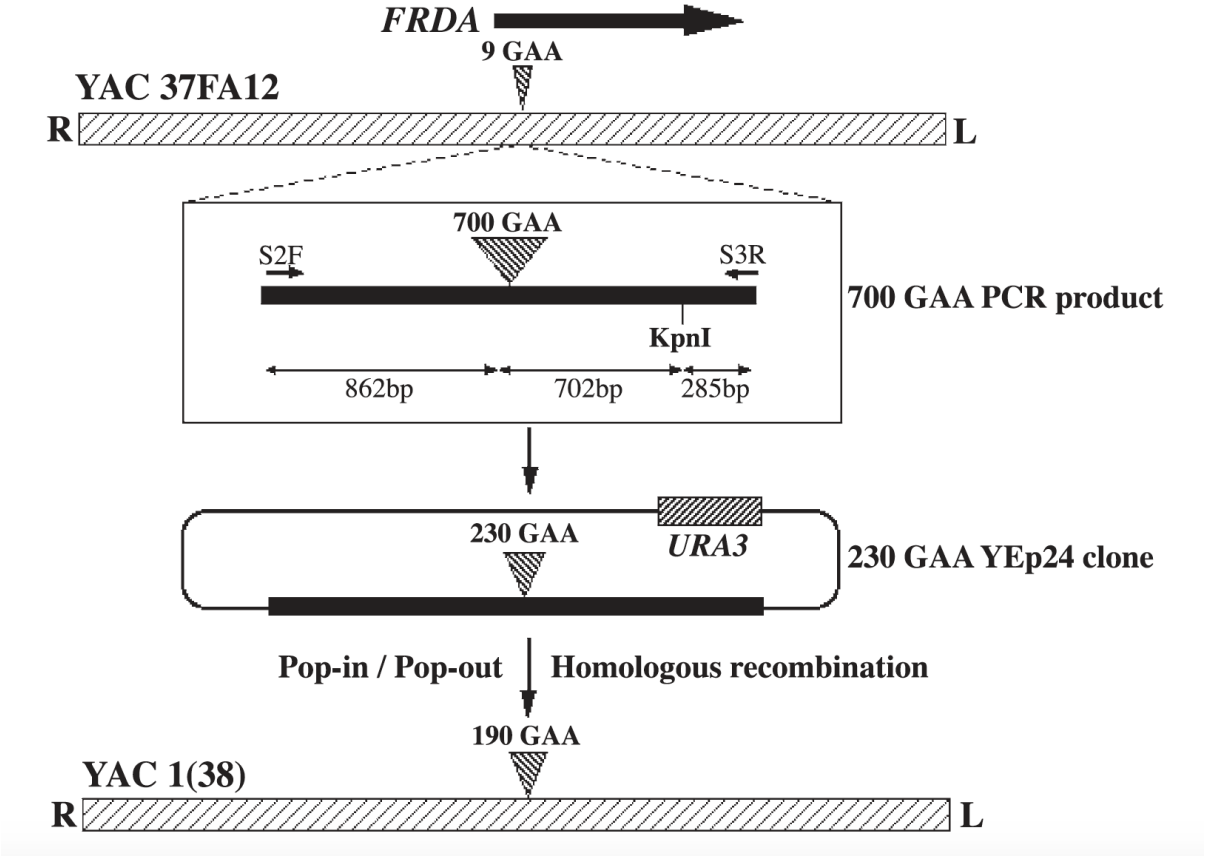

Figure 1. 19 - GAA repeat modification of YAC 37FA12. The position and orientation of the normal FRDA gene (9 GAA repeats) within the human YAC clone 37FA12 are indicated by the arrow. L and R indicate left and right arms of the YAC. A 700-GAA PCR product was amplified from FRDA patient DNA using primers S2F and S3R. The PCR product was first cloned into pCR2.1 (not shown) and then into YEp24, which contains a selectable URA3 gene, with resultant contraction to 230-GAA repeats. Pop-in/pop-out homologous recombination between Yep24 and YAC 37FA12 FRDA sequences produced the 190-GAA repeat YAC clone 1(38), which was subsequently used to generate the transgenic mice (Al-Mahdawi *et al.*, 2004).

Recently, a colony of a new YAC transgenic FRDA mouse model, designated YG8sR, has been established from intergenerational expansion, containing approximately 200 GAA repeats (Table 1.1). YG8sR mice were shown to have a single copy of the *FXN* transgene at a single site. Behavioural deficits, together with a degree of glucose intolerance and insulin hypersensitivity were identified in YG8sR FRDA mice compared with control Y47R and C57BL/6 (WT) mice. Additionally, YG8sR mice show increased somatic GAA repeat instability in the brain and cerebellum, together with a significantly reduced expression of *FXN* and aconitase enzyme activity, as compared to YG8R and YG22R models. Furthermore, the presence of pathological vacuoles within neurons of the DRG in YG8sR mice was also identified (Anjomani Virmouni *et al.*, 2015). Very recently, through further intergenerational expansion a new YAC transgenic mouse model have been established in our lab, designated YG8LR. YG8LR mice have shown to have a single copy of 440 GAA repeats, and have demonstrated a more severe disease phenotype (unpublished data). These novel GAA-repeat-expansion YAC transgenic FRDA mice, which exhibit progressive FRDA-like pathology similar to humans, are a good model for the investigation of FRDA disease mechanisms and therapy.

Table 1. 1 – Characterisation of the FRDA YAC transgenic mouse cell lines (Anjomani Virmouni *et al.*, 2015)

Transgenic Line	YAC transgenic integrity	*FXN* copy number	Founder GAA repeat length	Range of GAA repeats
YG8R	Complete	2	190+90	90 to 223
YG22R	Complete	1	190	190 to 235
YG8sR	Complete	1	200	120 to 240
YG8LR	Complete	1	440	440-450

1.6 Aims of the study

FRDA is a progressive neurodegenerative disorder with no effective therapy. Recently, it has been reported that the abnormal GAA expansion plays a role in histone modification, such as histone hypermethylation and histone hypoacetylation, subjecting the *FXN* gene to heterochromatin silencing (Herman *et al.*, 2006, Greene *et al.*, 2007, Al-Mahdawi *et al.*, 2008, De Biase *et al.*, 2009). Therefore, in efforts to reduce the repressive histone marks, in chapter 3 I investigated the efficacy and tolerability of two HMTase inhibitor compounds, BIX0194 (G9a-inhibitor) and GSK126 (EZH2-inhibitor), in FRDA human and mouse primary fibroblasts.

Moreover, the amount of residual frataxin critically affects the severity and progression of the disease; and recent advances in FRDA research have revealed the presence of the UPP pathway that regulates frataxin stability and degradation (Rufini *et al.*, 2011, 2015). Therefore, to restore physiological frataxin levels, in chapter 4 I investigated efficacy of various proteasome inhibitors (MG132, Bortezomib, Salinosporamide A and Ixazomib) using human primary fibroblasts.

Furthermore, it has been reported that increased degradation of D-serine by DAO overexpression results in ataxia, possibly due to low NMDAR functioning and impaired neural signalling in the cerebellum (Hashimoto *et al.*, 2005). Therefore, as an alternative FRDA therapeutic approach to target ataxia, in chapter 5 I carried out an *in vivo* investigation to test the efficacy of a newly developed DAO inhibitor, TAK-831, using the YG8sR FRDA YAC transgenic mouse model.

CHAPTER II - MATERIALS AND METHODS

2.1 Solution/ reagents

DMEM medium

- 1X DMEM medium, 10% fetal bovine serum (FBS), 2% Pen-Strep (5000U/ml penicillin and 5000mg/ml of streptomycin, Fisher Scientific).

Western blot analysis

- **Running buffer**: 25mM Tris, 190mM glycine, 3.5mM SDS
- **Sample buffer**: 80mM Tris-HCl (pH 6.8), 12.5% glycerol, 10% SDS, 0.5% BPB, 1% BME
- **Transfer buffer**: 25mM Tris, 190mM glycine, 10% methanol
- **PBS/T**: 0.2% Tween-20 in PBS
- **5% milk PBS/T**: 5% w/v milk, 0.2% Tween-20 in PBS

General Solutions

- **Tail digestion buffer**: 100mM Tris-HCl (pH 8), 5mM EDTA, 200mM NaCl, 0.2% SDS
- **RIPA buffer:** 10mM Tris-HCL (pH 8), 5mM EDTA, 200mM NaCl, 0.2% SDS
- **Orange G loading dye (6x)**: 0.35% Orange G dye, 30% sucrose
- **Tris/EDTA (TE) buffer**: 10mM Tris-HCl (pH 7.5), 1mM EDTA.
- **TBE buffer**: 90mM Tris, 90mM Boric acid, 2mM EDTA
- **TAE buffer**: 40mM Tris, 20mM Acetic acid, 1mM EDTA
- **PBS buffer**: For 1L – 8.0g NaCl, 1.15g Na2HPO4, 0.2g KH2PO4, 0.2g KCL
- **DEPC- treated water**: 1ml DEPC solution in 999ml sterilized water filtered then autoclaved twice

2.2 Primers

The primer sequences were either attained from previous studies or designed using Primer3 software (Rozen and Skaletsky, 2000). All primers were purchased from Sigma-Aldrich.

Table 2. 1 – FRDA YAC transgenic mice genotyping primers

Primer name	Sequence (5' – 3')	Product length
GAA repeat (Campuzano *et al*, 1996)		
GAA-F	GGGATTGGTTGCCAGTGCTTAAAAGTTAG	457bp + 3(GAA)n
GAA-R	GATCTAAGGACCATCATGGCCACACTTGCC	
FXN knockout (Cossee *et al*, 2000)		
WJ5	CTGTTTACCATGGCTGAGATCTC	
WN39 (WT specific)	CCAAGGATATAACAGACACCATT	520bp
WC76 (KO specific)	CGCCTCCCCTACCCGGTAGAATTC	245bp

Table 2. 2 - Quantification of *FXN* expression primers

Primer name	Sequence (5' – 3')	Product length
***FXN expression* (Human specific - Al-Mahdawi et al, 2008)**		
*FXN*RT-F	CAGAGGAAACGCTGGACTCT	172bp
*FXN*RT-R	AGCCAGATTTGCTTGTTTGGC	
***FXN* expression (Human and mouse - Pook *et al*, 2001)**		
FXN-FRT I	TTGAAGACCTTGCAGACAAG	121bp
FXN-RRT II	AGCCAGATTTGCTTGTTTGG	
***GAPDH* (Human - Al-Mahdawi et al, 2008)**		
GAPDH-h-F	GAAGGTGAAGGTCGGAGT	226bp
GAPDH-h-R	GAAGATGGTGATGGGATTTC	
***Gapdh* (Mouse - Al-Mahdawi et al, 2008)**		
Gapdh-m-F	ACCCAGAAGACTGTGGATGG	81bp
Gapdh-m-R	GGATGCAGGGATGATGTTCT	
***HPRT* (Human)**		
HPRT-h-F	GGTGAAAAGGACCCCACGA	90bp
HPRT-h-R	TCAAGGGCATATCCTACAACA	
***Hprt* (Mouse)**		
Hprt-m-F	ATGAAGGAGATGGGAGGCCA	80bp
Hprt-m-R	TCCAGCAGGTCAGCAAAGAA	

Table 2. 3 - ChIP qPCR primers

Primer name	Sequence (5' – 3')	Product length
***FXN* – 5'UTR**		
h-*FXN*-pro - F	AAGCAGGCTCTCCATTTTTG	186bp
h-*FXN*-pro - R	CGAGAGTCCACATGCTGCT	

2.3 Cell lines

Table 2. 4 - Details of the human primary fibroblasts

ID	Gender	Age (Years)	Ethnicity	Number of GAA repeats
GMO7492	Male	17	Caucasian	Normal
C4	ND	ND	Caucasian	Normal
Gmo3816	Female	36	Caucasian	330/380
FA1	ND	ND	Caucasian	416/590

ND = not determined

Table 2. 5 - Details of the mouse primary fibroblasts

ID	Gender	Average Age (Month)	Genotype	Number of GAA repeats
Y47R	Female	3.6	Transgenic Control	9
YG8sR	Male	11.3	FRDA YG8 small Rescue	220
YG8LR	Male	5.9	FRDA YG8 large Rescue	450

2.4 General techniques

Dilutions

All dilutions or stock solutions were mostly prepared in deionised water (18.2 MΩ) unless otherwise specified. However, for RNA dilutions and polymerase chain reaction (PCR) master-mix preparations, DNase-RNase-free DEPC-treated sterile water was used.

Centrifugations

For sample spin down, different centrifugation instrument was used according to the sample size and temperature necessity. A room temperature standard benchtop microcentrifuge (16K, BioRad) and a 4ºC refrigerated microcentrifuge (max speed 14K rpm, 5415R – Eppendorf) were used for small samples (≤ 1.5ml). Whereas, large volume samples (50ml) and plate centrifugation were carried out using a Centaur 2 centrifuge (Sanyo/MSE) and Legend T centrifuge (max speed 1000 rpm, Sorvall), respectively.

Incubations and pH regulation

Generally, water baths (Grant) were used for lower temperature incubation (37-60°C), whereas for higher temperatures (60-100ºC) a heating block (DB-2A, Techne) was used.

All genomic DNA (gDNA) containing solutions were stored at 4°C for a short time in the fridge and then in the cold room for long-term. Complementary DNA (cDNA) samples and PCR products were stored in -20ºC. All fresh tissues and RNA samples were snap frozen in liquid nitrogen and stored at -80°C. Reagent kits were stored according to the manufacturer recommendations at room temperature, 4ºC or 20ºC, or if needed in the dark. Antibodies were also stored according to the manufacturer recommendations, either at 4°C or -20°C. Frozen cells were stored overnight in a container with isopropanol at -80ºC and then transferred to the liquid nitrogen tank for long term storage. The pH of solutions was detected using a pH meter (Delta 340, Mettler) and pH adjustments were made by adding either concentrated HCl or NaOH.

Sterilisation

All necessary materials and reagents used in tissue culture and molecular analysis were sterilised in an autoclave at 121°C, 100kPa for 20 minutes.

2.4.1 Agarose gel electrophoresis

Agarose gel electrophoresis was used to detect and separate gDNA, cDNA or RNA fragments according to their size. Usually, the gels were prepared in the range of 1-2% with agarose (UltraPure electrophoresis grade; Invitrogen), in 1X TBE/TAE buffer. Initially, the agarose mixture was boiled in 1X TBE using a standard microwave then left to cool down. Ethidium bromide was then added to a final concentration of 0.025µg/ml, and immediately the gel mixture was dispensed into the casting tray with the appropriate well comb attached. The gel was then left to be set for 20 minutes at RT. Small gels (50ml capacity) were run in

mini gel tanks (Flowgen Biosciences). For some samples, before loading onto the gel, 6X orange G dye was added to a final concentration of 1X and then were run at 60V for 30 minutes. The gels were visualised and recorded using a UV transilluminator imaging system (Alpha Innotech).

2.5 General Cell culture maintenance

Similar cell culture procedures were carried out on both human and mouse fibroblast cell lines. The cells were routinely cultured in Dulbecco's Modified Eagle Medium (DMEM) (Invitrogen) which was filter sterilised through a 0.22µM pore filter unit (Nalgene) with 10% FBS, 100 units/ml penicillin and streptomycin (Invitrogen) supplementation. This was carried out in tissue culture biological safety cabinet, and the medium mixture was stored at 4ºC until required to use. Generally, cells were cultured in a T-25 flask (Fisher Scientific) at 37ºC in a 95% humidified atmosphere of 5% CO_2. All cell culture was carried out in a temperature-controlled laboratory.

2.5.1 Regeneration of cell lines

To avoid the risk of cell damage during ice crystal formation, frozen cells were rapidly thawed in the 37ºC water bath when taken from liquid nitrogen storage. To regenerate, the cells were then immediately transferred a 15ml conical tube containing 10ml pre-warmed culture medium and was gently mixed by pipetting up and down. The cells were collected by centrifugation at 1500 rpm for 5 minutes, then transferred to a T-25 flask containing new culture medium. The cells were incubated at 37ºC in a CO_2 incubator reach a confluent level.

2.5.2 Sub-culturing and passaging of cell lines

Sub-culturing was carried out when cells reached the log phase growth and were about 80% confluent. DMEM culture medium, 1X phosphate-buffered saline (PBS; Invitrogen) and 0.25% trypsin-EDTA (Invitrogen) solutions were pre-warmed at 37°C in water bath. The cell medium was removed by vacuum suction in a disinfected biological safety cabinet and were

washed gently with sterile PBS. 2ml 0.25% trypsin-EDTA was then used to detach the bound fibroblast cells for 5 minutes at 37°C, followed by gentle tapping, to bring them into complete suspension. 10ml DMEM culture medium was then added to the detached fibroblast cells to neutralise the trypsin/EDTA solution. The cells were then collected by centrifugation at 1500 rpm for 5 minutes. Depending on when the cells were required to use, cells were sub-cultured in 10ml DMEM culture medium at a 1:2, 1:4 or 1:6 ratios in a T-25 or T-75 flasks. The cells were then incubated at 37ºC, 5% CO_2 and 95% humidity, and growth was observed daily.

2.5.3 Cryopreservation of cell lines

To prevent the risk of microbial contamination and conserve a stock of cell lines for future studies, 1-2 vials of each line were cryopreserved in liquid nitrogen. The adherent cells were detached with 0.25% trypsin-EDTA, followed by cell quantification and viability assessment by trypan blue exclusion test (as described in 2.5.4). Subsequently, cells were pelleted by centrifugation at 1500 rpm for 5 minutes. The supernatant was discarded, and cells were resuspension in 1ml DMEM culture medium containing 10% (v/v) DMSO and transferred to the cryo-vials (Sarstedt). A good standard to freeze is 0.5-1x10^6 cells/ml. To avoid ice crystallization damage to the cells, cells were initially frozen slowly in -80ºC for up to 24hrs in a cooling box containing isopropanol (Sigma-Aldrich). Subsequently, cryo-vials were transferred to liquid nitrogen for long-term storage.

2.5.4 Cell quantification and viability (trypan blue exclusion assay)

Knowing the cell number in culture at a given stage is critical as it reports whether there are enough viable cells for an experimental procedure. Trypan Blue dye exclusion assay is based on the principle that live viable cells which have a bound membrane do not take up the dye, whereas dead non-viable cells do. In this analysis, cells were first trypsinised with 0.25%

trypsin-EDTA followed by centrifugation at 1500 rpm for 5 minutes and cell suspension in 1ml 1X PBS buffer. 10µl of the cell suspension were gently mixed with an equal volume of 0.4% (w/v) trypan blue (Sigma). Subsequently, a Countess® automated cell counter (Invitrogen) was used to count the cells, and the following formula determined their viability:

$$\text{Viability (\%)} = \left[\frac{\text{No of Viable Cells}}{\text{Total no. of Cells}} \right] \text{X } 100$$

2.5.5 Presto-Blue cell viability assay

For this assay, $2.5x10^4$ cells were seeded in a 24 well plate (Corning™) for 24hrs before drug treatment, followed by Presto-Blue® test to monitor the viability of the cells. The Presto-Blue® reagent (Invitrogen) contains a non-fluorescent blue cell-permeant compound. However, when added to cells, the Presto-Blue® reagent is modified by the reducing environment of the viable cells, and thus changes to a highly fluorescent red colour. This change can be detected using an absorbance measurement. Therefore, after specific drug treatment, cells were washed with PBS, then fresh pre-warmed culture medium was added with 1X Presto-Blue® solution from a 10X stock. The cells were then incubated for 3hrs at 37ºC, 5% CO_2 and 95% humidity. The change in solution fluorescent was then measured using a spectrophotometer (2000c, Invitrogen) at a wavelength of 570nm with 600nm reference.

2.5.6 Primary fibroblast drug treatment

All drug compounds were prepared as stock solutions and were stored at -20°C as specified until required to use. For every drug treatment, equal numbers of control and FRDA fibroblasts were seeded according to the size of the flask and experimental analysis

(confluency level of 50-60%). Successively, the medium was discarded, and cells were washed once with 1X PBS. Appropriate concentrations of drugs were diluted in pre-warmed DMEM medium from the stock solution to make the final drug concentration required and then supplemented to cultured cells. This was followed by incubation at 37ºC, 5% CO_2 and 90-95% humidity, for a specific duration (usually 72hr). At the end of the incubation period, the cells were washed once with PBS, followed by collection for various molecular analysis.

2.6 DNA extraction: Phenol/ Chloroform method

Generally, to extract good quality genomic DNA from mouse tissues, ear clips, and cell lines, phenol/chloroform method was carried out. Samples were collected in 1.5ml tubes (Eppendorf), followed by the addition of 400µl of tail digestion buffer and 10µl of proteinase K (50mg/ml). After a brief vortex the samples were incubated overnight at 55ºC. The digested samples were then vortexed, and 400µl of phenol (equilibrated with Tris-HCl pH 8.0) was added. Samples were mixed well by vortex twice for 15 seconds followed by centrifuged at 14K rpm for 5 minutes at RT. 380µl of the supernatant was then removed to a fresh tube containing 380µl of chloroform/isoamyl alcohol (24:1, v/v). Samples were vortexed briefly and centrifuged again at 14K rpm for 5 minutes at RT. From the resulting supernatant, 350µl was transferred to a fresh tube followed by the addition of 35µl of 3M Na-acetate (pH 5.2) and 700µl of absolute ethanol. The samples were mixed by inverting the tube several times and were subsequently incubated at -80ºC for 2hrs. This was followed by centrifugation at 14K rpm for 30 minutes at 4ºC to collect the precipitated DNA pellet. The ethanol was drained off, and the pellet washed with 1ml of 70% ethanol. The samples were centrifuged again at 14K rpm for 20 minutes at 4ºC. The ethanol was cautiously drained off, and the DNA pellet was air dried for 10 minutes. The DNA pellet was resuspended in 50µl of TE buffer and stored at 4ºC.

2.7 Total RNA extraction - Trizol® Method

Total RNA was isolated from the fibroblast cells or mouse tissues using the Trizol® reagent (Invitrogen) following the manufacturer's instruction. The cultured cells (~1x 10^6) were washed once with PBS and collected by centrifugation at 1.5K rpm for 5 minutes after trypsinisation. The cell pellet was loosened by gentle flicking and resuspended in 1ml Trizol®. For RNA extractions from tissues (20-30mg), 400µl of Trizol® was added initially, and the tissues were homogenized with homogeniser sticks, followed by the addition of the remaining 600µl of Trizol®. The samples were then incubated for 10 minutes at RT. 200µl of chloroform (Sigma-Aldrich) per 1ml of Trizol® was added to each sample, followed by vigorous vortexing of samples for 15 seconds and incubation for further 15 minutes at RT and then centrifuged at 14K rpm for 15 minutes at 4ºC. The chloroform affected the Trizol® to separate into a colourless aqueous phase and an organic phase. The upper aqueous phase (~500µl) was then transferred to a new labelled tube followed by the addition of 500µl of isopropanol alcohol (Sigma-Aldrich) to precipitate the RNA. Samples were incubated for 10 minutes at RT followed by centrifugation at 14K for 15 minutes at 4ºC. The supernatant was carefully removed and the RNA pellet was washed with 1ml of 75% ethanol, after a brief vortex the samples were centrifuged again at 14K rpm for 8 minutes at 4ºC. The supernatant was removed carefully and the RNA pellet was air dried for 5-10 minutes at RT and then resuspended in 20-50µl of RNase free water. The total RNA samples were stored at -80ºC if not used immediately.

2.8 RNA/DNA Quantity and Purity Check

A NanoDrop™ 2000c Spectrophotometer (NanoDrop, Thermo Scientific, UK) was used to determine the RNA/DNA concentration and purity. The absorption (A) of Ultra Violet light (UV-light) was measured at 260nm, and the quality was determined by $\mathbf{A}_{260/280}$ ratio using 1µl of the RNA/DNA samples. Additionally, the total RNA integrity was assessed on a 1% agarose gel electrophoresis by examining the ribosomal RNA (rRNA) bands under a UV transilluminator imaging system (Figure 2.1).

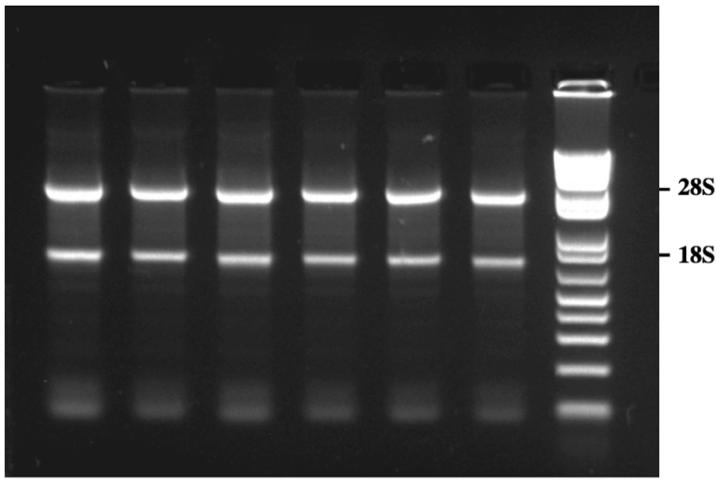

Figure 2. 1 - Gel electrophoresis of RNA samples using 1% agarose gel. The upper ribosomalband (28S) should be about twice the intensity of the lower band (18S) indicating intact RNA. For size evaluation a $1kb^{+}$ ladder (Invitrogen) was used.

2.9 DNase I treatment of RNA

To eliminate genomic DNA contamination during RNA purification procedures, DNase I treatment was carried out (DNase I, Amp Grade, Invitrogen). 1µg of total RNA was added to the reaction mixture consisting of 1µl 10X DNase I reaction buffer, 1µl of DNase I Amp Grade (1U/µl) and nuclease-free water to 10µl. The samples were incubated for 15 minutes at RT. 1µl of 25mM EDTA was added to inactivate the DNase I reaction mixture and heated for 10 minutes at 65ºC. The DNase I treated RNA samples were used immediately or store at -80ºC.

2.10 Complementary DNA (cDNA) synthesis

cDNA synthesis – using QuantiTect reverse transcription kit (Qiagen)

All reactions were carried out on ice. In an RNase free Eppendorf tube 1µg RNA was added, followed by 2µl 7X gDNA wipeout buffer, followed by the addition of RNase free water to make a total volume of 14µl. The mixture was then incubated for 2 minutes at 42ºC, followed by the addition of 1µl Quantiscript reverse transcriptase, 4µl of 5X Quantiscript RT buffer and 1µl of RT primer mix. The samples were incubated at 42ºC for 15 minutes, followed by 95ºC for 3 minutes to terminate the reaction and inactivate Quantiscript reverse transcription. The samples were then stored at -20ºC, if not used immediately.

cDNA synthesis – using cloned AMV first-strand cDNA synthesis kit (Invitrogen)

All reactions were carried out on ice. In an RNase free Eppendorf tube 1µg RNA was added, followed by the addition of 7µl of primer component master-mix (4µl of DEPC-water, 2µl 10mM dNTP mix and 1µl Oligo$(dT)_{20}$ primer). The RNA and primer were denatured by incubating at 65ºC for 5 minutes, followed by immediately placing the samples on ice. To each sample the following reagents were then added in order: 4µl 5X cDNA synthesis buffer, 1µl 0.1M DTT, 1µl cloned AMV RT (15U/µl). The 20µl reaction mixture was gently mixed by flicking the tube and briefly centrifuged to bring all the contents to the bottom. To initiate the reverse transcription process, samples were incubated at 55ºC for 60 minutes, followed by reaction terminations at 85ºC for 5 minutes. The cDNA samples were either used immediately or stored at -20ºC.

2.11 Conventional Reverse Transcription PCR

Various PCR amplification systems were utilised on DNA samples for mice genotyping, and to assess the cDNA and immunoprecipitated DNA quality.

Fxn-KO and – *FXN*-GAA PCR

A GAA repeat sequence and KO PCR amplification were carried out on mouse gDNA samples to detect the genotype. The *Fxn*-KO PCR was performed to identify the wild-type or knockout *Fxn* alleles, whereas *FXN*-GAA PCR identified the size of the GAA repeat. Using specific primers (primer sequence - Table 2.2), 1µl of template gDNA was added to the appropriate reactions mix prepared in a PCR tube (Fisher Scientific) as follows:

PCR MIX	
KO	**GAA**
-12.5µl of 2X Master-mix ($MgCl_2$, *Taq* DNA polymerase, dNTPs; Kapa Biosystem) - 0.5µl of 50µM WJ5 primer - 0.5µl of 50µM WN39 primer - 0.1µl of 50µM WC76 primer - Nuclease-free water to 25µl	-12.5µl of 2X master-mix ($MgCl_2$, *Taq* DNA polymerase, dNTPs; Qiagen) - 5µl of Q-buffer - 1µl of 50µl GAA forward primer - 1µl of 50µl GAA reverse primer - Nuclease-free water to 25µl

For *Fxn*-KO PCR amplification four controls were used: Wild-type, heterozygous, rescue and blank (dH_2O). Whereas for *FXN*-GAA PCR amplification three controls were used: positive, negative and blank (dH_2O). The samples were mixed, and the reaction was carried out in a PTC-225 Pelter Thermal Cycler (MJ Research) using the appropriate program as shown in Table 2.6.

Table 2. 6 - GAA and KO PCR programme

Steps	Temperature	Duration	Cycles
GAA PCR program			
Denaturation	94ºC	2 minutes	1
Denaturation	94ºC	10 sec	10
Annealing	60ºC	30 sec	
Elongation	68ºC	45 sec	
Denaturation	94ºC	10 sec	20
Annealing	60ºC	30 sec	
Elongation	68ºC	1 min, with 20 sec increment	
Extension	68ºC	10 minutes	1
KO PCR program			
Denaturation	94ºC	1 minute	1
Denaturation	94ºC	20 sec	30
Annealing	54ºC	20 sec	
Elongation	72ºC	20 sec	
Extension	72ºC	10 minutes	1

FXN PCR

Before performing *FXN* gene expression quantification, PCR amplification procedure was carried out to determine the quality of cDNA using *FXN*-FRT I and *FXN*-RRT II primers (primer sequence - Table 2.2). 1µl of cDNA sample was added to the following reagent mix:

- 12.5µl of 2X master-mix ($MgCl_2$, Taq DNA polymerase and dNTPs; Kapa Biosystem)
- 1µl of 5µM *FXN*-FRT I primer
- 1µl of 5µM *FXN*-RRT II primer
- Nuclease-free water to 25µl

Three controls were used: a positive, DNase treated total RNA, and blank (dH_2O). The samples were mixed, and the reaction was carried out using the programme shown in Table 2.7.

Table 2. 7 - *FXN* PCR programme

Steps	Temperature	Duration	Cycles
***FXN* PCR program**			
Denaturation	94ºC	1 minute	1
Denaturation	94ºC	30 sec	30
Annealing	52ºC	30 sec	
Elongation	72ºC	1 min	
Extension	72ºC	10 minutes	1

FXN Pro-5'UTR ChIP PCR

FXN Pro-5'UTR PCR was carried out to validate and assess the quality of the immunoprecipitation DNA obtained during ChIP analysis before the quantitative assessment. 2µl of immunoprecipitated DNA was added in the following reaction mix:

- 12.5µl of 2X master-mix ($MgCl_2$, Taq DNA polymerase and dNTPs; Kapa Biosystem)
- 1µl of 5µM *FXN*-pro forward primer
- 1µl of 5µM *FXN*-pro reverse primer } Primer sequence - Table 2.3
- Nuclease-free water to 25µl

For a control, a negative blank (dH_2O) was used. The samples were mixed, and the reaction was carried out using the following programme, Table 2.8.

Table 2. 8 – Pro-5'UTR ChIP PCR programme

Steps	Temperature	Duration	Cycles
Pro-5UTR' ChIP PCR program			
Denaturation	94ºC	1 minute	1
Denaturation	94ºC	30 sec	35
Annealing	60ºC	30 sec	
Elongation	72ºC	3 min	
Extension	72ºC	10 minutes	1

For the KO, *FXN* and ChIP DNA PCR reactions, to analyse the results, 10µl of PCR product was run in a 2% agarose gel alongside the controls and $1kb^+$ DNA size marker (Invitrogen) at 70V for around 30 minutes. For the GAA PCR, the products were mixed with and 2µl of 6X orange G dye and were run in a 1% agarose gel instead. The correct amplicons in each reaction were then visualised in a UV gel documentation system.

2.12 Quantitative Real-Time RT-PCR (qRT-PCR)

Quantitative real-time RT-PCR (qRT-PCR) was performed using 2X SYBR® Green PCR master-mix (Applied Biosystems), to quantify the expression of the gene of interest, in a real-time PCR machine (QuantStudio™ 6 Flex Real-Time PCR System; Applied Biosystems).

SYBR® Green dye functions by binding to cDNA as it forms and producing a fluorescent signal which is detected by the spectrophotometer continuously. This signal intensity is proportional to the level of cDNA present. Thus, in each step of the PCR reaction, the intensity increases as the amount of product increases. The qRT-PCR reaction was performed in triplicates in a 96-well plate (MicroAmp, Applied Biosystems). Each reaction well contained a final volume of 10µl containing the following: 2.5µl of 5X diluted cDNA products, 0.5µl of 50µM optimised respective forward and reverse primers (Table 2.2), 5µl of 2X SYBR Green master-mix and 2.5µl of nuclease-free water. Throughout the reaction preparation, the samples were exposed to low light. Target and endogenous master-mixes were prepared separately but added to the same plate. The diluted 5X cDNA were added last to the reaction plate. The plate was then sealed with real-time plate sealer (MicroAmp, Applied Biosystems) and centrifuged, for 30 seconds at 1000 rpm at 4ºC. The real-time PCR reaction was run at various temperatures for different cycles as shown in Figure 2.2. Following qRT-PCR, a dissociation curve run was performed by increasing the temperature gradually from 60ºC to 95ºC. Relative quantification values were determined by the $2^{-\Delta\Delta Ct}$ method by QuantStudio™ Real-Time PCR Software (Applied Biosystems).

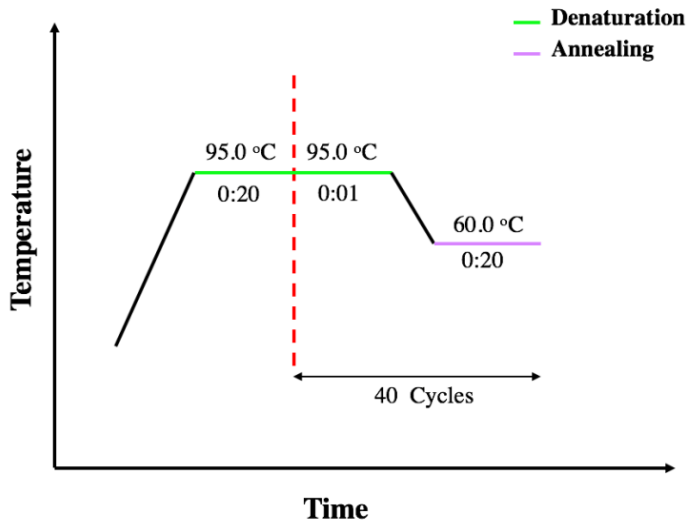

Figure 2. 2 - Schematic illustration of the real time PCR programme.

2.13 Chromatin Immunoprecipitation (ChIP) analysis

This procedure was performed using the Chromatrap® spin column ChIP kit for qPCR (Chromatrap). Around 5 million cells were washed with pre-warm PBS, followed by 10 minutes incubation at RT with 1% formaldehyde, prepared serum-free medium. The DNA/protein complex cross-linking was stopped by adding glycine solution at a final concentration of 0.65M and incubated for 5 minutes at RT. Glycine solution was then removed, and the cells were collected by scraping in cold PBS containing protease inhibitor cocktail (PIC, provided in the Chromatrap® kit) with 1:1000 dilution factor, followed by centrifugation at 3500xg for 5 minutes at 4ºC. The cell pellet was resuspended in 400µl hypotonic buffer and incubated on ice for 10 minutes, followed by centrifugation at 5000xg for 5 minutes at 4°C to collect the nuclei. The cell pellet was then resuspended in 300µl lysis buffer and then incubated at 4°C for 10 minutes. To achieve the desired lengths of <500bp DNA fragments, samples were sonicated for 10 cycles of 30s on/ 30s off program using Bioruptor® Pico sonicator (Diagenode), followed by centrifugation for 10 minutes at maximum speed and 4°C. The supernatant was collected, and 1µl of PIC was added to it. Before sample immunoprecipitation, the shearing quality of DNA was assessed. 5µl of 1 M NaHCO3 and 5µl of 5 M NaCl was added to each 25µl sheared chromatin aliquot and was made up to 50µl with nuclease-free water. The samples were mixed and then incubated for 2hrs at 65°C to reverse the cross-linking. After a brief centrifuge, 1µl of the Proteinase K solution was then added, mixed thoroughly and incubated for 1hr at 37°C. Subsequently, 2µl Proteinase K stop solution was added, and DNA concentration was quantified by Nanodrop. To assess the DNA fragment size, 10µl of the sheared chromatin (mixed with 2µl 6X orange loading dye) was run on 1.5% agarose gel. As a control, the respective 2X diluted un-sheared DNA was used (Figure 2.3). The DNA was either immediately submitted to immunoprecipitation (IP) or stored in -80ºC.

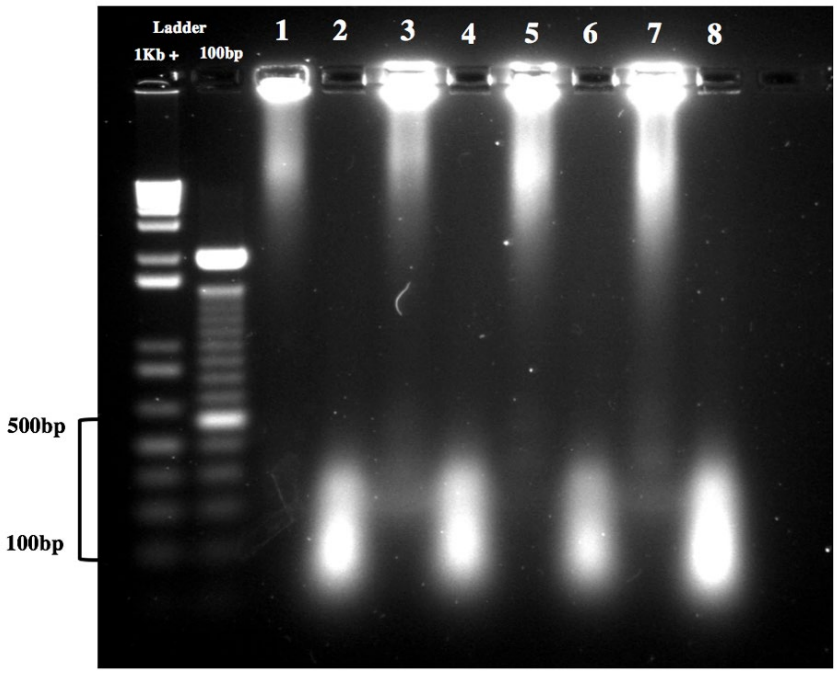

Figure 2. 3 - Gel electrophoresis to assess the quality of the sonication DNA using 1.5% agarose gel. Lane 1,3,5 and 7 represent the unsheared DNA-chromatin samples. Lane 2,4,6 and 8 show the successfully sheared DNA-chromatin fragment less than 500bp in size.

Immunoprecipitation (IP)

The sheared chromatin was centrifuged at max speed and 4ºC for 10 minutes. The clear supernatant was subsequently used for IP slurry mixture containing 2:1 – antibody: chromatin ratio and were prepared as follows:

- nuclease free dH_2O to 40µl
- 5µl of wash buffer 1
- 1µl of PIC
- 2µg of sheared chromatin
- 4µg ChIP certified antibody specific to the protein of interest (Table 2.9)

Each sample had a negative control (-Ab), where 2µg of immunoglobulin G (IgG; Upstate) was used. Additionally, for input control, 2µg of sheared chromatin was made up to 20µl with nuclease-free dH_2O and stored in -80^{o}C for later use. The IP slurries were gently mixed and were kept on ice while the spin columns were being activated (add 600µl of column conditioning buffer to the columns 3 times and allow flow through under gravity).

Table 2. 9 - List of antibodies used in ChIP analysis

Antibody	Company of purchase
Anti-H3K9ac rabbit polyclonal	Merck Millipore (06-942)
Anti-H3K9me3 rabbit polyclonal	Merck Millipore (07-442)
Anti-H3K27me3 rabbit polyclonal	Merck Millipore (07-449)

The slurries were transferred to spin columns and incubate for 1hr at 4ºC on a rocking platform with gentle agitation. This was followed by washing the columns 5X with 600µl of wash buffer 1 and centrifugation at 4000xg for 30 seconds at RT to discard the buffer each time. This was repeated for wash buffer 2 and 3. The columns were then dry centrifuged at top speed for 30 seconds at RT. 50µl of elution buffer was added to the columns and incubated at RT for 15 minutes. Subsequently, the immunoprecipitated chromatin was eluted by centrifuging the columns at top speed for 30 seconds.

Reverse cross-linking

To release the DNA from protein-bound complexes, the chromatin samples were first reverse cross-linked. The Proteins were degraded by proteinase K digestion before DNA purification.

To each 50µl eluted chromatin the following were added:

- 50µl 0.1M NaOH
- 5µl 1M $NaHCO_3$

Additionally, the 20µl input control was reintroduced, and the following were added:

- 40µl elution buffer
- 40µl 0.1M NaOH
- 5µl 1M $NaHCO_3$

The content was mixed thoroughly and incubate for 2hrs at 65ºC. 1µl of Proteinase K (0.5µg /µl) was then added to each IP and input samples and incubated for 1hr at 37ºC. 2µl of Proteinase K stop solution was added to all tubes, followed by a brief vortex and a short spin.

DNA clean up using phenol/chloroform with glycogen

The total volume of IP and input samples were brought up to 300µl with clean TE buffer. 300µl phenol was added then centrifuged at max speed for 5 minutes at RT. The supernatant was transferred to a new tube and mixed with 270µl chloroform: isoamyl (24:1), followed by centrifugation at max speed for 5 minutes at RT. The supernatant was transferred again to a new tube containing 2.5µl glycogen (20mg/ml), 30µl 3M NaAc (pH 5.2) and 600µl 100% ethanol. The tubes were gently agitated and incubated overnight at -80ºC. Subsequently, the samples were centrifuged at max speed for 30 minutes at 4ºC. The pellet obtained was washed in 1ml 70% ethanol, followed by a quick shake and centrifugation at max speed for 5 minutes at RT. The supernatant was carefully discarded, and the pellet was air dried. The pellet was then resuspended in 25µl of TE buffer. The samples were stored at 4ºC for 24hrs, then moved to -20ºC storage if not needed immediately.

ChIP qPCR

Relative qPCR amplification was carried out to validate the ChIP samples with SYBR Green (Applied Biosystems) in a QuantStudio™ 6 Flex Real-Time PCR instrument (Applied Biosystems), as previously described (section 2.12). Reactions were carried out in triplicates in a final volume of 10µl containing 12.5pmol of each of the respective forward and reverse primers (Table 2.3). Relative quantification values were normalised to input and minus antibody samples and finally determined in relation to a control region.

2.14 Nuclear Extraction

This procedure was carried out on drug-treated cells using the EpiQuik™ nuclear extraction kit (EpiGenTek). All reactions were carried out on ice. Cells were collected as a pellet and were resuspended in 100µl of 1X pre-extraction buffer per million cells, followed by incubation on ice for 10 minutes. The samples were then vigorously vortexed for 10 seconds and centrifuged for 1 minute at 12K rpm at 4ºC. The cytoplasmic supernatant was carefully

removed, and to the nuclear pellet, two volumes of extraction buffer containing PIC (1:1000 diluted) was added. The extracts were incubated on ice for 15 minutes with vigorous vortexing every 3 minutes, followed by centrifugation for 10 minutes at 14k rpm and 4°C. The supernatant obtained was then transferred carefully to a new tube. The protein concentration of the nuclear extract was subsequently measured using BCA protein quantification assay as described below (section 2.18).

2.15 Histone Methyltransferase Activity Assay

This analysis was carried out using the EpiQuik™ histone methyltransferase activity assay kit (EpiGenTek). This assay is based on the principle that the HMTase enzyme G9a and EZH2, transfers a methyl group from *S*-Adenosyl methionine (Adomet) to lysine 9 and 27 of histone H3, respectively. The level of methylated histone H3K9 / H3K27 is then recognised with a high-affinity antibody, which is directly proportional to enzyme activity. This was quantified through horseradish peroxidase (HRP) conjugated secondary antibody-colour development system. Using strip wells, which captures the methylated histone substrates, the reaction mix for HMTase activity were prepared alongside positive and negative blank controls, as shown in Table 2.10.

Table 2. 10 - HMTase activity assay reaction mix

HMT activity	Positive Control	Blank
- 24µl of 1X Histone Assay Buffer - 1.5µl of Adomet solution - 2µl of Biotinylated Substrate - 3µ of Nuclear Extract	- 26µl of 1X Histone Assay Buffer - 1.5µl of Adomet solution - 2µl of Biotinylated Substrate - 1µl of Control Enzyme	- 27µl of 1X Histone Assay Buffer - 1.5µl of Adomet Solution - 2µl of Biotinylated Substrate

The strip wells were mixed and covered with Parafilm M (Sigma Aldrich) and incubated at 37°C for 60-90 minutes. 150µl of 1X histone assay buffer was then used to wash the strip wells three times. 50µl of 1:100 diluted capture antibody (specific to either G9a or EZH2)

was then added, followed by incubation at RT for 1hr on an orbital shaker (50-100 rpm). Subsequently, the strip wells were washed 5X with 150µl of 1X histone assay buffer, followed by the addition of 50µl of 1:1000 diluted detection antibody and incubation at RT for 30 minutes. The detection antibody was washed away 5X with 150µl of 1X wash buffer. 100µl of developing solution was then added and incubated at room temperature for 2-10 minutes away from light. Subsequently, 50µl of stop solution was added to each well to stop enzyme reaction, and the absorption from the colour change was monitored within 2-15 minutes at 450nm. The enzymatic activity of the samples was calculated using the following formula:

$$\text{Activity (OD/h/mg)} = \frac{\text{OD (No inhibitor – Blank)}}{\text{Protein amount (µg)* x hour**}} \times 1000$$

* Amount of protein added in µg
** Reaction mix incubation time before capture antibody addition

2.16 Trypsin-like and chymotrypsin-like cell-based assay

The trypsin-like and the chymotrypsin-like cell-based assay was carried out using the Proteasome-Glo™ Cell-based kits (Promega). This test provides a specific luminogenic proteasome substrates in buffers, which is cleaved by the proteasomes when added to cells in culture, releasing luciferin. Luciferase then consumes luciferin, and a rapid luminescent signal is generated that correlates directly to the trypsin-like or chymotrypsin-like protease activity. This assay was highly sensitive to the presence of minute quantities of trypsin or chymotrypsin present in the cell suspension used for plating. Therefore, before cells were counted, the suspended cells were washed 3X in complete medium. Subsequently, the suspended cells were counted by trypan-blue exclusion assay as described above (section 2.5.4). In a white-walled 96-well plate (Corning), 5000 fibroblast cells were seeded with

100µl culture medium, followed by incubation for 24hrs at 37ºC, 5% CO2 and 95% humidity, before drug treatment. The plate was then equilibrated at RT before performing the Proteasome-Glo™ assay. For reagent preparation, 10ml of Proteasome-Glo™ cell-based buffer was added to luciferin detection reagent. For the chymotrypsin-like assay, only Proteasome-Glo™ substrate was added, whereas for trypsin-like assay inhibitor 1 and inhibitor mix 2 was also added. After a gentle mix, the cell-based reagents were incubated for 30 minutes at RT. Subsequently, 100µl of either the trypsin-like or chymotrypsin-like prepared Proteasome-Glo™ cell-based reagent was added to each cell sample well. The content was mixed at 700 rpm on a shaker for 2 minutes, followed by incubation at RT for a minimum of 10 minutes. The luminescence of the samples, which determined the trypsin-like or chymotrypsin-like protease activity, was then measured using Glomax™ 96-well microplate luminometer (Promega).

2.17 Preparation of cell lysates

To extract protein, cell pellets containing just over 1x 10^6 cells were homogenized in 192µl of Radio-Immunoprecipitation Assay (RIPA) buffer (Sigma-Aldrich) and 8µl of 25X Roche protease inhibitor (Sigma Aldrich) and centrifuged at 4ºC for 30 minutes at a max speed of 14K rcf. Subsequently, the supernatant consisting of total protein was separated from the pellet (cellular debris) and transferred to a clean Eppendorf tube. The protein concentration was determined using the BCA protein assay (as described below), followed by the addition of Dithiothreitol (DTT) at the final concentration of 1mM. If not used immediately, the samples were stored at -80℃.

2.18 Determination of protein concentrations using BCA protein assay

Protein samples were quantified using a Pierce® BCA protein assay kit (Thermo Scientific) following the manufacturer's instructions. The BCA protein assay is based on the reduction of Cu^{2+} to Cu^{1+} by protein in an alkaline medium with highly sensitive and selective colorimetric detection of the cuprous cation (Cu^{1+}) using bicinchoninic acid (BCA). To determine the protein concentration, BCA protein assay reagents A and B were mixed in a ratio of 50:1, respectively. Additionally, a set of protein standards (with known protein concentration) was prepared by a serial dilution of bovine serum albumin (BSA) (0.025mg/ml-1.5mg/ml, Table 2.11) to construct a standard curve. 200µl of the BCA solution (A+B) were added to individual wells of a 96-well microplate. 10µl of protein lysates (diluted 1:10 with homogenising buffer) and 10µl of the BSA standards were then added to respective wells, followed by gentle mix. The plate was incubated at 37ºC for 30 minutes and then allowed to cool at RT. The protein concentration was measured at 562nm absorption using a plate reader (Biohit HealthCare).

Table 2. 11 - BSA standards preparation for BCA analysis

Tube	dH_2O Volume	BSA Volume	Final Volume	Final BSA concentration
A	10µl	30µl	20µl	**1500 µg/ml**
B	20µl	20µl	20µl	**1000 µg/ml**
C	20µl	20µl of tube **A**	40µl	**750 µg/ml**
D	20µl	20µl of tube **B**	20µl	**500 µg/ml**
E	20µl	20µl of tube **D**	20µl	**250 µg/ml**
F	20µl	20µl of tube **E**	30µl	**125 µg/ml**
G	40µl	10µl of tube **F**	50µl	**25 µg/ml**
H	40µl	-	40µl	**0 µg/ml**

2.19 Western Blotting

Polyacrylamide gel electrophoresis (PAGE)

A 12% resolving polyacrylamide gel (37:5:1 acrylamide (Bio-Rad), 0.5mM Tris (pH 8.8), 0.1% SDS) was prepared in a glass flask, followed by the addition of 0.05% TEMED (Fisher Scientific) to initiate polymerisation. The resolving gel was then gently poured between the gel plates (set up on the Bio-Rad mini gel casting stand) up to 1cm below the comb. Water saturated butanol was immediately added over the gel mix to prevent air contact, and the gel was left to polymerise for 30-40 minutes. The butanol was then rinsed off with dH_2O, and a 4% stacking polyacrylamide gel (37:5:1 acrylamide, 0.125mM Tris (pH 6.8), 0.1% SDS) was then prepared, followed by the addition of 0.1% TEMED. The stacking gel was then gently poured on top of the set resolving gel, and the well comb was fitted carefully. The gel was allowed another 45 minutes to polymerise. The casting gel was then placed inside the PAGE tank (Mini-PROTEAN® Tetra Cell (Bio-Rad) and approximately 1L of 1X running buffer were poured into the two compartments to establish an electric current through the gel. The comb was then removed and the wells were flushed with running buffer, using a syringe and needle. Before loading the samples, the protein amount (Table 2.12) was prepared in 1X working sample buffer to a final volume of 20µl and heated at 95°C for 5 minutes to fully denature and reduce the proteins. Subsequently, the protein samples and a 10µl Low molecular weight (LMW) protein marker (Precision Plus Protein™ standard – Bio-Rad) were carefully loaded into the wells, and the SDS-PAGE gels were run at 120V for 2-3hrs.

Table 2. 12 - List of protein amounts used for the appropriate antibody for western blotting

Protein detection	Protein amount used
Frataxin	100µg
c-Jun	20µg
p27	20µg
PSMß5	20µg

Protein transfer to membrane

After electrophoresis, proteins transfer was carried out by either a wet-system (Mini Trans-Blot®; Bio-Rad) or a semi-dry system (Trans-Blot Turbo System; Bio-Rad).

Wet-transfer system

After the SDS-PAGE was completed, the stacking gel was removed from the resolving gel and was equilibrated in 1X transfer buffer for 5 minutes. One piece of PVDF membrane (Amersham Biosciences) and four pieces of filter papers (3MM Whatman; Fisher scientific) were cut according to the gel size. The top corner of the PVDF membrane was marked with a pencil to distinguish the right side of the membrane. The PVDF membrane was then activated by equilibrating in 1X transfer buffer for 20 minutes. Additionally, both the filter papers and the blotting sponges were soaked in 1X transfer buffer for 5 minutes. The blotting system was assembled in 1X transfer buffer, as shown in Figure 2.4. At every step of layering, a roller was used to remove any air bubbles. The blotting cassette was placed in the transfer tank in a vertical position orientation, filled with ice-cold 1X transfer buffer and an additional ice-block. Thus the negatively charged molecules would migrate towards the grey anode efficiently, transferring the protein from the gel into the PVDF membrane. The transfer was carried out at constant 400mA, and 100-110V for 1hr 10 minutes.

Semi-dry transfer system

The same procedure was applied for semi-dry transfer system in preparing the filter papers and membrane, but very little transfer buffer is required. The transfer sandwich was assembled on the anode cassette base (Figure 2.4), by placing two pieces of wet filter paper, and then the PVDF membrane, the gel, and finally the remainder of the wet filter papers on top. The cathode cassette top was positioned on the sandwich and locked. The cassette was placed in the transfer system, and a transfer was carried out at constant 2.5A, 25V for 20 minutes.

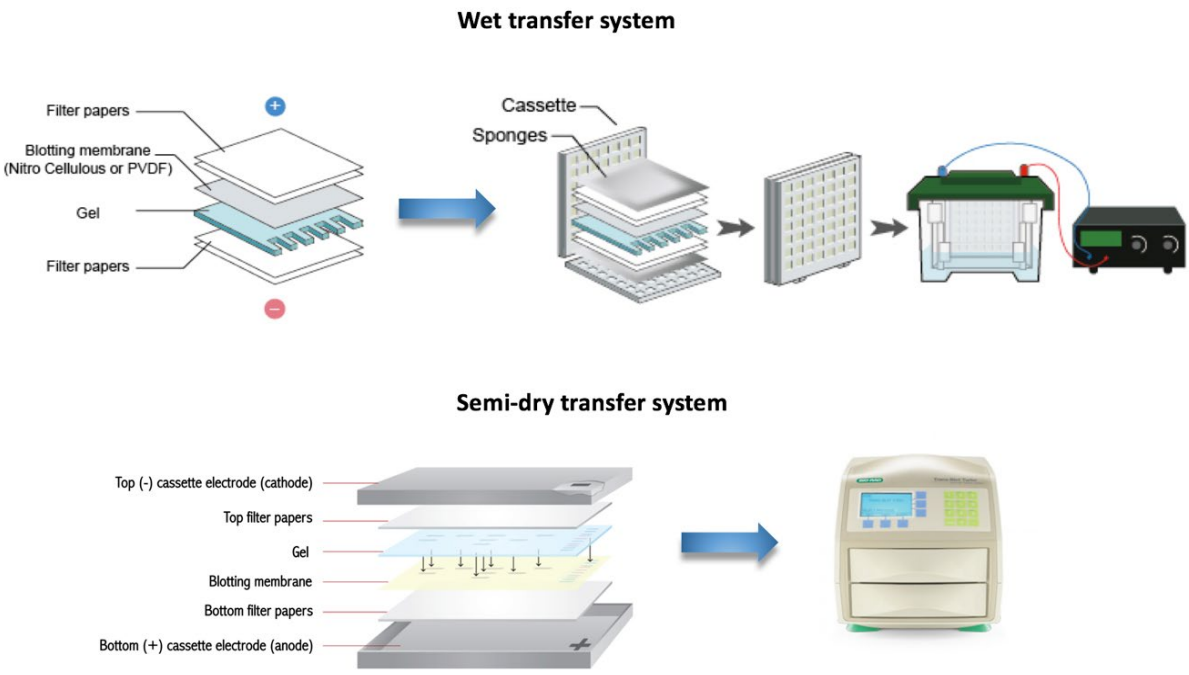

Figure 2. 4 - Schematic illustration of the blotting sandwich transfer cassette assembly for the two electro-transfer techniques: wet transfer and semi-dry transfer.

Gel and membrane staining

At the end of the transfer, the gel and the membrane was briefly washed in dH_2O. To assess and visualise the residual proteins left on the gel, it was stained with Coomassie blue reagent (Instant Blue; Expedeon) on a shaker for 30 minutes and then washed with dH_2O. The stained gel was placed on a piece of 3MM Whatman paper, covered with cling film and dried on a gel dryer (5040, Fisherbrand) under vacuum and ramp temperature of 80°C for 2hr. Additionally, to understand the effectiveness of the protein transfer, the membrane was stained with 1X Ponceau solution (Sigma Aldrich) on a shaker for 10 minutes. To de-stain the membrane after protein transfer assessment, membranes were washed twice with 5% acetic acid and once with dH_2O for 10 minutes.

Hybridization of membrane with antibodies

The PVDF membrane was briefly washed in PBS/T and then blocked in 5% w/v milk in PBS/T for 30 minutes at RT with gentle agitation. The membranes were then incubated with the corresponding primary antibodies (Table 2.13), at 4°C overnight with gentle agitation. The following day, unbound primary antibody was washed 3 times in PBS/T buffer for 30 minutes, at RT. Secondary antibody, specific to the primary antibody and conjugated with HRP (Dako), was diluted by 1:2000 in 5% milk or BSA and added to the membrane. The membrane was then incubated at RT for 30 minutes with gentle agitation. The membrane was washed again 3 times in PBS/T buffer for 30 minutes.

Table 2. 13 - Primary antibodies with their dilution factor and observed molecular weight sizes

Protein name	Antibody	Observed MW (kDa)	Antibody dilution	Source
Frataxin	Mouse anti-frataxin monoclonal Ab	14m, 18i, 21-26p	1 in 100 in 5 % BSA	Abcam (ab110328)
p27	Rabbit anti-p27 KIP1 polyclonal Ab	22-25	1 in 200 in 5% non-fat milk	Abcam (ab7961)
c-Jun	Rabbit anti-c-Jun monoclonal Ab	40	I in 2000 in 5% non-fat milk	Abcam (ab32137)
PSMß5	Rabbit anti-PSMB5 Polyclonal Ab	19	I in 100 in 5% non-fat milk	Sigma (HPA049618)
Actin	Rabbit anti-actin polyclonal Ab	42	1 in 2000 in 5% BSA/ non-fat milk	Sigma (SAB4301137)
Tubulin	Rat anti-tubulin monoclonal Ab	55	1 in 10,000 in 5% BSA/ non-fat milk	Abcam (ab6160)

Chemiluminescent visualisation and X-ray film processing

A SuperSignal West-Pico (Perbio) or a Clarity™ Western (Bio-Rad) enhanced chemiluminescent (ECL) substrate was used for the detection of high and low abundance proteins, respectively. Initially, the membrane was transferred onto a saran wrap with the protein side upwards. The chemiluminescent reagent mix was prepared according to the manufacturer's instruction (1:1 ratio of substrate components) in a total volume of 2ml. This was then pipetted onto each membrane covering its entire surface and incubated for 5 minutes at RT. The reagent was drained and the membrane was tightly covered with Saran

wrap. To detect the luminescence, the membrane was then exposed to Amersham Hyperfilm ECL films (GE Healthcare) for various lengths of time up to 1hr in x-ray cassettes. The films were developed in the dark using an automatic firm processing unit (Xograph) .

Western Blot quantifications

Western blot signals were quantified using the Java-based image processing programme ImageJ (public domain). The developed hyperfilms were scanned and were saved as .jpg. The image file was then opened in ImageJ where the single protein bands were measured, resulting in one profile blot for each captured signal. Profile blots showed the relative density of the respective lanes, with darker signals giving higher peaks and broader signals resulting in lower peaks (Figure 2.5). Background signals were subtracted from the final quantification value by drawing a baseline on the bottom of each peak, thereby excluding the underlying area from the peak area measurements. The obtained numbers for the measured areas under the peaks showed arbitrary units and could thus only be compared within the context of one single blot. This was also carried out for their respective endogenous control protein bands, to which the sample protein's peak area values were normalized to.

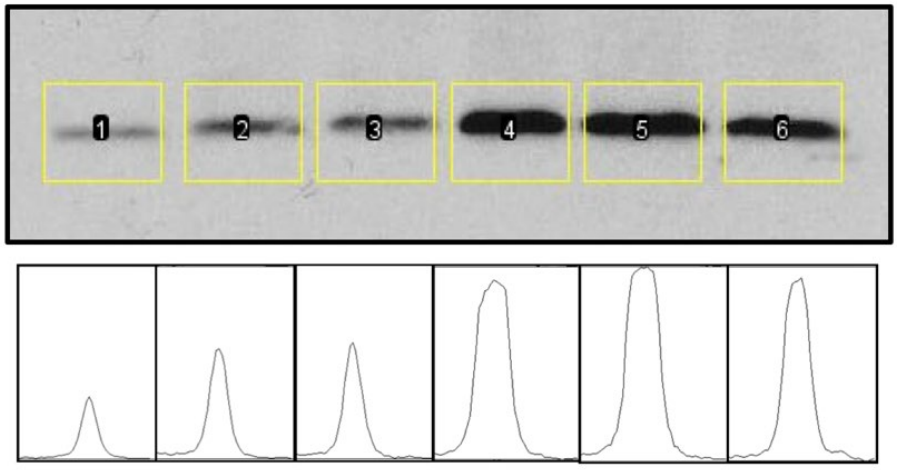

Figure 2. 5 - Quantification of western blot signals by using ImageJ.

2.20 Frataxin protein measurement – Mitosciences dipstick assay

The level of frataxin protein was measured by lateral flow immunoassay with the Frataxin Protein Quantity Dipstick Assay Kit (MitoSciences) according to the manufacturer's instructions. 2µg of protein in 25µl of extraction buffer (buffer A) was mixed with 25µl of 2X blocking buffer (buffer B) and was added to individual wells on a 96-well plate with gold-conjugated monoclonal antibody at the bottom of each well. The samples were incubated for 5 minutes, allowing the gold-conjugate to hydrate. The mixture was then resuspended gently using a pipette and dipsticks were inserted into the wells. Subsequently, frataxin within each sample was immunocaptured onto designated capture zones on the dipstick, and the signal appeared 5-7 mm from the bottom of the dipstick in approximately 20 minutes. When the signal was developed, the dipsticks were washed for 20 minutes, with 30µl of washing buffer (buffer C) in an empty well of the microplate. The dipstick was air-dried for approximately 20 minutes and the signal intensity (Figure 2.6) was measured with an MS-1000 Immunochromatographic Reader (MitoSciences).

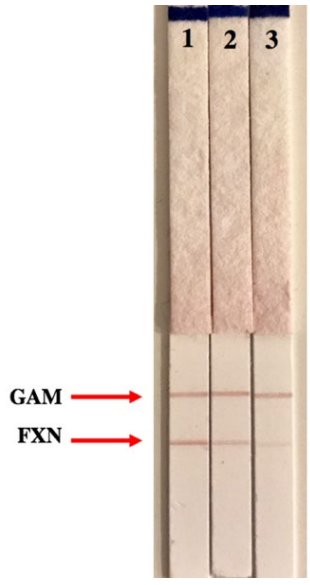

Figure 2. 6 - Quantification of mouse fibroblast frataxin (FXN) expression level using dipstick immunoassay. Upper bands correspond to internal control (goat anti-mouse antibody (GAM); lower bands correspond to mouse FXN. Lanes correspond to Y47 (1), YG8s (2) and YG8L (3).

2.21 Aconitase Assay

Aconitase activity assay was performed in cell lysates to determine conversion of citrate to isocitrate catalysed by aconitase, a Fe-S cluster protein. This procedure was carried out using the Cayman Chemical aconitase assay kit (USA, Cat. No. 705502).

To perform the assay, whole-cell extracts of human fibroblast cell lines were resuspended in Cell-Lytic extraction buffer (Sigma) to 10% w/v. Lysates were centrifuged at 14K rpm for 15 minutes at 4ºC and used immediately. A substrate reaction premix was made, as shown in Table 2.14, and 200µl of substrate premix was added to each well of a preheated 96-well plate. The reactions were then initiated by adding 50µl of the diluted (1:10) samples to each well, in triplicates. Reactions were incubated at 37ºC for 15 minutes in the dark and then the absorbance was measured once every minute at 340 nm for 15 minutes at 37ºC using a spectrophotometer. The absorption monitors the formation of NADPH and the production of NADPH is proportional to the aconitase activity. The aconitase activity was then determined by the slope of the graph once the absorbance was plotted over time.

Table 2. 14 - Aconitase assay substrate reaction premix

Component	Final Concentration
Tris/HCl (pH 7.4)	50mM
NADP	0.4mM
Na Citrate	5mM
MgCl2	0.6mM
Isocitrate dehydrogenase	1U

2.22 TAK-831 drug preparation for *in vivo* study

TAK-831 was synthesized and provided to us by Takeda Cambridge Limited. The drug was supplied in a solid form and stored at -20ºC until required to use. Initially, 30mg of TAK-831 was weighed and completely resuspended in 1ml Tween-80. This was then added to 99ml of 0.5% (w/v) methylcellulose, to make a final volume of 100ml drug solution (0.3mg/ml). The drug dispersions were stored in 2ml aliquots at -20ºC. A placebo/ vehicle solution was also prepared in the same way with 0.5% (w/v) methylcellulose containing 1% (v/v) Tween-80, and was stored at 4ºC.

2.23 Functional studies during drug treatment

To assess the functional outcome of FRDA mice and the drug effect on their functional capacity, body weight measurement, locomotor activity, beam walk and accelerated rotarod tests were conducted.

2.23.1 Body weight analysis

Mouse body weights were recorded before and after treatment, to aid in drug dose preparation and to observe drug toleration on body weight. This was conducted using an LBK Compact Bench Scale (Adam equipment) (Figure 2.7).

Figure 2. 7 - Mice body weight analysis

2.23.2 Beam breaker test

A beam breaker activity monitor (MED-OFA-510 activity chamber, Med Associates) (Figure 2.8) was used to measure the locomotor activity of the mice. The system consisted of 2 subject containment environment (chamber) each measure 27.3cm X 27.3cm with 16-beam infrared (I/R) transmitters connected to the computer with data analysis software (SOF-811). Each chamber could only take one mouse per run, and it assessed various standard parameters: jump counts, jump time, average velocity, ambulatory episodes, ambulatory distance, ambulatory time, ambulatory counts, stereotypic time, stereotypic counts, resting time, vertical counts and vertical time. These parameters were measured and recorded every 1 minute for 5 minutes. Data analysis and processing was performed using Graphpad Prism 7 program.

Figure 2. 8 - Beam-breaker activity monitor chambers

2.23.3 Beam walk test

Beam-walk test was performed to compare the motor coordination and balance capabilities of FRDA transgenic and control mice. The test was carried out with two wooden beams of 90cm long, one with an external diameter of 12mm and the other 22mm (Figure 2.9). The beams were placed horizontally 10cm above the bench surface with one end mounted on a narrow support with a 60W lamp while a darkened escape box was located at the other end of the beam. Motor function was assessed by measuring the time taken for the mouse to cross the beam and enter the escape box. The mice received two trainings on the beam followed assessments four times on the wider and narrower beams respectively with a rest period of 5 minutes between each trial.

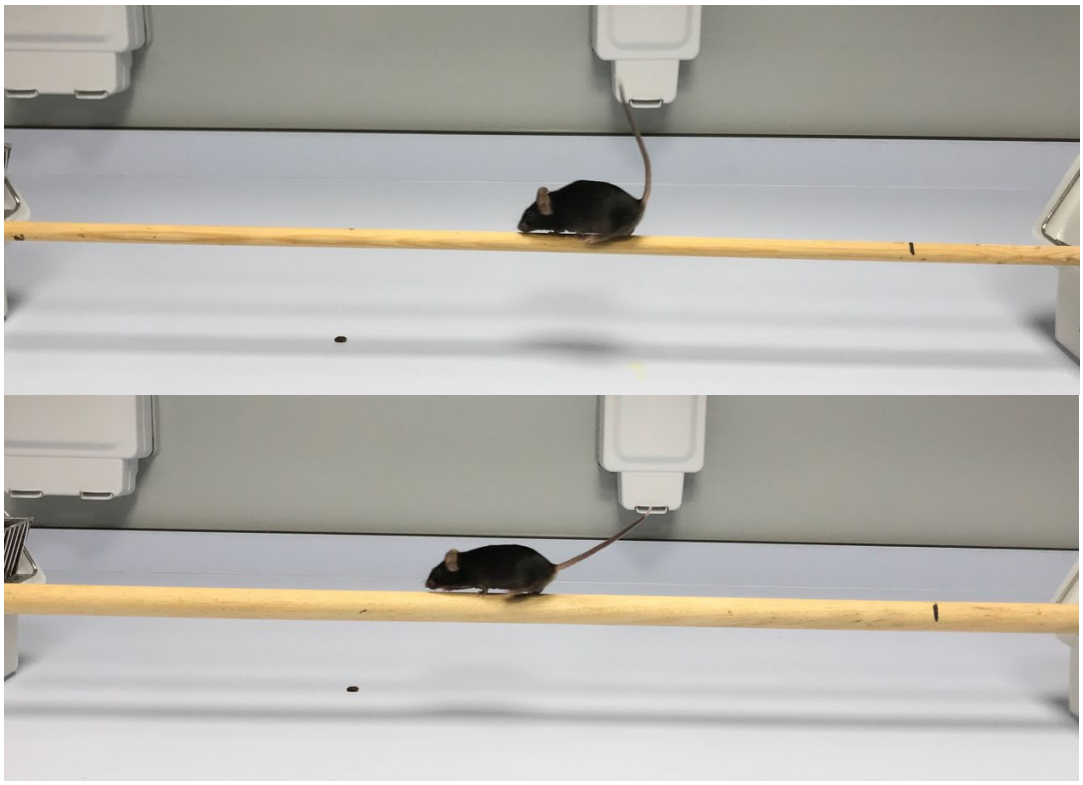

Figure 2. 9 - Beam walk analysis device. Motor function of the mice was measured using a 12x900mm (top) and a 22x900mm (bottom) beams.

2.23.4 Accelerating rotarod

The motor deficits associated with FRDA were assessed using a Ugo-Basille 7650 accelerating rotarod treadmill apparatus (Figure 2.10), designated for testing the balance and coordination characteristics of general motor function. The rotarod device consisted of a rotating rod, driven by an electric motor, upon which the animals were placed. Mutant and control littermate mice were placed on the rods, and four trials were performed with the speed of the rotation gradually increasing from 4 to 40 rpm. The time score where the mouse completes the task (by staying on the rotarod for 400s) or falls from the apparatus was recorded. Four runs were performed, and a minimum of 5 minutes' rest was given between each run.

Figure 2. 10 - Rotarod apparatus

2.24 Post treatment mice tissue collection

At the end of each drug treatment course, the mice were culled by cervical dislocation. This was followed by tissues collection, which included the brain (B), cerebellum (C), blood (Bl) and plasma (Pl) from both the male and female mice. The collected tissues were snap-frozen in liquid nitrogen and stored at -80^{o}C. All procedures were carried out in accordance with the UK Home Office 'Animals (Scientific Procedures) Act 1986'. Biochemical analysis and frataxin expression will be carried out on these tissues.

2.25 Statistical analysis

Statistical analyses, such as detailed measurements, and graphical visualisation were done using Microsoft excel 2016 software and Graphpad Prism7. Functional measurements (weight, locomotor activity, accelerated rotarod and beam walk performance) were statistically analysed using two-way analysis of variance (ANOVA) and /or Student's *t*-test. Two-way ANOVA analysis compares the mean differences between groups with two independent variables; therefore, allowed us to investigate if there is an interaction between the two independent variables on the dependent variable. All other measurements comparing two sample groups at a specific time point were analysed using student's *t*-test to determine if the mean values differed significantly or not. In all cases a p value of ≤ 0.05 was chosen as the significance threshold in all cases.

CHAPTER III - HMTASE INHIBITORS *IN VITRO* THERAPEUTIC STUDIES

3.1 Introduction

3.1.1 Mechanism of histone modification and transcriptional regulation

The term epigenetics is commonly defined as heritable changes in gene expression without altering the DNA sequence. One of the vital constituents of epigenetic mechanisms that govern chromatin-based nuclear processes is histone post-translational modification. To date, more than 60 different histone modifications have been identified, including acetylation, methylation, ubiquitination, phosphorylation, and sumoylation (Table 3.1), all of which can serve as epigenetic tags (Kouzarides, 2007, Rothbart and Strahl, 2014). With the aid of specific enzymes, biochemical modification of histones predominantly occurs on the protruding N-terminal tails of H3 and H4 histones. Consequently, this influences higher-order chromatin structure formation, by affecting the inter-nucleosome or histone-DNA interactions, which then renders the gene accessibility to the transcriptional machinery. These histone modifications also act as a signalling platform by integrating responses to multiple biochemical signalling cascades, to recruit or repel the transcriptional machinery and chromatin remodelling signal complexes, which ultimately induces distinct biological responses (Bannister and Kouzarides, 2011). For this reason, histone modifications are increasingly recognized as having a substantial role to play in both normal cellular and disease physiology (Cheung and Lau, 2005, Morera *et al.*, 2016).

Table 3. 1- Different classes of modification identified on histones (Kouzarides, 2007)

Chromatin Modifications	Residues Modified	Functions Regulated
Acetylation	**K**-ac	Transcription, Repair, Replication, Condensation
Methylation (lysines)	**K**-me1 **K**-me2 **K**-me3	Transcription, Repair
Methylation (arginines)	**R**-me1 **R**-me2a **R**-me2s	Transcription
Phosphorylation	**S**-ph **T**-ph	Transcription, Repair, Condensation
Ubiquitylation	**K**-ub	Transcription, Repair
Sumoylation	**K**-su	Transcription
ADP ribosylation	**E**-ar	Transcription
Deimination	**R > Cit**	Transcription
Proline Isomerization	**P-cis > P-trans**	Transcription

The most prevalent and well-studied histone modifications are acetylation and methylation of lysine (K) residues. Generally, histone acetylation is associated with euchromatin formation and modulation of gene transcription. Acetylation is targeted to regions of chromatin by the recognition and binding of DNA sequence-specific transcription factors, that recruit histone acetyl transferase (HAT) cofactors such as CREB binding protein (CBP). Subsequently, the addition of the acetyl groups reduces the positive charge, which locally modifies the histone affinity towards DNA and promotes gene regulation (Lee and Workman, 2007, Abel and Zukin, 2008, Handy *et al.*, 2011). The effects of the HATs on acetylation can be reversed by HDACs, which remove acetyl groups from the histone tails. Deacetylation of histones proteins shifts the balance towards chromatin condensation and thereby silences gene expression (Abel and Zukin, 2008).

On the other hand, histone lysine methylation (mono-, di-, tri-methylated) patterns and their effects on transcription are more complex compared to acetylation. The addition of single or multiple methyl groups does not change the electrostatic charges of histones but allows conformational changes due to hydrophobic alterations. Therefore, the outcome of some methylation sites on transcription could be either activation (adopting euchromatin structure) or repression (inducing heterochromatin structure) (Bannister and Kouzarides, 2011). For instance, H3K27me3 and H3K9me2/3 states are associated with silencing, whereas the H3K4me1/2/3 and H3K36me3 states are typically transcriptionally permissive modifications (Figure 3.1) (Handy *et al.*, 2011, Black *et al.*, 2012).

Histone methylation is catalysed by various HMTases which utilise SAM (S-adenosyl methionine) as the methyl-group donor. So far, several families of HMTase have been identified, with most having a SET homology domain and a high specificity for a particular lysine residues and the degree of methylation (Volkel and Angrand, 2007). In constitutive heterochromatin, the HMTase Drosophila suppressor of variegation 3-9 (human homologue)

(SUV39H) catalyses H3K9me3, which is recognised by HP1 (Yandim *et al.*, 2013). HP1 self-dimerises and is therefore thought to create a 'glue effect' on chromatin by holding adjacent nucleosomes together. Importantly, HP1 was shown to also recruit and interact with SUV39H methyltransferase, to further methylate H3K9. This creates a positive feedback loop and is thought to be the basis of the spreading behaviour of heterochromatin. In addition to SUV39H, other HMTase such as G9a and SETDB1 are known to act mostly on inactivated gene promoters (Kouzarides, 2007).

Furthermore, H3K27me3 is another vital methylated residue associated with facultative heterochromatin formation. The activity of H3K27 methylation has been tightly linked to polycomb system, where one polycomb repressive complex (PRC2) catalyses the methylation of H3K27 and another one (PRC1) recognises methylated residues. PRC1 mono-ubiquitinates the globular H2AK119, which prohibits chromatin remodelling and hence successive elongation of RNAPII. Intramolecular interactions of PRC2 complex are thought to be responsible for a low-level chromatin compaction and its spreading (Francis *et al.*, 2004, Grau *et al.*, 2011, Yandim *et al.*, 2013).

Moreover, various studies have confirm the presence of multiple HDMs capable of reversing the HMTase efforts by demethylating histones in a gene specific manner (Kouzarides, 2007). HDMs are classified into two distinct enzyme families: the nuclear amine oxidase homologues (e.g. LSD1) and the JmjC-domain proteins (e.g. JHDM1) (Shi *et al.*, 2004, Sandi *et al.*, 2014). The opposite functions of between HMTases and HDMs act to maintain the balanced histone methylation levels that are required for gene transcription regulation (Figure 3.1).

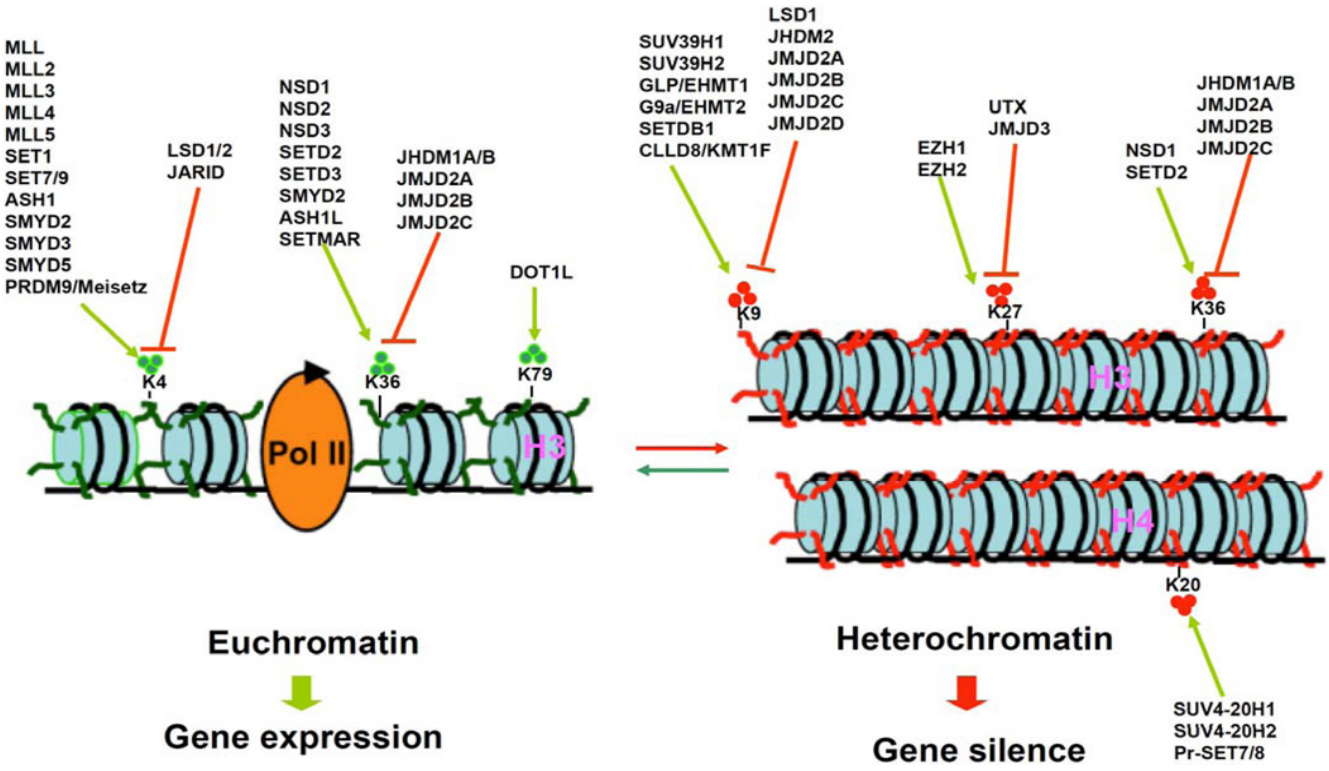

Figure 3. 1 - Schematic illustration of histone lysine methylation and demethylation regulated by HMTases and HDMs for gene transcription. Presently known histone H3 and H4 lysine HMTases (green arrows) and HDMs (red arrows). In general, methylation of H3K4, H3K36, and H3K79 is associated with euchromatin and transcriptional activation, whereas methylation of H3K9, H3K27, H4K20 and H3K36 is related to heterochromatin and transcriptional repression (Black *et al.*, 2012).

3.1.2 Histone modification in FRDA

As previously discussed in Chapter I, in FRDA high levels of heterochromatin marks were reported in the first intron of the pathologically silenced *FXN,* particularly in the immediate flanking region of GAA repeats (Figure 3.2). Histone modifications in the mutated *FXN* locus were first observed in FRDA lymphoblastoid cell lines, where an elevation in di- and tri-methylation of H3K9 (H3K9me2/3) and decrease in acetylation of H3 and H4 was reported in the upstream region of the expanded GAA repeat tract (Herman *et al.*, 2006, Greene *et al.*, 2007).

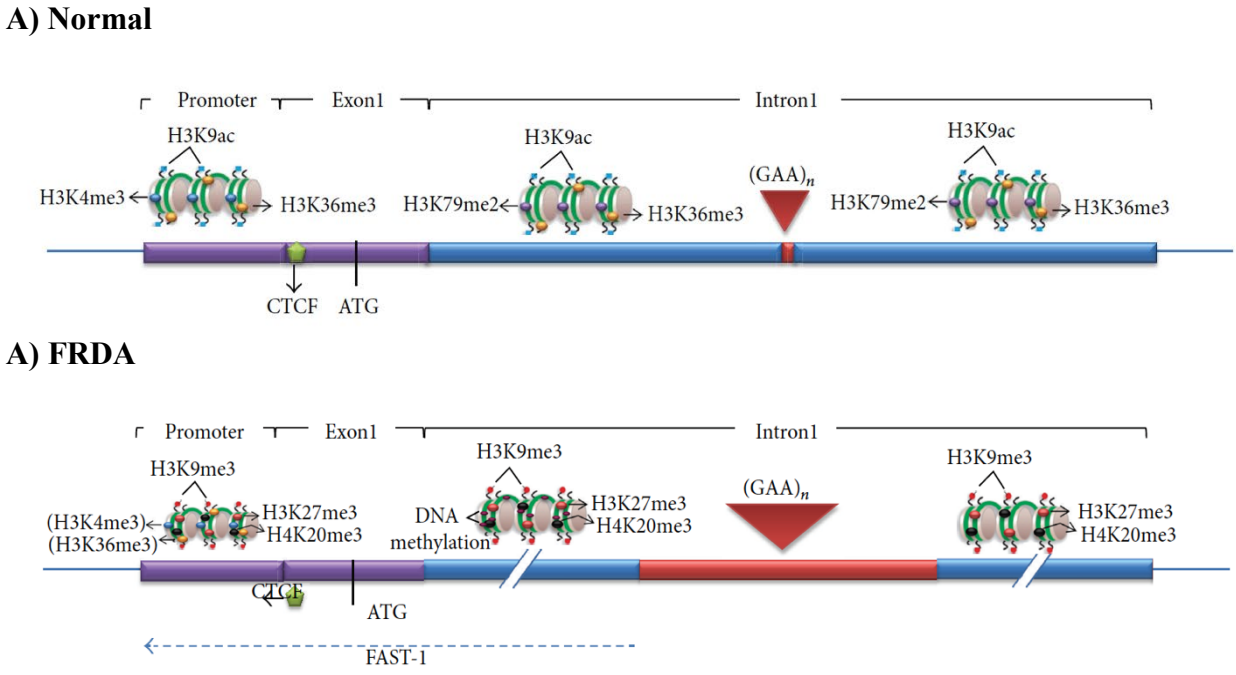

Figure 3. 2 - A schematic illustration of the *FXN* chromatin organization in normal individuals and FRDA patients. (A) In normal individuals, H3K9ac is seen in all regions which induces an active open chromatin. Histone marks involved in the transcription initiation and elongation is seen in the promoter (H3K4me3 and H3K36me3) and downstream regions (H3K79me2 and H3K36me3). Additionally, normal CTCF binding is found at the 5'UTR. (B) In FRDA, repressive histone marks H3K27me3, H3K9me3 and H4K20me3, are observed throughout the gene, but most prominently at the upstream GAA repeat region, along with an increased DNA methylation. The levels of H3K36me3 and H3K79me2 at the upstream GAA region are significantly reduced, whereas H3K4me3 and H3K36me3 levels are not substantially changed in the promoter region. This suggests a defect of transcription elongation rather than initiation in FRDA. Depletion of CTCF may trigger the FAST-1 antisense transcription that may lead to the deacetylation of histones and the increase of H3K9me3 at the promoter and other regions of the gene (Sandi *et al.*, 2013).

Subsequently, Al-Mahdawi *et al.* (2008) described various histone modifications in the *FXN* promoter, upstream and downstream GAA regions, in autopsy brain tissues from two FRDA patients (Figure 3.3). An overall decreased acetylation of H3 and H4 was confirmed, particularly in the downstream GAA regions, with a consistent increased levels of di- and trimethylation of H3K9 in all three of the *FXN* regions. De Biase *et al.* (2009) then reported a significant increase in heterochromatin HP1 levels in the silenced *FXN* locus of FRDA derived fibroblasts, alongside an elevation on the classical heterochromatin marks, H3K9me3 and H3K27me3 levels at the *FXN* 5' UTR promoter region (Figure 3.4).

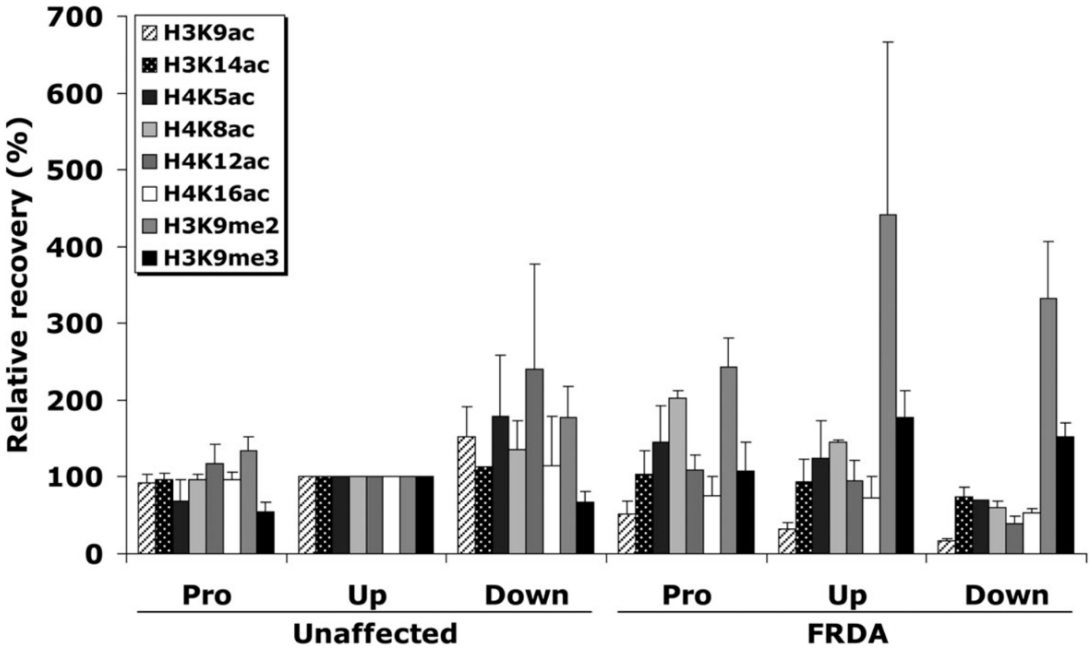

Figure 3. 3 - Analysis of histone modification in human brain tissues. ChIP quantitative PCR results for the *FXN* promoter/exon1 (Pro), upstream GAA (Up) and downstream (Down) amplified regions are represented as the relative amount of immunoprecipitated DNA compared with input DNA, having taken negligible –Ab control values into account. *FXN* values were normalized with human *GAPDH* and all values have been adjusted so that all of the upstream GAA mean values from the unaffected individuals are 100%. The means and SEMs of these values are shown (Al-Mahdawi *et al.*, 2008).

Moreover, ChIP analysis have also revealed decreases in H3K36me3 and H3K79me3 levels flanking the GAA repeat regions in FRDA cells. These latter histone methylation marks are contrastingly associated with a more open chromatin state and elongation of gene transcriptions, suggesting that a transcription elongation defect is possibly at fault in FRDA. Additionally, a decrease in H3K4me3 levels, a transcription initiation mark, has been reported at the upstream GAA repeat region, but not at the promoter region. This indicates a more pronounced defect of the post-initiation elongation stage of *FXN* gene expression, rather than an early transcription initiation defect (reviewed in Sandi *et al.* (2014)).

Nonetheless, although the exact mechanism remains elusive, there is good evidence that the reduction of frataxin protein levels in FRDA is primarily caused by GAA repeat expansion induced transcriptional silencing, which is associated with specific post-translational heterochromatin modifications.

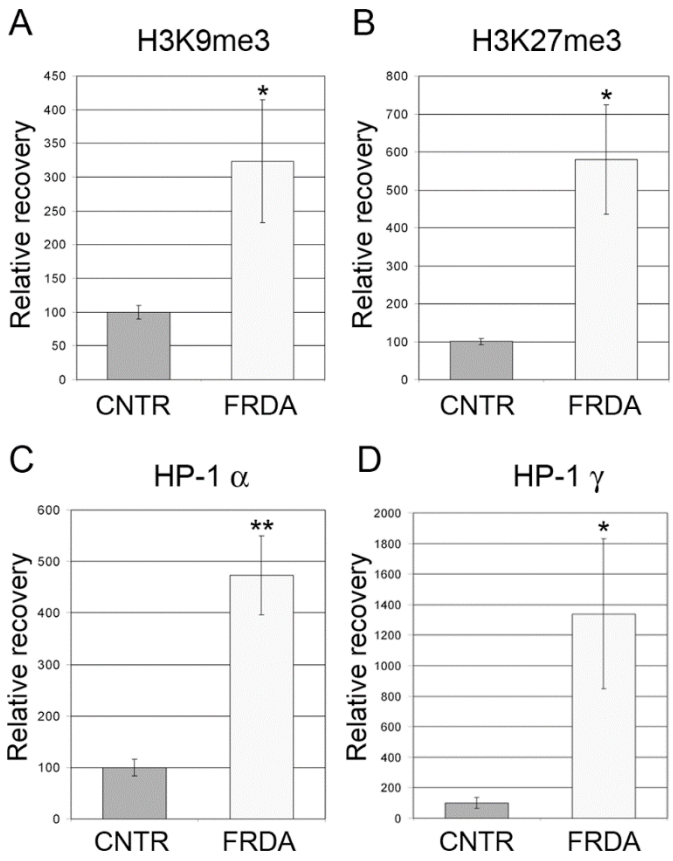

Figure 3. 4 - Heterochromatin formation in the *FXN* 5′UTR in FRDA patients. ChIP assays showing enrichment of (**A**) H3K9me3, (**B**) H3K27me3, and (**C, D**) heterochromatin protein 1 subunits HP-1α and HP-1γ, specifically in FRDA fibroblast cell lines versus non-FRDA controls (CNTR). All bars represent cumulative data from two fibroblast cell lines (FRDA or non-FRDA control), ChIP performed in triplicate, on two independent chromatin preparations. The means and SEMs of these values are shown (*P<0.05, **P<0.01) (De Biase *et al.*, 2009).

3.1.3 Use of HMTase inhibitors as a therapy for FRDA

Due to the identification of several associated epigenetic marks, FRDA can now be considered as an epigenetic disease, and drug treatments are being developed to target these epigenetic changes in attempts to ameliorate the disease phenotype.

So far, a number of studies have demonstrated that specific HDAC inhibitors are capable of enhancing histone acetylation and thus increase the *FXN* expression in FRDA cells (Herman *et al.*, 2006, Rai *et al.*, 2008, Sandi *et al.*, 2011). However, the repressive histone mark, H3K9me3, observed in the proximity of long GAA repeats is sustained during HDAC inhibitor treatment (Herman *et al.*, 2006, Rai *et al.*, 2008). Therefore, as an additional epigenetic-based therapeutic approach for FRDA, HMTase inhibitors are now also being considered to counteract the repressive histone marks and induce a more open chromatin structure at the *FXN* locus (Sandi *et al.*, 2014). Recently, several studies have reported that G9a methyltransferase is responsible for H3K9 methylation by forming a heterodimeric complex with a G9a-like protein (GLP) (Tachibana *et al.*, 2005, Black *et al.*, 2012). The G9a-GLP complex is believed to play an important role in various biological processes including embryo development, immune response and tumour growth (Feldman *et al.*, 2006, Chen *et al.*, 2006, Thomas *et al.*, 2008, Lehnertz *et al.*, 2010, Huang *et al.*, 2010, Antignano *et al.*, 2014). Therefore, as a potential therapeutic target for various human pathophysiology, several compounds have been developed that can inhibit the G9a catalytic activity and its epigenetic machinery. The first disclosed potent and selective inhibitor of G9a-GLP complex was BIX01294 (adiazepin-quinazolin-amine derivative), which was discovered in a combined virtual and high-throughput screen approach (Kubicek *et al.*, 2007). BIX-01294 binds to the SET domain of GLP in the same grove at which the target lysine (H3K9) binds. This prevents the binding of the peptide substrate and consequently, the deposition of methylation marks at H3K9 (Chang *et al.*, 2009, Sandi *et al.*, 2014). Cultured cells treated

with BIX01294 showed to decrease global H3K9me2, induce apoptosis and inhibit the proliferation, migration, and invasion of cancer cells (Varier and Timmers, 2011, Kim *et al.*, 2013, Ke *et al.*, 2014, Oh *et al.*, 2015). Additionally, the efficacy of BIX01294 has previously been tested in FRDA lymphoblastoid cells. Although H3K9me2 was erased from the expanded GAA repeats by BIX-01294 treatment, *FXN* mRNA levels remained unaffected. However, lymphoblastoid cells are known to develop different epigenetic patterns compared to primary cells and they may respond to epigenetic-based drugs differently (Punga and Buhler, 2010).

Furthermore, enhancer of zeste homologue 2 (EZH2) is the methyltransferase responsible for H3K27 trimethylation. As the catalytic subunit of PRC2, EZH2 plays a key role in transcriptional repression and its overexpression is associated with several human cancers (Morera *et al.*, 2016). Therefore, identifying potential compounds which can inhibit its catalytic activity may have a beneficial therapeutic outcome. In 2012, McCabe *et al* performed a high throughput biochemical screening and identified GSK126 as a potent, highly specific inhibitor of EZH2. Lymphoma cells treated with GSK126 display genome-wide loss of H3K27 methylation and reactivates silenced PRC2 target genes with minimal off-target effects (McCabe *et al.*, 2012). Furthermore, myeloma cells treated with GSK126 showed effective abrogation of H3K27me3 levels, and this inhibition was concomitant with enhanced cellular apoptosis (Zeng *et al.*, 2017). The growth inhibitory effects of GSK126 were also observed in several other malignant tissues, including small cell lung cancers and prostate cancers (Takeshima *et al.*, 2015). Moreover, GSK126 treatment in combination with a DNA demethylating agent has significantly decreased H3K27me3 and increased the levels of *FMR1* transcripts in fragile X syndrome (FXS) cells (Kumari and Usdin, 2016). Therefore, as hypermethylated H3K9me3 and H3K27me3 is associated with *FXN* gene repression in

FRDA, inhibition of G9a and EZH2 activity by small molecule inhibitors, may have a beneficial therapeutic effect by reactivating *FXN* gene transcription.

3.2 Therapeutic testing of BIX01294 and GSK126

At present, there are limited FRDA studies which have investigated the use of HMTase inhibitors to induce an open chromatin structure and alleviate *FXN* gene silencing. Therefore, with aims to reduce the repressive histone marks H3K9me2/3 and H3K27me3, I decided to investigate the efficacy and tolerability of BIX01294 and GSK126, respectively, as a therapy for FRDA (Figure 3.5).

As sensory neurons are challenging to obtain from FRDA patients and may not survive long-term in culture, in this study, we have used FRDA human fibroblasts (GMO3816, 330 and 380 GAA repeats) and fibroblasts established from FRDA YAC transgenic mouse models (YG8sR, YG8LR and Y47R) to unravel any frataxin-increasing capabilities following BIX01294 and GSK126 treatment. The three FRDA mouse models all express human *FXN* in a mouse-*Fxn*-null background. YG8sR and YG8LR carry 220 and 450 units of GAA repeats respectively, whereas Y47R contain normal-sized $(GAA)_9$ repeat in intron 1 of a human *FXN* transgene (Pook *et al.*, 2001, Anjomani Virmouni *et al.*, 2015). In line with FRDA-like phenotype, YG8sR and YG8LR, both exhibit GAA repeat-mediated *FXN* gene silencing associated with decreased H3K9 acetylation and increased H3K9 tri-methylation at *FXN* 5'UTR promoter region, compared to Y47R controls (unpublished data). Therefore, cells derived from YG8sR and YG8LR are considered to be suitable systems in which to investigate the efficacy of BIX01294 and GSK126 as a potential epigenetic-based FRDA therapy.

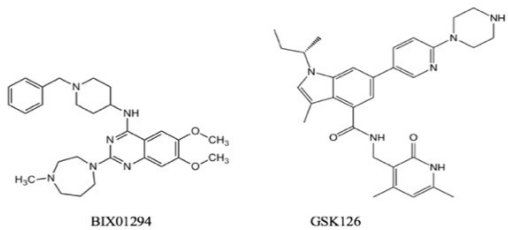

Figure 3. 5 - Chemical structure of BIX01294 and GSK126.

3.3 Results

3.3.1 Cell viability assessment

To investigate the safety and cellular tolerability of BIX01294 and GSK126 treatment, PrestoBlue cell viability assay was carried out (as described in Chapter 2, section 2.5.5), to quantitatively measure the proliferation of cells. Human and mouse primary cell lines were treated with BIX01294 (1nM - 10μM) and GSK126 (1nM - 10μM) in triplicates for 72hrs. Subsequently, the reducing environment of the viable cells modified the PrestoBlue reagent which released a highly fluorescent colour. This was detected by spectrophotometer at an absorbance filter 570nm and 600nm reference. A mean value of vehicle and drug treated triplicates were used for calibration, where the untreated normal / control cells were set arbitrarily as 100%.

Both human and mouse fibroblasts revealed to safely tolerate BIX01294 treatment with concentrations ranging from 1nM to 100nM, whereas, higher concentrations significantly decreased the cellular viability (Figure 3.6 A-B). Furthermore, in comparison to BIX01294 treatment, cells were generally less sensitive to GSK126 treatment (Figure 3.6 C-D). Both normal and FRDA human fibroblasts indicated no significant change in viability with 1nM to 2μM GSK126 treatment (Figure 3.6 C). However, cellular treatment with 10μM GSK126 indicated to be lethal, as the cell viability was significantly reduced. A similar pattern was also observed in mouse fibroblasts treated with GSK126, however, YG8sR and YG8LR cells showed reduced tolerance with 2μM GSK126 ($P<0.05$) (Figure 3.6 D). These results gave a valuable indication of the optimal compound dosing required for subsequent molecular analysis to determine the efficacy of BIX01294 and GSK125 for FRDA therapy.

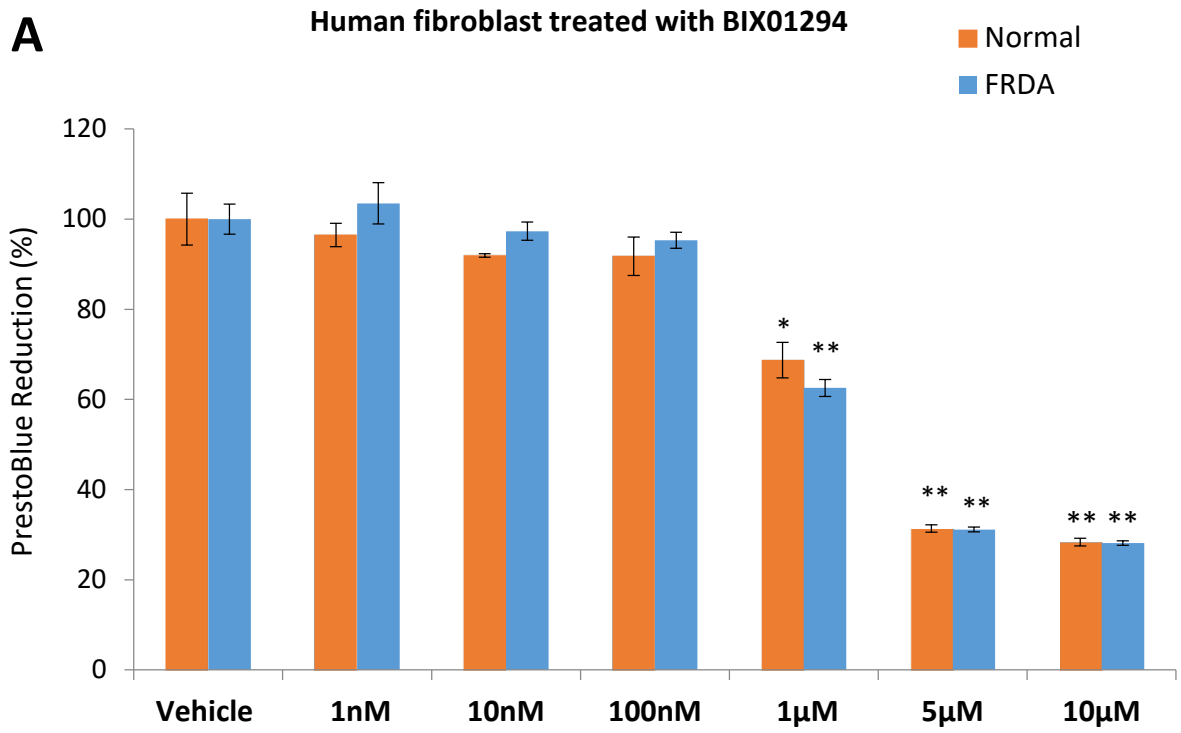
A
Human fibroblast treated with BIX01294
Normal
FRDA
PrestoBlue Reduction (%)
120
100
80
60
40
20
0
*
**
**
**
**
**
**
Vehicle
1nM
10nM
100nM
1µM
5µM
10µM

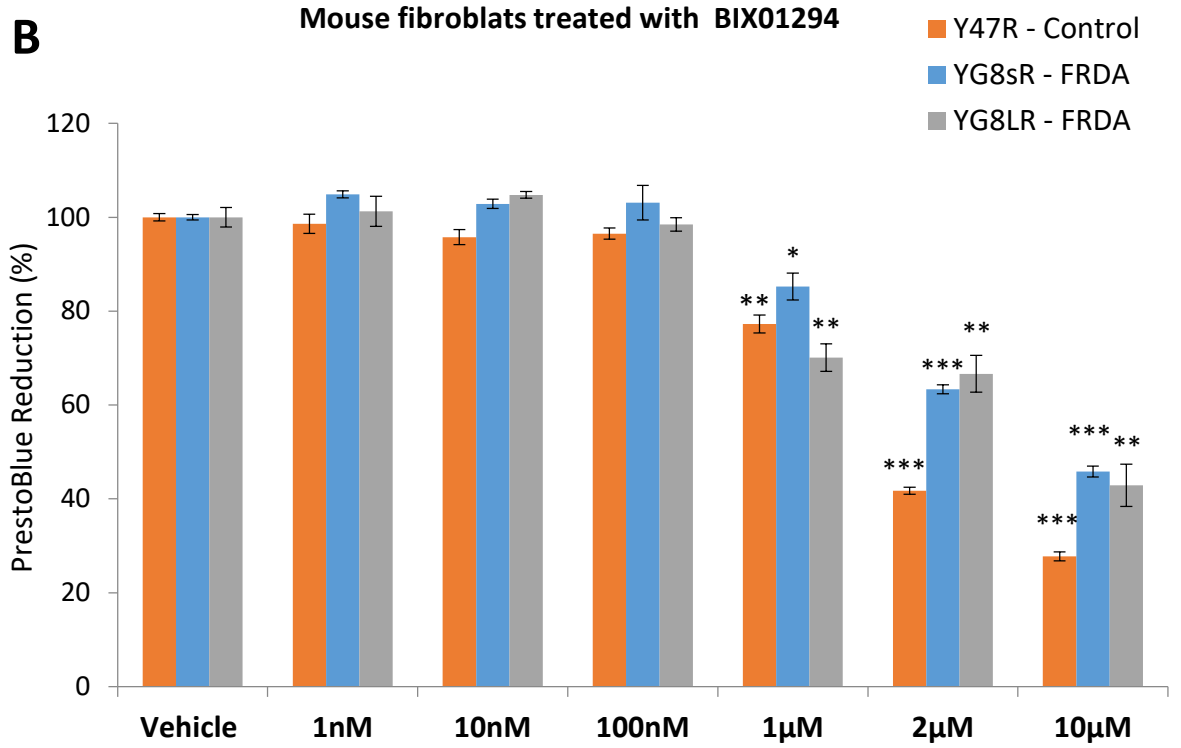
B
Mouse fibroblats treated with BIX01294
Y47R - Control
YG8sR - FRDA
YG8LR - FRDA
PrestoBlue Reduction (%)
120
100
80
60
40
20
0
**
*
**
***
**
***
***
**
Vehicle
1nM
10nM
100nM
1µM
2µM
10µM

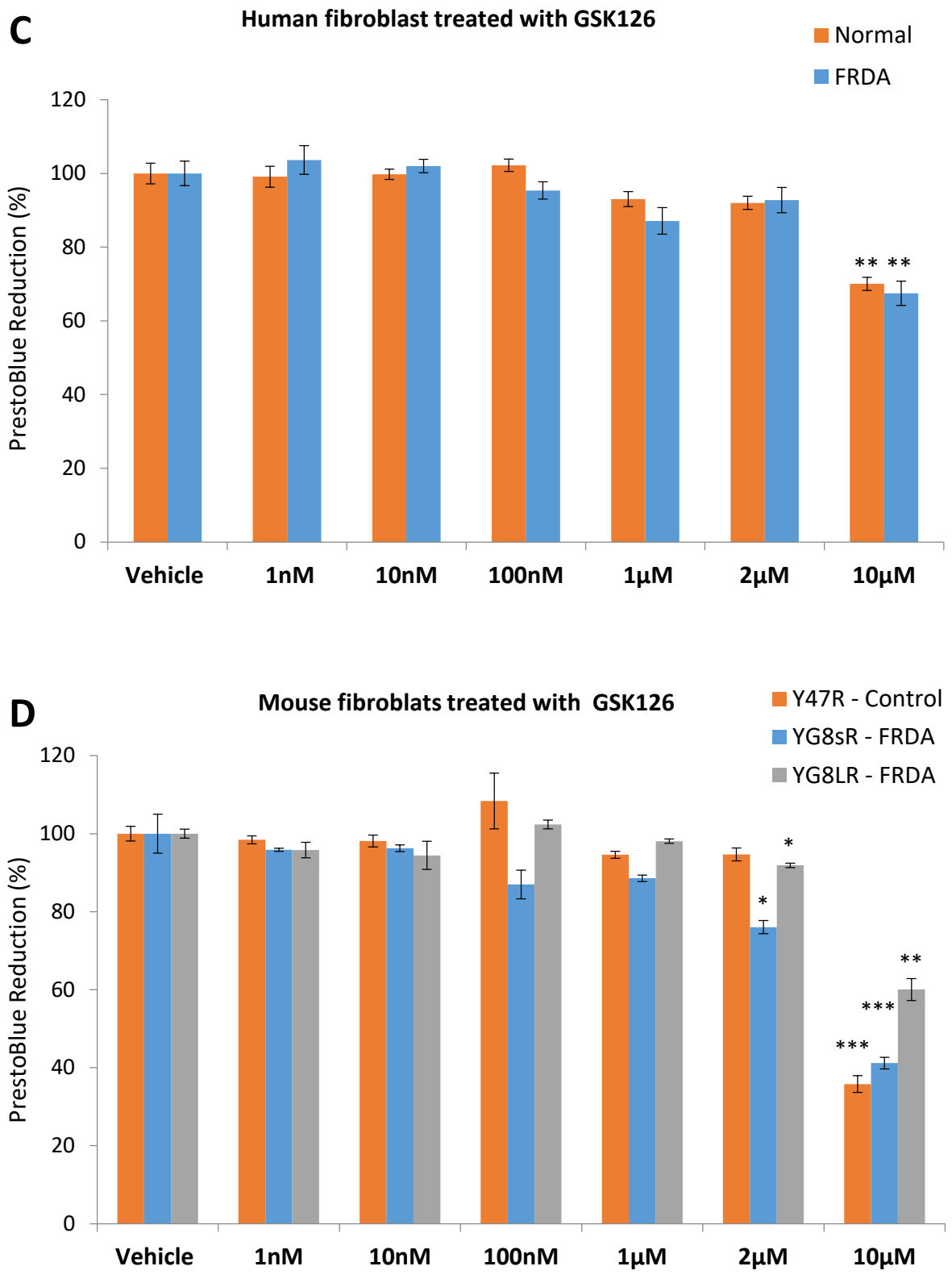

Figure 3. 6 - PrestoBlue cell viability analysis following 72hr HMTase inhibitor treatment. BIX01294 treatment analysis in A) human FRDA and B) mouse FRDA fibroblasts. GSK126 treatment analysis in C) human FRDA and D) mouse FRDA fibroblasts. The mean value of all data was normalised to the PrestoBlue reduction of vehicle treated cells (set at 100%). Error bars indicate SEM and values represent mean ±SEM (n=3). Asterisks indicate significant differences between drug and vehicle treated cell lines, assessed by Student's *t*-test (*P<0.05, **P<0.01, ***P<0.001).

3.3.2 Quantification of *FXN* mRNA levels in human primary fibroblast

In order to test the effects of BIX01294 and GSK126 on *FXN* gene reactivation, normal and FRDA human primary fibroblasts were treated with 100nM, 500nM and 1μM of BIX01294, and 1μM and 2μM of GSK126. The drug concentrations were prepared in DMEM medium and the cells were treated with the drug(s) either individually or in combination over a period of 72hrs. The *FXN* mRNA levels were measured by performing qRT-PCR analysis (as described in Chapter 2, section 2.12). Briefly, RNA was extracted from about 1 million cells by the Trizol® method (as described in section 2.7) and converted into cDNA, followed by qRT-PCR using primers designed to detect *FXN* human frataxin cDNA (Table 2.2). In order to account for possible differences in gene expression efficiency, at the mRNA levels, the Ct values obtained for *FXN* were normalised to the *HPRT* gene as an endogenous control. Each sample was run in triplicates and each experiment was performed at least twice. The mean value of each triplets was used for further analysis, using $2^{-\Delta\Delta Ct}$ method to obtain relative quantification (RQ) values. The relative levels of mRNA expression in FRDA and normal fibroblasts were then calibrated by calculating the means of the RQ values, where the mean values of vehicle treated normal fibroblasts was set arbitrarily at 100%. The passage numbers of all primary fibroblasts were closely matched, throughout all the mRNA quantification experiments to avoid any possible cell culture variabilities.

Treatment of cells with BIX01294 did not significantly increase *FXN* gene expression levels, except for 500nM concentrations, where an increase of 19% ($P< 0.05$) is seen in FRDA cell lines (Figure 3.7). Similarly, individual treatments of GSK126 did not have a great effect in *FXN* mRNA expression levels in FRDA cells, where in fact a significant decrease is seen with 1μM (22%, $P<0.05$) and 2μM (38%, $p<0.01$) concentrations.

Interestingly, all combination treatments of BIX01294 and GSK126 in FRDA cell lines were shown to significantly increase the *FXN* gene levels. The highest significant increase of 88% ($P<0.01$) was observed with 100nM BIX01294 + 2μM GSK126 treatment, followed by 34% ($P<0.01$) increase with 1μM BIX01294 + 1μM GSK126 treatment, then 26% ($P<0.01$) increase with 500nM BIX01294 + 1μM GSK126 treatment. This suggests that simultaneous inhibition of both H3K9me2/3 and H3K27me3 with BIX01294 and GSK126, respectively, is beneficial in reversing the histone modifications and in activating the *FXN* gene. However, none of the synergistic treatment in FRDA fibroblasts increased the *FXN* gene expression to the same level as in the normal fibroblasts. Nevertheless, normal fibroblasts were generally unaffected, except for a combination treatment of 500nM BIX01294 + 1μM GSK126, where a significant decrease of 18% ($P<0.01$) in *FXN* gene expression is seen.

Furthermore, after determining the synergistic effect with 100nM BIX01294 + 2μM GSK126 as the optimum drug dosing, we then investigated the effect of this combination treatment on *FXN* gene expression levels with different time points (2, 3, 6 and 9-day) in FRDA cell lines (Figure 3.8). In this experiment, the cell culture medium was replaced with fresh drug containing medium every 3 days. The results indicated a gradual significant increase in *FXN* transcription in FRDA cell lines after 2 and 3-day treatments by 15% ($P<0.01$) and 88% ($P<0.01$). However, the significant increase in *FXN* gene expression then reduced to 30% by 9-day treatment, with no change seen with 6-day treatment. This indicates that 3-day was the optimum treating course in enhancing *FXN* gene levels in FRDA cell lines.

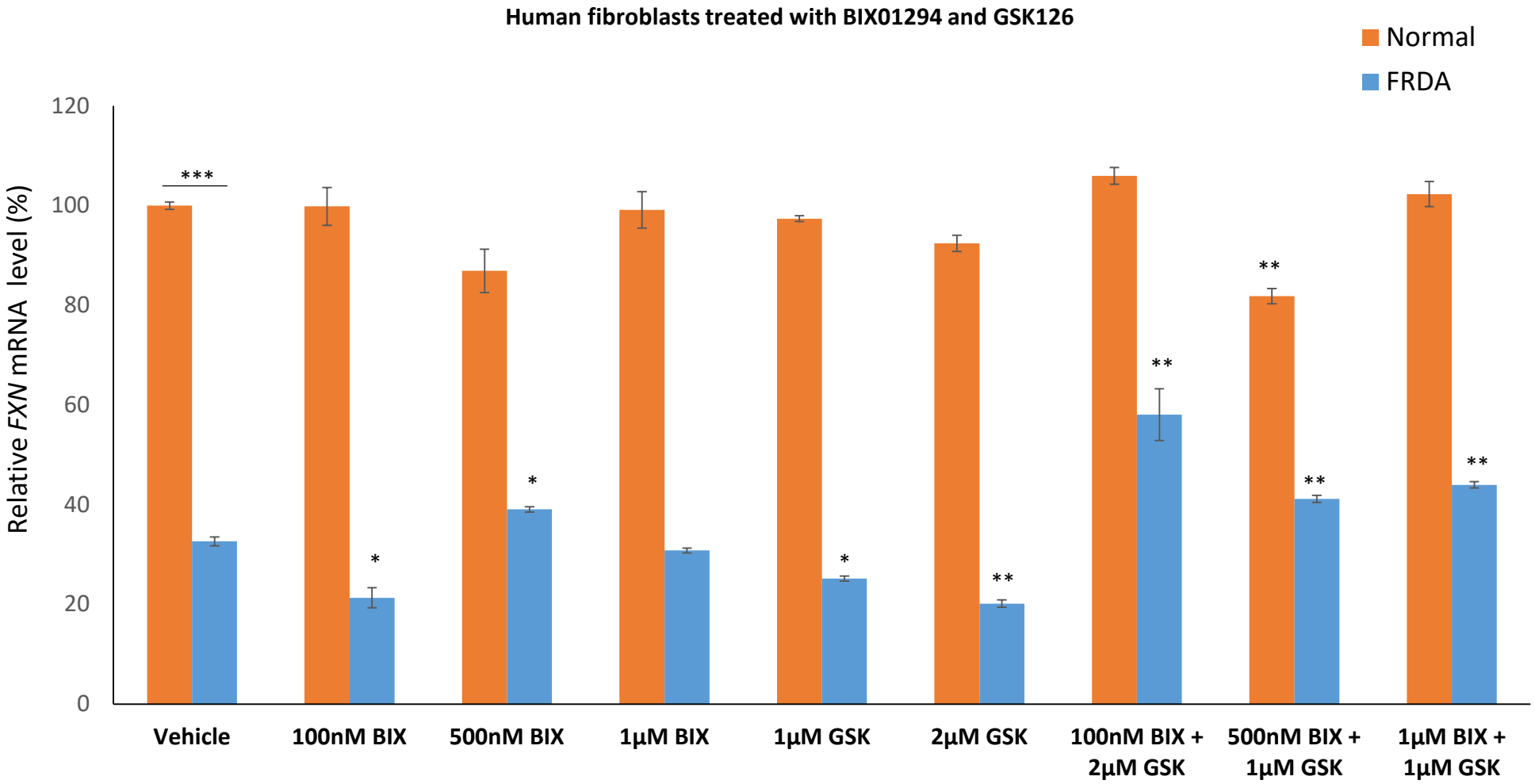

Figure 3. 7 – qRT-PCR analysis indicating the relative *FXN* mRNA levels following treatment with BIX01294 and GSK126 individually and synergistically in human primary fibroblasts. Each result displayed is the mean of two independent experiments and the *FXN* mRNA levels of each sample were normalised to *HPRT* mRNA levels. The values were expressed as a ratio to the vehicle treated samples of normal fibroblasts. Error bars indicate SEM and values represent mean ±SEM. Asterisks indicate significant differences between drug and vehicle treated cell lines, assessed by Student's *t*-test (*P<0.05, **P<0.01, ***P<0.001).

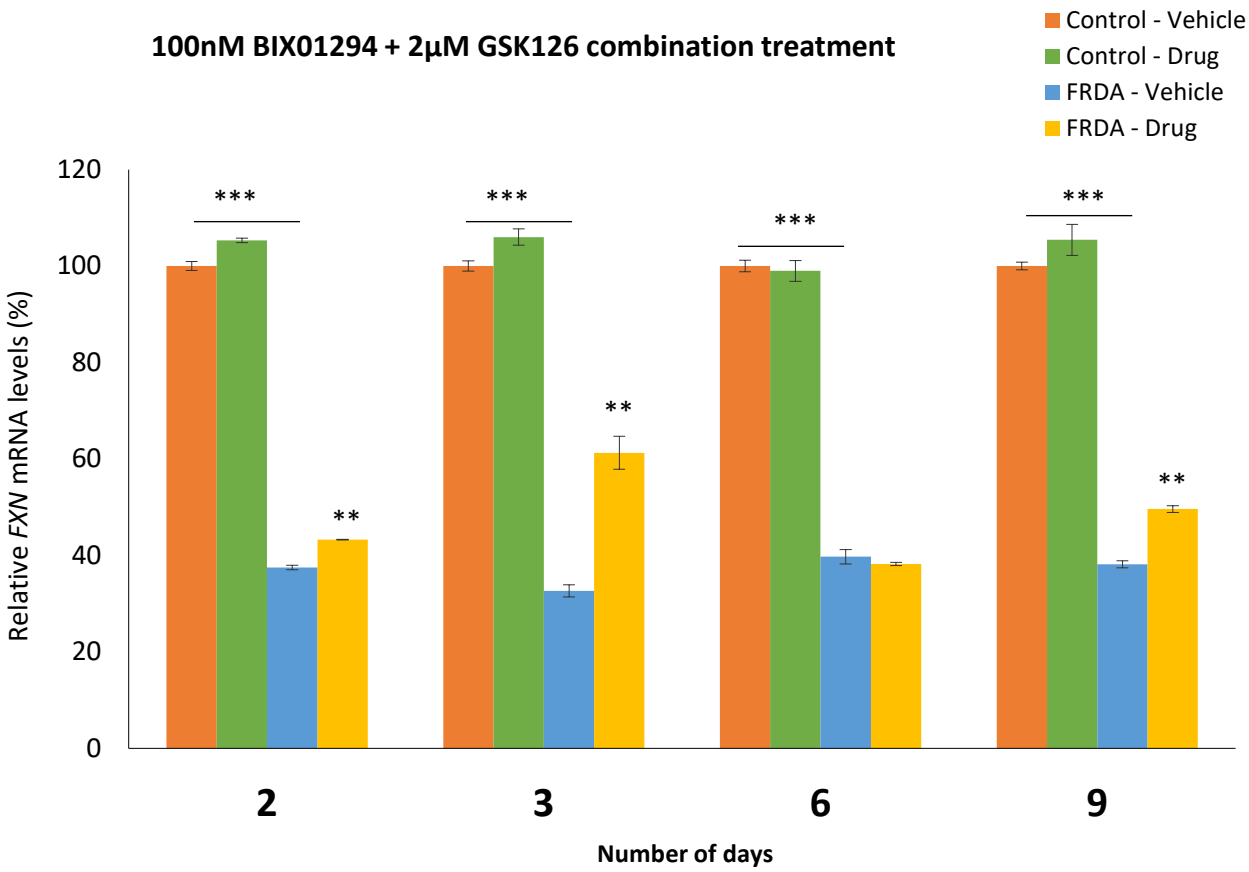

Figure 3. 8 - qRT-PCR analysis indicating the relative *FXN* mRNA levels following BIX01294 + GSK126 combination treatment in human primary fibroblasts for different time points. For this treatment, the cell culture medium was replaced with fresh drug containing medium every 3 days. The mean *FXN* mRNA levels of each sample were normalised to *HPRT* mRNA levels. The values were expressed as a ratio to the vehicle treated samples of normal fibroblasts at the corresponding time point. Error bars indicate SEM and values represent mean ±SEM (n=3). Asterisks indicate significant differences between drug and vehicle treated cell lines, assessed by Student's *t*-test (**P<0.01, ***P<0.001).

3.3.3 Quantification of *FXN* mRNA levels in mouse primary fibroblasts

Similar to human fibroblasts, the mouse primary fibroblasts were treated with 1nM and 100nM of BIX01294, and, 100nM and 1μM of GSK126. The cells were treated with the drug(s) either individually or in combination for 72hrs, followed by *FXN* mRNA expression quantification, tested by qRT-PCR. The vehicle treated Y47R-control values were used as a calibrator for the YG8sR and YG8LR *FXN* gene expression values, relatively.

Generally, no significant changes in *FXN* gene expression levels were observed in YG8sR cells after individual treatments with BIX01294 and GSK126 (Figure 3.9). However, similar to human FRDA fibroblasts, 1μM GSK126 treatment significantly reduced *FXN* mRNA expression levels in YG8sR cells (39%, $P<0.01$). A similar pattern was also seen in YG8LR cell lines, except for 100nM BIX01294 treatment where a significant increase of 51% ($P<0.01$) in *FXN* transcription was seen. Interestingly, combination treatments of 100nM BIX01294 + 100nM GSK126 and 100nM BIX01294 + 1μM GSK126, both have significantly increased the *FXN* mRNA expression levels in YG8sR cells by 16% ($P<0.01$) and 37% ($P<0.01$), respectively. Whereas, YG8LR cell lines indicated a significant increase of 78% with synergistic treatment of 1nM BIX01294 + 1μM GSK126. This correlates well with the results obtained from the human fibroblasts, where simultaneously targeting H3K9me2/3 and H3K27me3 histone repressive marks, with combination treatment of BIX01294 and GSK126, indicated to have a beneficial therapeutic effect in FRDA. However, some combination treatment seems to have a non-cell type specific effect, as significant increases in *FXN* gene levels are also observed in Y47R- control cells. Moreover, since a combination treatment of BIX01294 and GSK126 induced the highest change in *FXN* gene expression (in YG8sR fibroblasts), we then decided to investigate the effect of 100nM BIX01294 + 2μM GSK126 synergistic treatment at different time points (2, 3, 6 and 9 days) (Figure 3.10). In this experiment the cell culture medium was replaced with fresh drug

containing medium every 3 days. Overall, the results indicated that 3-day treatment induced the best change in *FXN* gene expression, where an increase was seen in both the YG8sR and YG8LR cell lines. However, increases were statistically non-significant in YG8LR cells (P=0.1).

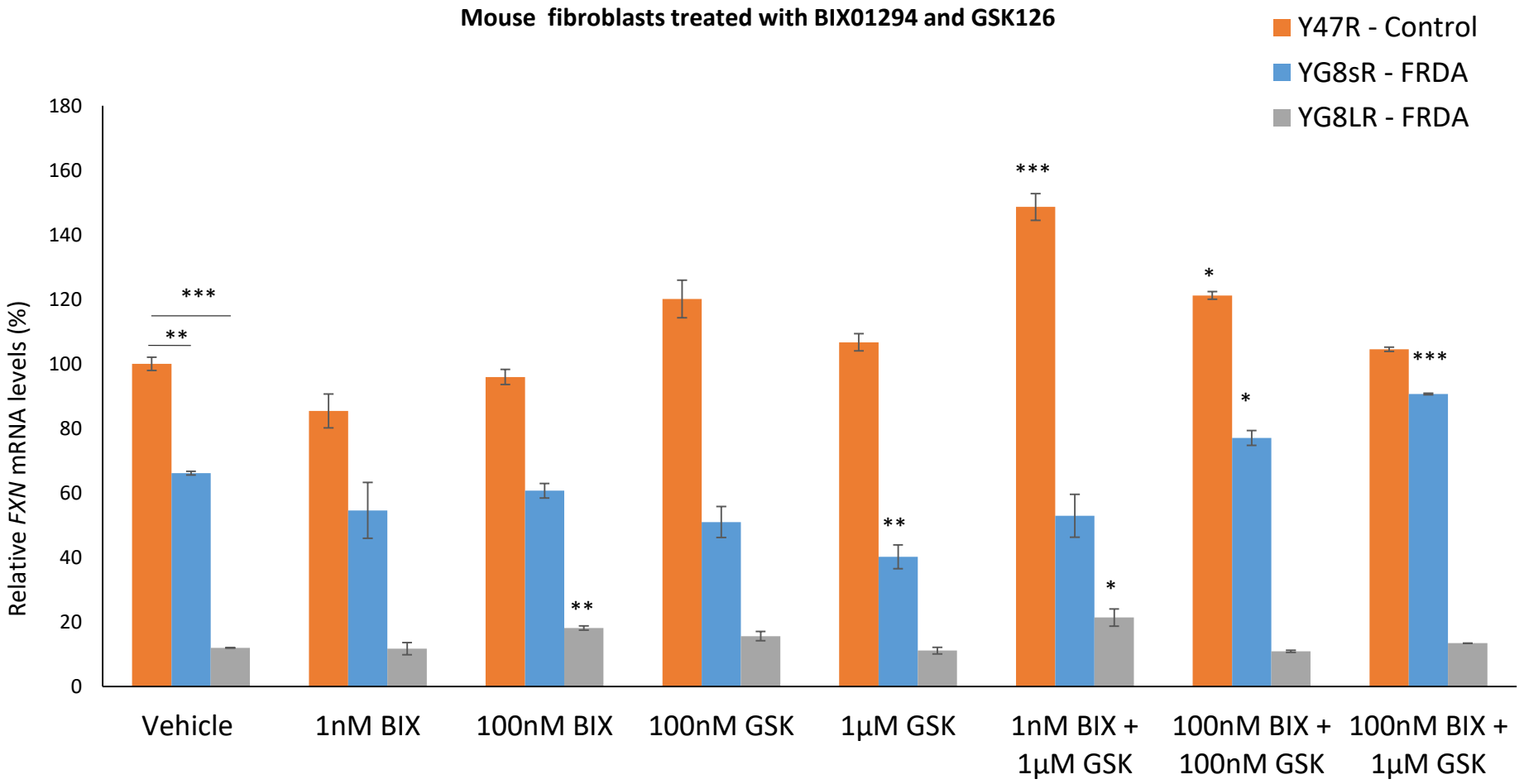

Figure 3. 9 – qRT-PCR analysis indicating the relative FXN mRNA levels following treatment with BIX01294 and GSK126 individually and synergistically in mouse primary fibroblasts. Each result displayed is the mean of two independent experiments and the *FXN* mRNA levels of each sample were normalised to *Hprt* mRNA levels. The values were expressed as a ratio to the vehicle treated samples of normal fibroblasts. Error bars indicate SEM and values represent mean ±SEM. Asterisks indicate significant differences between drug and vehicle treated cell lines, assessed by Student's *t*-test (*P<0.05, **P<0.01, ***P<0.001).

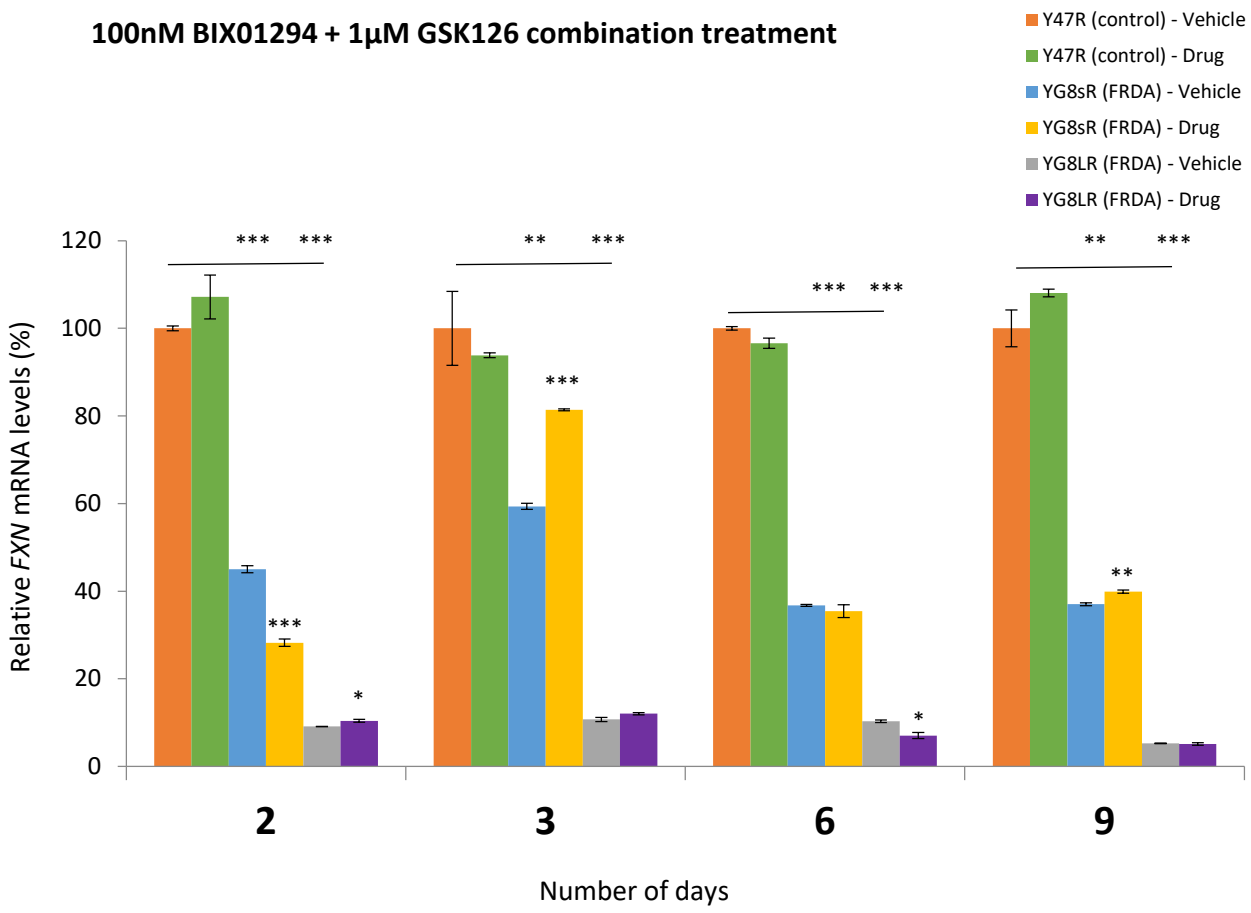

Figure 3. 10 – qRT-PCR analysis indicating the relative *FXN* mRNA levels following BIX01294 + GSK126 combination treatment in mouse primary fibroblasts for different time points. For this treatment, the cell culture medium was replaced with fresh drug containing medium every 3 days. The mean *FXN* mRNA levels of each sample were normalised to *Hprt* mRNA levels. The values were expressed as a ratio to the vehicle treated samples of normal fibroblasts at the corresponding time point. Error bars indicate SEM and values represent mean ±SEM (n=3). Asterisks indicate significant differences between drug and vehicle treated cell lines, assessed by Students *t*-test (**P<0.01, ***P<0.001).

3.3.4 Frataxin protein quantification

To determine the change in frataxin protein expression in human and mouse fibroblasts, combination treatments were carried out with 100nM BIX01294 + 2μM GSK126 and 100nM BIX01294 + 1μM GSK126, respectively, for different time points (2-9 days). Total protein was extracted and the protein concentration was measured using a Pierce™ BCA Protein Assay Kit (Thermo Scientific), as described in Chapter 2, section 2.17-18. Subsequently, the protein samples were subjected to frataxin protein quantity dipstick assay kit (MitoSciences) and the levels of frataxin protein expression was determined by lateral flow immunoassay (as described in Chapter 2, section 2.20). Although a significant reduction in frataxin protein levels are observed in both human and mouse FRDA fibroblasts as compared to normal fibroblasts; generally, no significant change was observed after drug treatment at any time point (Figure 3.11 A-B). This suggests that perhaps the *FXN* mRNA expression did not reach the level where it would have a significant impact on the frataxin protein expression levels. Furthermore, there may also be other post-translational mechanisms which may play a role in frataxin protein regulation.

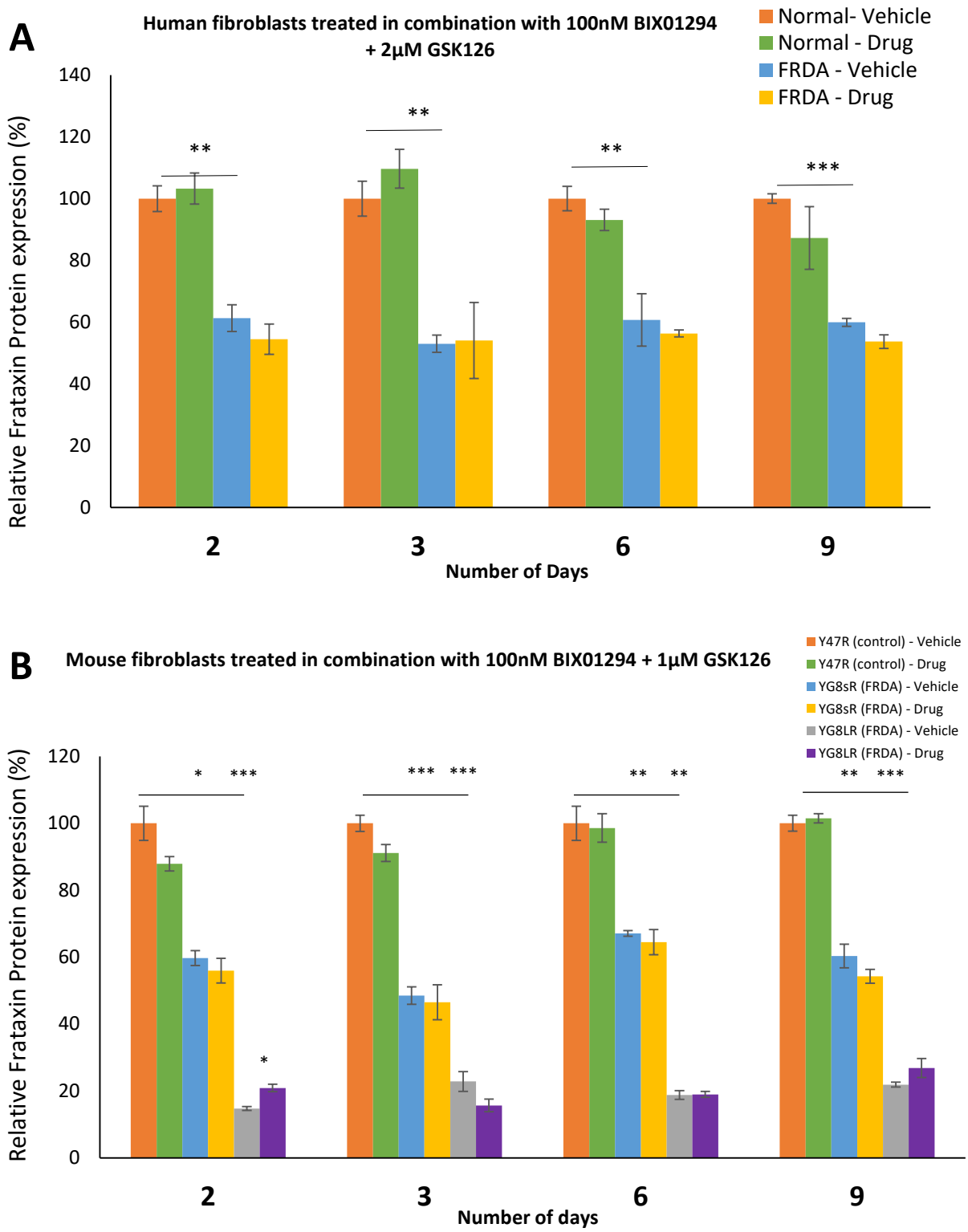

Figure 3. 11 – qRT-PCR analysis indicating the relative frataxin protein expression levels in human and mouse primary fibroblasts following BIX01294 + GSK126 combination treatment for different time points. The change in frataxin levels in A) human and B) mouse fibroblasts were determined by the dipstick immunoassay. The values were expressed as a ratio to the vehicle treated samples of normal fibroblasts at the corresponding time point. Error bars indicate SEM and values represent mean ±SEM (n=3). Asterisks indicate significant differences between drug and vehicle treated cell lines, assessed by Student's *t*-test (**P<0.01, ***P<0.001).

3.3.5 HMTase enzymatic assessment

To assess the inhibitory effects of BIX01294 and GSK126, I investigated the enzymatic activity levels of EZH2 and G9a, respectively, following treatment in human primary fibroblasts. As compared to the mouse FRDA cellular models, human primary fibroblasts are derived from actual FRDA patients. Therefore, it is a better cellular-model system for drug treatment. For this study, we treated the cells with 100nM BIX01294 and 2μM GSK126 either individually or in combination for 72 hours, followed by nuclear extract preparations (as described in Chapter 2, section 2.14). Subsequently, HMTase enzymatic assay kits (EpiQuik™) were used to measure the levels of methylated H3K9 and H3K27 by a high-affinity primary antibody and an HRP conjugated secondary antibody-colour developing system, as described in Chapter 2, section 2.15. Each of the samples were run in triplicates, and the mean values of HMTase activity in FRDA and normal fibroblasts were calibrated to vehicle-treated normal fibroblasts subjectively set as 100%. Curiously, the EZH2 activity is significantly higher by 53% ($P<0.01$) in vehicle treated FRDA fibroblasts as compared to normal fibroblasts (Figure 3.12 A). However, 2μM GSK and a combination treatment of 2μM GSK126 + 100nM BIX01294 in FRDA fibroblasts have shown to significantly reduce the EZH2 levels by 28% ($P<0.05$) and 20% ($P<0.05$), respectively. Similarly, FRDA fibroblasts were shown to have a 59% significantly higher G9a enzymatic activity as compared to normal fibroblasts (Figure 3.12 B). This activity was significantly reduced by 25% ($P<0.01$) and 20% ($P<0.01$) with 100nM BIX01294 and combination treatment of 2μM GSK126 + 100nM BIX01294, respectively. There was no significant change in EZH2 and G9a activity levels between individual and synergistic drug treatment in FRDA cells. This suggest that the combination treatment of BIX01294 and GSK126 does not interfere with each of the drugs specific inhibitory effects. However, a similar change in EZH2 and G9a enzymatic activity

was also observed in normal fibroblasts after treatment. This indicates that BIX01294 and GSK126 have a non-cell type specific inhibitory effect.

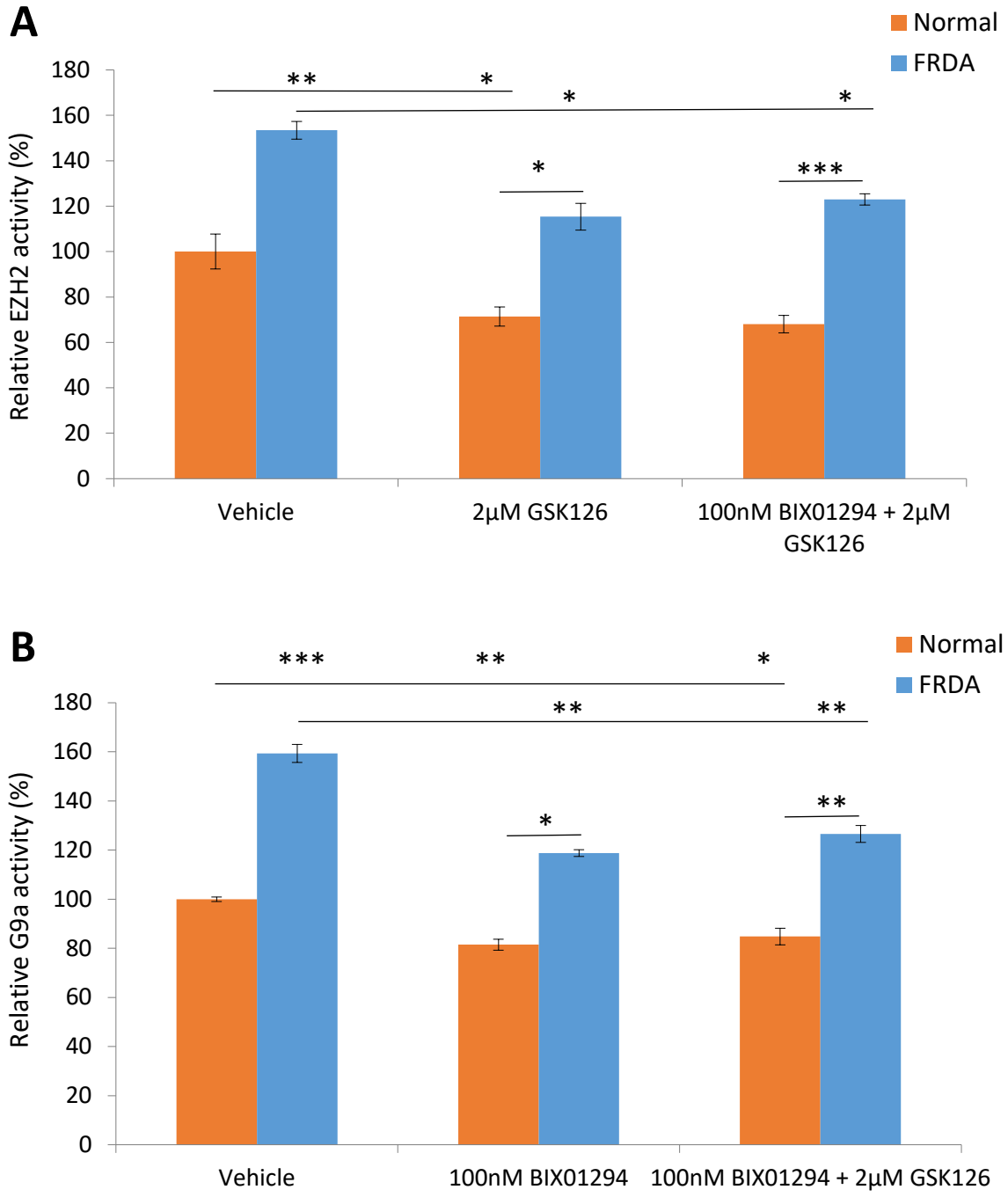

Figure 3. 12 - HMTase enzymatic activity analysis in human fibroblasts treated individually and in combination with BIX01294 and GSK126. A) EZH2 activity levels and B) G9a activity levels. The values were expressed as a ratio to the vehicle treated samples of normal fibroblasts. Error bars indicate SEM and values represent mean ±SEM (n=3). Asterisks indicate significant differences between drug and vehicle treated cell lines, assessed by Student's *t*-test (*P<0.05, **P<0.01, ***P<0.001).

3.3.6 Histone modification assessment

To examine the effects of BIX01294 and GSK126 on histone modifications, human primary fibroblasts were treated with a combination of 100nM BIX01294 + 2μM GSK126 for 72hrs, followed by performing ChIP assay, to determine the histone modification changes in the *FXN* 5'UTR promoter region (as discussed in Chapter 2, section 2.13). The histone modification levels in each sample were normalised to input and minus antibody samples and finally determined to the vehicle treated normal fibroblasts, which was arbitrarily set as 100%.

Immunoprecipitation with anti-H3K9ac antibody revealed a significant reduction of 81% ($P<0.001$) in FRDA fibroblasts treated with vehicle as compared to normal fibroblasts. However, this was increased by 242% ($P<0.001$) with BIX01294 and GSK126 combination treatment (Figure 3.13). Moreover, FRDA cell lines indicated a significant increase of 231% ($P<0.001$) and 168% ($P<0.001$) in H3K9me3 and H3K27me3 levels, respectively. However, after drug treatment, the methylation levels significantly decreased by 42% ($P<0.01$) and 51% ($P<0.01$), respectively. Nonetheless, an increase in H3K9ac and decrease in H3K9me3 and H3K27me3 levels is also observed in normal fibroblasts after drug treatment, indicating that BIX01294 and GSK126 have non-cell type specific drug effect. These results correlate well with the change in EZH2 and G9a enzymatic activity after combination treatment with BIX01294 and GSK126. Overall, the change in histone modification after drug treatment in FRDA fibroblasts did not reach the regular levels as seen in normal fibroblasts.

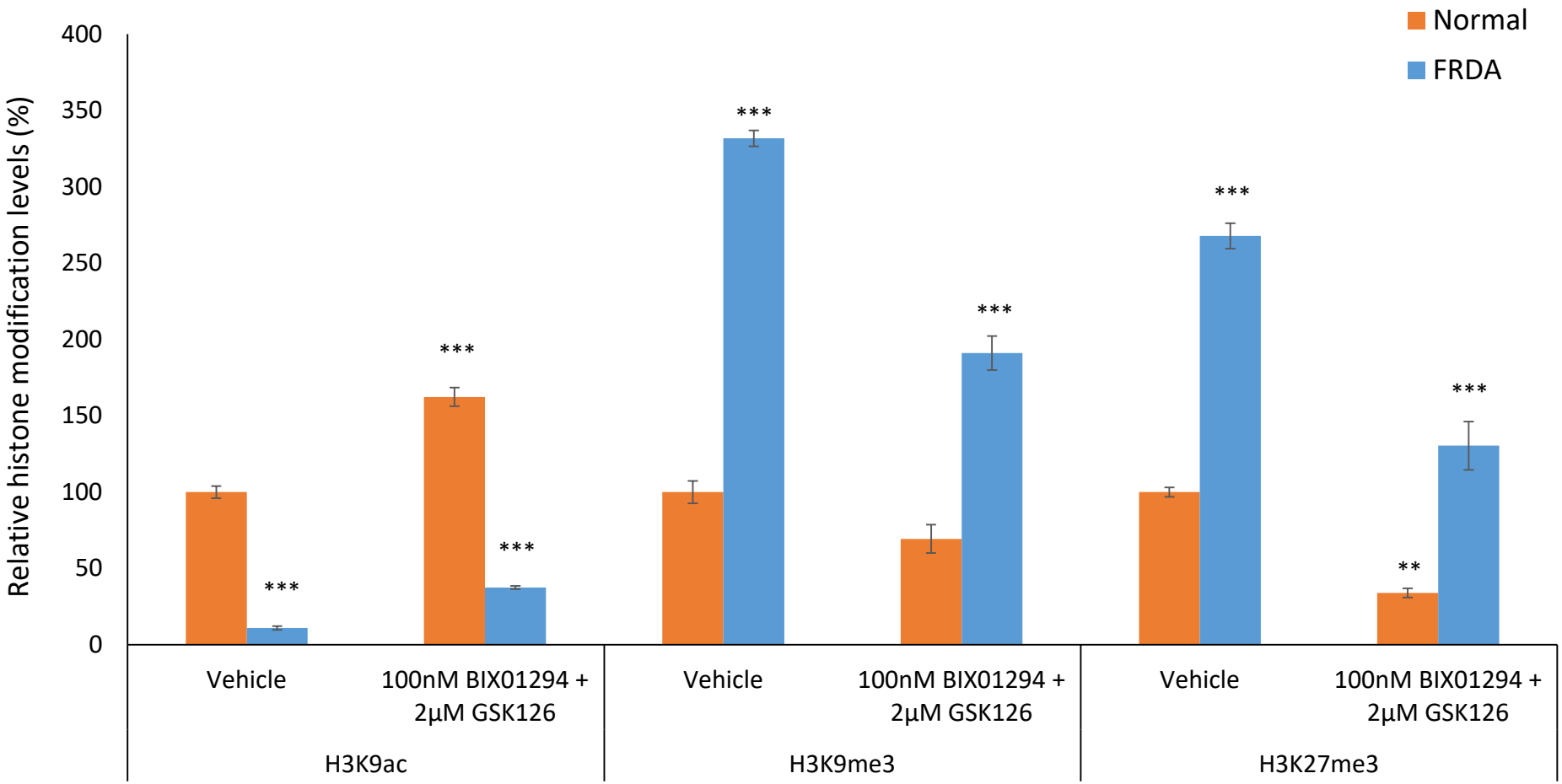

Figure 3. 13 - Histone modification changes in the *FXN* 5'UTR promoter region, after 72hr combination treatment with BIX01294 + GSK126 in normal and FRDA fibroblasts. The values were expressed as a ratio to the vehicle treated samples of normal fibroblasts. Error bars indicate SEM and values represent mean ±SEM (technical repeats, n=3). Asterisks indicate significant differences between drug and vehicle treated cell lines, assessed by Student's *t*-test (**P<0.01, ***P<0.001).

3.3.7 General gene quantification

Like any epigenetic-based therapies, HMTase inhibitors are expected to induce a widespread effect on gene expression by altering global histone modification levels, and thus have a potential off-target effects. Therefore, to evaluate the possibility of BIX01294 and GSK126 off-target effects in FRDA, we treated human and mouse fibroblasts with a combination treatment of the two drugs (100nM BIX01293 + 1uM/2uM GSK126), which had exerted a change in *FXN* gene expression levels (Figure 3.7), for 72hrs. We then quantitatively measured changes in a panel of endogenous control gene expression by qRT-PCR using specific primer sets (TATAA Biocenter) for human and mouse.

The results obtained show that there is no significant change in any of the genes explored in either the mouse or human fibroblasts after treatment (Figure 3.14 A-B). This suggests that BIX01294 and GSK126 exerts minimal off-target effects outside of *FXN* gene regulation.

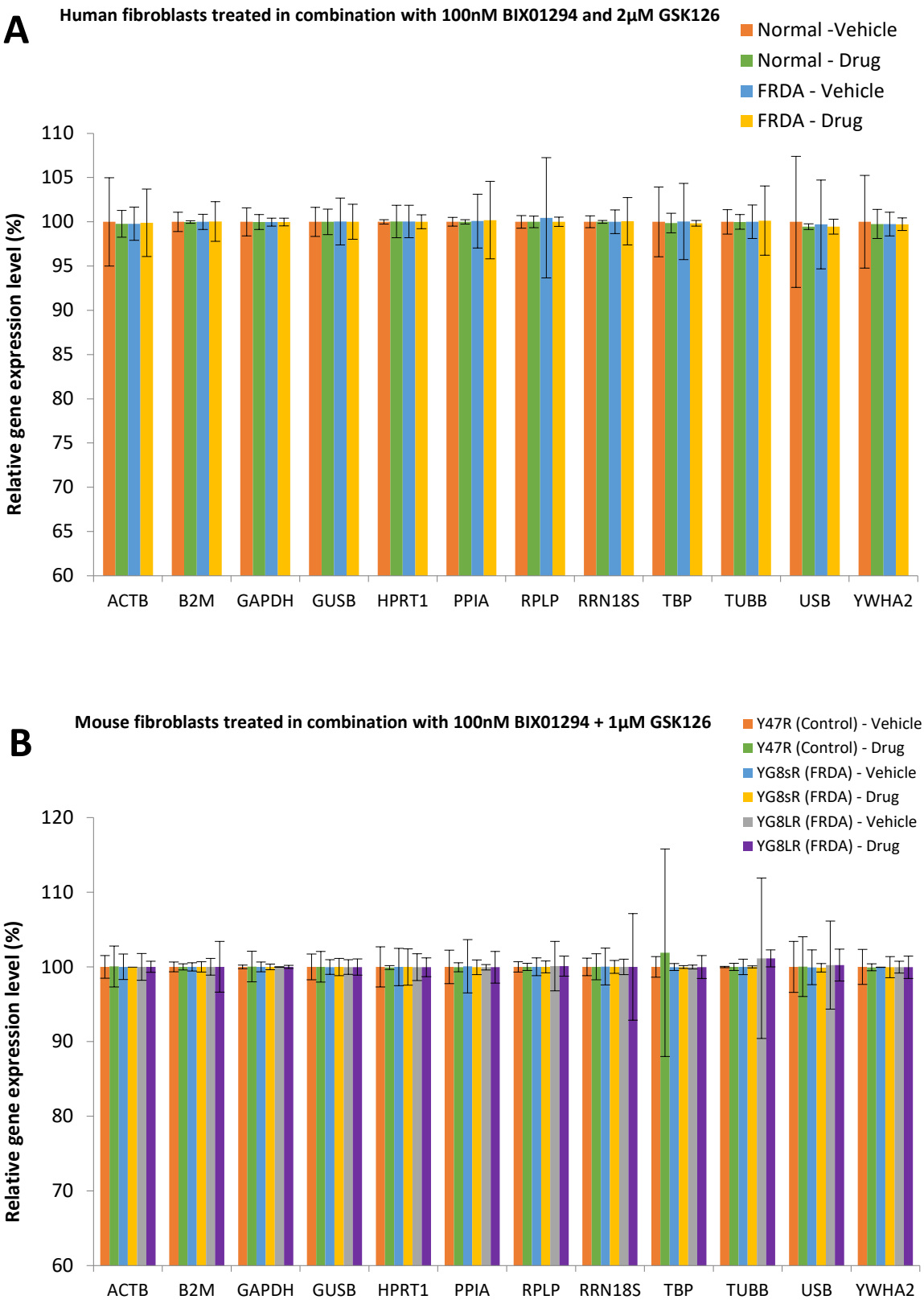

Figure 3. 14 - Relative change in endogenous control gene expression levels in A) human and B) mouse primary fibroblasts following BIX01294 + GSK126 combination treatment. The values were expressed as a ratio to the vehicle treated samples of normal fibroblasts. Error bars indicate SEM and values represent mean ±SEM (n=3).

3.4 Discussion

It has been reported that 98% of FRDA patients have a homozygous GAA trinucleotide repeat expansion within the first intron of the *FXN* gene, leading to reduced expression of frataxin (Campuzano *et al.*, 1996). Although the mechanism by which the GAA repeat expansion leads to decreased levels of frataxin are currently unknown, it is generally accepted that FRDA may be caused by a heterochromatin-mediated silencing effect of the *FXN* gene (Saveliev *et al.*, 2003, Festenstein, 2006). In support of this hypothesis, differential DNA methylation in FRDA patients accompanied by various histone modifications have been identified in FRDA patients within the vicinity of the expanded GAA repeats and near the promoter region of the *FXN* gene. This includes elevated methylation of histone residues, such as H3K9me2/3 and H3K27me3, with hypoacetylation of H3K9 (Herman *et al.*, 2006, Greene *et al.*, 2007, Al-Mahdawi *et al.*, 2008, De Biase *et al.*, 2009). Such DNA and histone modifications can be reversed, representing a suitable target for epigenetic-based therapy. Moreover, since the expanded GAA repeat in FRDA does not alter the amino acid sequence of frataxin, gene reactivation would be of therapeutic benefit (Sandi *et al.*, 2014).

In the present study, we have demonstrated the *in vitro* feasibility of two HMTase inhibitors, BIX01294 (G9a-inhibitor) and GSK126 (EZH2-inhibitor), to potentially increase frataxin expression, by reducing histone methylation levels at the *FXN* locus, and improve the disease phenotype in FRDA patient-derived fibroblasts and also fibroblasts established from YG8sR and YG8LR FRDA mouse models.

Notably, 72hr treatment with BIX01294 or GSK126 did not induce a great effect on the *FXN* gene expression in either the human or mouse FRDA fibroblasts. In fact, a dose-dependent significant decrease in *FXN* gene expression level is seen with GSK126 treatments. Previously, it was reported that chemical inhibition of G9a with BIX01294 treatment showed to decrease H3K9 methylation at the *FXN* locus but failed to up-regulate *FXN* to a significant

high level (Punga and Buhler, 2010). A possible explanation for this could be that H3K9 methylation may have a redundant role or it may cooperate with another heterochromatin mark in silencing the *FXN* gene. It is interesting to note, that on the silenced *FXN* locus there is presence of both H3K9 and H3K27 methylation at high levels. As explained above, H3K9 methylation is associated with HP1 mediated silencing of highly heterochromatinised satellite repeats whereas H3K27 is linked to polycomb-mediated silencing of formerly euchromatin genes. Typically, these two marks do not overlap in the mammalian genome (Yandim *et al.*, 2013). Therefore, one could hypothesis that there is a cooperation between the H3K9 and H3K27 methylation marks on the *FXN* locus. In fact, a study in 2003 reported an accumulation of H3K27me3 in SUV39H double null cells may partially substitute for lack H3K9me3 histone marks (Peters *et al.*, 2003).

Therefore, carrying out a combination treatment with BIX01294 and GSK126 showed to promote a safe induction of *FXN* mRNA expression levels in both the human and mouse FRDA fibroblasts, predominantly after a 3-day treatment period. This indicates that simultaneous inhibition of G9a and EZH2, which targets H3K9me2/3 and H3K27me3 repressive histone marks, may have beneficial effect, to some extent, in increasing *FXN* gene expression levels in FRDA. However, frataxin dipstick analysis revealed that frataxin protein expression levels remained unaffected after combined treatment with BIX01294 and GSK126, in both the human and mouse FRDA fibroblasts. This suggests that there may be other post-translational mechanisms at play, affecting either the *FXN* mRNA stability or frataxin protein translation, stability or degradation, that will require further investigation. Moreover, it would be interesting to assess the changes in frataxin precursor and intermediate forms after drug treatment. Therefore, future western blot analysis is a consideration.

Interestingly, we also identified significantly increased levels of EZH2 and G9a activity in FRDA human fibroblasts as compared to normal fibroblasts. This agrees with previous

proposals that stalled RNAPII, during RNA:DNA hybrid formation, may be recruiting high levels of HMTases to methylate histones locally and reducing *FXN* gene transcription, as a defence mechanism (Yandim *et al.*, 2013). Furthermore, following individual and combination treatment of BIX01294 and GSK126, the G9a and EZH2 levels were significantly reduced, respectively, in both the normal and FRDA human fibroblasts. This suggests that the drugs target and inhibit their corresponding HMTase activities in a non-cell type specific manner.

Moreover, significantly increased H3K9me3 and H3K27me3 levels, alongside decreased H3K9ac levels, were seen in the *FXN* 5'UTR promoter region in human FRDA fibroblasts, as previously reported (De Biase *et al.*, 2009, Sandi *et al.*, 2014). However, after combined treatment of BIX01294 and GSK126, a non-cell type specific reduction in H3K9me3 and H3K27me3, and an increase in H3K9ac was seen, which correlated well with the changes in G9a and EZH2 levels. For future studies, it would be interesting to measure the changes of these histone modifications in the flanking regions of GAA repeats, in addition to individual treatments of BIX01294 and GSK126. Furthermore, no off-target effects were observed with combined treatment of BIX01294 and GSK126. However, this was only assessed in a limited panel of endogenous control genes for both human and mouse, which did not contain any cancer-related genes. From the selection of genes investigated, TBP, USB1 and HPRT1 are known to have lower expression levels. ChIP-sequencing signals from ENCODE/SYDH in UCSE Genome Browser (genome.ucsc.edu) (Kent *et al.*, 2002) reveal that generally these genes have higher histone acetylation marks near the promoter region, with elevated H3K36me3 enrichment alongside lower H3K9me3 and H3K27me3 enrichments throughout the gene. However, thus far no studies have reported that these genes can be affected by HMTase inhibitors.

Overall, our results indicated that a combination treatment of BIX01294 and GSK126 may be effective in increasing the *FXN* gene expression levels in FRDA, by simultaneously targeting H3K9me3 and H3K27m3 repressive marks. However, based on our findings of frataxin expression levels after drug treatment, *in vivo* animal studies are not proposed at this stage.

Compared to other epigenetic-based therapies, the use of HMTase inhibitors is still highly underexplored in FRDA. Since larger expanded GAA repeats are highly associated with heterochromatin mediated *FXN* gene silencing, it is crucial to carry out future *in vitro* studies using patient-derived cells with higher GAA repeats, and possibly different cell culture systems. Furthermore, it would be interesting to also investigate the synergistic effect of HMTase inhibitors with other epigenetic-based drugs, such as HDAC inhibitor or DNMT inhibitors, in the activation of *FXN* gene transcription. Recent FXS studies revealed positive results using a combination treatment with both GSK126 and 5-azadC, which significantly increased *FMR1* gene expression in FXS cells (Kumari and Usdin, 2016). Moreover, since HDAC inhibitors have been shown to increase frataxin expression levels previously in cellular and animal models (reviewed in Nageshwaran and Festenstein (2015)), simultaneous administration of both HDAC inhibitors and HMTase inhibitors may produce beneficial therapeutic effects in FRDA. Overall, our study encourages the use of simultaneous administration of two or more epigenetic-based drugs for further preliminary studies to improve disease phenotype in FRDA.

CHAPTER IV - PROTEASOME INHIBITOR *IN VITRO* THERAPEUTIC STUDIES

4.1 Introduction

4.1.1 Proteasomal degradation of proteins

Nearly all proteins in mammalian cells are continually being degraded and replaced by *de novo* synthesis. Protein turnover is crucial for the cell fate and is predominantly regulated by the ubiquitin proteasome pathway (UPP), a highly conserved system from yeast to mammals (Bochtler *et al.*, 1999). The UPP plays a pivotal role in the degradation of regulatory proteins involved in essential cellular pathways, including cell cycle progression, DNA repair, apoptosis, transcription and immune response (Table 4.1). The orderly degradation of cellular proteins by UPP is critical to maintain cellular homeostasis (Glickman and Ciechanover, 2002, Nawaz and O'Malley, 2004). The UPP consists of enzymes that link substrate proteins with an ubiquitin chain, in an ATP-dependent process, to tag them for their subsequent recognition and degradation by the 26S proteasome (Baumeister *et al.*, 1998, Glickman and Ciechanover, 2002, Pickart and Eddins, 2004) (Figure 4.1). The process begins with the E1 ubiquitin activating enzyme, which first adenylates the C terminus of ubiquitin (via ATP hydrolysis) to form a reactive thioester bond with a surface cysteine residue. E1 then transfers the activated ubiquitin to an E2 ubiquitin-conjugating enzyme to form a new thioester. One of the over 600 E3 ligases then acts as an adaptor which promote the formation of a third thioester intermediate to bring the E2–ubiquitin complex into proximity with the target protein, and thus facilitate the transfer of ubiquitin to a surface lysine residue to form an isopeptide bond. Once the first ubiquitin is bound to its target, E2 and E3 enzymes repeat the addition of ubiquitin units to the N terminus or lysine residues of ubiquitin to form a poly-ubiquitin chain. This is then sufficient to transfer the target protein for degradation by the 26S proteasome (Hershko *et al.*, 1983, Lecker *et al.*, 2006, Bedford *et al.*, 2011). Notably, ubiquitination is dynamic and can be reversed by the action of various deubiquitinating enzymes (DUBs) (Amerik and Hochstrasser, 2004).

Eukaryotic proteasomes are often found as large 26S holoenzymes complexes, consisting of a catalytic 20S core particle and a 19S regulatory particle at either or both of its ends (Nickell *et al.*, 2009, Bedford *et al.*, 2011). In the cylindrical central core, the 20S particle is composed of four stacked rings formed by two outer heptameric α-subunits (α1-7) and two inner heptameric ß-subunits (ß1-7). The interior face of the cylinder, the ß-rings, contain up to three catalytic residues that are responsible for protein cleavages: ß1 (caspase-like), ß2 (trypsin-like) and ß5 (chymotrypsin-like) subunits. The two outer α-rings, serve as a docking domain for the 19S regulatory particle and form a gated channel leading to the inner proteolytic chamber (Groll *et al.*, 1999). The 19S regulatory particle, which is made up of a 'base' and a 'lid' is responsible for the recognition of the ubiquitin signal and directing the substrate into the 20S core particle. The outer lid contains a subunit which recognizes the polyubiquitin chain, cleaves it from the substrate and recycles the ubiquitin (Glickman and Ciechanover, 2002). Whereas, the inner base contains six ATPases, which uses ATP hydrolysis to encourage unfolding and translocation of the substrate into the 20S catalytic chamber, where they are degraded to oligopeptides (Benaroudj *et al.*, 2003).

This highly complex and tightly regulated ubiquitin-proteasome system also acts as a protein quality control, where it selectively eliminates misfolded or mutant proteins with abnormal conformations, before they build up and produce harm to the cell (Goldberg, 2003). For this reason, any aberration in this pathway has been implicated in various pathological conditions, from cancer to neurodegenerative diseases (Mani and Gelmann, 2005, Chen and Dou, 2010, Zheng *et al.*, 2016).

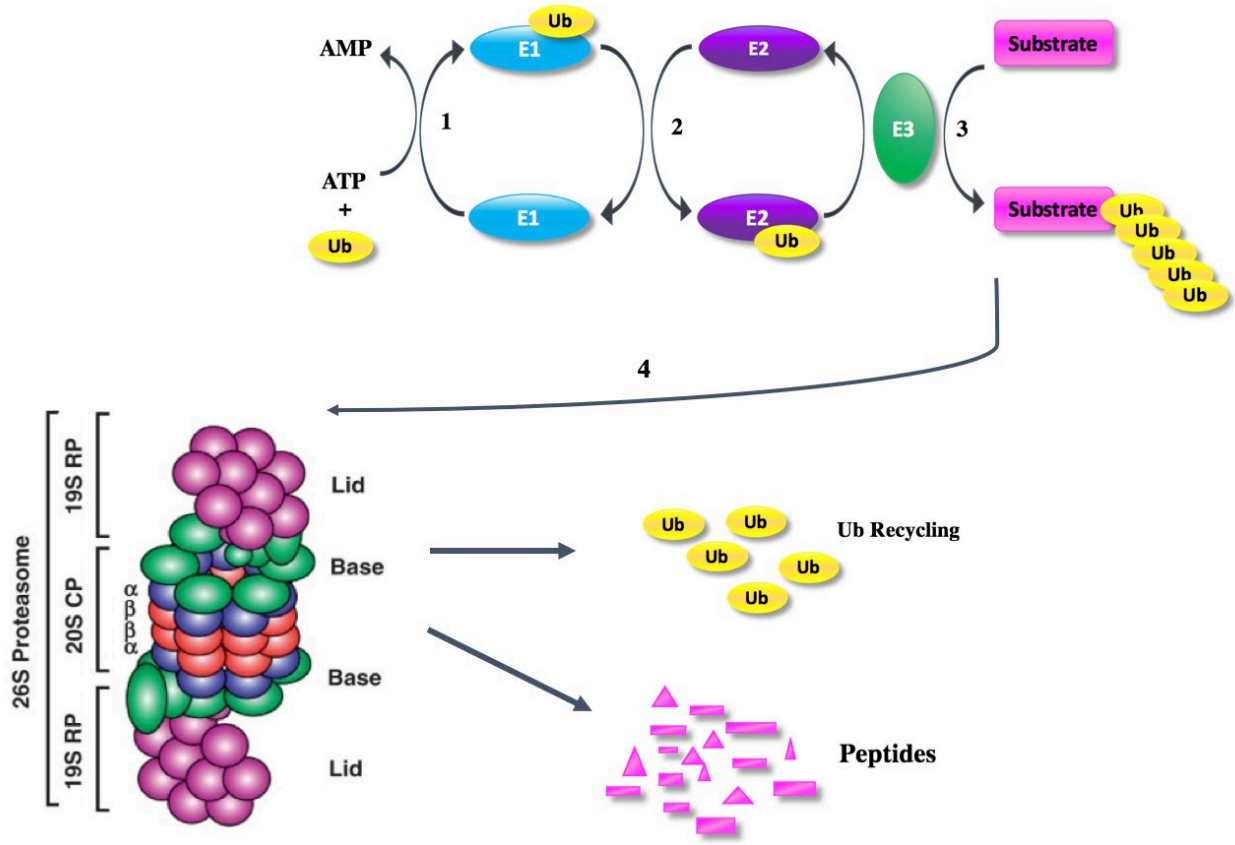

Figure 4. 1- Summary of the ubiquitin-proteasome pathway. 1) Ubiquitin (Ub) activation by the E1 ubiquitin activating enzyme; and (2) transferred to an E2 ubiquitin conjugating enzyme; (3) The E2 enzyme then transfers ubiquitin to a target protein with the assistance of an E3 ubiquitin ligase. This process is then repeated to form polyubiquitin chains, (4) that are recognized by 26S proteasome leading to degradation of the target protein and the recycling of the ubiquitin units (Image annotated from Erales and Coffino (2014).

4.1.2 Proteasome-mediated degradation of frataxin protein

Rufini *et al.* (2011), investigated whether the ubiquitin-proteasome system plays a role in modulating frataxin protein stability and its physiological turnover. By treating HEK-293 cells, which stably expresses frataxin, with an effective proteasome inhibitor, they revealed a remarkable accumulation of frataxin precursor and mature levels (Figure 4.2). This suggests that a significant fraction of frataxin (especially the precursor form) is constitutively targeted to the UPP for degradation. Moreover, by co-immunoprecipitation approaches, they also showed that frataxin can be mono- and poly-ubiquitinated in culture following proteasome inhibition. This verified that frataxin precursor is targeted to proteasomal degradation by ubiquitin labelling. Subsequent analysis then identified a single lysine residue, K^{147}, within frataxin as the ubiquitination targeting site for degradation. The substitution of this single K^{147} residue with arginine has shown to prolong the frataxin half-life and abrogat virtually all the mono-ubiquitination signal. This effect was then shown to be corrected with the reintroduction of K^{147} (Rufini *et al.*, 2011). These findings were also confirmed in human lung adenocarcinoma (Calu-6) cells stably expressing frataxin (Lavecchia *et al.*, 2013).

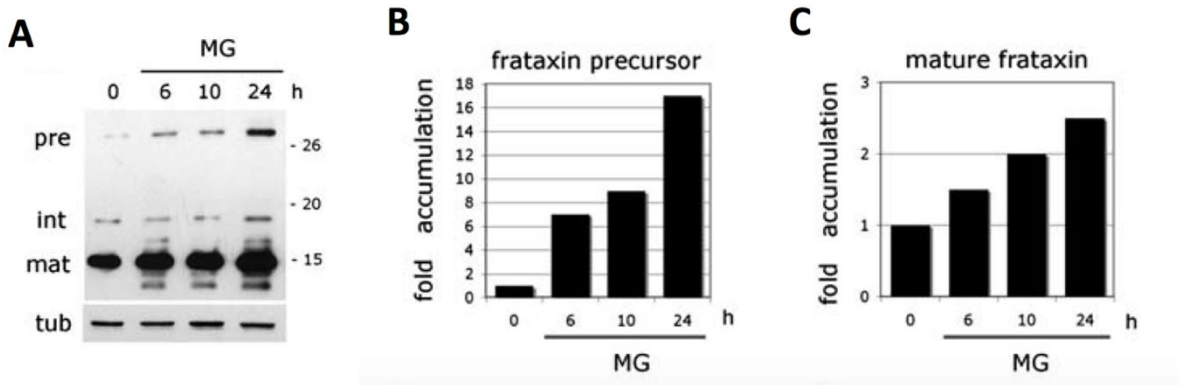

Figure 4. 2 - Frataxin abundance is controlled by the proteasome. A) HEK-293 Flp-In cells stably transfected with frataxin$^{1-210}$ were treated for the indicated times with 10 mM MG132. Total cell extracts were analyzed by SDS–PAGE and revealed by immunoblotting with anti-frataxin antibody (upper panel) or anti-tubulin (lower panel). One representative experiment out of four performed with similar results is shown. MG - MG132; Pre - precursor; int - intermediate; mat - mature; tub - tubulin. B and C) Quantitative analysis of frataxin precursor and mature accumulation upon MG132 treatment of HEK-293 Flp-In cells, as shown in (A) (Rufini *et al.*, 2011).

4.1.3 Preventing frataxin ubiquitin-proteasome degradation

The recognition that frataxin stability is regulated by the UPP has opened up a new avenue to the possibility of using small molecule compounds to prevent its ubiquitination. This can be achieved by directly docking at the ubiquitin-binding site K^{147}, and subsequently rescuing intracellular frataxin deficiency. Currently, ubiquitin competing molecules (UCM) are in the discovery phase of development and have been proposed as a potential promise in FRDA treatment. Thus far, treatments of FRDA patient cells with NSC620301 and the newly developed second-generation UCMs, UCM53, UCM108 and UCM71, have been shown to inhibit ubiquitination on K^{147} and to significantly increase frataxin expression. Additionally, no modifications in frataxin protein function were observed with the treatments, and the aconitase and ATP defects were restored (Rufini *et al.*, 2011, Rufini *et al.*, 2015). Moreover, as a complementary approach to prevent frataxin degradation, Benini *et al.* (2017) identified the RING-type E3 ubiquitin ligase, RNF126, as the specific enzyme responsible for frataxin recognition and ubiquitination targeting. These findings may encourage the design of small molecules to inhibit the specific interaction between frataxin and RNF126, without disturbing its catalytic activity, as a novel FRDA therapy (Benini *et al.*, 2017).

4.2 Use of proteasome inhibitors as a therapy for FRDA

As an additional therapeutic strategy for FRDA, small molecule inhibitors have been developed, which are especially designed to target different steps of the UPP. These include proteasome inhibitors (PI), some of which are now approved for cancer treatments and have been shown to modulate frataxin turnover in FRDA (Richardson *et al.*, 2006, Rufini *et al.*, 2011, Kisselev *et al.*, 2012, Rentsch *et al.*, 2013, Rufini *et al.*, 2015). Therefore, in collaboration with the pharmaceutical company, Takeda Cambridge limited, we have carried out an extensive investigation on the efficacy of various PIs (MG132, Bortezomib, Salinosporamide A and Ixazomib) in preventing frataxin degradation, using human FRDA fibroblasts (GMO3816 with 330 and 380 GAA repeats, and FA1 with 416 and 590 GAA repeats). Cells derived from FRDA patients constitute the most relevant frataxin-deficient cell model as they carry the complete frataxin locus together with GAA repeat expansions and all the regulatory sequences. Moreover, as sensory neurons and cardiomyocytes (which are particularly affected in FRDA) are hard to obtain from patients, primary fibroblasts are easily accessible and offer an alternative source of cell material to study therapeutic candidates in modulating frataxin levels.

4.2.1 Results

4.2.2 Therapeutic testing of MG132

The peptide aldehyde, MG132 (Z-Leu-Leu-Leu-CHO), constructed by Roc et al in 1994, was the first discovered inhibitor of the 20S proteasomes (Vinitsky *et al.*, 1992, Rock *et al.*, 1994) (Figure 4.3). Chemically, MG132 reacts with the hydroxyl group of the N-terminal threonine of the active site β5-subunit, to form a reversible hemiacetal, which blocks the chymotrypsin like activity of the 26S proteasomes (Zhang *et al.*, 2013). Although, MG132 has never been tested clinically due to its rapid oxidation, it has proved to be a valuable research tool for *in vitro* investigation (Pellom and Shanker, 2012). In culture, MG132 has been shown to inhibit the growth of tumour cells by inducing the cell cycle arrest, as well as triggering apoptosis (Guo and Peng, 2013). Moreover, HEK-293 Flip-In cells stably expressing frataxin$^{1\text{-}210}$ treated with MG132 have also shown a 15-fold and 2.5-fold accumulation of frataxin precursor and mature forms, respectively (Figure 4.2) (Rufini *et al.*, 2011). Therefore, in an effort to overcome impaired frataxin processing, we have investigated MG132 as a potential therapy for FRDA.

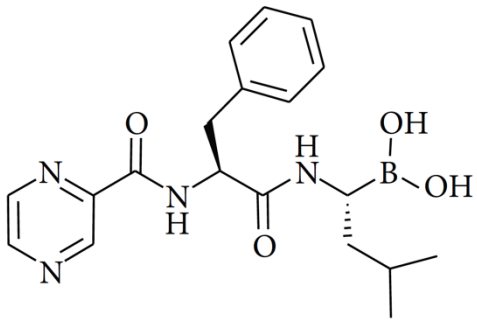

Figure 4. 3 - Molecular structure of MG132

4.2.2.1 Cell viability assessment

To assess the cellular toxicity of MG132, human fibroblasts were treated for 72hrs in triplicates with 1nM to 10µM MG132, followed by PrestoBlue (Invitrogen) cell viability assay to quantitatively measure the proliferation of cells. The mean value of the triplicates was normalised to the corresponding vehicle treated fibroblasts, which was set as 100% arbitrarily. Surprisingly, all MG132 treatments with up to 10µM concentration were considerably safe and tolerable, where no significant reduction in cell viability was observed after treatment, in both the normal and FRDA human fibroblasts (Figure 4.4). Therefore, to understand the therapeutic efficacy of MG132 in FRDA, subsequent molecular analysis was carried out using 100nM and 10µM concentrations as the optimal dosing.

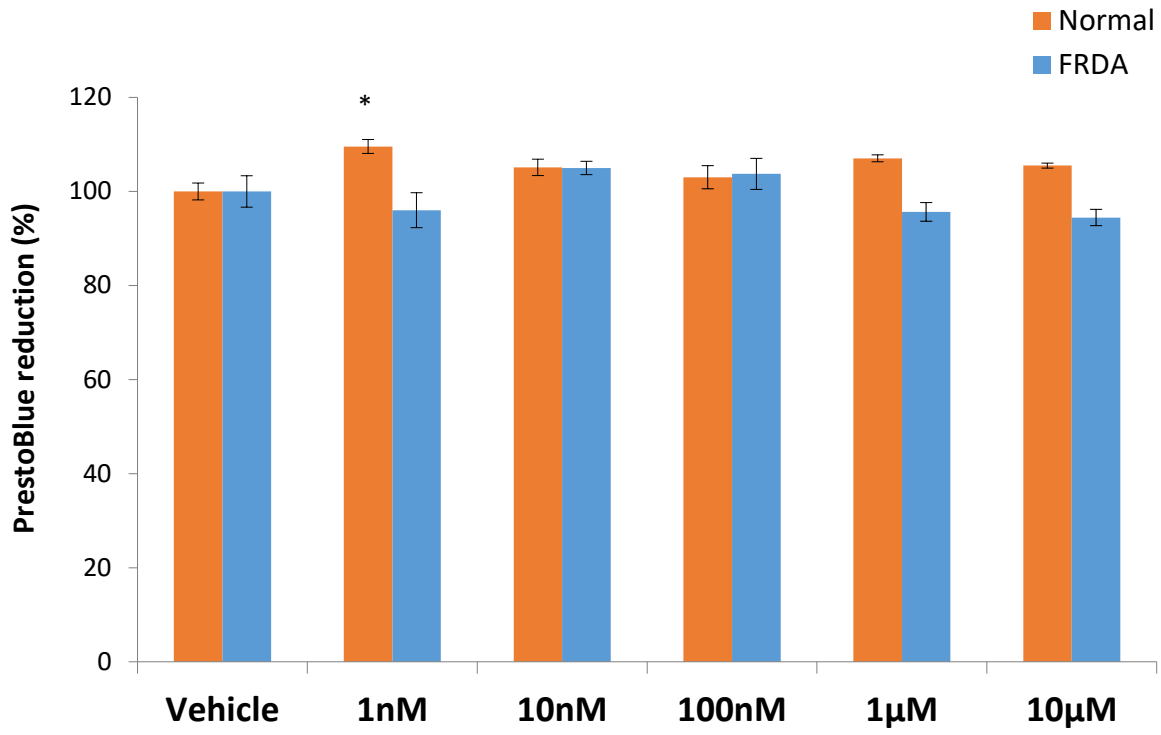

Figure 4. 4 - PrestoBlue cell viability analysis of human primary fibroblasts following 72hr MG132 treatment. All data was normalised to the mean average PrestoBlue reduction of the corresponding vehicle treated cell lines (set at 100%). Error bars indicate SEM and values represent mean ±SEM (n=3). Asterisks indicate significant differences between drug and vehicle treated cell lines, assessed by Student's *t*-test (*P<0.01).

4.2.2.2 Protein quantification assessment

In order to understand the effectiveness of MG132 treatment in FRDA, comparative protein expression levels of c-Jun (a UPP substrate), $p27^{Kip1}$ (a key cell cycle regulator controlled by UPP), PSMB5 (20S proteasome subunit ß-5) and mature frataxin forms were identified by western blotting. Human primary fibroblasts were treated with 100nM and 10µM MG132 for 72hrs, followed by protein extraction and protein concentration determination using the Pierce™ BCA protein assay kit (Thermo Scientific), as described in Chapter 2, section 2.17-18. Western analysis was then carried out to identify protein expression levels using specific primary antibodies and secondary-HRP conjugated antibodies, as described in Chapter 2, section 2.19. Densitometry was carried out using ImageJ software and the values were normalised to those of actin. MG132 treatment in FRDA fibroblasts revealed a dose dependent increase of 32% and 39% in frataxin expression with 100nM and 10µM treatment, respectively, compared to vehicle treated cells. However, the increases were statistically not significant (Figure 4.5 A-B). To confirm these results, similar frataxin expression changes were also obtained in FRDA cells after MG132 treatment by lateral flow immunoassay dipstick analysis (MitoSciences) (Figure 4.6). Moreover, to assess the proteasome inhibitory effect of MG132, c-Jun expression levels were determined following treatment. FRDA fibroblasts show a significant increase in c-Jun levels as compared to normal fibroblasts, as previously described by Pianese et al (2002) (Figure 4.5 A and C). However, after MG132 treatment, no significant changes in c-Jun levels were detected in FRDA cells. Comparably, MG132 treatment did not induce any significant changes in the cellular stress marker levels, $p27^{Kip1}$, and in the proteasome complex activity, PSMB5, in either the normal or FRDA fibroblast cells (Figure 4.5 A, D-E). This suggest, that the proteasomal inhibitory activity of MG132 at 100nM and 10µM is considerably ineffective in FRDA primary fibroblasts.

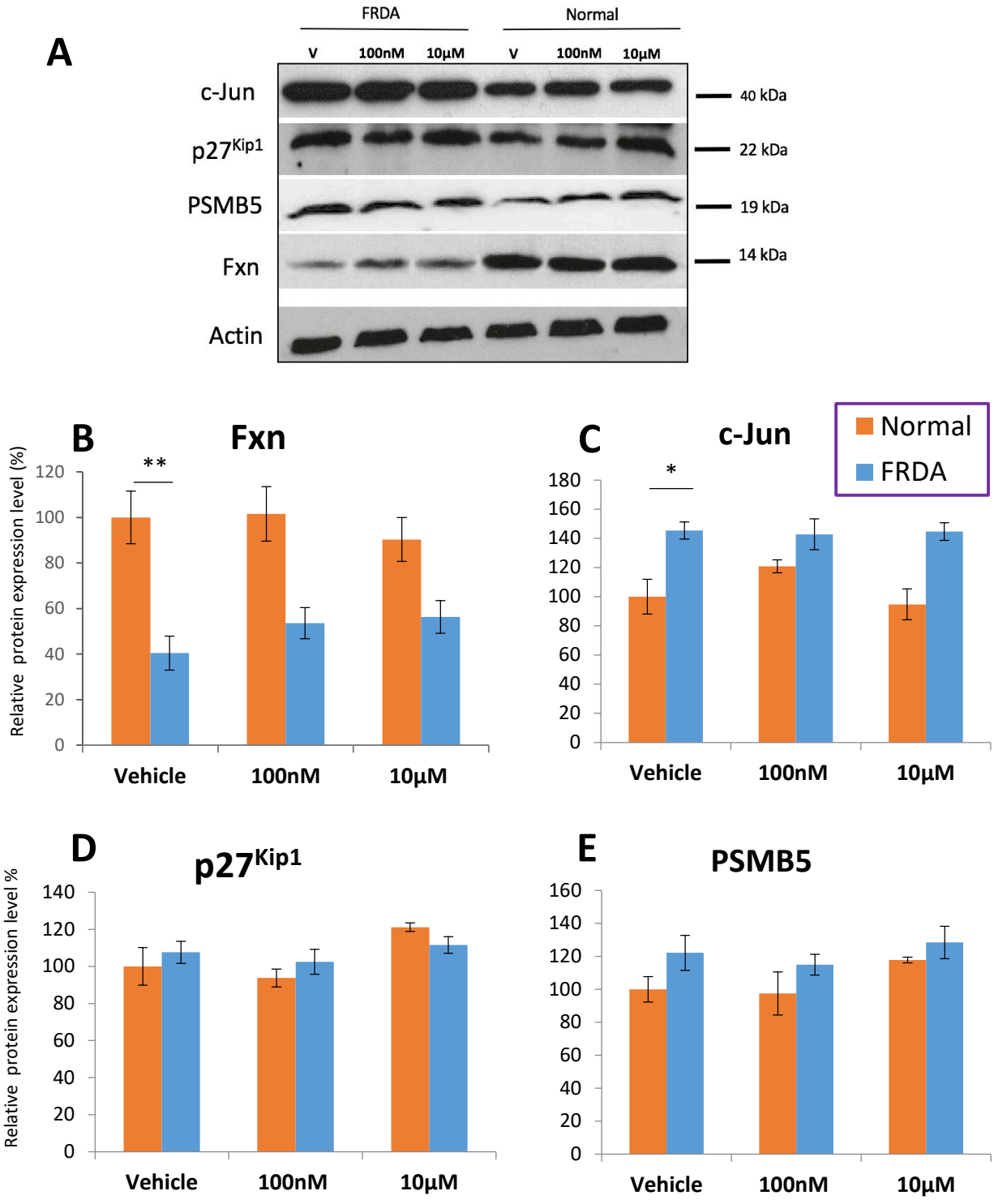

Figure 4. 5 - Dose-response western analysis of human FRDA and normal fibroblast cells treated with MG132 for 72hrs. A) Total cell extracts were analysed by SDS-PAGE and revealed by immunoblotting with anti-frataxin, anti-cJun, anti-p27^{Kip1} and anti-PSMB5, and anti-actin as a control. One representative experiment out of three performed with similar results is shown. V- vehicle (DMSO). B-E) Densitometry analysis of frataxin, c-Jun, p27^{Kip1}, PSMB5 upon MG132 treatment of human fibroblasts as shown in (A). The values were expressed as a ratio to the vehicle treated samples of normal fibroblasts. (*P<0.05, **P<0.01, error bars ±SEM).

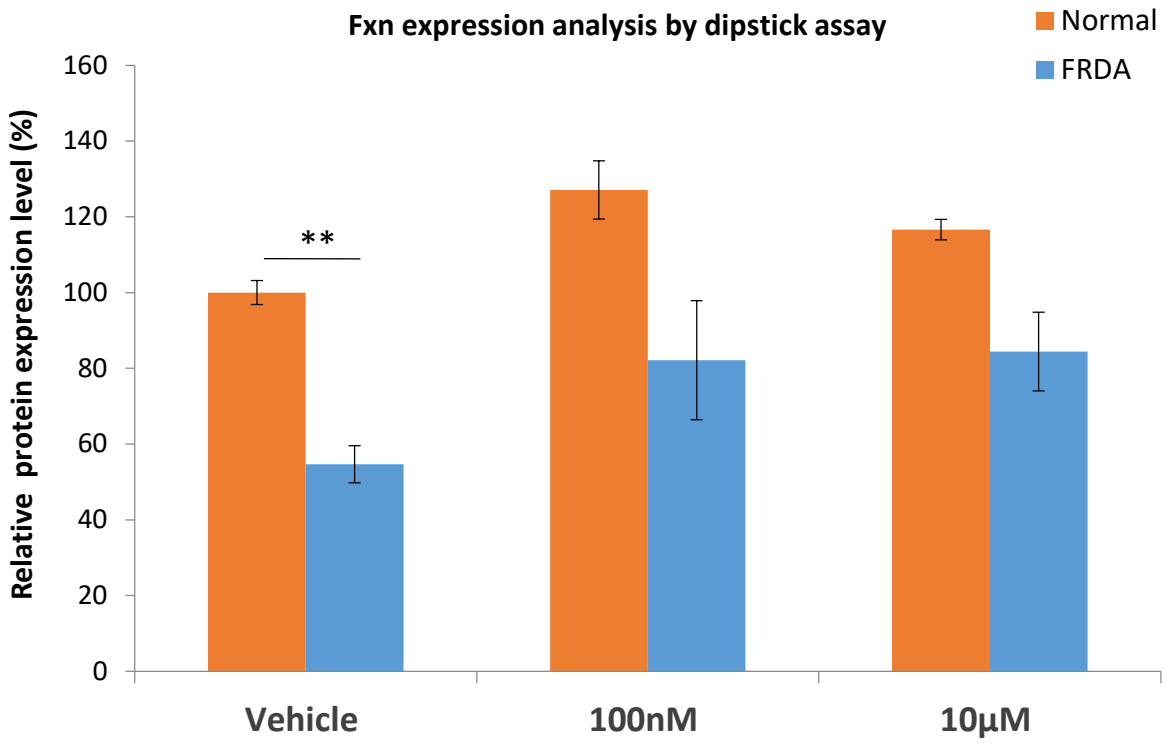

Figure 4. 6 - Relative frataxin protein expression levels in human normal and FRDA primary fibroblasts following MG132 treatment for 72hrs. The change in frataxin levels were determined by the dipstick immunoassay. The values were expressed as a ratio to the vehicle treated samples of normal fibroblasts. Error bars indicate SEM and values represent mean ±SEM (n=3). Asterisks indicate significant differences between drug and vehicle treated cell lines, assessed by Student's *t*-test (*P<0.01).

4.2.2.3 Proteasomal activity analysis

The inhibitory effect of MG132 was also analysed by determining the proteasome chymotrypsin-like activity in normal and FRDA fibroblasts. Cells were treated with 100nM and 10µM MG132 for 72hrs, followed by proteasome-Glo cell based assay assessment (Promega). When added to cultured cells, proteasomes cleave off luciferin from the specific luminogenic proteasome substrates in buffers. This is consumed by luciferin, and a rapid luminescent signal is generated that correlates directly to the chymotrypsin-like protease activity. The mean value of the vehicle and drug treated triplicates were used for calibration to untreated normal cells, which was set as 100% arbitrarily. Results obtained indicated that MG132 does not induce any changes to the chymotrypsin-like activity of the proteasome at 100nM and 10µM concentrations, in both the normal and FRDA primary fibroblasts (Figure 4.7). Although a decrease in chymotrypsin-like activity is seen in normal fibroblast cells after 10µM treatment, the difference was statistically insignificant.

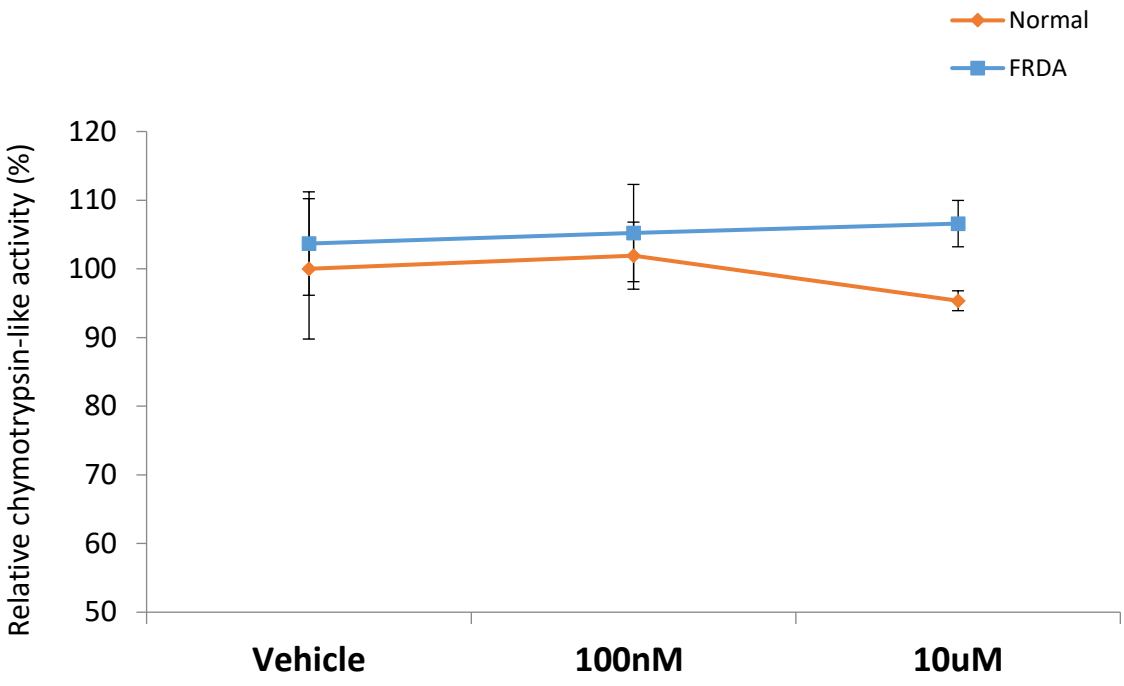

Figure 4. 7 - Relative change in chymotrypsin-like activity in FRDA and normal fibroblasts after 72hrs of MG132 treatment. The values were expressed as a ratio to the vehicle treated samples of normal fibroblasts. Error bars indicate SEM and values represent mean ±SEM (n=3).

4.2.3 Therapeutic testing of bortezomib

Bortezomib (Velcade®) is a PIs approved by the FDA for the treatment of multiple myeloma by targeting the proteasome (Kane *et al.*, 2003, Kane *et al.*, 2006, Richardson *et al.*, 2009) (Figure 4.8). Similar to MG132, bortezomib is chemically a dipeptidyl boronic acid derivative, which forms a reversible complex with the active site of threonine hydroxyl group in the β5-subunit, blocking the chymotrypsin-like activity of the proteasome. It also binds the β1 subunit with lower affinity, inhibiting its caspase-like activity (Adams and Kauffman, 2004, Crawford *et al.*, 2006, Chen *et al.*, 2011). This is then responsible for the disruption of various signalling pathways, resulting in cell cycle arrest and apoptotic induction in tumour cells (Chen *et al.*, 2011). Moreover, previous FRDA studies using His-frataxin transfected Calu-6 cells, revealed a 2.6-fold increase in frataxin levels after bortezomib treatment (Lavecchia *et al.*, 2013). Therefore, based on these encouraging reports, we decided to investigate whether bortezomib will rescue the impaired frataxin expression in human FRDA fibroblasts.

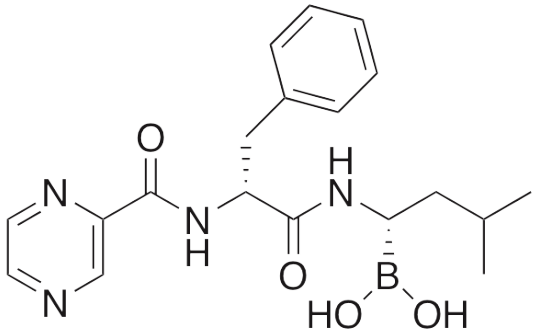

Figure 4. 8 - Molecular structure of bortezomib

4.2.3.1 Cell viability assessment

The safety and cellular tolerability of bortezomib was investigated by the PrestoBlue cell viability assay. The human primary fibroblasts (normal and FRDA) were treated in triplicates with 0.5nM to 1µM bortezomib for 72hrs, followed by PrestoBlue analysis. Bortezomib treatment at concentrations ranging from 0.5nM to 5nM revealed to be considerably safe for administration in both the normal and FRDA human fibroblasts, as no significant change in cell viability was seen when compared to vehicle treated cells (Figure 4.9). However, treatment with higher bortezomib concentrations showed to be significantly harmful to the cell lines, where a reduction in cell viability is observed in a dose-dependently. Therefore, for subsequent molecular analysis we decided to use 0.5nM and 2nM of bortezomib as the optimal compound dosing in the human fibroblast treatment.

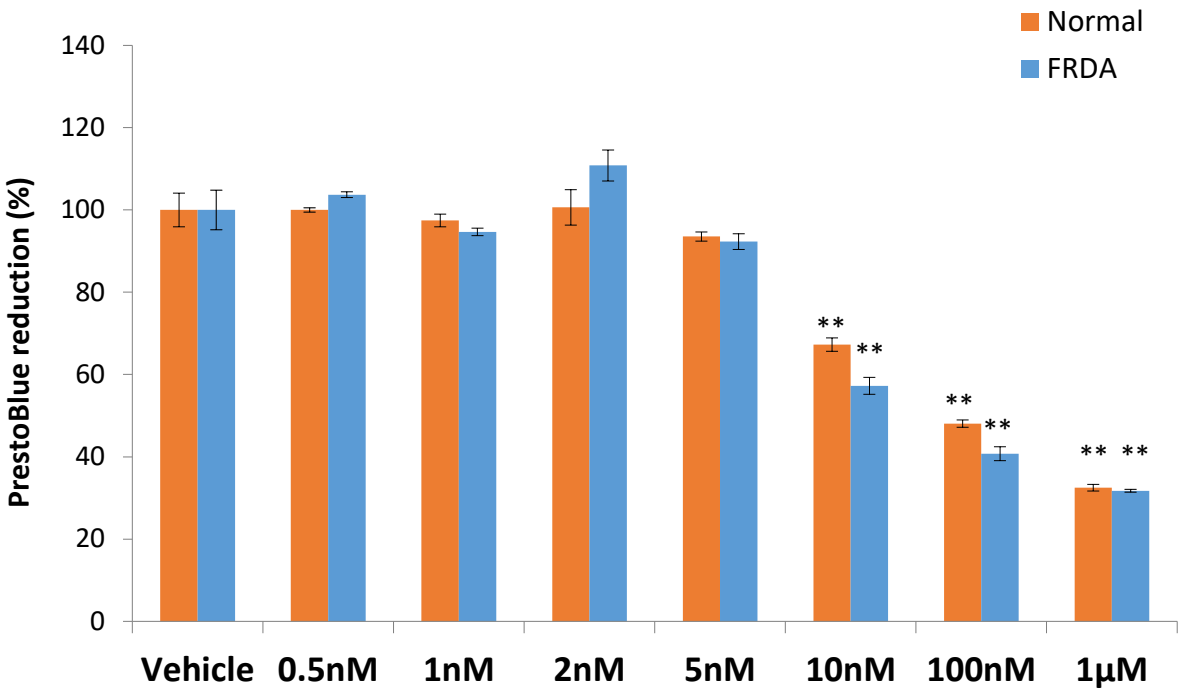

Figure 4. 9 - PrestoBlue cell viability analysis of human primary fibroblasts following 72hr bortezomib treatment. All data was normalised to the mean average of PrestoBlue reduction of the corresponding vehicle treated cell line (set at 100%). Error bars indicate SEM and values represent mean ±SEM (n=3). Asterisks indicate significant differences between drug and vehicle treated cell lines, assessed by Student's *t*-test (**P<0.01).

4.2.3.2 Protein quantification assessment

In order to assess the effectiveness of bortezomib in FRDA, human fibroblasts were treated with 0.5nM and 2nM concentration for 72hrs. Subsequently, cells were collected and protein expression levels of mature frataxin, c-Jun, $p27^{Kip1}$ and PSMB5 were assessed by western analysis with specific primary antibodies.

Bortezomib treatment revealed no significant change in frataxin expression levels in both the normal and FRDA human primary fibroblasts, compared to vehicle treatment (Figure 4.10 A-B). Additionally, comparable frataxin expression levels were also obtained following bortezomib treatment by the lateral flow immunoassay dipstick kit (Figure 4.11). This suggests that bortezomib, at concentrations of 0.5nM and 2nM, does not prevent frataxin degradation via the UPP in FRDA fibroblasts. Moreover, no significant change in the proteasome substrate level, c-Jun, was seen after treatment in both the normal and FRDA fibroblasts (Figure 4.10 A and C). Similarly, no significant change in the cellular stress marker, $p27^{Kip1}$, and the proteasome activity, PSMB5 levels, were observed after treatment (Figure 4.10 A, D-E). Although, FRDA cells indicated 30% increase in $p27^{Kip1}$ levels after 2nM bortezomib treatment, it was statistically insignificant (P=0.08). This suggests that the proteasomal inhibitory activity of 0.5nM and 2nM bortezomib is considerably ineffective in human primary fibroblasts.

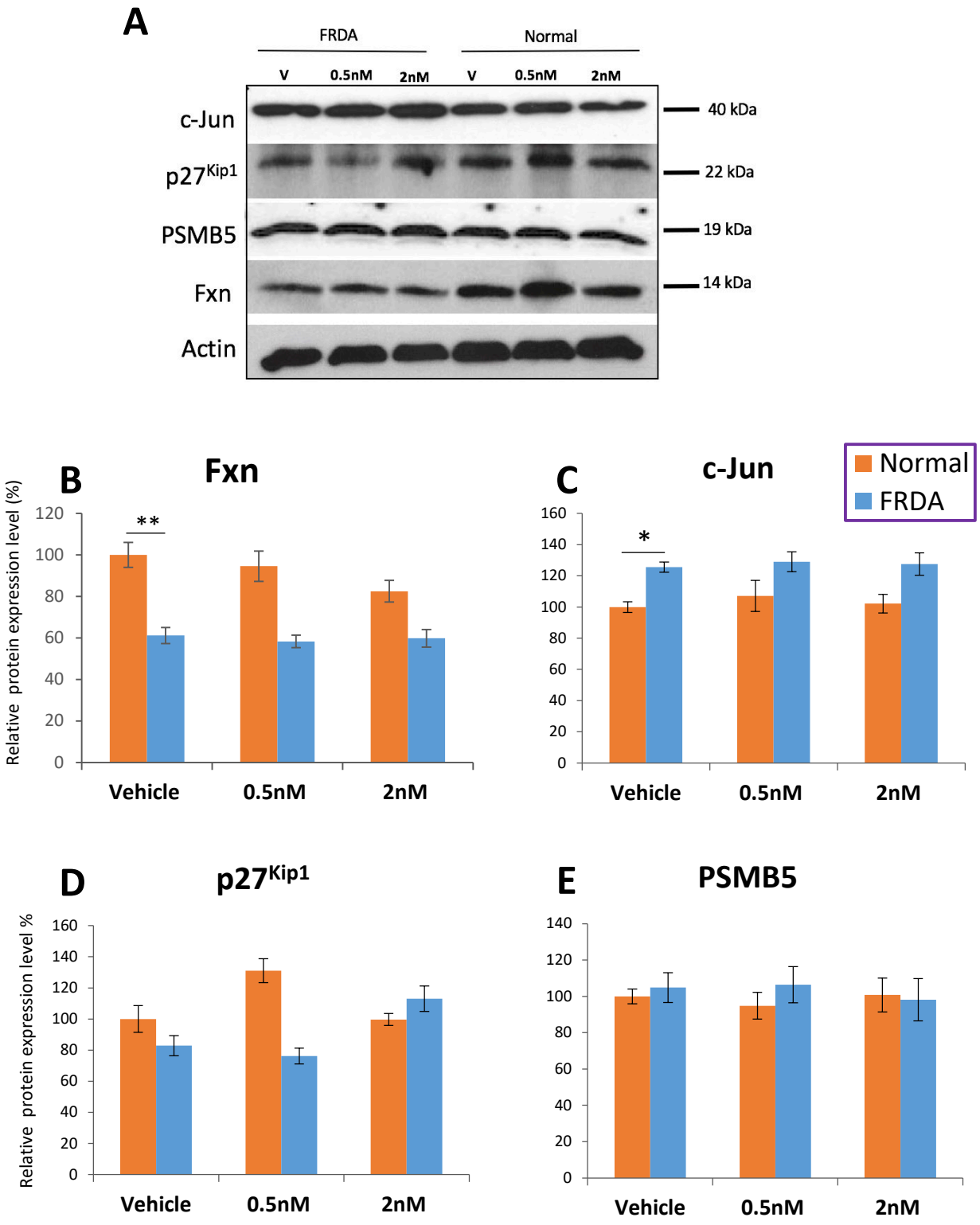

Figure 4. 10 - Dose-response western analysis of human FRDA and normal fibroblast cells treated with bortezomib for 72hrs. A) Total cell extracts were analysed by SDS-PAGE and revealed by immunoblotting with anti-frataxin, anti-cJun, anti-p27^{Kip1} and anti-PSMB5, and anti-tubulin as a control. One representative experiment out of three performed with similar results is shown. V-vehicle (DMSO). B-E) Densitometry analysis of frataxin, c-Jun, p27^{Kip1}, PSMB5 upon bortezomib treatment of human fibroblasts as shown in (A). The values were expressed as a ratio to the vehicle treated samples of normal fibroblasts. (*P<0.05, **P<0.01, error bars ±SEM).

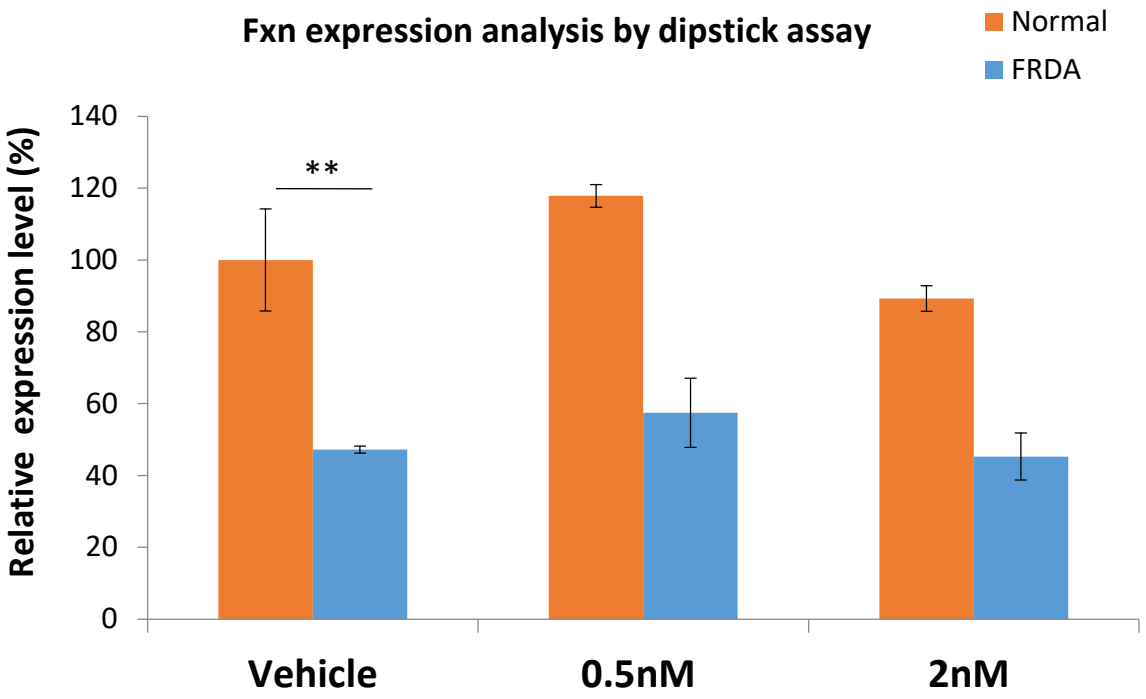

Figure 4. 11 - Relative frataxin protein expression levels in human normal and FRDA primary fibroblasts following bortezomib treatment for 72hrs. The change in frataxin levels were determined by the dipstick immunoassay. The values were expressed as a ratio to the vehicle treated samples of normal fibroblasts. Error bars indicate SEM and values represent mean ±SEM (n=3). Asterisks indicate significant differences between drug and vehicle treated cell lines, assessed by Student's *t*-test (**P<0.01).

4.2.3.3 Proteasomal activity analysis

In order to understand the proteasomal inhibitory effect of bortezomib treatment, the trypsin-like and chymotrypsin-like activity were analysed in the human FRDA primary fibroblasts. Cells were treated with 0.5nM and 2nM bortezomib for 72hrs, followed by assessment with specific proteasome-Glo cell based assay. As expected, bortezomib treatment has significantly reduced the proteasomes chymotrypsin-like activity in FRDA primary fibroblasts with 1nM (by 71%, $P<0.001$) and 10nM (by 45%, $P<0.05$) (Figure 4.12). However, a similar effect is also seen in normal cells after bortezomib treatment, suggesting that bortezomib may have a non-cell type specific effect in reducing the chymotrypsin-like activity. Moreover, it is interesting to note that the trypsin-like activity was found to be significantly higher by 95% ($P<0.001$) in FRDA cells, compared to normal cells. Nonetheless, this activity was reduced dose-dependently after bortezomib treatment, but the changes were statistically non-significant. No changes were observed in trypsin-like activity levels in the normal fibroblasts after treatment.

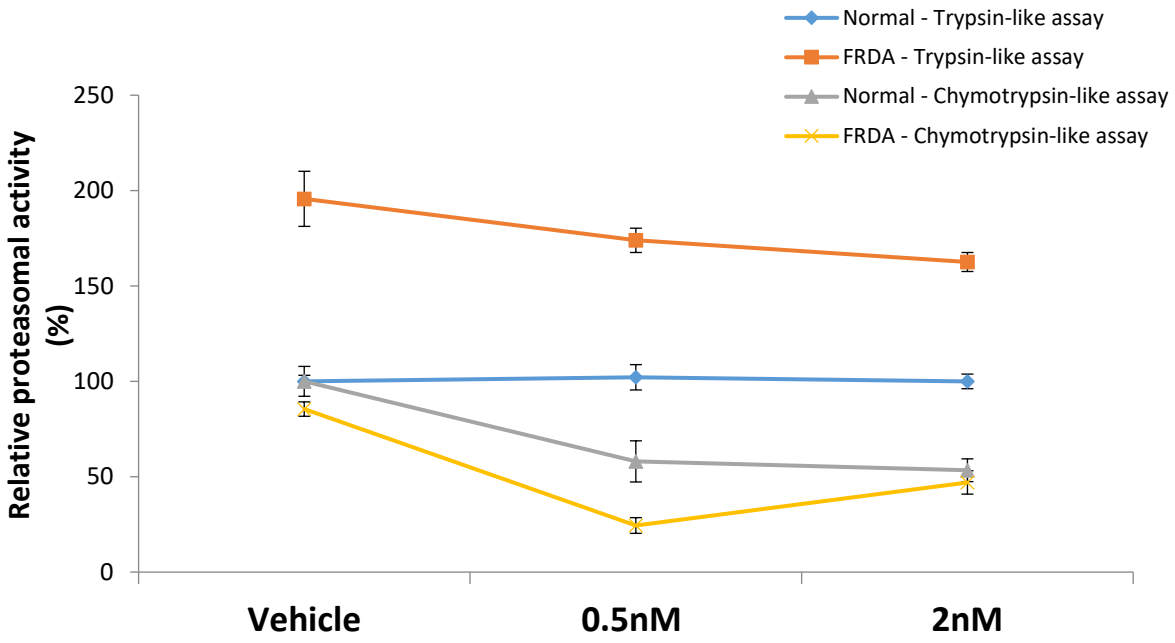

Figure 4. 12 - Relative change in trypsin-like and chymotrypsin-like activity in FRDA and normal fibroblasts after 72hrs of bortezomib treatment. The values were expressed as a ratio to the vehicle treated samples of normal fibroblasts. Error bars indicate SEM and values represent mean ±SEM (n=3).

4.2.4 Therapeutic testing of Ixazomib

The second generation PI, Ixazomib (trade name Ninlaro), is the first orally-administered PI to be approved by FDA for patients with multiple myeloma (Muz *et al.*, 2016). Ixazomib was initially developed as MLN9708, a stable citrate ester that of boranic acid. When exposed to aqueous solution or plasma, MLN9708 immediately hydrolyses to the free boric acid metabolite, MLN2238, which is the biologically active form (Figure 4.13). Similar to bortezomib and MG132, MLN2238 is a selective, potent and reversible PI that preferentially binds to and inhibits the β5 (chymotrypsin-like) proteolytic site of the 20S proteasome. At higher concentrations, the inhibition of β1 (caspase-like) and β2 (trypsin-like) proteolytic sites are also seen (Kupperman *et al.*, 2010).

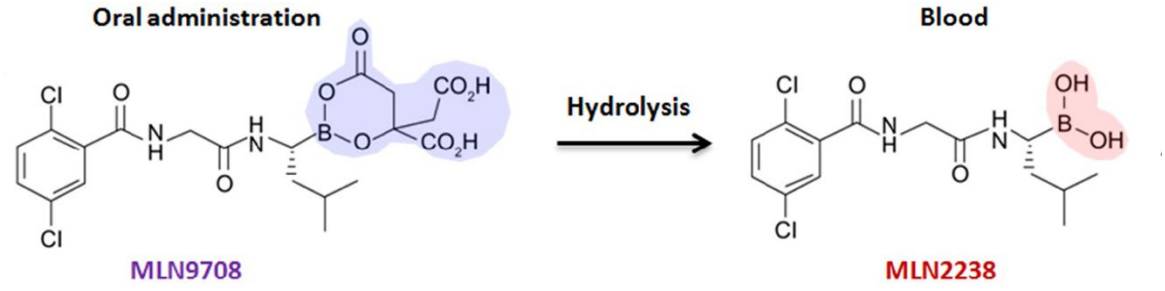

Figure 4. 13 - Chemical structure of the two forms of ixazomib (MLN9708 and MLN2238). MLN9708 administered orally as a capsule, is rapidly absorbed and hydrolyzed to the biologically active form, MLN2238, when it comes in contact with aqueous plasma.

Although the potency and selectivity of MLN2238 were generally similar to bortezomib, the proteasome dissociation half-life is approximately sixfold faster for ixazomib than bortezomib, which is believed to contribute to its superior tissue penetration and wider distribution (Al-Salama *et al.*, 2017). *In vitro*, MLN2238 reduces tumour progression in several human multiple myeloma cell lines by inducing apoptosis, and disrupts the interaction of MM cells with the BM microenvironment resulting in decreased angiogenesis and osteolytic lesions (Muz *et al.*, 2016). These results were consistent with *in vivo* findings

where oral doses of MLN2238 induced a significant anti-tumour activity and increase in survival, in tumour xenograft models (Kupperman *et al.*, 2010) and multiple myeloma models (Chauhan *et al.*, 2011).

Since, bortezomib and MG132 have been reported previously to rescue frataxin from UPP degradation, we decided to also investigate the potential therapeutic effect of ixazomib in FRDA, using human FRDA fibroblasts.

4.2.4.1 Cell viability assessment after drug treatment

To investigate the safety and cellular tolerability of ixazomib, both normal and FRDA human fibroblasts were treated in triplicates with 1nM to 10µM ixazomib for 72hrs. This was followed by PrestoBlue cell viability analysis, to quantitatively measure the proliferation of cells after treatment. The mean value of the triplicates was normalised to vehicle treated normal fibroblasts, which was set as 100% arbitrarily. The results obtained indicated that ixazomib treatment was significantly toxic to human fibroblasts with 100nM to 10µM concentrations, where a dose-dependent reduction in cell viability was seen (Figure 4.14). However, lower concentrations (1nM and 10nM) of ixazomib were considered safe to human fibroblasts, as no significant changes in cell viability was observed. Therefore, 1nM and 10nM were then chosen as the optimum ixazomib concentrations for further analysis.

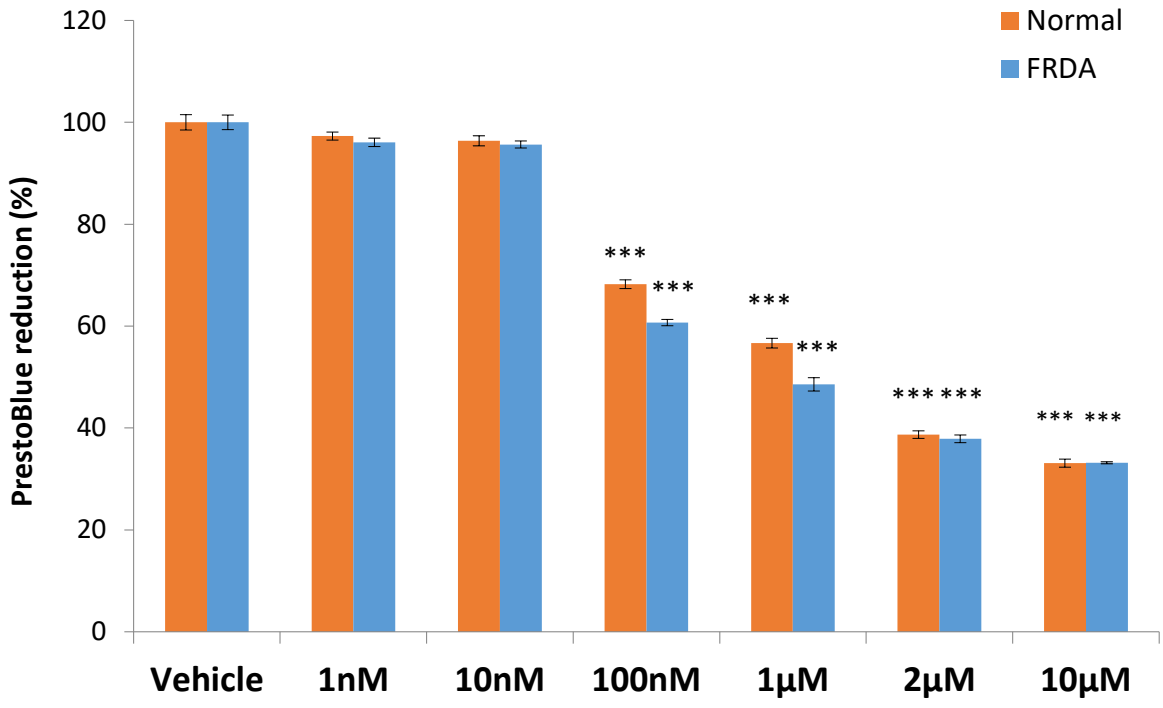

Figure 4. 14 - PrestoBlue cell viability analysis of human primary fibroblasts following 72hr ixazomib treatment. All data was normalised to the mean average of PrestoBlue reduction of control cells (set at 100%). Error bars indicate SEM and values represent mean ±SEM (n=3). Asterisks indicate significant differences between drug and vehicle treated cell lines, assessed by Student's *t*-test (***P<0.001).

4.2.4.2 Protein quantification assessment

The efficacy of ixazomib in FRDA was subsequently investigated by treating normal and FRDA human primary fibroblasts with 1nM and 10nM concentrations for 72hrs. This was followed by cell collection and protein expression analysis of frataxin, c-Jun, $p27^{Kip1}$ and PSMB5, by western analysis using specific primary antibodies. Densitometry was carried out using ImageJ software, where the values were normalised to those of tubulin as an endogenous control. Western blot analysis revealed an increase in frataxin expression levels after 1nM and 10nM ixazomib treatment in FRDA fibroblasts by 23% and 27%, respectively (Figure 4.15 A-B). However, the changes were statistically not significant. These changes in frataxin were also confirmed by the lateral flow immunoassay dipstick kit (MitoSciences), where a statistically significant increase of 76% ($P<0.05$) and 69% (0.05) was noted in frataxin expression levels with 1nM and 10nM treatment, respectively (Figure 4.16). Moreover, a dose-dependent increase was seen in c-Jun and $p27^{Kip1}$ levels, with 33% significant increase ($P<0.05$) in $p27^{Kip1}$ levels after 10nM ixazomib treatment in FRDA fibroblast (Figure 4.15 A, C-D). However, no significant changes were seen in PSMB5 levels after treatment in both normal and FRDA fibroblasts (Figure 4.15 A, E). This suggests that ixazomib may have some therapeutic effects in preventing frataxin proteasomal degradation.

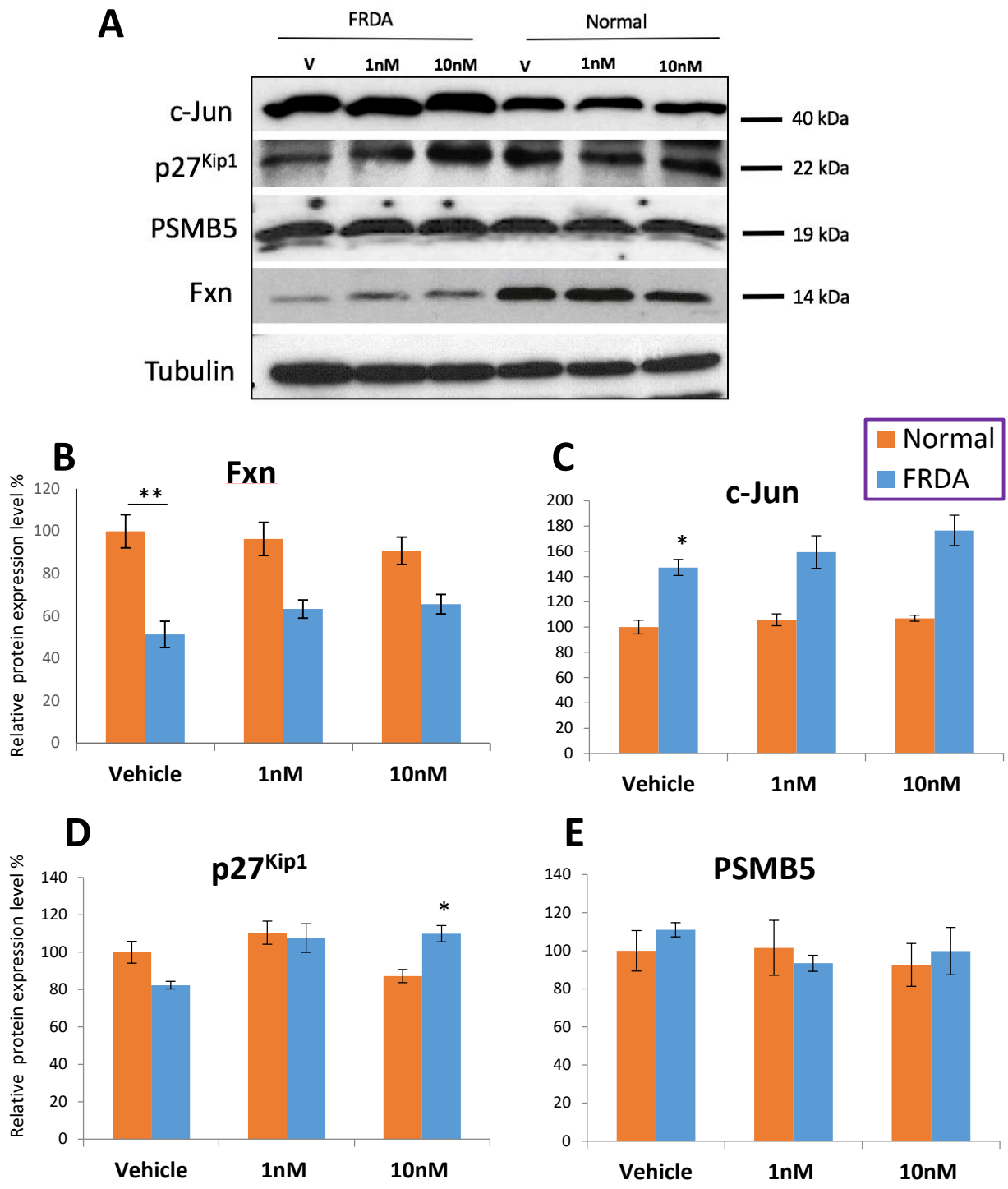

Figure 4. 15 - Dose-response western analysis of human FRDA and normal fibroblast cells treated with ixazomib for 72hrs. A) Total cell extracts were analysed by SDS-PAGE and revealed by immunoblotting with anti-frataxin, anti-cJun, anti-p27^{Kip1} and anti-PSMB5, and anti-tubulin as a control. One representative experiment out of three performed with similar results shown. V- Vehicle (DMSO). B-E) Densitometry analysis of frataxin, c-Jun, p27^{Kip1}, PSMB5 upon ixazomib treatment of human fibroblasts as shown in (A). The values were expressed as a ratio to the vehicle treated samples of normal fibroblasts. (*P<0.05, **P<0.01, error bars ±SEM).

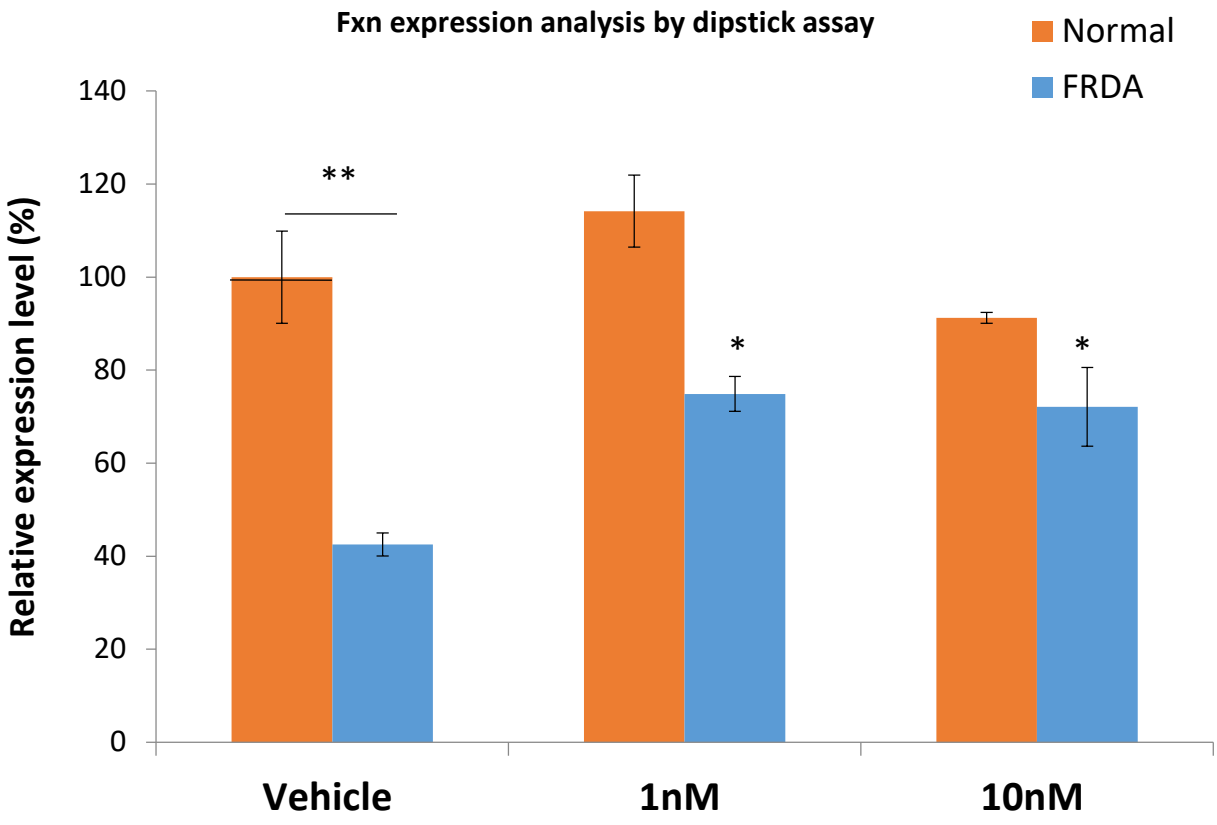

Figure 4. 16 - Relative frataxin protein expression levels in human normal and FRDA primary fibroblasts following ixazomib treatment for 72hrs. The change in frataxin levels were determined by the dipstick immunoassay. The values were expressed as a ratio to the vehicle treated samples of normal fibroblasts. Error bars indicate SEM and values represent mean ±SEM (n=3). Asterisks indicate significant differences between drug and vehicle treated cell lines, assessed by Student's *t*-test (*P<0.05, **P<0.01).

4.2.4.3 Proteasomal activity analysis

The proteasomal inhibitory effect of ixazomib in FRDA was analysed by determining the trypsin-like and the chymotrypsin-like activity in normal and FRDA fibroblasts. Cells were treated with 1nM and 10nM ixazomib for 72hrs, followed by specific proteasome-Glo cell based assay assessment. The mean value of the vehicle and drug treated triplicates were used for calibration to untreated normal cells, which was set as 100% arbitrarily. As expected, ixazomib treatment reduced the chymotrypsin-like activity with 1nM (48%, $P<0.05$) and 10nM (35%, $P=0.02$) treatment in FRDA cell line (Figure 4.17). However, no significant change in trypsin-like activity was seen after ixazomib treatment in FRDA cells. Ixazomib had no significant effect, on either the trypsin-like or chymotrypsin-like activity, in normal fibroblasts.

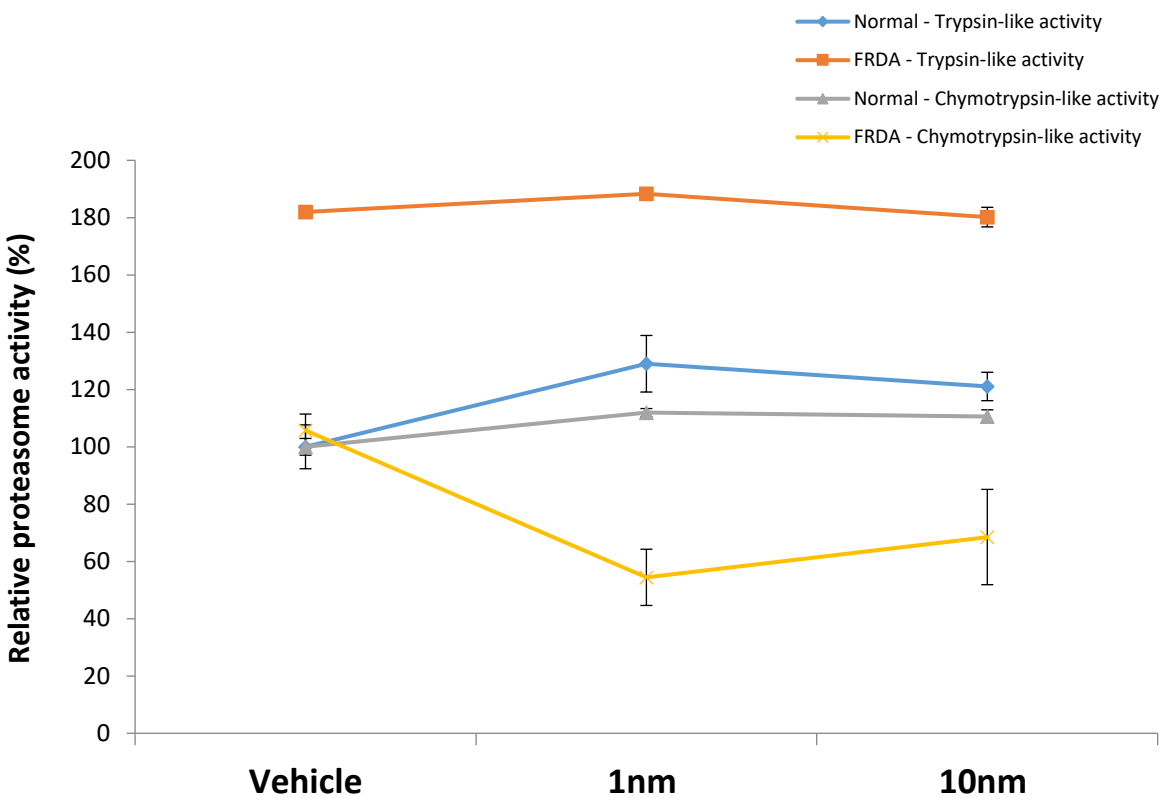

Figure 4. 17 - Relative change in trypsin-like and chymotrypsin-like activity in FRDA and normal fibroblasts after 72hrs of ixazomib treatment. The values were expressed as a ratio to the vehicle treated samples of normal fibroblasts. Error bars indicate SEM and values represent mean ±SEM (n=3).

4.2.4.4 Biochemical analysis following ixazomib treatment

Aconitase is an Fe-S cluster protein involved in iron homeostasis that is defective in FRDA cells. Aconitase activity can undergo reversible citrate-dependent modulation in response to pro-oxidants. Frataxin is an iron chaperone protein that protects the aconitase iron sulphur cluster from disassembly and promotes enzyme reactivation. Loss of aconitase activity in cells or other biological samples treated with pro-oxidants has been interpreted as a measure of oxidative damage. Therefore, we have investigated whether ixazomib treatment is able to ameliorate the impaired aconitase enzymatic activity in FRDA human fibroblasts, using the aconitase assay kit (Cayman Chemicals). In this assay, citrate is converted by aconitase into isocitrate, which is further processed resulting in a product that converts a nearly colourless probe into an intensely coloured form with MAX 450nm (Chapter 2, section 2.21). The mean values of the vehicle and drug-treated triplicates were calibrated to vehicle treated normal fibroblasts, which was arbitrarily set as 100%. As expected, the aconitase activity of human FRDA fibroblast was significantly lower (65%, $P<0.001$), as compared to normal fibroblasts (Figure 4.18). However, after 1nM and 10nM ixazomib treatment, a significant increase in aconitase activity was seen in both cell lines. This may suggest that ixazomib has non-cell type specific effects in increasing aconitase activity.

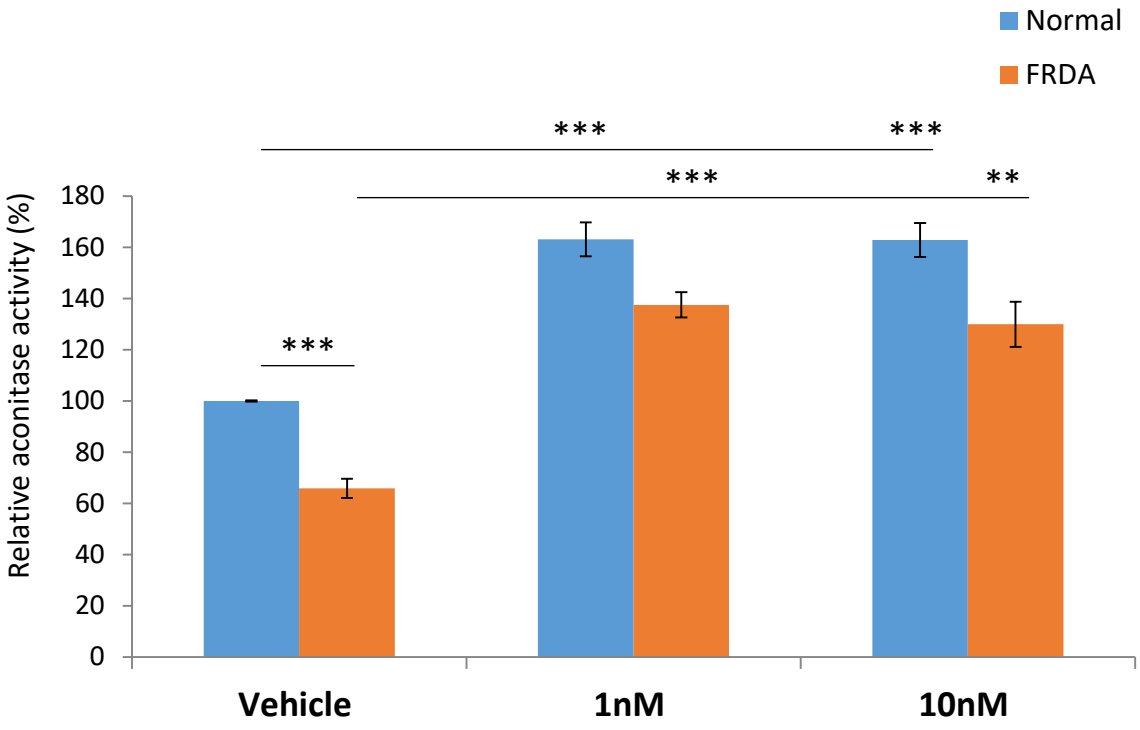

Figure 4. 18 - Relative aconitase activity levels in normal and FRDA human fibroblasts after ixazomib treatment for 72hrs. The mean aconitase activity of each sample was first normalised to the activity of the activity of vehicle treated normal fibroblasts (set to 100%). After 1nM and 10nM ixazomib treatment, the aconitase activity increased from 65% to 165% and 162%, respectively, in FRDA fibroblasts and an increase of 63% and 62%, is seen in normal fibroblasts, respectively. Error bars indicate SEM and values represent mean ±SEM (n=3). Asterisks indicate significant differences between drug and vehicle treated cell lines, assessed by Student's *t*-test (**P<0.01, ***P<0.001).

4.2.5 Therapeutic testing of salinosporamide A

Salinosporamide A (also known as marizomib or NPI-0052) (Figure 4.19) is a second-generation PI isolated from marine bacterium, *Salinispora tropica*. It was the first natural PI to be used in clinical trials for the treatment of myeloma (Fenical and Jensen, 2006). Chemically, salinosporamide A is bicycle ß-lactone-γ-lactam, and is structurally distinct from bortezomib, MG132 and ixazomib, due to its lack of peptide chain. Additionally, unlike other PIs, salinosporamide A has a unique ability to effectively inhibit all three proteolytic activities of the proteasome, by irreversibly binding with high affinity to the chymotrypsin-like (ß5), trypsin-like (ß2), and with lower affinity to the caspase-like (ß1) catalytic sites (Chauhan *et al.*, 2005). Studies have shown, that the irreversible proteasome binding of the ligand is responsible for the slower efflux, longer duration and greater potency of action of salinosporamide A, relative to other PIs (Obaidat *et al.*, 2011). Therefore, due to the encouraging reports on the proteasomal inhibitory effects of salinoporamide A, we decided to assess its potential therapeutic effects in FRDA.

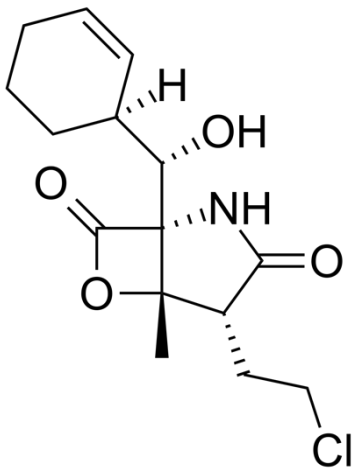

Figure 4. 19 - Molecular structure of salinosporamide A

4.2.5.1 Cell viability assessment after drug treatment

In order to evaluate the safety and cellular tolerability of salinosporamide A, both normal and FRDA primary fibroblasts were treated with 1nM to 1µM salinosporamide A for 72hrs, followed by PrestoBlue cell viability analysis. Interestingly, 1nM to 100nM salinosporamide A treatments did not produce cellular toxicity in either normal and FRDA cell lines, as no significant changes in PrestoBlue cell viability were observed (Figure 4.20). However, 1µM salinosporamide A treatment significantly reduced the cell viability by 15% ($P<0.01$) in normal fibroblasts, compared to vehicle treated cells. Therefore, as cellular tolerability was observed with 1nM to 100nM salinosporamide A treatment in both normal and FRDA fibroblasts, we continued the subsequent molecular analysis with 1nM and 100nM concentrations to investigate the efficacy of salinosporamide A.

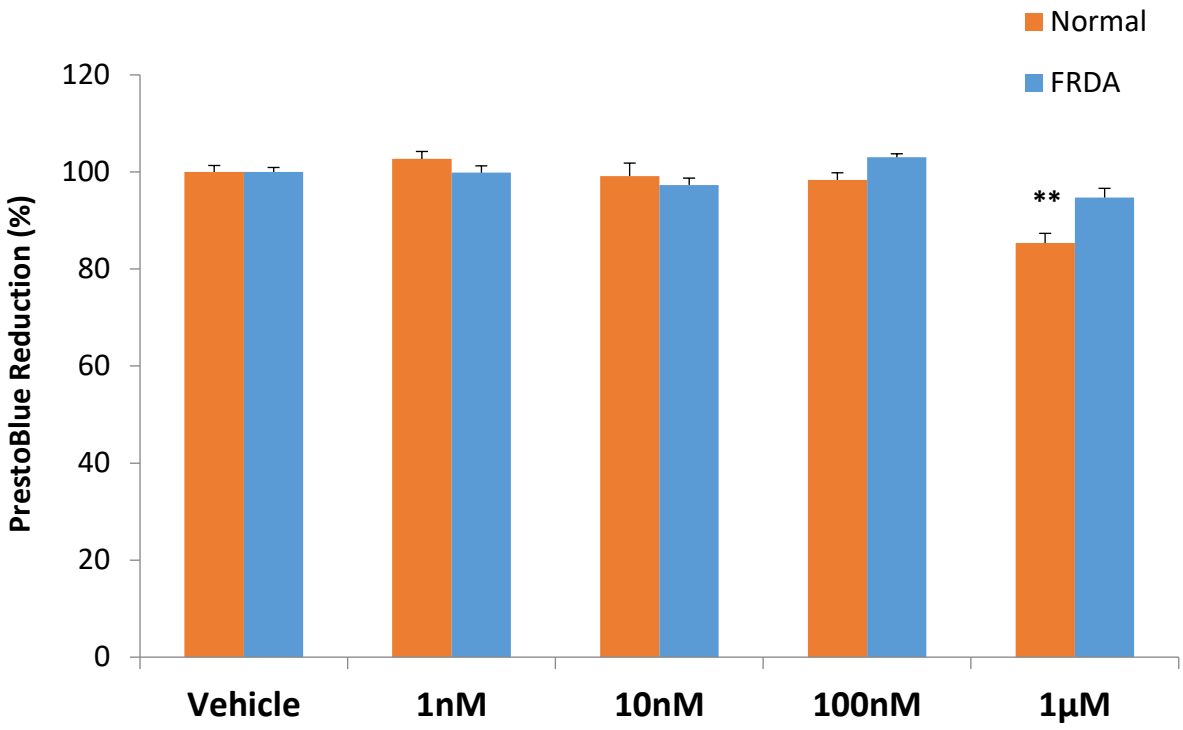

Figure 4. 20 - PrestoBlue cell viability analysis of human primary fibroblasts following 72hr salinosporamide A treatment. All data was normalised to the mean average of PrestoBlue reduction of the corresponding vehicle treated cell line (set at 100%). Error bars indicate SEM and values represent mean ±SEM (n=3). Asterisks indicate significant differences between drug and vehicle treated cell lines, assessed by Student's *t*-test (**P<0.001).

4.2.5.2 Protein quantification assessment

The effect of salinosporamide A on FRDA was subsequently investigated by treating normal and FRDA human primary fibroblasts with 1nM and 100nM concentrations for 72hrs. This was followed by cell collection and protein expression assessment of frataxin, c-Jun, $p27^{Kip1}$ and PSMB5 by western analysis with specific primary antibodies. 1nM salinosporamide A treatment of FRDA fibroblasts revealed an increase of 35% in frataxin expression levels, compared to vehicle treated cells, but the increase was statistically insignificant (Figure 4.21 A-B). No significant change in frataxin expression was seen with 100nM salinosporamide A treatment in either normal or the FRDA fibroblasts. Furthermore, western analysis indicated an increase of 5% in c-Jun expression levels with 1nM drug treatment, in FRDA cells (Figure 4.21 A, C), whereas in normal fibroblasts, a decrease of 42% was seen. However, these changes in c-Jun expression levels were statistically insignificant. Comparably, 1nM salinosporamide A treatment increased the $p27^{Kip1}$ cellular stress marker levels by 18% and 46% in normal and FRDA fibroblasts, respectively (Figure 4.21 A, D). Nevertheless, this was reduced with 100nM treatment. No significant changes in the PSMB5 proteasome complex activity levels were observed after treatment (Figure 4.21 A,E).

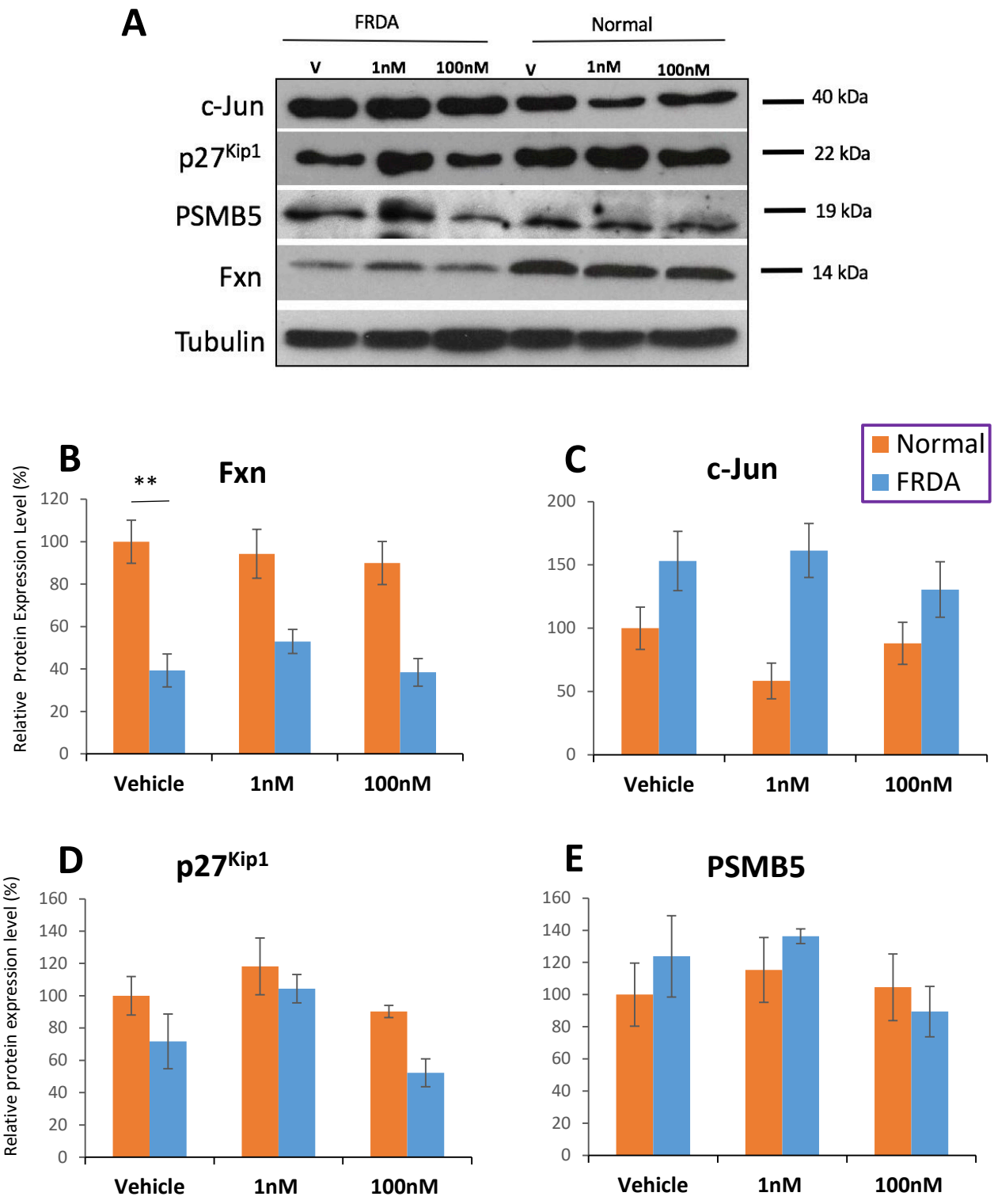

Figure 4. 21 - Dose-response western analysis of human FRDA and normal fibroblast cells treated with salinosporamide A for 72hrs. A) Total cell extracts were analysed by SDS-PAGE and revealed by immunoblotting with anti-frataxin, anti-cJun, anti-p27^{Kip1} and anti-PSMB5, and anti-tubulin as a control. One representative experiment out of three performed with similar results shown. V- Vehicle (DMSO). B-E) Densitometry analysis of frataxin, c-Jun, p27^{Kip1}, PSMB5 upon salinosporamide A treatment of human fibroblasts as shown in (A). The values were expressed as a ratio to the vehicle treated samples of normal fibroblasts. (*P<0.05, **P<0.01, error bars ±SEM**).**

4.2.5.3 Proteasomal activity analysis

In order to assess proteasomal inhibitory effect of salinosporamide A in FRDA, the trypsin-like and chymotrypsin-like catalytic activity of the proteasomes were determined. The human primary fibroblasts were treated with 1nM and 100nM of salinosporamide A for 72hrs, followed by specific proteasome-Glo cell based assay assessment. A mean value of the vehicle and drug treated triplicates were used, compared to untreated normal cells, which were set as 100% arbitrarily. A significant reduction of 59% ($P<0.01$) in chymotrypsin-like activity was observed in FRDA cells treated with 100nM salinosporamide A, whereas no changes were seen with 1Nm (Figure 4.22). Moreover, a dose-dependent reduction in chymotrypsin-like activity was also seen in normal fibroblasts, whereas 100nM salinosporamide A treatment instigated a 47% ($P<0.05$) reduction. No changes were observed in the trypsin-like activity of either cell lines after treatments.

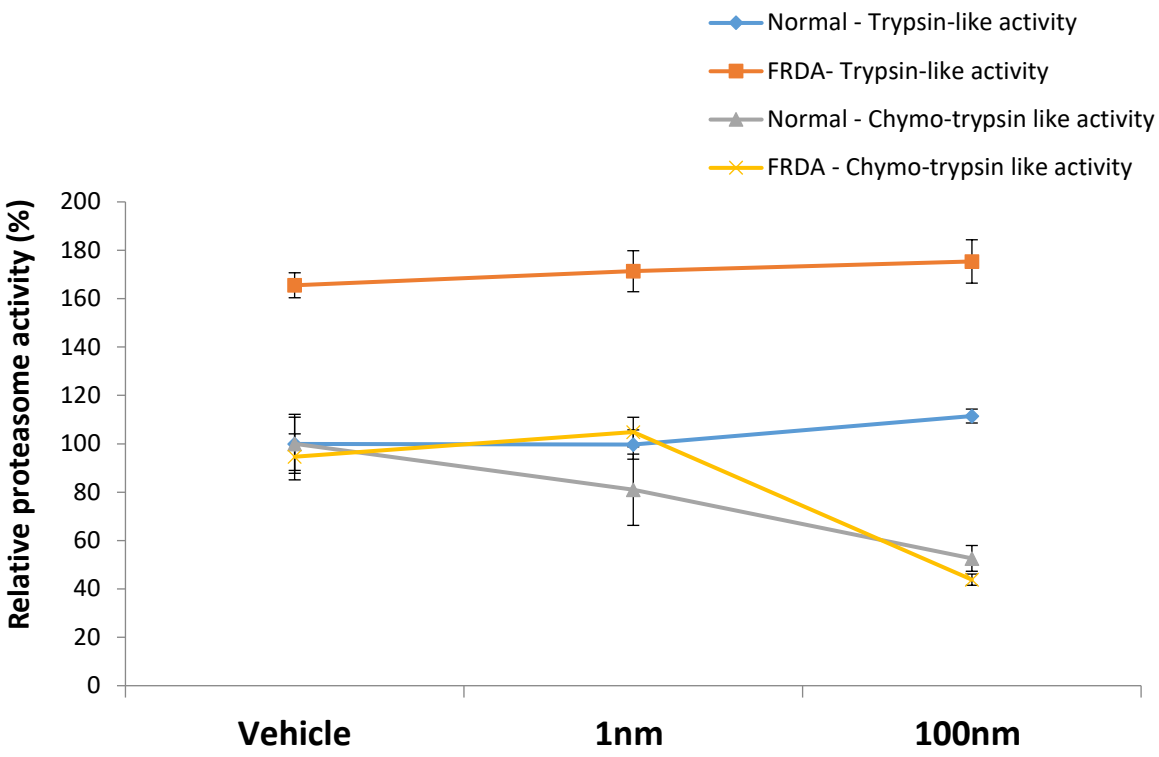

Figure 4. 22 - Relative change in trypsin-like and chymotrypsin-like activity in FRDA and normal fibroblasts after 72hrs of salinosporamide A treatment. The values were expressed as a ratio to the vehicle treated samples of normal fibroblasts. Error bars indicate SEM and values represent mean ±SEM (n=3).

4.3 Discussion

FRDA is an inherited progressive neurodegenerative disorder caused by an unstable GAA repeat expansion mutation within intron 1 of the *FXN* gene, which partly silences *de novo* transcription, leading to reduction in intracellular frataxin protein levels. Frataxin is an essential mitochondrial protein, and is involved in iron metabolism and oxidative stress control (Babcock *et al.*, 1997, Foury and Cazzalini, 1997). Decreased residual frataxin results in mitochondrial dysfunction and ultimately causs pathology in affected tissues, where the severity of the disease is directly correlated to the extent of the reduction (Chutake et al, 2014b). Therefore, strategies which aim to restore physiological frataxin levels are desirable, and are likely to be therapeutically beneficial for FRDA patients (Wilson, 2012, Soragni *et al.*, 2014, Nabhan *et al.*, 2015). Most current therapeutic approaches aim to induce frataxin expression from the pathogenic *FXN* locus (Strawser et al, 2014), or to intervene in the pathogenic cascade downstream of frataxin deficiency. In contrast, frataxin post-translation modulation has not been explored extensively. Recent advances in FRDA research have reported that the UPP pathway degrades precursor frataxin (Rufini *et al.*, 2011, 2015), and that UPP inhibition can prevent frataxin precursor degradation to ultimately upsurge mature frataxin levels.

Thereby, in this study we have reported the *in vitro* efficacy of four 26S proteasome inhibitors (MG132, bortezomib, salinosporamide A and ixazomib) using FRDA patient-derived fibroblasts, to potentially increase frataxin protein expression and ameliorate the disease phenotype.

Western analysis of human FRDA fibroblasts confirmed to be significant reduction in frataxin, as compared to normal fibroblasts. Subsequently treatment with MG132 or bortezomib, at non-toxic concentrations, produced no significant change in frataxin levels. Additionally, no significant change was observed in the UPP substrate, c-Jun, and the cell

cycle stress control modulator, $P27^{Kip1}$. Moreover, while no change was seen in the PSMB5 levels by western analysis, the proteasome-Glo luciferase assay revealed a slight decrease in chymotrypsin-like activity in normal fibroblasts with 10μM MG132 treatment. On the other hand, bortezomib treatment induced a non-cell specific significant decrease in the chymotrypsin-like activity. This suggests that although these treatments inhibit the chymotrypsin-like activity of the 26S proteasomes to some extent, no downstream effects can be observed of increasing frataxin protein expression levels in FRDA fibroblasts.

Although it was previously reported that MG132 treatment increased precursor and mature frataxin levels, this experiment was performed in HEK-293 cells which stably expressed frataxin at more physiological level (Rufini *et al.*, 2011, 2015), and not in cells derived from FRDA patients. Furthermore, in agreement with our findings, Nabhan *et al.* (2015) demonstrated that UPP-inhibition with MG132 or bortezomib treatment did not increase mature frataxin levels in 293T cells, with a decrease in mature frataxin levels in FRDA patient-derived lymphoblastoid cells after bortezomib treatment.

Similarly, our results showed no significant change in frataxin protein expression levels with salinosporamide A treatment. Although a small increase in $P27^{Kip1}$ was seen with 1nM drug concentration in FRDA fibroblasts, the chymotrypsin-like activity was significantly reduced at 100nM treatment in both normal and FRDA fibroblasts. This suggests that higher concentrations of salinosporamide A have a non-cell specific effect on the chymotrypsin-like activity of the proteasomes; but have no effect on frataxin expression levels.

Furthermore, ixazomib treatment at non-toxic concentrations resulted in a slight increase in frataxin protein expression in FRDA fibroblasts, and this increase was statistically significant with frataxin dipstick assay. Although western analysis revealed no significant changes in c-Jun and PSMB5 levels, the chymotrypsin-like activity of the 26S proteasome was significantly reduced with ixazomib treatment in FRDA fibroblasts, alongside a dose-

dependent increase in $p27^{Kip1}$ levels. This indicates that ixazomib has a specific FRDA effect. However, since the cell cycle stress control modulators were triggered, it may produce some detrimental effects, to some extent. Moreover, since reduced frataxin in FRDA is associated with impaired mitochondrial activity and cytosolic aconitase, we then investigated the effect of ixazomib on aconitase activity in FRDA firboblasts. Interestingly, our results indicated a non-cell specific significant increase in the aconitase activity, where the increase was above normal, suggesting that ixazomib may have an indirect effect on the aconitase activity.

Interestingly, c-Jun expression levels were found to be significantly higher in FRDA fibroblasts as compared to normal cells. This was reported previously by Pianese *et al.* (2002) in FRDA fibroblasts, where they proposed that lack of frataxin in FRDA may trigger increased c-Jun phosphorylation and hyperactive stress signalling pathway, probably due to increased ROS levels. Moreover, it is important to note that no change was seen in the chymotrypsin-like activity levels between the normal and FRDA fibroblasts, but a significant increase in trypsin-like activity was seen in FRDA fibroblast ($P<0.001$). This suggests that perhaps the increased frataxin UPP-mediated degradation in FRDA may be related to the increased trypsin-like activity, as supposed to chymotrypsin-like activity of the 20S proteasome. This has not been reported before, and requires further investigations.

Overall, out of the four proteasome inhibitors investigated, only ixazomib treatment increased frataxin protein expression levels. However, the significance of these results is unclear since an increase in cellular stress marker, $p27^{Kip1}$, is also seen. Therefore, at this stage we do not propose *in vivo* animal studies, and our results do not support the use of proteasome inhibitors as a therapeutic approach for FRDA. However, it would be interesting to investigate the precursor and intermediate frataxin protein forms, alongside a broad range of UPP substrates, after proteasome inhibitor treatment in FRDA patient-derived cells. Therefore, further western analysis is a consideration.

CHAPTER V - DAO INHIBITOR *IN VIVO* THERAPEUTIC STUDIES

5.1 Introduction

Synaptic transmission is essential for the nervous system to process and store information. Synapses are specialised contacts between neurons, where the release of neurotransmitters by the presynaptic neurons activates neurotransmitter receptors on the membrane of the postsynaptic neuron (Vyklicky *et al.*, 2014). One of the key excitatory neurotransmitter receptors in the brain are the *N*-methyl D-aspartate receptors (NMDARs), which are involved in many physiological processes, including memory formation, synaptic plasticity and development of the central nervous system (CNS) (Danysz and Parsons, 1998). Consequently, abnormal NMDAR function have been implicated in numerous neurological disorders and pathological conditions, including cerebellar ataxia (Zhou and Sheng, 2013). NMDARs are a class of ionotropic glutamate receptors, whose functional activation requires the binding of two ligands and membrane depolarization, removing a magnesium ion from the binding site within the ion conduction pore (Danysz and Parsons, 1998). The main NMDAR agonist, glutamate, does not activate the receptor unless a co-agonist is bound simultaneously (Johnson and Ascher, 1987). Studies have reported that D-serine may be the dominant co-agonist of NMDARs, mediating several NMDAR-dependent processes (Mothet *et al.*, 2000). Endogenous D-serine is synthesized from L-serine by serine racemase (SRR) (De Miranda *et al.*, 2002), an enzyme that is expressed in both glia and the neurons in the brain (Takayasu *et al.*, 2008). Upon synaptic transduction, glial cells detect changes in their environment, which induces the release of D-serine from these cells in culture, where it plays a critical role in long-term potentiation (Figure 5.1) (Mothet *et al.*, 2005). Degradation of mammalian D-serine is mediated by the peroxisomal flavoprotein, D-amino acid oxidase (DAO), an enzyme highly present in astrocytes of the hindbrain and cerebellum (Sacchi, 2013).

DAO catalyses D-serine oxidation to form the corresponding keto acid, ammonia and hydrogen peroxide (Pollegioni *et al.*, 2007, Verrall *et al.*, 2007).

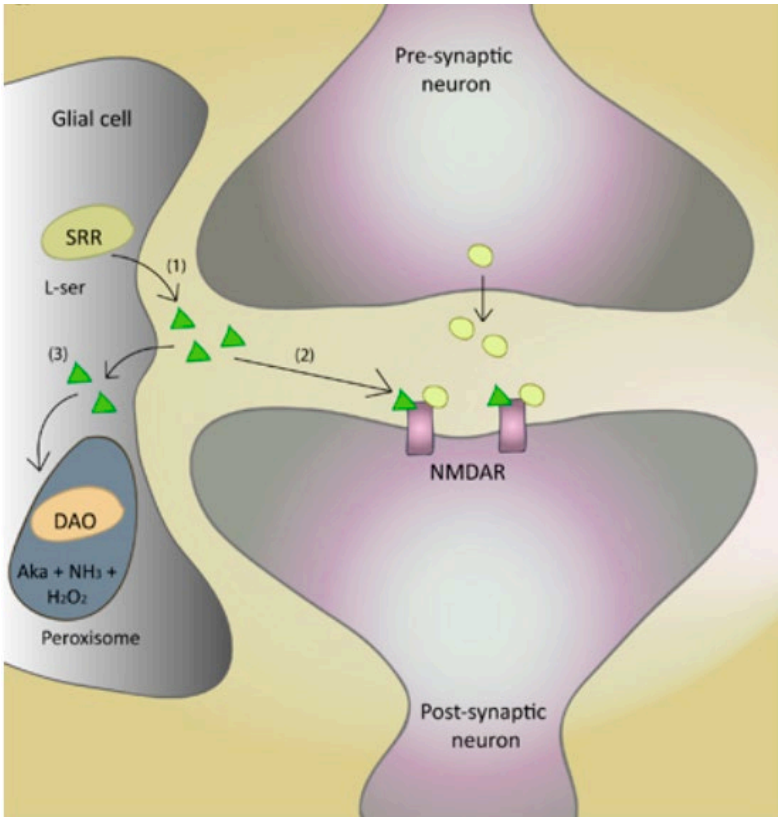

Figure 5. 1 - Synaptic regulation and D-serine catabolism. 1) Glial SRR synthesizes D-serine (green triangles) from L-serine. 2) D-serine is released at tripartite synapses to facilitate the action of synaptic glutamate (yellow circles) at NMDARs. 3) Synaptic D-serine is then taken up into glia and broken down within glia by peroxisomal DAO, forming the alpha keto acid (Aka), ammonia and hydrogen peroxide (Verrall *et al.*, 2010).

Studies have reported that impaired glutamate-mediated signalling may be associated in the pathogenesis and progression of cerebellar ataxia both in humans and animal models (Ogawa *et al.*, 2003). For instance, gene disruption of the NMDAR subunits in mice resulted in lack of motor coordination and ataxia (Kadotani *et al.*, 1996), suggesting that NMDA-type glutamate receptor functioning is vital for correct motor coordination. Successively, ataxia symptoms induced by NMDAR uncompetitive antagonists such as PCP (1-phenylcyclohexyl piperidine) and MK-801 (di-zocilpine) in rodents, were reduced when the animals were given

injections of D-serine (Tanii *et al.*, 1994). This suggests that D-serine is vital in modulating normal NMDAR functioning and improves ataxia produced by cerebellar dysfunction. Furthermore, Hashimoto *et al.* (2005) later reported that mice lacking DAO activity displayed significant attenuation of stereotypy, as well as ataxia induced by PCP and MK-801, due to increased levels of D-serine in the brain and enhancement of NMDAR-mediated synaptic transmission. This indicates that overexpression and hyperactivity of brain DAO may be associated to excessive D-serine degradation and NMDAR hypofunction in cerebellar degeneration (Verrall *et al.*, 2010). Therefore, as a potential neuromodulation therapy for cerebellar ataxia, small molecule inhibitors of DAO could be used to prevent D-serine degradation and alleviate ataxic symptoms.

5.2 Therapeutic testing of TAK-831

It has been hypothesised that excessive degradation of D-serine by DAO may lead to low NMDAR functioning and impaired neural signalling in the cerebellum, resulting in ataxia. Therefore, as a potential therapeutic approach, in collaboration with the pharmaceutical company Takeda Cambridge Limited, we decided to investigate the efficacy of a small molecule inhibitor of DAO, TAK-831, in our FRDA YAC transgenic mice, YG8sR (220 GAA repeats). Similar to FRDA patients, the YG8sR mice demonstrate progressive behavioural deficits, together with significant decreases of *FXN* and frataxin protein expression compared with control mice (Anjomani Virmouni *et al.*, 2015), thus, making them an excellent model to investigate potential FRDA therapies.

5.3 Study design and drug administration

In order to observe the therapeutic efficacy of TAK-831 in FRDA, two dosing experiments were performed on the same YG8sR and C57B6/J (WT) mice. The first dosing experiment was carried out when the mice were on average 4 months of age (T1), then the mice were left to age normally to reach 8 months, followed by the second dosing experiment (T2). Mice were either administered vehicle or 3mg/kg TAK-831 by daily oral gavage for 14 days. In each group, 10 age- and sex-matched mice were used, where the YG8sR mice were treated with vehicle or 3mg/kg TAK-831, and WT mice were treated with vehicle (Table 5.1).

Table 5. 1- Study design of TAK-831 in WT and YG8sR mice

Genotype	Male	Female	Dose
WT	5	5	Vehicle
YG8sR	5	5	Vehicle
YG8sR	5	5	TAK-831 3mg/kg

Weight and beam walk measurements were taken before and after treatment in both of the dosing experiments (T1 and T2), whereas locomotor activity was measured in the first dosing (T1), and rotarod performance was measured in the second dosing experiment (T2). At the completion of the drug treatment all of the mice were appropriately culled and samples were collected (as described in Chapter 2, section 2.23) for molecular analysis.

5.4 Results

5.4.1 Weight analysis

Mouse weight analysis was carried out during both T1 and T2 experiments, before and after drug treatment. Within respective groups, the mean weight of mice at each time point was normalised to the average weight at T1-day 0, which was set to 100%. At the start of T1 drug treatment, all mouse groups showed similar weight distribution. However, a considerable increase in weight was seen after 3 months of no treatment, with YG8sR mice having a higher body weight as compared to WT mice. Two-way analysis of variance (ANOVA) conducted across both T1 and T2 experiments (Table 5.2) confirmed that there was no significant difference in overall average body weight between YG8sR mice as compared to WT mice treated with vehicle, or YG8sR TAK-831-treated mice as compared to YG8sR vehicle-treated mice (Figure 5.2), suggesting that TAK-831 was well tolerated and the treatment did not have any significant effect on the FRDA mouse body weight. This was also true for female values analysed separately (Figure 5.2 B). However, male YG8sR mice treated with the vehicle had a higher average body weight as compared to WT vehicle-treated mice ($P<0.0001$) (Figure 5.2 B). Moreover, a significant reduction in body weight was seen in male YG8sR TAK-831-treated mice compared to male YG8sR vehicle-treated mice over time ($P<0.001$).

Table 5. 2 - Two-way ANOVA analysis of body weight in YG8sR or WT mice throughout treatment

Groups	*P* value	Sex	*P* value
Vehicle YG8sR Vs WT	0.1505	Male	<0.0001
		Female	0.6782
YG8sR TAK-831 Vs YG8sR Vehicle	0.9395	Male	0.0011
		Female	0.3023

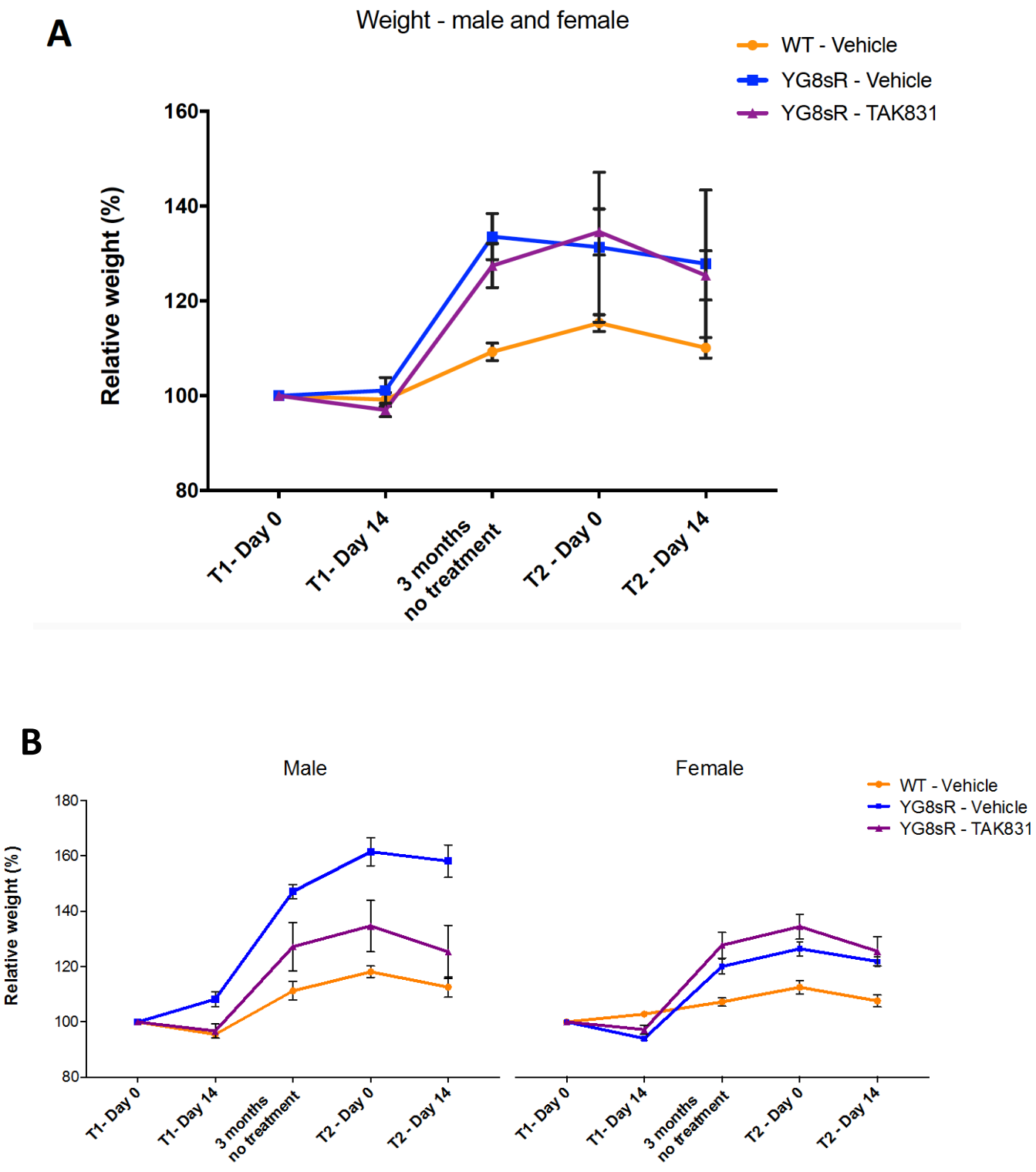

Figure 5. 2 - Mouse body weight analysis during treatment with TAK-831. Relative weight analysis of YG8sR mice treated with vehicle and TAK-831, compared to WT vehicle treated mice, when A) both male and female values were taken together (*n*=10 mice per group), B) male and female values analysed separately (*n*=5 mice per group). Error bars indicate SEM and values represent mean ±SEM.

5.4.2 Beam-walk assessment

Beam-walk performances were assessed to investigate the coordination ability of YG8sR FRDA mice before and after oral TAK-831 or vehicle treatment, while B6 mice treated with vehicle were used as WT controls. 10 mice, 5 males and 5 females, were assessed for each group and the average beam crossing time of 4 trials on 22x900mm and 12x900mm beams were recorded. The data obtained within each group were normalised to baseline (T1- Day 0), which was arbitrarily set as 100%. The significance of these observation was confirmed by two-way ANOVA (Table 5.3) and Student's *t* test (Table 5.4).

As shown in Figure 5.3 A, in the first dosing treatment (T1-day 0 to T1-day 14), no specific TAK-831 drug-induced effect was observed, as the YG8sR TAK-31-treated mice showed no significant change in the time taken to cross either the 22mm and 12mm beam when compared to controls groups. However, after 3 months without treatment, we observed a progressive FRDA-like disease effect in YG8sR mice when compared to WT mice. YG8sR mice took significantly longer to cross both the 22mm and 12mm beams (Table 5.4). Nevertheless, after the second dose of TAK-831 treatment (T2-day 14), a clear drug-induced effect was seen in YG8sR mice, as the time taken to cross the 22mm beam was significantly reduced in comparison to vehicle-treated YG8sR mice. This indicates that TAK-831 significantly improved the balance and motor coordination ability of YG8sR mice at 8 months of age when the disease effect was prominent. The same trend was also observed when female values were considered alone (Figure 5.3 B). YG8sR female mice took significantly longer than WT female mice to cross the 22mm and 12mm beam at an older age, but this effect was improved significantly with TAK-831 treatment. Similar results were also obtained when analysing YG8sR male mice crossing the 22mm beam (Figure 5.3 C). However, detailed analysis of YG8sR and WT male values crossing the 12mm beam showed variabilities throughout the time points. This could be attributed to the differences in male

and female average body weight, which could affect their balance and performance on the narrow beam. This could have also contributed to the lack of drug-induced changes observed with the 12mm beam.

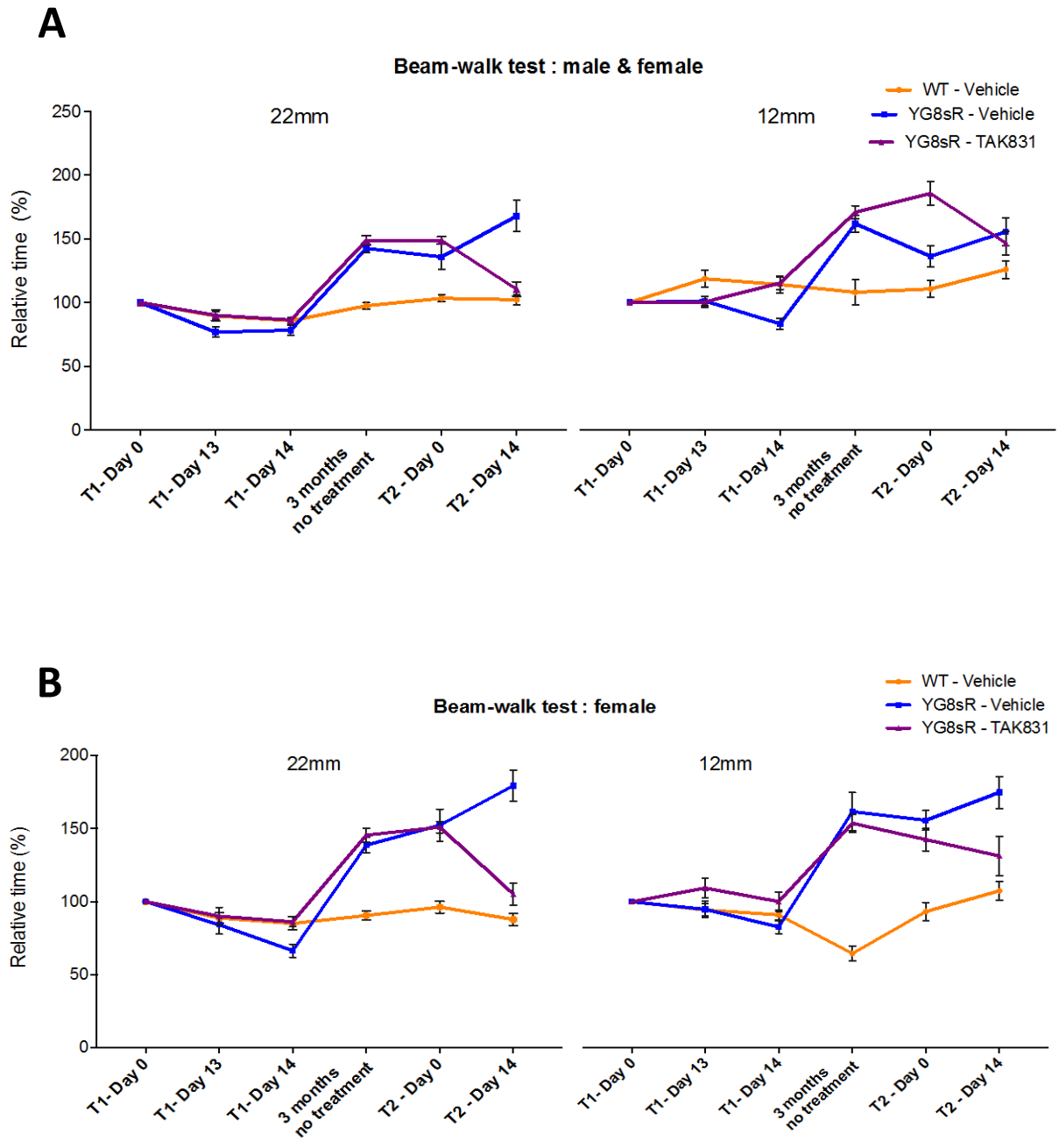

Figure 5. 3 - Mouse beam walk analysis during TAK-831 treatment. Relative time taken to cross the 22mm and 12mm beam in A) male and female B) male and C) female WT and YG8sR mice. Error bars indicate SEM and values represent mean ±SEM.

Table 5. 3 - Two-way ANOVA analysis of beam-walk performance in YG8sR or WT mice throughout treatment

Beam size	Groups	*P* value	Sex	*P* value
22mm	Vehicle YG8sR versus WT	<0.0001	Male	0.0003
			Female	<0.0001
	YG8sR TAK-831 versus YG8sR Vehicle	<0.0001	Male	0.0009
			Female	<0.0001
12mm	Vehicle YG8sR versus WT	<0.0001	Male	0.0003
			Female	<0.0001
	YG8sR TAK-831 versus YG8sR Vehicle	<0.0001	Male	<0.0001
			Female	0.0007

Table 5. 4 - Student's *t* test analysis of beam-walk performance in YG8sR or WT mice throughout treatment

				T1				T2	
Beam Size	**FRDA mouse**	**Gender**	**Versus**	**Day 0**	**Day 13**	**Day 14**	**3 months no treatment**	**Day 0**	**Day 14**
22mm	YG8sR - Vehicle	Male and female	B6 - Vehicle	>0.9999	0.1488	0.5281	<0.0001	<0.0001	<0.0001
			YG8sR-TAK831	>0.9999	0.1247	0.4754	0.6248	0.1364	<0.0001
	YG8sR - Vehicle	Male	B6 - Vehicle	>0.9999	0.1351	0.9280	0.0004	0.6903	0.0007
			YG8sR-TAK831	>0.9999	0.1351	0.9280	0.8531	0.0329	0.0006
	YG8sR - Vehicle	Female	B6 - Vehicle	>0.9999	0.8268	0.0453	<0.0001	<0.0001	<0.0001
			YG8sR-TAK831	>0.9999	0.7415	0.0306	0.6625	0.9840	<0.0001
12mm	YG8sR - Vehicle	Male and female	B6 - Vehicle	>0.9999	0.1570	0.0028	<0.0001	0.0172	0.0046
			YG8sR-TAK831	>0.9999	0.9946	0.0019	0.6087	<0.0001	0.6103
	YG8sR - Vehicle	Male	B6 - Vehicle	>0.9999	0.0253	0.0002	0.7026	0.6880	0.8211
			YG8sR-TAK831	>0.9999	0.4379	0.0016	0.1327	<0.0001	0.1339
	YG8sR - Vehicle	Female	B6 - Vehicle	>0.9999	0.9989	0.6790	<0.0001	<0.0001	<0.0001
			YG8sR-TAK831	>0.9999	0.3094	0.1904	0.7032	0.3814	<0.0001

5.4.3 Rotarod assessment

Since YG8sR mice revealed a progressive FRDA-like disease effect at an older age, we then additionally decided to investigate the motor coordination performance of YG8sR mice in the second TAK-831 dosing experiment (T2) using a rotarod treadmill. As shown in Figure 5.4, the coordination ability of vehicle-treated YG8sR mice was significantly reduced compared to vehicle-treated WT mice after 3 months without treatment when analysed by Student's *t* test (Table 5.5). However, the YG8sR mice that had previously been dosed with TAK-831 at 4 months of age where found to stay on the rotarod treadmill for significantly longer than the vehicle-treated YG8sR mice. After the second dosing treatment (T2- Day 14), the time on the rotarod for YG8sR mice treated with TAK-831 continued to show significant improvement compared to YG8sR mice treated with the vehicle (P<0.001), suggesting a drug-induced effect. No significant changes were observed in TAK-831 treated YG8sR and vehicle treated WT mice throughout the T2 time points. This trend was observed when both male and female values were taken together (Figure 5.4 A), or when male and females were considered alone (Figure 5.4 B). In general, male YG8sR mice were shown to stay on the rotarod for a shorter period of time as compared to female YG8sR mice. A possible explanation for this could be due to difference in mice body weight.

Table 5. 5 - Student's *t* test analysis of rotarod performance in YG8sR or WT mice throughout treatment

				T2	
FRDA mouse	**Gender**	**Versus**	**3 months no treatment**	**Day 0**	**Day 14**
YG8sR - Vehicle	Male and female	B6 - Vehicle	<0.0001	<0.0001	<0.0001
		YG8sR- TAK831	0.0027	<0.0001	<0.0001
YG8sR - Vehicle	Male	B6 - Vehicle	<0.0001	<0.0001	<0.0001
		YG8sR- TAK831	0.0029	<0.0001	<0.0001
YG8sR - Vehicle	Female	B6 - Vehicle	<0.0001	<0.0001	<0.0001
		YG8sR- TAK831	0.0368	0.0005	<0.0001

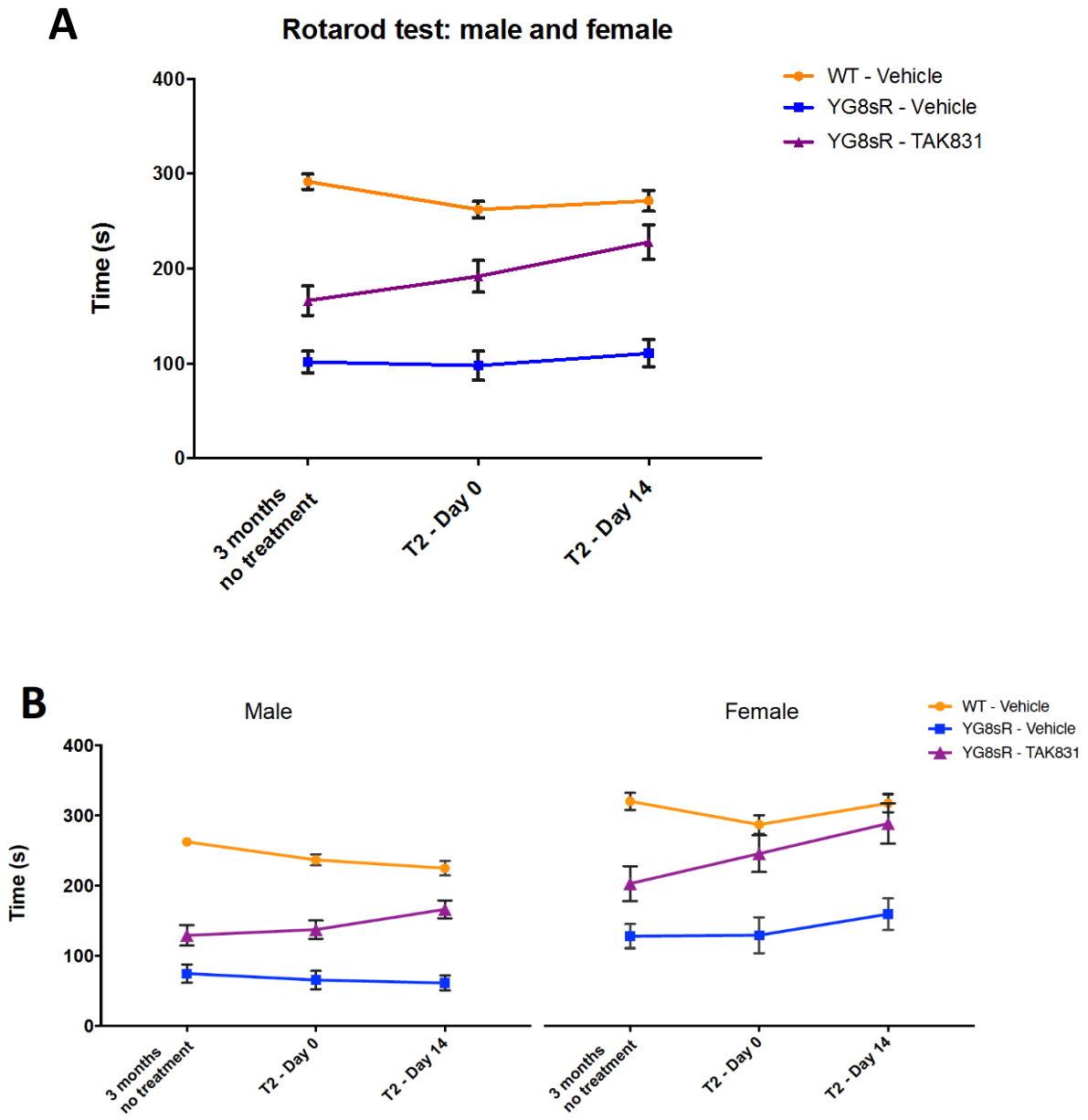

Figure 5. 4 - Mouse rotarod analysis during TAK-831 treatment. The average time on the rotarod in A) male and female together, and B) male and female WT and YG8sR mice separately. Error bars indicate SEM and values represent mean ±SEM.

5.4.4 Beam-breaker locomotor activity assessment

The locomotor activity of the mice, including average velocity, jump counts and stereotypic counts were monitored in all groups during the first dosing experiment and after 3 months without treatment. The functional measurements were recorded over a 5-minute period and repeated four times for each mouse using a beam-breaker activity monitor. For all experimental results, statistical analysis was performed by two-way ANOVA (Table 5.6).

As shown in Figure 5.5 A, no significant change in the average velocity (total distance covered divided by the total time elapsed) was observed in YG8sR mice compared to WT vehicle treated mice, and when TAK-831-treated YG8sR mice were compared to vehicle-treated YG8sR mice throughout the time points. Although, a drop in average velocity is seen in all mouse groups at T1-Day 14 (post-treatment), this could be due to the mice becoming familiar with their environment and lessening in explorative behaviour. A similar trend was observed when males and females were analysed separately (Figure 5.5 B).

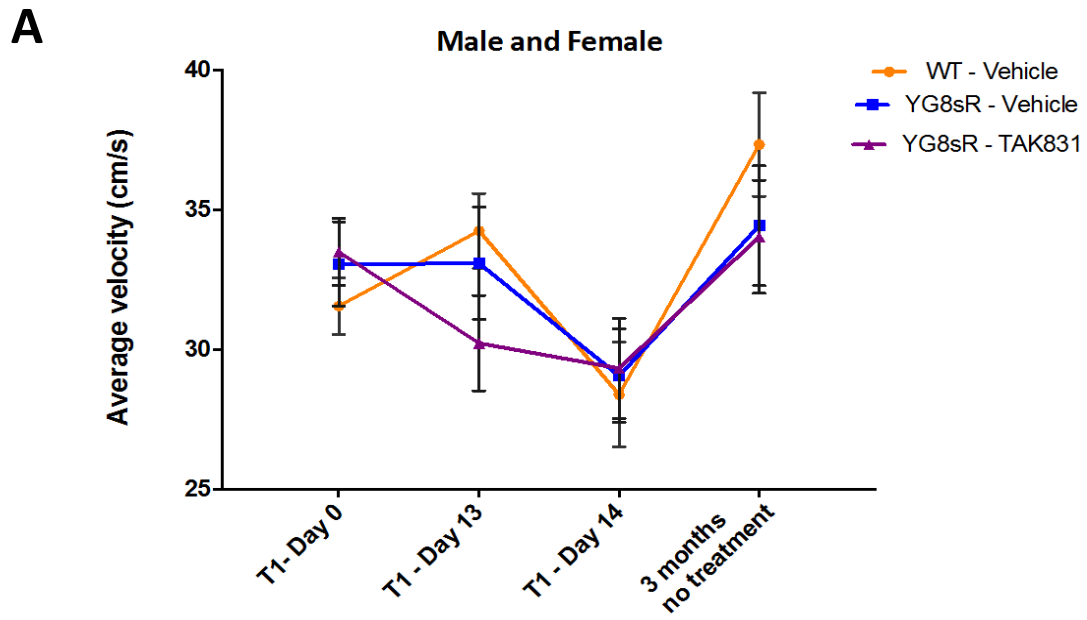

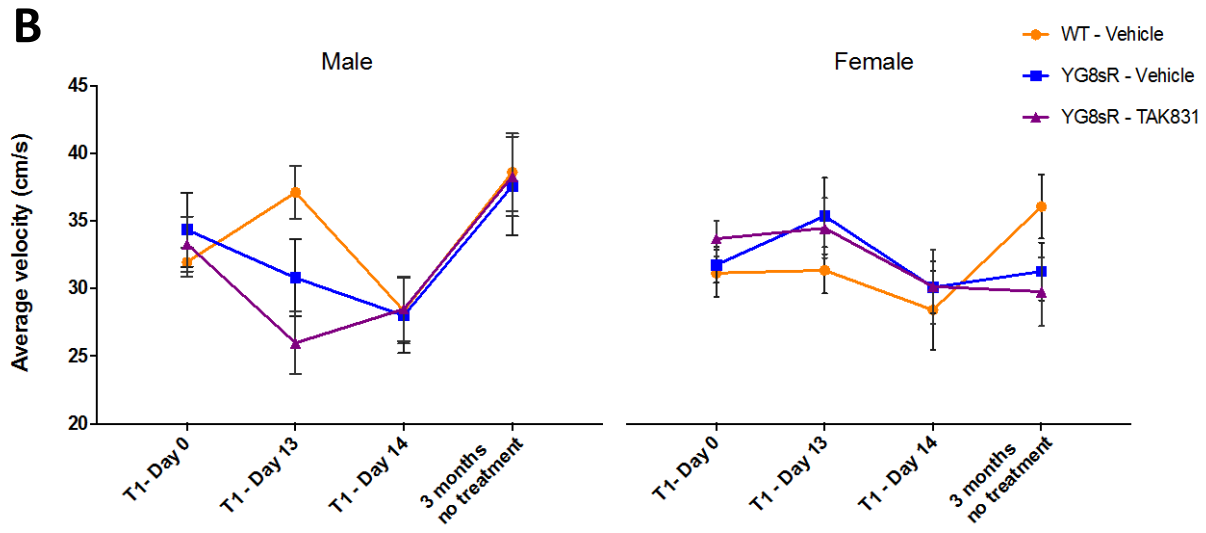

Figure 5. 5 - Average velocity analysis during TAK-831 treatment in YG8sR in A) male and female together, and B) male and female mice separately. Error bars indicate SEM and values represent mean ±SEM.

The jump count (total number of times that the mouse jumps) were also recorded. As shown in Figure 5.6 A, overtime the YG8sR mice showed a significant decrease in jump counts compared to WT mice, when analysing males and females together. This could have been influenced by the male values, where YG8sR mice jump count was significantly lower than the WT mice ($P<0.004$) (Figure 5.6 B). However, female YG8sR mice showed to have a higher jump count compared to WT mice. This difference in male and female jump count could be due to their weight differences. Moreover, no significant difference in jump counts was observed in YG8sR TAK-831-treated mice compared to YG8sR vehicle-treated overt the time-points.

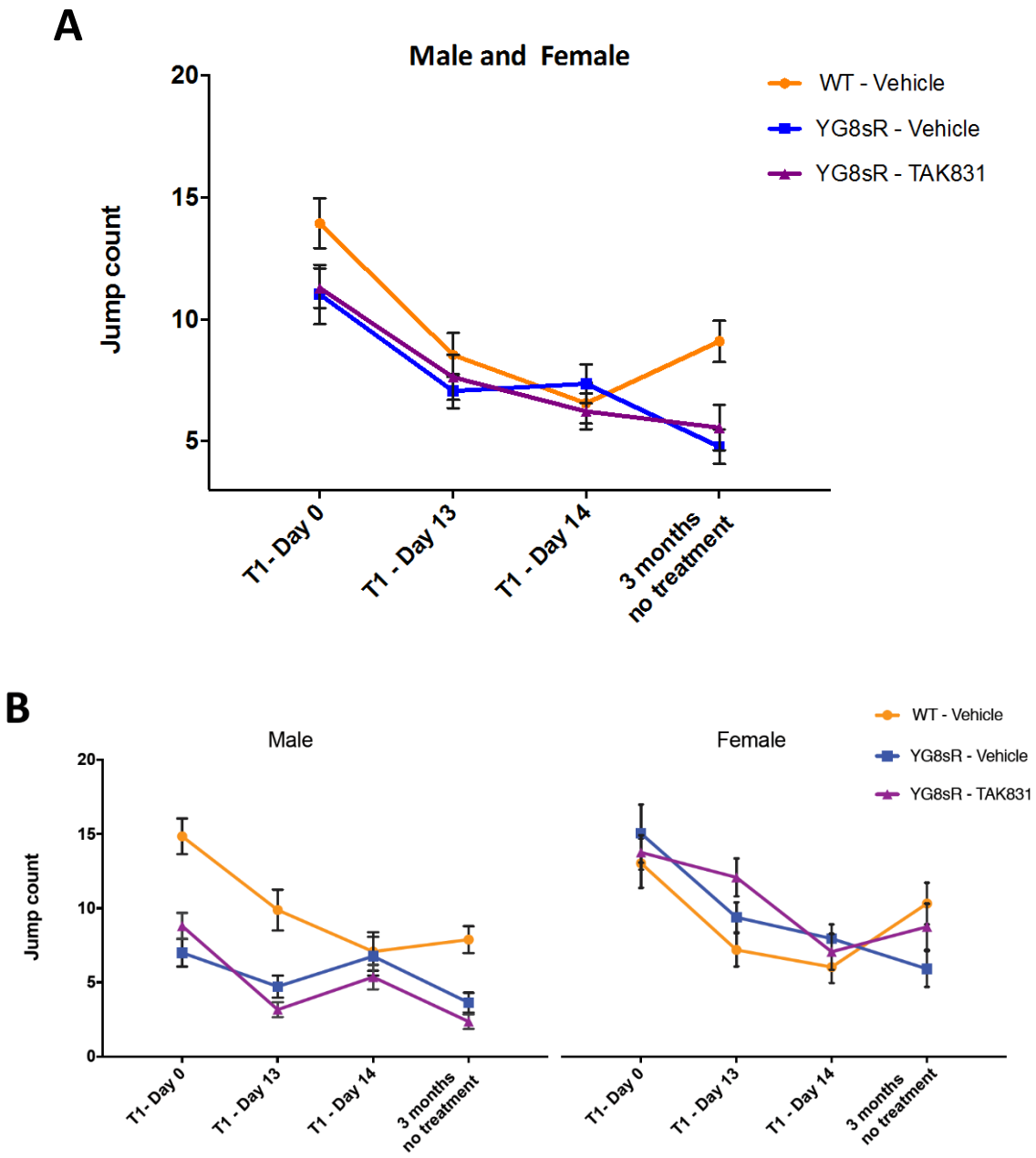

Figure 5. 6 - Average jump count analysis during TAK-831 treatment in YG8sR in A) male and female together, and B) male and female mice separately. Error bars indicate SEM and values represent mean ±SEM.

The stereotypic count assesses the total number of mouse motor responses, that are repetitive, invariant and seemingly without purpose (such as grooming). YG8sR mice showed to have a significantly lower stereotypic count as compared to WT mice, when both male and female values were taken together, throughout the time points, with an emerging FRDA-like disease phenotype of reduced stereotypic activity after 3 months without treatment (Figure 5.7 A).

However, there is no significant difference in the stereotypic count of TAK-831 treated YG8sR mice as compared to the vehicle treated group, indicating no specific drug-induced effect is seen. Moreover, female YG8sR mice treated with TAK-831 showed a higher stereotypic count compared to YG8sR mice treated with vehicle at the 3 months without treatment time point, an effect that was not observed in the male YG8sR mice (Figure 5.7 B).

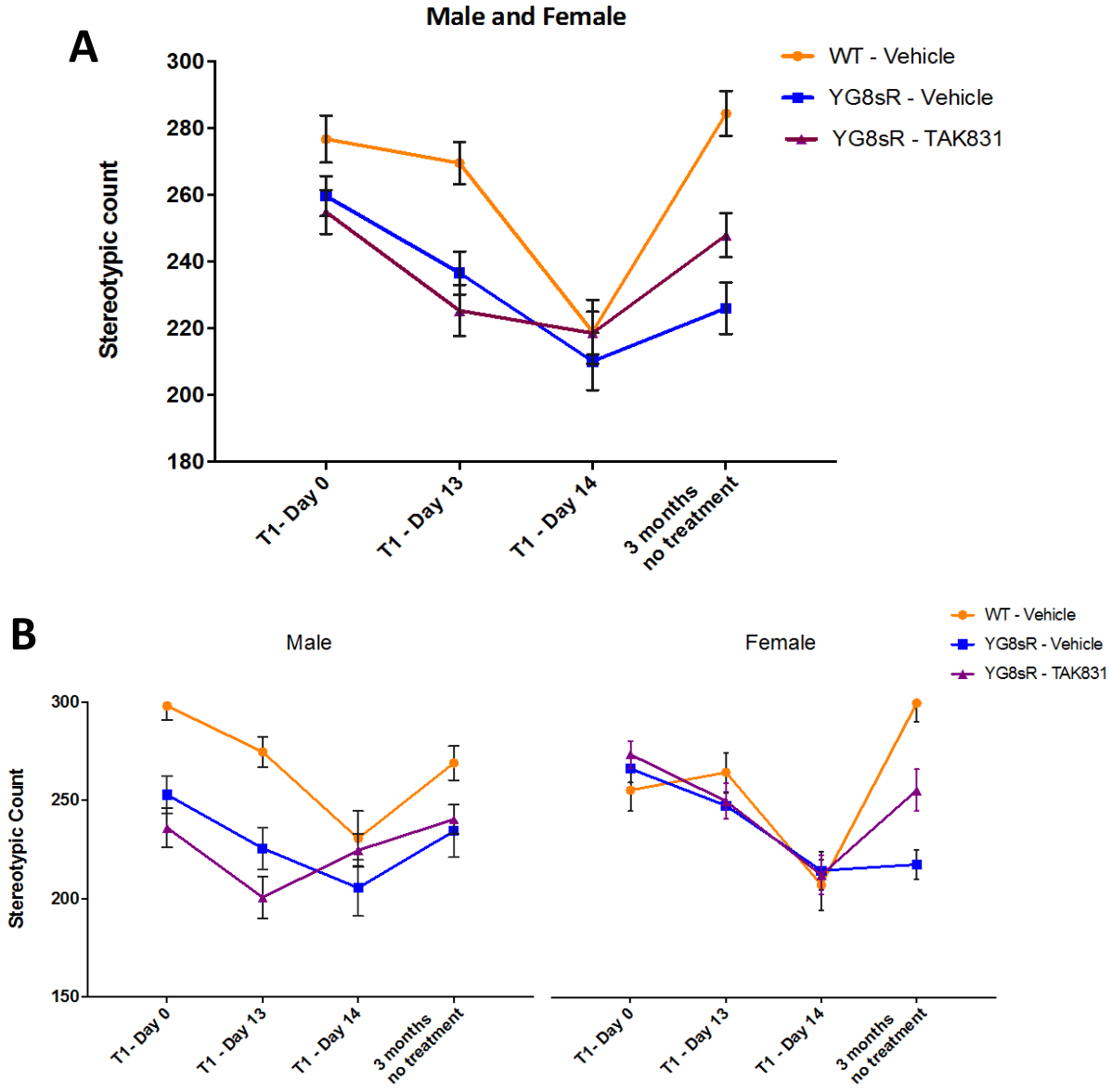

Figure 5. 7 - Average stereotypic count analysis during TAK-831 treatment in YG8sR in A) male and female together, and B) male and female mice separately. Error bars indicate SEM and values represent mean ±SEM.

Table 5. 6 - Two-way ANOVA analysis of locomotor activity in YG8sR and WT mice throughout treatment

	Groups	*P* value	Sex	*P* value
Average velocity	Vehicle YG8sR Vs WT	0.5587	Male	0.4154
			Female	0.1767
	YG8sR TAK-831 Vs YG8sR Vehicle	0.7896	Male	0.7506
			Female	0.8693
Jump count	Vehicle YG8sR Vs WT	0.0096	Male	0.0038
			Female	0.0102
	YG8sR TAK-831 Vs YG8sR Vehicle	0.5548	Male	0.0779
			Female	0.1650
Stereotypic count	Vehicle YG8sR Vs WT	0.0038	Male	0.6582
			Female	<0.0001
	YG8sR TAK-831 Vs YG8sR Vehicle	0.5548	Male	0.1254
			Female	0.0570

5.4.5 Quantification of *FXN* mRNA levels following TAK-831 treatment

Investigation of *FXN* mRNA

Following the second dose period of TAK-831 treatment (T2), the levels of *FXN* mRNA expression were measured in the cerebellum and heart of the drug-treated and vehicle-treated mice by qRT-PCR analysis. The relative *FXN* mRNA expression level was quantified using mRNA specific primers for *FXN*, and mouse *Hprt* was used as an endogenous control. Relative quantification values were determined by the $2^{-\Delta\Delta}$ method using the SDS 2.1 software (Applied Biosystems). Six mice from each group were used for the analysis (Table 5.7) and qRT-PCRs were performed in triplicates for each sample.

Table 5. 7 - Number of mice investigated for the FXN mRNA quantification

Group	Genotype	Cerebellum	Heart
Vehicle	WT	6	6
	YG8sR	6	6
TAK-831	YG8sR	6	6

As expected, qRT-PCR analysis revealed a significant decrease in *FXN* mRNA expression in both the cerebellum ($P<0.001$) (Figure 5.8 A) and heart samples ($P<0.001$) (Figure 5.8 B) of the YG8sR mice, compared to WT mice. However, no significant changes in *FXN* mRNA expression were identified in YG8sR mice following treatment with TAK-831 in either tissue, compared to vehicle-treated YG8sR mice. This suggests that TAK-831 had no effect on *FXN* gene expression, indicating that the beneficial behavioural effects were not likely to be due in any way to increased *FXN* expression.

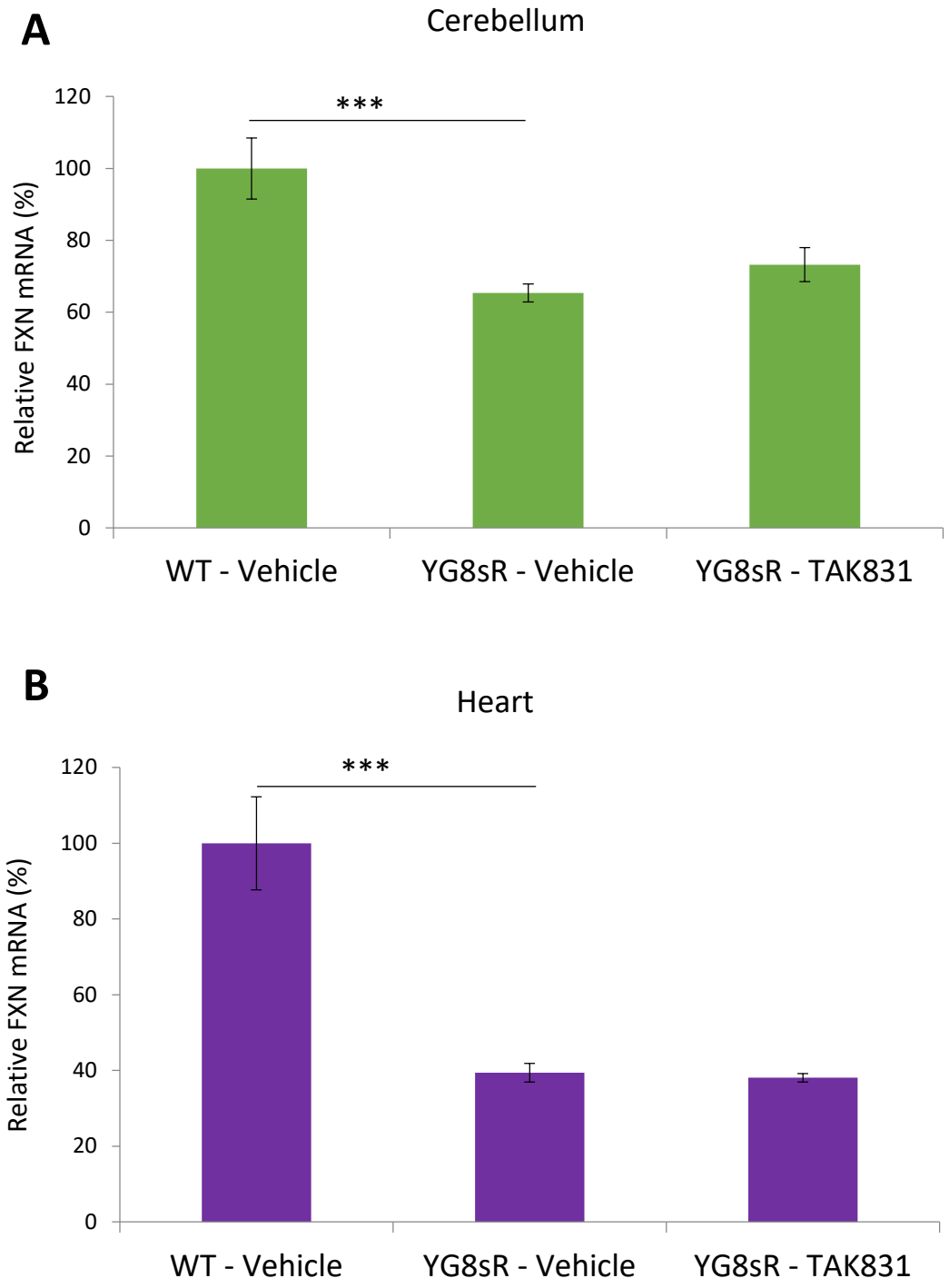

Figure 5. 8 – qRT-PCR analysis indicating the relative FXN mRNA levels in YG8s rescue mice following treatment with TAK-831 in A) cerebellum and B) heart tissues. Error bars indicate SEM and values represent mean ±SEM (n=3).

5.5 Discussion

The neurodegenerative disorder, FRDA, is the most common form of autosomal recessive cerebellar ataxia, with pathological features of peripheral sensory neuropathy, spinal degeneration and progressive cerebellar dysfunction. Recently, it has been reported that excessive degradation of D-serine by DAO overexpression, may lead to low NMDAR functioning and impair neural signalling in the cerebellum, resulting in ataxia. Therefore, regulation of the D-serine function via pharmacological manipulation of DAO represents currently an important research and development target.

In this study we have demonstrated the *in vivo* feasibility of a small molecule compound inhibitor of DAO, TAK-831, in our FRDA YAC transgenic mouse model to ameliorate the disease phenotype. Two dosing experiments were performed on the same FRDA mice by administering either vehicle or 3mg/kg TAK-831 compound by oral gavage daily for 14 days, first when the mice were at 4 months of age and then again at 8 months of age. Throughout the dosing regime, no apparent toxicity was observed in any of the mice, indicating a safe administration of compound.

We previously reported that YG8sR mice have a higher average body weight as compared to the C57BL6/J (WT) mice (Anjomani Virmouni *et al.*, 2015). This was also observed in this study with 8 months old YG8sR mice; along with no significant change in mouse body weight with TAK-831-treatment. However, a significant reduction was seen in male YG8sR mice average body weight with TAK-831 treatment, which were generally overweight as compared to the female YG8sR mice. Therefore, TAK-831 may have a specific effect on obese FRDA mice by increasing body metabolism.

The balance and motor coordination performance as determined by beam-walk analysis revealed no specific FRDA-like disease phenotype in YG8sR mice aged 4 months and no specific TAK-831 drug effect. However, as the mice aged to 8 months, YG8sR mice took a

significant longer time to cross both the 22mm and 12mm beams compared to WT mice ($P<0.001$), indicating a progressive FRDA-like disease effect. This progressive FRDA-like pathology of YG8sR mice has been previously reported by Anjomani Virmouni *et al.* (2015), when characterising this mouse model. Furthermore, as the disease effect became prominent in YG8sR mice, the second dosing of TAK-831 revealed promising results, due to the finding that TAK-831-treated YG8sR mice displayed a significant improvement in balance and coordination ability compared to the vehicle-treated group ($P<0.0001$). To elaborate on these results, the accelerated rotarod analysis carried out in second dosing experiment, also confirmed a progressive FRDA-like disease effect in YG8sR mice, as the mice took significantly lower time on the rotarod as compared to WT mice ($P<0.0001$). Moreover, after TAK-831 treatment, a significant improvement in rotarod performance was observed in YG8sR mice compared to vehicle-treated group ($P<0.0001$). Interestingly, after 3 months without treatment, TAK-831-treated YG8sR mice (in the first dosing experiment) were performing better on the rotarod than the vehicle-treated group ($P<0.003$). This suggests that treating FRDA with TAK-831 at an early age (before disease prominence) may be beneficial in reducing the progressive disease effect later in life. Therefore, taking together the beam walk and the rotarod results, treatment with TAK-831 may prove beneficial to improve ataxia motor coordination deficits, which are associated with FRDA.

In contrast, no-specific TAK-831 drug effect was observed when analysing the average velocity, jump count, stereotypic count in YG8sR mice aged 4 months, compared to control groups. Furthermore, the qRT-PCR results revealed no significant changes in *FXN* gene expression levels in the cerebellum and heart samples of TAK-831-treated YG8sR mice, indicating that the beneficial effect of the TAK-831 was not due to increased *FXN* gene expression levels.

Presently, the therapeutic potential of DAO inhibitors are still relatively unexplored and

preclinical studies have primarily addressed the relevance of these compounds mainly for the neuropsychiatric disorder, schizophrenia. Similar to cerebellar ataxia, studies have revealed a reduction in D-serine levels in the plasma and cerebrospinal fluid of schizophrenia patients, which is explained by the excessive D-serine oxidation due to elevated DAO activity (Verrall *et al.*, 2007, Sacchi *et al.*, 2008, Madeira *et al.*, 2008). Collectively, the small number of structurally diverse DAO inhibitors tested have been shown, when given systemically, to increase D-serine concentrations in the brain and plasma. However, the efficacy of these compounds in behavioral assays, that measure antipsychotic potential and pro-cognitive effects in animal models, has been fairly modest and inconsistent (Smith *et al.*, 2010, Sacchi *et al.*, 2013).

As a result, several authors then investigated the effects of co-administering DAO inhibitors in conjunction with systemic D-serine on brain neurochemistry and behavioural assays.

Ferraris *et al.* (2008) reported that oral administration of a potent DAO inhibitor, 6-chloro-benzo[d]isoxazol-3-ol (CBIO), in conjunction with 30mg/kg D-serine significantly enhanced plasma and brain D-serine, relative to either CBIO or D-serine administered alone. Hashimoto *et al.* (2009) extended this finding by showing effects on cortical D-serine levels, and the reversal of MK-801-induced deficit in prepulse inhibition (PPI) in mice with co-administration of CBIO and D-serine, whereas D-serine had no effect on its own. Similar results were also reported by Smith *et al.* (2010) with co-administering another potent DAO inhibitor, compound 4 (pyrrole carboxylic acid) with D-serine in rodents.

However, as yet there have been no studies that have reported the use DAO inhibitors in FRDA. Our study is the first and reveal that TAK-831 is well tolerated and elicits improved balance and motor coordination in mice with prominent FRDA-like disease effect. Very recently, TAK-831 has entered a randomized Phase 2 clinical trials in USA, sponsored by Takeda Cambridge Limited. This study will assess the safety, tolerability, pharmacokinetics

and efficacy of multiple doses of the compound in adult FRDA patients.

Furthermore, it is of paramount importance to assess the correlation between the DAO activity and DAO inhibitor drug concentration with D-serine accumulation in the plasma and cerebellum after TAK-831 treatment. Additionally, since the co-administration of DAO inhibitors and D-serine have revealed promising results in treating schizophrenia, it might be worth to investigate TAK-831 co-administration with D –serine or D-serine ethylester (D-cycloserine) a partial NMDA allosteric agonist. Previous studies have reported that systemic administration of D-cycloserine diminishes ataxia in mice carrying inherited or chemically induced cerebellar degeneration. Subsequently, D-cycloserine was then given to patients and ataxia was reduced after 14-day treatment (Ogawa *et al.*, 2003). Moreover, the co-administration of TAK-831 with D-serine may reduce the potential side effects associated with high D-serine dose administration, such as nephrotoxicity.

Overall, our preliminary findings support the use of TAK-831, as a small molecule DAO inhibitor, in clinical development as a novel therapeutic approach for FRDA.

CHAPTER VI - GENERAL DISCUSSION

FRDA is a rare autosomal recessive neurodegenerative disease caused by GAA repeat expansion within the first intron of the *FXN* gene encoding 'frataxin', an essential mitochondrial protein (Campuzano *et al.*, 1996). Lack of frataxin expression in FRDA leads to oxidative stress, mitochondrial iron accumulation and ultimately causes pathology in affected tissues (Chutake *et al.*, 2014). Recent *in vitro* and *in vivo* investigations have indicated that the GAA hyperexpansion interferes with *FXN* transcription by inducing heterochromatin-mediated silencing in FRDA (Saveliev *et al.*, 2003, Festenstein, 2006).
Currently, there is no effective therapy for FRDA (Delatycki, 2009). However, research on prospective pharmacological treatments has significantly advanced over the last two decades. Potential therapeutic strategies that aim to delay disease progression by intervening in the pathogenetic cascade downstream of frataxin, are currently undergoing clinical trial evaluations (Aranca *et al.*, 2016, Burk, 2017). However, there is still a high unmet clinical need to develop a therapy for this devastating disorder.

The identification of abnormal histone modifications in FRDA encouraged us to investigate the efficacy of two HMTase inhibitor compounds, BIX01294 and GSK126, as a potential epigenetic-based therapy for FRDA, with aims of reversing the *FXN* gene silencing in human and mouse FRDA-derived fibroblasts. Notably, the combination treatment of BIX01294 and GSK126 has been shown to induce a safe induction of *FXN* mRNA expression levels, in both human and mouse FRDA fibroblasts. Alongside this, a significant reduction was also seen in G9a and EZH2 levels, which was initially found to be higher in human FRDA fibroblasts. Moreover, a significant reduction in H3K9me3 and H3K27me3 levels and an increase in H3K9ac levels were seen in the *FXN* 5'UTR promoter region after BIX01294 and GSK126 combination treatment. Therefore, simultaneous inhibition of G9a and EZH2, which target H3K9me2/3 and H3K27m3 repressive histone marks, may be favourable in inducing *FXN*

gene expression levels in FRDA. However, the change in HMTases and histone modifications levels were non-cell specific, which falls into the general non-specificity of epigenetic based therapies. Therefore, the development of drugs that preferentially target the *FXN* locus in FRDA may require further consideration. Furthermore, no changes in frataxin expression levels were identified following synergistic HMTase inhibitor treatments, which may be due to other post-translational mechanisms taking place that require further investigation. Nevertheless, HMTase inhibitors should still be pursued for further preclinical studies, perhaps with other synergistic epigenetic-based compounds, such as HDAC inhibitors and DNMT inhibitors.

Similar to HMTase inhibitors, HDAC inhibitors could potentially reduce epigenetic silencing of an affected gene by targeting the heterochromatin state. In FRDA, the HDAC inhibitors 109/RG2833 and nicotinamide (vitamin B3) have shown the most promising results in restoring frataxin to normal levels by increasing histone acetylation at the *FXN* locus (Burk, 2017). Moreover, alongside abnormal histone modification, numerous studies have reported an increase in DNA methylation levels in the pathogenic *FXN* alleles. Thus far, no studies have reported the effects of DNA demethylation agents in treating FRDA. However recent reports investigating the TNR disorder FXS, have shown promising results using the DNMT inhibitor, 5-aza-CdR, either alone or in combination with HDAC inhibitors (Chiurazzi *et al.*, 1999) or with HMTase inhibitors (Kumari and Usdin, 2016) to effectively reduce the *FMR1* promoter hypermethylation and reinstating mRNA and protein levels to normal in FXS patient cells. Therefore, it would be interesting to investigate the synergistic effects of HMTase inhibitors with HDAC inhibitor compounds and/or DNMT inhibitors in the reactivation of *FXN* gene transcription.

At present, therapeutic approaches predominantly aim to induce frataxin expression from the pathogenic *FXN* locus (Strawser *et al.*, 2014), or to intrude in the pathogenic cascade downstream of frataxin deficiency. However, recent studies have reported that UPP pathway controls frataxin stability (Rufini *et al.*, 2011, 2015), thus leading to the development of new therapeutic approaches aimed at preventing the degradation of frataxin.

Therefore, we investigated the efficacy of a number of proteasome inhibitors in human FRDA fibroblasts to ameliorate the disease phenotype by increasing frataxin levels. The proteasome inhibitors, MG132, bortezomib and salinosporamide A affected the chymotrypsin-like activity of the 26S proteasomes to some extent in FRDA fibroblasts. However, no downstream effects were observed in increasing frataxin expression levels. Conversely, treatments using ixazomib displayed an upregulation in frataxin levels, alongside a dose-dependent reduction in the chymotrypsin-like activity in FRDA fibroblasts. Yet, the significance of these results are unclear since an increase in the cell cycle stress modulator, $p27^{Kip1}$, was also seen. Therefore, taking together the findings from this study and previous studies, which reported no significant increase in frataxin levels by general proteasomal inhibition (Nabhan *et al.*, 2015), the use of these proteasome inhibitors as a therapy for FRDA is not recommended at this stage.

Previously, Rufini *et al.* (2011) identified K147 as the critical lysine residue on frataxin which is targeted for ubiquitination, alongside identifying a set of UCM molecules predicted to increase frataxin stability by inhibiting ubiquitination on K147. Therefore, due to their specificity, UCMs may offer a novel therapeutic approach to treat FRDA and are currently being explored for further studies (Rufini *et al.*, 2011, 2015). Subsequently, Benini *et al.* (2017) identified RNF126 as the specific frataxin E3 ligase that causes frataxin ubiquitination and degradation. E3 ligase enzymes are responsible for substrate recognition and confer specificity to the ubiquitination process. Therefore, inhibition of RNF126 may further

represent an attractive and more selective pharmacological target for potential FRDA therapy.

Overall, and also based on our results, targeting the proteasomes, as a whole, is a highly unspecific approach and may result in an undesired outcome. Therefore, the need for a more specific therapeutic target among UPP components is crucial for the design of more selective therapies.

A different FRDA therapeutic approach to target ataxia, more generally, was instigated by reports that increased degradation of D-serine by DAO overexpression results in ataxia, possibly due to low NMDAR functioning and impaired neural signalling in the cerebellum (Hashimoto *et al.* (2005). Therefore, in collaboration with Takeda Cambridge Limited, we carried out an *in vivo* investigation to test the efficacy of a newly developed DAO inhibitor, TAK-831, using our YG8sR FRDA mouse model. Functional studies, such as beam walk and rotarod testing, revealed that YG8sR mice developed a progressive FRDA-like disease effect at older age, which was significantly reduced following TAK-831 treatment. Furthermore, our results also suggested that treating FRDA with TAK-831 at an early stage of the disease, may be beneficial in improving the progressive disease phenotype later in life.

Our study, which is the first to report the use of DAO inhibitors in a FRDA model, revealed that TAK-831 was well tolerated and helped in ameliorating ataxia motor coordination deficits. This indicated that TAK-831 should be pursued further as a potential therapy for FRDA, and indeed FARA have recently announced enrolment for a Phase 2 study of TAK-831, sponsored by Takeda (http://www.curefa.org/clinical-trials/clinical-trials-active-enrolling/phase-2-study-of-tak-831-takeda). However, it would be also interesting to assess the association of DAO activity and D-serine levels following TAK-831 treatment of FRDA

mice. Additionally, co-administration of TAK-831 with D-serine is also proposed to have beneficial effects.

Other promising therapeutic approaches which are currently being developed as a treatment for FRDA include gene replacement and protein replacement therapies. Vyas and colleagues constructed an innovative delivery system known as trans-activator of transcription (TAT) to transport human frataxin protein to mitochondria in patient-derived cells and in conditional FRDA mouse models. TAT-frataxin fusion proteins improved growth, increased lifespan by 53%, increased cardiac functions, and improved aconitase activity (Vyas *et al.*, 2012). On the other hand, there are a number of strategies currently being explored for gene replacement therapy with aims of correcting frataxin loss in FRDA (as discussed in chapter 1). Although, experimental data predominantly demonstrate effectiveness of gene replacement approaches, the challenges of targeted delivery, genotoxicity and controlled expression are yet unsolved (Evans-Galea *et al.*, 2014b). Nonetheless, a recent gene replacement therapy, using CRISPR-Cas9 system has been shown to successfully excise the GAA repeat and restore frataxin levels in YG8R and YG8sR-derived fibroblasts and YG8R mouse models (Ouellet *et al.*, 2017).

In conclusion, the evaluation of therapeutic agents for FRDA has rapidly advanced in the last few decades, with the finding of numerous pharmacological agents at different stages of development. To add to this list, our studies have also shown encouraging results with the use of HMTase inhibitors and TAK-831 as potential FRDA therapeutic approaches.

REFERENCES

ABEL, T. & ZUKIN, R. S. 2008. Epigenetic targets of HDAC inhibition in neurodegenerative and psychiatric disorders. *Curr Opin Pharmacol,* 8**,** 57-64.

ACQUAVIVA, F., CASTALDO, I., FILLA, A., GIACCHETTI, M., MARMOLINO, D., MONTICELLI, A., PINELLI, M., SACCA, F. & COCOZZA, S. 2008. Recombinant human erythropoietin increases frataxin protein expression without increasing mRNA expression. *Cerebellum,* 7**,** 360-5.

ADAMEC, J., RUSNAK, F., OWEN, W. G., NAYLOR, S., BENSON, L. M., GACY, A. M. & ISAYA, G. 2000. Iron-dependent self-assembly of recombinant yeast frataxin: implications for Friedreich ataxia. *Am J Hum Genet,* 67**,** 549-62.

ADAMS, J. & KAUFFMAN, M. 2004. Development of the proteasome inhibitor Velcade (Bortezomib). *Cancer Invest,* 22**,** 304-11.

ADINOLFI, S., IANNUZZI, C., PRISCHI, F., PASTORE, C., IAMETTI, S., MARTIN, S. R., BONOMI, F. & PASTORE, A. 2009. Bacterial frataxin CyaY is the gatekeeper of iron-sulfur cluster formation catalyzed by IscS. *Nat Struct Mol Biol,* 16**,** 390-6.

ADINOLFI, S., TRIFUOGGI, M., POLITOU, A. S., MARTIN, S. & PASTORE, A. 2002. A structural approach to understanding the iron-binding properties of phylogenetically different frataxins. *Hum Mol Genet,* 11**,** 1865-77.

AL-MAHDAWI, S., PINTO, R. M., ISMAIL, O., VARSHNEY, D., LYMPERI, S., SANDI, C., TRABZUNI, D. & POOK, M. 2008. The Friedreich ataxia GAA repeat expansion mutation induces comparable epigenetic changes in human and transgenic mouse brain and heart tissues. *Hum Mol Genet,* 17**,** 735-46.

AL-MAHDAWI, S., PINTO, R. M., RUDDLE, P., CARROLL, C., WEBSTER, Z. & POOK, M. 2004. GAA repeat instability in Friedreich ataxia YAC transgenic mice. *Genomics,* 84**,** 301-10.

AL-SALAMA, Z. T., GARNOCK-JONES, K. P. & SCOTT, L. J. 2017. Ixazomib: A Review in Relapsed and/or Refractory Multiple Myeloma. *Target Oncol,* 12**,** 535-542.

ALPER, G. & NARAYANAN, V. 2003. Friedreich's ataxia. *Pediatr Neurol,* 28**,** 335-41.

AMERIK, A. Y. & HOCHSTRASSER, M. 2004. Mechanism and function of deubiquitinating enzymes. *Biochim Biophys Acta,* 1695**,** 189-207.

ANJOMANI VIRMOUNI, S., EZZATIZADEH, V., SANDI, C., SANDI, M., AL-MAHDAWI, S., CHUTAKE, Y. & POOK, M. A. 2015. A novel GAA-repeat-expansion-based mouse model of Friedreich's ataxia. *Dis Model Mech,* 8**,** 225-35.

ANTIGNANO, F., BURROWS, K., HUGHES, M. R., HAN, J. M., KRON, K. J., PENROD, N. M., OUDHOFF, M. J., WANG, S. K., MIN, P. H., GOLD, M. J., CHENERY, A. L., BRAAM, M. J., FUNG, T. C., ROSSI, F. M., MCNAGNY, K. M., ARROWSMITH, C. H., LUPIEN, M., LEVINGS, M. K. & ZAPH, C. 2014. Methyltransferase G9A regulates T cell differentiation during murine intestinal inflammation. *J Clin Invest,* 124**,** 1945-55.

ARANCA, T. V., JONES, T. M., SHAW, J. D., STAFFETTI, J. S., ASHIZAWA, T., KUO, S. H., FOGEL, B. L., WILMOT, G. R., PERLMAN, S. L., ONYIKE, C. U., YING, S. H. & ZESIEWICZ, T. A. 2016. Emerging therapies in Friedreich's ataxia. *Neurodegener Dis Manag,* 6**,** 49-65.

BABCOCK, M., DE SILVA, D., OAKS, R., DAVIS-KAPLAN, S., JIRALERSPONG, S., MONTERMINI, L., PANDOLFO, M. & KAPLAN, J. 1997. Regulation of mitochondrial iron accumulation by Yfh1p, a putative homolog of frataxin. *Science,* 276**,** 1709-12.

BACOLLA, A., WANG, G. & VASQUEZ, K. M. 2015. New Perspectives on DNA and RNA Triplexes As Effectors of Biological Activity. *PLoS Genet,* 11**,** e1005696.

BANNISTER, A. J. & KOUZARIDES, T. 2011. Regulation of chromatin by histone modifications. *Cell Res,* 21**,** 381-95.

BAUMEISTER, W., WALZ, J., ZUHL, F. & SEEMULLER, E. 1998. The proteasome: paradigm of a self-compartmentalizing protease. *Cell,* 92**,** 367-80.

BAYOT, A. & RUSTIN, P. 2013. Friedreich's ataxia, frataxin, PIP5K1B: echo of a distant fracas. *Oxid Med Cell Longev,* 2013**,** 725635.

BEDFORD, L., LOWE, J., DICK, L. R., MAYER, R. J. & BROWNELL, J. E. 2011. Ubiquitin-like protein conjugation and the ubiquitin-proteasome system as drug targets. *Nat Rev Drug Discov,* 10**,** 29-46.

BENAROUDJ, N., ZWICKL, P., SEEMULLER, E., BAUMEISTER, W. & GOLDBERG, A. L. 2003. ATP hydrolysis by the proteasome regulatory complex PAN serves multiple functions in protein degradation. *Mol Cell,* 11**,** 69-78.

BENCZE, K. Z., YOON, T., MILLAN-PACHECO, C., BRADLEY, P. B., PASTOR, N., COWAN, J. A. & STEMMLER, T. L. 2007. Human frataxin: iron and ferrochelatase binding surface. *Chem Commun (Camb)***,** 1798-800.

BENINI, M., FORTUNI, S., CONDO, I., ALFEDI, G., MALISAN, F., TOSCHI, N., SERIO, D., MASSARO, D. S., ARCURI, G., TESTI, R. & RUFINI, A. 2017. E3 Ligase RNF126 Directly Ubiquitinates Frataxin, Promoting Its Degradation: Identification of a Potential Therapeutic Target for Friedreich Ataxia. *Cell Rep,* 18**,** 2007-2017.

BIDICHANDANI, S. I., GARCIA, C. A., PATEL, P. I. & DIMACHKIE, M. M. 2000. Very late-onset Friedreich ataxia despite large GAA triplet repeat expansions. *Arch Neurol,* 57**,** 246-51.

BLACK, J. C., VAN RECHEM, C. & WHETSTINE, J. R. 2012. Histone lysine methylation dynamics: establishment, regulation, and biological impact. *Mol Cell,* 48**,** 491-507.

BOCHTLER, M., DITZEL, L., GROLL, M., HARTMANN, C. & HUBER, R. 1999. The proteasome. *Annu Rev Biophys Biomol Struct,* 28**,** 295-317.

BODDAERT, N., LE QUAN SANG, K. H., ROTIG, A., LEROY-WILLIG, A., GALLET, S., BRUNELLE, F., SIDI, D., THALABARD, J. C., MUNNICH, A. & CABANTCHIK, Z. I. 2007. Selective iron chelation in Friedreich ataxia: biologic and clinical implications. *Blood,* 110**,** 401-8.

BOESCH, S., NACHBAUER, W., MARIOTTI, C., SACCA, F., FILLA, A., KLOCKGETHER, T., KLOPSTOCK, T., SCHOLS, L., JACOBI, H., BUCHNER, B., VOM HAGEN, J. M., NANETTI, L. & MANICOM, K. 2014. Safety and tolerability of carbamylated erythropoietin in Friedreich's ataxia. *Mov Disord,* 29**,** 935-9.

BOESCH, S., STURM, B., HERING, S., GOLDENBERG, H., POEWE, W. & SCHEIBER-MOJDEHKAR, B. 2007. Friedreich's ataxia: clinical pilot trial with recombinant human erythropoietin. *Ann Neurol,* 62**,** 521-4.

BOESCH, S., STURM, B., HERING, S., SCHEIBER-MOJDEHKAR, B., STEINKELLNER, H., GOLDENBERG, H. & POEWE, W. 2008. Neurological effects of recombinant human erythropoietin in Friedreich's ataxia: a clinical pilot trial. *Mov Disord,* 23**,** 1940-4.

BOU-ABDALLAH, F., ADINOLFI, S., PASTORE, A., LAUE, T. M. & DENNIS CHASTEEN, N. 2004. Iron binding and oxidation kinetics in frataxin CyaY of Escherichia coli. *J Mol Biol,* 341**,** 605-15.

BRADLEY, J. L., BLAKE, J. C., CHAMBERLAIN, S., THOMAS, P. K., COOPER, J. M. & SCHAPIRA, A. H. 2000. Clinical, biochemical and molecular genetic correlations in Friedreich's ataxia. *Hum Mol Genet,* 9**,** 275-82.

BULTEAU, A. L., O'NEILL, H. A., KENNEDY, M. C., IKEDA-SAITO, M., ISAYA, G. & SZWEDA, L. I. 2004. Frataxin acts as an iron chaperone protein to modulate mitochondrial aconitase activity. *Science,* 305**,** 242-5.

BURK, K. 2017. Friedreich Ataxia: current status and future prospects. *Cerebellum Ataxias,* 4**,** 4.

BURNETT, R., MELANDER, C., PUCKETT, J. W., SON, L. S., WELLS, R. D., DERVAN, P. B. & GOTTESFELD, J. M. 2006. DNA sequence-specific polyamides alleviate transcription inhibition associated with long GAA.TTC repeats in Friedreich's ataxia. *Proc Natl Acad Sci U S A,* 103**,** 11497-502.

CALABRESE, V., LODI, R., TONON, C., D'AGATA, V., SAPIENZA, M., SCAPAGNINI, G., MANGIAMELI, A., PENNISI, G., STELLA, A. M. & BUTTERFIELD, D. A. 2005. Oxidative stress, mitochondrial dysfunction and cellular stress response in Friedreich's ataxia. *J Neurol Sci,* 233**,** 145-62.

CAMPUZANO, V., MONTERMINI, L., LUTZ, Y., COVA, L., HINDELANG, C., JIRALERSPONG, S., TROTTIER, Y., KISH, S. J., FAUCHEUX, B., TROUILLAS, P., AUTHIER, F. J., DURR, A., MANDEL, J. L., VESCOVI, A., PANDOLFO, M. & KOENIG, M. 1997. Frataxin is reduced in Friedreich ataxia patients and is associated with mitochondrial membranes. *Hum Mol Genet,* 6**,** 1771-80.

CAMPUZANO, V., MONTERMINI, L., MOLTO, M. D., PIANESE, L., COSSEE, M., CAVALCANTI, F., MONROS, E., RODIUS, F., DUCLOS, F., MONTICELLI, A., ZARA, F., CANIZARES, J., KOUTNIKOVA, H., BIDICHANDANI, S. I., GELLERA, C., BRICE, A., TROUILLAS, P., DE MICHELE, G., FILLA, A., DE FRUTOS, R., PALAU, F., PATEL, P. I., DI DONATO, S., MANDEL, J. L., COCOZZA, S., KOENIG, M. & PANDOLFO, M. 1996. Friedreich's ataxia: autosomal recessive disease caused by an intronic GAA triplet repeat expansion. *Science,* 271**,** 1423-7.

CAVADINI, P., GELLERA, C., PATEL, P. I. & ISAYA, G. 2000. Human frataxin maintains mitochondrial iron homeostasis in Saccharomyces cerevisiae. *Hum Mol Genet,* 9**,** 2523-30.

CEMAL, C. K., HUXLEY, C. & CHAMBERLAIN, S. 1999. Insertion of expanded CAG trinucleotide repeat motifs into a yeast artificial chromosome containing the human Machado-Joseph disease gene. *Gene,* 236**,** 53-61.

CHAMBERLAIN, S., SHAW, J., ROWLAND, A., WALLIS, J., SOUTH, S., NAKAMURA, Y., VON GABAIN, A., FARRALL, M. & WILLIAMSON, R. 1988. Mapping of mutation causing Friedreich's ataxia to human chromosome 9. *Nature,* 334**,** 248-50.

CHAN, P. K., TORRES, R., YANDIM, C., LAW, P. P., KHADAYATE, S., MAURI, M., GROSAN, C., CHAPMAN-ROTHE, N., GIUNTI, P., POOK, M. & FESTENSTEIN, R. 2013. Heterochromatinization induced by GAA-repeat hyperexpansion in Friedreich's ataxia can be reduced upon HDAC inhibition by vitamin B3. *Hum Mol Genet,* 22**,** 2662-75.

CHANG, Y., ZHANG, X., HORTON, J. R., UPADHYAY, A. K., SPANNHOFF, A., LIU, J., SNYDER, J. P., BEDFORD, M. T. & CHENG, X. 2009. Structural basis for G9a-like protein lysine methyltransferase inhibition by BIX-01294. *Nat Struct Mol Biol,* 16**,** 312-7.

CHANTREL-GROUSSARD, K., GEROMEL, V., PUCCIO, H., KOENIG, M., MUNNICH, A., ROTIG, A. & RUSTIN, P. 2001. Disabled early recruitment of antioxidant defenses in Friedreich's ataxia. *Hum Mol Genet,* 10**,** 2061-7.

CHAUHAN, D., CATLEY, L., LI, G., PODAR, K., HIDESHIMA, T., VELANKAR, M., MITSIADES, C., MITSIADES, N., YASUI, H., LETAI, A., OVAA, H., BERKERS, C., NICHOLSON, B., CHAO, T.

H., NEUTEBOOM, S. T., RICHARDSON, P., PALLADINO, M. A. & ANDERSON, K. C. 2005. A novel orally active proteasome inhibitor induces apoptosis in multiple myeloma cells with mechanisms distinct from Bortezomib. *Cancer Cell,* 8**,** 407-19.

CHAUHAN, D., TIAN, Z., ZHOU, B., KUHN, D., ORLOWSKI, R., RAJE, N., RICHARDSON, P. & ANDERSON, K. C. 2011. In vitro and in vivo selective antitumor activity of a novel orally bioavailable proteasome inhibitor MLN9708 against multiple myeloma cells. *Clin Cancer Res,* 17**,** 5311-21.

CHEN, D. & DOU, Q. P. 2010. The ubiquitin-proteasome system as a prospective molecular target for cancer treatment and prevention. *Curr Protein Pept Sci,* 11**,** 459-70.

CHEN, D., FREZZA, M., SCHMITT, S., KANWAR, J. & DOU, Q. P. 2011. Bortezomib as the first proteasome inhibitor anticancer drug: current status and future perspectives. *Curr Cancer Drug Targets,* 11**,** 239-53.

CHEN, H., YAN, Y., DAVIDSON, T. L., SHINKAI, Y. & COSTA, M. 2006. Hypoxic stress induces dimethylated histone H3 lysine 9 through histone methyltransferase G9a in mammalian cells. *Cancer Res,* 66**,** 9009-16.

CHEUNG, P. & LAU, P. 2005. Epigenetic regulation by histone methylation and histone variants. *Mol Endocrinol,* 19**,** 563-73.

CHIURAZZI, P., POMPONI, M. G., PIETROBONO, R., BAKKER, C. E., NERI, G. & OOSTRA, B. A. 1999. Synergistic effect of histone hyperacetylation and DNA demethylation in the reactivation of the FMR1 gene. *Hum Mol Genet,* 8**,** 2317-23.

CHUTAKE, Y. K., LAM, C., COSTELLO, W. N., ANDERSON, M. & BIDICHANDANI, S. I. 2014. Epigenetic promoter silencing in Friedreich ataxia is dependent on repeat length. *Ann Neurol,* 76**,** 522-8.

CNOP, M., IGOILLO-ESTEVE, M., RAI, M., BEGU, A., SERROUKH, Y., DEPONDT, C., MUSUAYA, A. E., MARHFOUR, I., LADRIERE, L., MOLES LOPEZ, X., LEFKADITIS, D., MOORE, F., BRION, J. P., COOPER, J. M., SCHAPIRA, A. H., CLARK, A., KOEPPEN, A. H., MARCHETTI, P., PANDOLFO, M., EIZIRIK, D. L. & FERY, F. 2012. Central role and mechanisms of beta-cell dysfunction and death in friedreich ataxia-associated diabetes. *Ann Neurol,* 72**,** 971-82.

CODAZZI, F., HU, A., RAI, M., DONATELLO, S., SALERNO SCARZELLA, F., MANGIAMELI, E., PELIZZONI, I., GROHOVAZ, F. & PANDOLFO, M. 2016. Friedreich ataxia-induced pluripotent stem cell-derived neurons show a cellular phenotype that is corrected by a benzamide HDAC inhibitor. *Hum Mol Genet,* 25**,** 4847-4855.

CONDO, I., VENTURA, N., MALISAN, F., RUFINI, A., TOMASSINI, B. & TESTI, R. 2007. In vivo maturation of human frataxin. *Hum Mol Genet,* 16**,** 1534-40.

COOPER, J. M. & SCHAPIRA, A. H. 2007. Friedreich's ataxia: coenzyme Q10 and vitamin E therapy. *Mitochondrion,* 7 Suppl**,** S127-35.

COSSEE, M., PUCCIO, H., GANSMULLER, A., KOUTNIKOVA, H., DIERICH, A., LEMEUR, M., FISCHBECK, K., DOLLE, P. & KOENIG, M. 2000. Inactivation of the Friedreich ataxia mouse gene leads to early embryonic lethality without iron accumulation. *Hum Mol Genet,* 9**,** 1219-26.

COSSEE, M., SCHMITT, M., CAMPUZANO, V., REUTENAUER, L., MOUTOU, C., MANDEL, J. L. & KOENIG, M. 1997. Evolution of the Friedreich's ataxia trinucleotide repeat expansion: founder effect and premutations. *Proc Natl Acad Sci U S A,* 94**,** 7452-7.

CRAWFORD, L. J., WALKER, B., OVAA, H., CHAUHAN, D., ANDERSON, K. C., MORRIS, T. C. & IRVINE, A. E. 2006. Comparative selectivity and specificity of the proteasome inhibitors BzLLLCOCHO, PS-341, and MG-132. *Cancer Res,* 66**,** 6379-86.

CUMMINGS, C. J. & ZOGHBI, H. Y. 2000. Trinucleotide repeats: mechanisms and pathophysiology. *Annu Rev Genomics Hum Genet,* 1**,** 281-328.

DANYSZ, W. & PARSONS, C. G. 1998. Glycine and N-methyl-D-aspartate receptors: physiological significance and possible therapeutic applications. *Pharmacol Rev,* 50**,** 597-664.

DE BIASE, I., CHUTAKE, Y. K., RINDLER, P. M. & BIDICHANDANI, S. I. 2009. Epigenetic silencing in Friedreich ataxia is associated with depletion of CTCF (CCCTC-binding factor) and antisense transcription. *PLoS One,* 4**,** e7914.

DE BIASE, I., RASMUSSEN, A., ENDRES, D., AL-MAHDAWI, S., MONTICELLI, A., COCOZZA, S., POOK, M. & BIDICHANDANI, S. I. 2007a. Progressive GAA expansions in dorsal root ganglia of Friedreich's ataxia patients. *Ann Neurol,* 61**,** 55-60.

DE BIASE, I., RASMUSSEN, A., MONTICELLI, A., AL-MAHDAWI, S., POOK, M., COCOZZA, S. & BIDICHANDANI, S. I. 2007b. Somatic instability of the expanded GAA triplet-repeat sequence in Friedreich ataxia progresses throughout life. *Genomics,* 90**,** 1-5.

DE MICHELE, G., CAVALCANTI, F., CRISCUOLO, C., PIANESE, L., MONTICELLI, A., FILLA, A. & COCOZZA, S. 1998. Parental gender, age at birth and expansion length influence GAA repeat intergenerational instability in the X25 gene: pedigree studies and analysis of sperm from patients with Friedreich's ataxia. *Hum Mol Genet,* 7**,** 1901-6.

DE MICHELE, G., FILLA, A., CAVALCANTI, F., DI MAIO, L., PIANESE, L., CASTALDO, I., CALABRESE, O., MONTICELLI, A., VARRONE, S., CAMPANELLA, G. & ET AL. 1994. Late onset Friedreich's disease: clinical features and mapping of mutation to the FRDA locus. *J Neurol Neurosurg Psychiatry,* 57**,** 977-9.

DE MIRANDA, J., PANIZZUTTI, R., FOLTYN, V. N. & WOLOSKER, H. 2002. Cofactors of serine racemase that physiologically stimulate the synthesis of the N-methyl-D-aspartate (NMDA) receptor coagonist D-serine. *Proc Natl Acad Sci U S A,* 99**,** 14542-7.

DELATYCKI, M. B. 2009. Evaluating the progression of Friedreich ataxia and its treatment. *J Neurol,* 256 Suppl 1**,** 36-41.

DELATYCKI, M. B., PARIS, D., GARDNER, R. J., FORSHAW, K., NICHOLSON, G. A., NASSIF, N., WILLIAMSON, R. & FORREST, S. M. 1998. Sperm DNA analysis in a Friedreich ataxia premutation carrier suggests both meiotic and mitotic expansion in the FRDA gene. *J Med Genet,* 35**,** 713-6.

DELATYCKI, M. B., WILLIAMSON, R. & FORREST, S. M. 2000. Friedreich ataxia: an overview. *J Med Genet,* 37**,** 1-8.

DHE-PAGANON, S., SHIGETA, R., CHI, Y. I., RISTOW, M. & SHOELSON, S. E. 2000. Crystal structure of human frataxin. *J Biol Chem,* 275**,** 30753-6.

DI PROSPERO, N. A., BAKER, A., JEFFRIES, N. & FISCHBECK, K. H. 2007a. Neurological effects of high-dose idebenone in patients with Friedreich's ataxia: a randomised, placebo-controlled trial. *Lancet Neurol,* 6**,** 878-86.

DI PROSPERO, N. A., SUMNER, C. J., PENZAK, S. R., RAVINA, B., FISCHBECK, K. H. & TAYLOR, J. P. 2007b. Safety, tolerability, and pharmacokinetics of high-dose idebenone in patients with Friedreich ataxia. *Arch Neurol,* 64**,** 803-8.

DILLON, N. & FESTENSTEIN, R. 2002. Unravelling heterochromatin: competition between positive and negative factors regulates accessibility. *Trends Genet,* 18**,** 252-8.

DURR, A., COSSEE, M., AGID, Y., CAMPUZANO, V., MIGNARD, C., PENET, C., MANDEL, J. L., BRICE, A. & KOENIG, M. 1996. Clinical and genetic abnormalities in patients with Friedreich's ataxia. *N Engl J Med,* 335**,** 1169-75.

ELGIN, S. C. & REUTER, G. 2013. Position-effect variegation, heterochromatin formation, and gene silencing in Drosophila. *Cold Spring Harb Perspect Biol,* 5**,** a017780.

EMOND, M., LEPAGE, G., VANASSE, M. & PANDOLFO, M. 2000. Increased levels of plasma malondialdehyde in Friedreich ataxia. *Neurology,* 55**,** 1752-3.

ERALES, J. & COFFINO, P. 2014. Ubiquitin-independent proteasomal degradation. *Biochim Biophys Acta,* 1843**,** 216-21.

ERWIN, G. S., GRIESHOP, M. P., ALI, A., QI, J., LAWLOR, M., KUMAR, D., AHMAD, I., MCNALLY, A., TEIDER, N., WORRINGER, K., SIVASANKARAN, R., SYED, D. N., EGUCHI, A., ASHRAF, M., JEFFERY, J., XU, M., PARK, P. M. C., MUKHTAR, H., SRIVASTAVA, A. K., FARUQ, M., BRADNER, J. E. & ANSARI, A. Z. 2017. Synthetic transcription elongation factors license transcription across repressive chromatin. *Science,* 358**,** 1617-1622.

ETZION, Y. & GROSSMAN, Y. 2001. Highly 4-aminopyridine sensitive delayed rectifier current modulates the excitability of guinea pig cerebellar Purkinje cells. *Exp Brain Res,* 139**,** 419-25.

EVANS-GALEA, M. V., CARRODUS, N., ROWLEY, S. M., CORBEN, L. A., TAI, G., SAFFERY, R., GALATI, J. C., WONG, N. C., CRAIG, J. M., LYNCH, D. R., REGNER, S. R., BROCHT, A. F., PERLMAN, S. L., BUSHARA, K. O., GOMEZ, C. M., WILMOT, G. R., LI, L., VARLEY, E., DELATYCKI, M. B. & SARSERO, J. P. 2012. FXN methylation predicts expression and clinical outcome in Friedreich ataxia. *Ann Neurol,* 71**,** 487-97.

EVANS-GALEA, M. V., LOCKHART, P. J., GALEA, C. A., HANNAN, A. J. & DELATYCKI, M. B. 2014a. Beyond loss of frataxin: the complex molecular pathology of Friedreich ataxia. *Discov Med,* 17**,** 25-35.

EVANS-GALEA, M. V., PEBAY, A., DOTTORI, M., CORBEN, L. A., ONG, S. H., LOCKHART, P. J. & DELATYCKI, M. B. 2014b. Cell and gene therapy for Friedreich ataxia: progress to date. *Hum Gene Ther,* 25**,** 684-93.

FEIL, K., BREMOVA, T., MUTH, C., SCHNIEPP, R., TEUFEL, J. & STRUPP, M. 2016. Update on the Pharmacotherapy of Cerebellar Ataxia and Nystagmus. *Cerebellum,* 15**,** 38-42.

FEIL, K., CLAASSEN, J., BARDINS, S., TEUFEL, J., KRAFCZYK, S., SCHNEIDER, E., SCHNIEPP, R., JAHN, K., KALLA, R. & STRUPP, M. 2013. Effect of chlorzoxazone in patients with downbeat nystagmus: a pilot trial. *Neurology,* 81**,** 1152-8.

FELDMAN, N., GERSON, A., FANG, J., LI, E., ZHANG, Y., SHINKAI, Y., CEDAR, H. & BERGMAN, Y. 2006. G9a-mediated irreversible epigenetic inactivation of Oct-3/4 during early embryogenesis. *Nat Cell Biol,* 8**,** 188-94.

FENICAL, W. & JENSEN, P. R. 2006. Developing a new resource for drug discovery: marine actinomycete bacteria. *Nat Chem Biol,* 2**,** 666-73.

FERRARIS, D., DUVALL, B., KO, Y. S., THOMAS, A. G., ROJAS, C., MAJER, P., HASHIMOTO, K. & TSUKAMOTO, T. 2008. Synthesis and biological evaluation of D-amino acid oxidase inhibitors. *J Med Chem,* 51**,** 3357-9.

FESTENSTEIN, R. 2006. Breaking the silence in Friedreich's ataxia. *Nat Chem Biol,* 2**,** 512-3.

FESTENSTEIN, R., SHARGHI-NAMINI, S., FOX, M., RODERICK, K., TOLAINI, M., NORTON, T., SAVELIEV, A., KIOUSSIS, D. & SINGH, P. 1999. Heterochromatin protein 1 modifies mammalian PEV in a dose- and chromosomal-context-dependent manner. *Nat Genet,* 23**,** 457-61.

FESTENSTEIN, R., TOLAINI, M., CORBELLA, P., MAMALAKI, C., PARRINGTON, J., FOX, M., MILIOU, A., JONES, M. & KIOUSSIS, D. 1996. Locus control region function and heterochromatin-induced position effect variegation. *Science,* 271**,** 1123-5.

FILLA, A., DE MICHELE, G., CAVALCANTI, F., PIANESE, L., MONTICELLI, A., CAMPANELLA, G. & COCOZZA, S. 1996. The relationship between trinucleotide (GAA) repeat length and clinical features in Friedreich ataxia. *Am J Hum Genet,* 59**,** 554-60.

FLEMING, J., SPINOULAS, A., ZHENG, M., CUNNINGHAM, S. C., GINN, S. L., MCQUILTY, R. C., ROWE, P. B. & ALEXANDER, I. E. 2005. Partial correction of sensitivity to oxidant stress in Friedreich ataxia patient fibroblasts by frataxin-encoding adeno-associated virus and lentivirus vectors. *Hum Gene Ther,* 16**,** 947-56.

FOURY, F. & CAZZALINI, O. 1997. Deletion of the yeast homologue of the human gene associated with Friedreich's ataxia elicits iron accumulation in mitochondria. *FEBS Lett,* 411**,** 373-7.

FRANCIS, N. J., KINGSTON, R. E. & WOODCOCK, C. L. 2004. Chromatin compaction by a polycomb group protein complex. *Science,* 306**,** 1574-7.

FRANK-KAMENETSKII, M. D. & MIRKIN, S. M. 1995. Triplex DNA structures. *Annu Rev Biochem,* 64**,** 65-95.

FRIEDREICH, N. 1863a. Ueber degenerative Atrophie der spinalen Hinterstränge (On degenerative atrophy of the spinal dorsal columns). *Virchows Arch Pathol Anat Physiol Klin Med,* 26**,** 391–419.

FRIEDREICH, N. 1863b. Ueber degenerative Atrophie der spinalen Hinterstränge (On degenerative atrophy of the spinal dorsal columns). *Virchows Arch Pathol Anat Physiol Klin Med,* 26**,** 433–459.

FRIEDREICH, N. 1863c. Ueber degenerative Atrophie der spinalen Hinterstränge (On degenerative atrophy of the spinal dorsal columns). *Virchows Arch Pathol Anat Physiol Klin Med,* 27**,** 1–26.

FRIEDREICH, N. 1876. Ueber Ataxie mit besonderer Berücksichtigung der hereditären Formen (About ataxia with special consideration of the hereditary forms). *Virchows Arch Pathol Anat Physiol Klin Med,* 68**,** 145–245.

FRIEDREICH, N. 1877. Ueber Ataxie mit besonderer Berücksichtigung der hereditären Formen. Nachtrag (About ataxia with special consideration of the hereditary forms. Postscriptum). *Virchows Arch Pathol Anat Physiol Klin Med,* 70**,** 140–152.

GACY, A. M., GOELLNER, G. M., SPIRO, C., CHEN, X., GUPTA, G., BRADBURY, E. M., DYER, R. B., MIKESELL, M. J., YAO, J. Z., JOHNSON, A. J., RICHTER, A., MELANCON, S. B. & MCMURRAY, C. T. 1998. GAA instability in Friedreich's Ataxia shares a common, DNA-directed and intraallelic mechanism with other trinucleotide diseases. *Mol Cell,* 1**,** 583-93.

GAKH, O., ADAMEC, J., GACY, A. M., TWESTEN, R. D., OWEN, W. G. & ISAYA, G. 2002. Physical evidence that yeast frataxin is an iron storage protein. *Biochemistry,* 41**,** 6798-804.

GERARD, C., XIAO, X., FILALI, M., COULOMBE, Z., ARSENAULT, M., COUET, J., LI, J., DROLET, M. C., CHAPDELAINE, P., CHIKH, A. & TREMBLAY, J. P. 2014. An AAV9 coding for frataxin clearly improved the symptoms and prolonged the life of Friedreich ataxia mouse models. *Mol Ther Methods Clin Dev,* 1**,** 14044.

GERBER, J., MUHLENHOFF, U. & LILL, R. 2003. An interaction between frataxin and Isu1/Nfs1 that is crucial for Fe/S cluster synthesis on Isu1. *EMBO Rep,* 4**,** 906-11.

GIBSON, T. J., KOONIN, E. V., MUSCO, G., PASTORE, A. & BORK, P. 1996. Friedreich's ataxia protein: phylogenetic evidence for mitochondrial dysfunction. *Trends Neurosci,* 19**,** 465-8.

GLICKMAN, M. H. & CIECHANOVER, A. 2002. The ubiquitin-proteasome proteolytic pathway: destruction for the sake of construction. *Physiol Rev,* 82**,** 373-428.

GLICKSTEIN, H., EL, R. B., SHVARTSMAN, M. & CABANTCHIK, Z. I. 2005. Intracellular labile iron pools as direct targets of iron chelators: a fluorescence study of chelator action in living cells. *Blood,* 106**,** 3242-50.

GOLDBERG, A. L. 2003. Protein degradation and protection against misfolded or damaged proteins. *Nature,* 426**,** 895-9.

GONCALVES, S., PAUPE, V., DASSA, E. P. & RUSTIN, P. 2008. Deferiprone targets aconitase: implication for Friedreich's ataxia treatment. *BMC Neurol,* 8**,** 20.

GOTTESFELD, J. M. 2007. Small molecules affecting transcription in Friedreich ataxia. *Pharmacol Ther,* 116**,** 236-48.

GOTTESFELD, J. M., RUSCHE, J. R. & PANDOLFO, M. 2013. Increasing frataxin gene expression with histone deacetylase inhibitors as a therapeutic approach for Friedreich's ataxia. *J Neurochem,* 126 Suppl 1**,** 147-54.

GRABCZYK, E., MANCUSO, M. & SAMMARCO, M. C. 2007. A persistent RNA.DNA hybrid formed by transcription of the Friedreich ataxia triplet repeat in live bacteria, and by T7 RNAP in vitro. *Nucleic Acids Res,* 35**,** 5351-9.

GRABCZYK, E. & USDIN, K. 2000. The GAA*TTC triplet repeat expanded in Friedreich's ataxia impedes transcription elongation by T7 RNA polymerase in a length and supercoil dependent manner. *Nucleic Acids Res,* 28**,** 2815-22.

GRASSO, G., SFACTERIA, A., MELI, F., PASSALACQUA, M., FODALE, V., BUEMI, M., GIAMBARTINO, F., IACOPINO, D. G. & TOMASELLO, F. 2007. The role of erythropoietin in neuroprotection: therapeutic perspectives. *Drug News Perspect,* 20**,** 315-20.

GRAU, D. J., CHAPMAN, B. A., GARLICK, J. D., BOROWSKY, M., FRANCIS, N. J. & KINGSTON, R. E. 2011. Compaction of chromatin by diverse Polycomb group proteins requires localized regions of high charge. *Genes Dev,* 25**,** 2210-21.

GREENE, E., MAHISHI, L., ENTEZAM, A., KUMARI, D. & USDIN, K. 2007. Repeat-induced epigenetic changes in intron 1 of the frataxin gene and its consequences in Friedreich ataxia. *Nucleic Acids Res,* 35**,** 3383-90.

GROH, M., LUFINO, M. M., WADE-MARTINS, R. & GROMAK, N. 2014. R-loops associated with triplet repeat expansions promote gene silencing in Friedreich ataxia and fragile X syndrome. *PLoS Genet,* 10**,** e1004318.

GROLL, M., HEINEMEYER, W., JAGER, S., ULLRICH, T., BOCHTLER, M., WOLF, D. H. & HUBER, R. 1999. The catalytic sites of 20S proteasomes and their role in subunit maturation: a mutational and crystallographic study. *Proc Natl Acad Sci U S A,* 96**,** 10976-83.

GUO, N. & PENG, Z. 2013. MG132, a proteasome inhibitor, induces apoptosis in tumor cells. *Asia Pac J Clin Oncol,* 9**,** 6-11.

HANDY, D. E., CASTRO, R. & LOSCALZO, J. 2011. Epigenetic modifications: basic mechanisms and role in cardiovascular disease. *Circulation,* 123**,** 2145-56.

HARDING, A. E. 1981. Early onset cerebellar ataxia with retained tendon reflexes: a clinical and genetic study of a disorder distinct from Friedreich's ataxia. *J Neurol Neurosurg Psychiatry,* 44**,** 503-8.

HARDING, A. E., DIENGDOH, J. V. & LEES, A. J. 1984. Autosomal recessive late onset multisystem disorder with cerebellar cortical atrophy at necropsy: report of a family. *J Neurol Neurosurg Psychiatry,* 47**,** 853-6.

HART, P. E., LODI, R., RAJAGOPALAN, B., BRADLEY, J. L., CRILLEY, J. G., TURNER, C., BLAMIRE, A. M., MANNERS, D., STYLES, P., SCHAPIRA, A. H. & COOPER, J. M. 2005. Antioxidant treatment of patients with Friedreich ataxia: four-year follow-up. *Arch Neurol,* 62**,** 621-6.

HASHIMOTO, A., YOSHIKAWA, M., NIWA, A. & KONNO, R. 2005. Mice lacking D-amino acid oxidase activity display marked attenuation of stereotypy and ataxia induced by MK-801. *Brain Res,* 1033**,** 210-5.

HASHIMOTO, K., FUJITA, Y., HORIO, M., KUNITACHI, S., IYO, M., FERRARIS, D. & TSUKAMOTO, T. 2009. Co-administration of a D-amino acid oxidase inhibitor potentiates the efficacy of D-serine in attenuating prepulse inhibition deficits after administration of dizocilpine. *Biol Psychiatry,* 65**,** 1103-6.

HEIDARI, M. M., HOUSHMAND, M., HOSSEINKHANI, S., NAFISSI, S. & KHATAMI, M. 2009. Complex I and ATP content deficiency in lymphocytes from Friedreich's ataxia. *Can J Neurol Sci,* 36**,** 26-31.

HERMAN, D., JENSSEN, K., BURNETT, R., SORAGNI, E., PERLMAN, S. L. & GOTTESFELD, J. M. 2006. Histone deacetylase inhibitors reverse gene silencing in Friedreich's ataxia. *Nat Chem Biol,* 2**,** 551-8.

HERSHKO, A., HELLER, H., ELIAS, S. & CIECHANOVER, A. 1983. Components of ubiquitin-protein ligase system. Resolution, affinity purification, and role in protein breakdown. *J Biol Chem,* 258**,** 8206-14.

HICK, A., WATTENHOFER-DONZE, M., CHINTAWAR, S., TROPEL, P., SIMARD, J. P., VAUCAMPS, N., GALL, D., LAMBOT, L., ANDRE, C., REUTENAUER, L., RAI, M., TELETIN, M., MESSADDEQ, N., SCHIFFMANN, S. N., VIVILLE, S., PEARSON, C. E., PANDOLFO, M. & PUCCIO, H. 2013. Neurons and cardiomyocytes derived from induced pluripotent stem cells as a model for mitochondrial defects in Friedreich's ataxia. *Dis Model Mech,* 6**,** 608-21.

HOUREZ, R., SERVAIS, L., ORDUZ, D., GALL, D., MILLARD, I., DE KERCHOVE D'EXAERDE, A., CHERON, G., ORR, H. T., PANDOLFO, M. & SCHIFFMANN, S. N. 2011. Aminopyridines correct early dysfunction and delay neurodegeneration in a mouse model of spinocerebellar ataxia type 1. *J Neurosci,* 31**,** 11795-807.

HOUSHMAND, M., PANAHI, M. S., NAFISI, S., SOLTANZADEH, A. & ALKANDARI, F. M. 2006. Identification and sizing of GAA trinucleotide repeat expansion, investigation for D-loop variations and mitochondrial deletions in Iranian patients with Friedreich's ataxia. *Mitochondrion,* 6**,** 82-8.

HUANG, J., DIZIN, E. & COWAN, J. A. 2008. Mapping iron binding sites on human frataxin: implications for cluster assembly on the ISU Fe-S cluster scaffold protein. *J Biol Inorg Chem,* 13**,** 825-36.

HUANG, J., DORSEY, J., CHUIKOV, S., PEREZ-BURGOS, L., ZHANG, X., JENUWEIN, T., REINBERG, D. & BERGER, S. L. 2010. G9a and Glp methylate lysine 373 in the tumor suppressor p53. *J Biol Chem,* 285**,** 9636-41.

HUGHES, J. T., BROWNELL, B. & HEWER, R. L. 1968. The peripheral sensory pathway in friedreich's ataxia. An examination by light and electron microscopy of the posterior nerve roots, posterior root ganglia, and peripheral sensory nerves in cases of friedreich's ataxia. *Brain,* 91**,** 803-18.

ILG, W., BASTIAN, A. J., BOESCH, S., BURCIU, R. G., CELNIK, P., CLAASSEN, J., FEIL, K., KALLA, R., MIYAI, I., NACHBAUER, W., SCHOLS, L., STRUPP, M., SYNOFZIK, M., TEUFEL, J. &

TIMMANN, D. 2014. Consensus paper: management of degenerative cerebellar disorders. *Cerebellum,* 13**,** 248-68.

JAIN, A., RAJESWARI, M. R. & AHMED, F. 2002. Formation and thermodynamic stability of intermolecular (R*R*Y) DNA triplex in GAA/TTC repeats associated with Freidreich's ataxia. *J Biomol Struct Dyn,* 19**,** 691-9.

JIRALERSPONG, S., GE, B., HUDSON, T. J. & PANDOLFO, M. 2001. Manganese superoxide dismutase induction by iron is impaired in Friedreich ataxia cells. *FEBS Lett,* 509**,** 101-5.

JOHNSON, J. W. & ASCHER, P. 1987. Glycine potentiates the NMDA response in cultured mouse brain neurons. *Nature,* 325**,** 529-31.

KADOTANI, H., HIRANO, T., MASUGI, M., NAKAMURA, K., NAKAO, K., KATSUKI, M. & NAKANISHI, S. 1996. Motor discoordination results from combined gene disruption of the NMDA receptor NR2A and NR2C subunits, but not from single disruption of the NR2A or NR2C subunit. *J Neurosci,* 16**,** 7859-67.

KAKHLON, O., MANNING, H., BREUER, W., MELAMED-BOOK, N., LU, C., CORTOPASSI, G., MUNNICH, A. & CABANTCHIK, Z. I. 2008. Cell functions impaired by frataxin deficiency are restored by drug-mediated iron relocation. *Blood,* 112**,** 5219-27.

KANE, R. C., BROSS, P. F., FARRELL, A. T. & PAZDUR, R. 2003. Velcade: U.S. FDA approval for the treatment of multiple myeloma progressing on prior therapy. *Oncologist,* 8**,** 508-13.

KANE, R. C., FARRELL, A. T., SRIDHARA, R. & PAZDUR, R. 2006. United States Food and Drug Administration approval summary: bortezomib for the treatment of progressive multiple myeloma after one prior therapy. *Clin Cancer Res,* 12**,** 2955-60.

KAYTOR, M. D., BURRIGHT, E. N., DUVICK, L. A., ZOGHBI, H. Y. & ORR, H. T. 1997. Increased trinucleotide repeat instability with advanced maternal age. *Hum Mol Genet,* 6**,** 2135-9.

KE, X. X., ZHANG, D., ZHU, S., XIA, Q., XIANG, Z. & CUI, H. 2014. Inhibition of H3K9 methyltransferase G9a repressed cell proliferation and induced autophagy in neuroblastoma cells. *PLoS One,* 9**,** e106962.

KENT, W. J., SUGNET, C. W., FUREY, T. S., ROSKIN, K. M., PRINGLE, T. H., ZAHLER, A. M. & HAUSSLER, D. 2002. The human genome browser at UCSC. *Genome Res,* 12**,** 996-1006.

KHONSARI, H., SCHNEIDER, M., AL-MAHDAWI, S., CHIANEA, Y. G., THEMIS, M., PARRIS, C., POOK, M. A. & THEMIS, M. 2016. Lentivirus-meditated frataxin gene delivery reverses genome instability in Friedreich ataxia patient and mouse model fibroblasts. *Gene Ther,* 23**,** 846-856.

KIM, Y., KIM, Y. S., KIM, D. E., LEE, J. S., SONG, J. H., KIM, H. G., CHO, D. H., JEONG, S. Y., JIN, D. H., JANG, S. J., SEOL, H. S., SUH, Y. A., LEE, S. J., KIM, C. S., KOH, J. Y. & HWANG, J. J. 2013. BIX-01294 induces autophagy-associated cell death via EHMT2/G9a dysfunction and intracellular reactive oxygen species production. *Autophagy,* 9**,** 2126-39.

KISSELEV, A. F., VAN DER LINDEN, W. A. & OVERKLEEFT, H. S. 2012. Proteasome inhibitors: an expanding army attacking a unique target. *Chem Biol,* 19**,** 99-115.

KOEPPEN, A. H. 2011. Friedreich's ataxia: pathology, pathogenesis, and molecular genetics. *J Neurol Sci,* 303**,** 1-12.

KOEPPEN, A. H. & MAZURKIEWICZ, J. E. 2013. Friedreich ataxia: neuropathology revised. *J Neuropathol Exp Neurol,* 72**,** 78-90.

KOEPPEN, A. H., MICHAEL, S. C., KNUTSON, M. D., HAILE, D. J., QIAN, J., LEVI, S., SANTAMBROGIO, P., GARRICK, M. D. & LAMARCHE, J. B. 2007. The dentate nucleus in Friedreich's ataxia: the role of iron-responsive proteins. *Acta Neuropathol,* 114**,** 163-73.

KOUTNIKOVA, H., CAMPUZANO, V., FOURY, F., DOLLE, P., CAZZALINI, O. & KOENIG, M. 1997. Studies of human, mouse and yeast homologues indicate a mitochondrial function for frataxin. *Nat Genet,* 16**,** 345-51.

KOUTNIKOVA, H., CAMPUZANO, V. & KOENIG, M. 1998. Maturation of wild-type and mutated frataxin by the mitochondrial processing peptidase. *Hum Mol Genet,* 7**,** 1485-9.

KOUZARIDES, T. 2007. Chromatin modifications and their function. *Cell,* 128**,** 693-705.

KU, S., SORAGNI, E., CAMPAU, E., THOMAS, E. A., ALTUN, G., LAURENT, L. C., LORING, J. F., NAPIERALA, M. & GOTTESFELD, J. M. 2010. Friedreich's ataxia induced pluripotent stem cells model intergenerational GAATTC triplet repeat instability. *Cell Stem Cell,* 7**,** 631-7.

KUBICEK, S., O'SULLIVAN, R. J., AUGUST, E. M., HICKEY, E. R., ZHANG, Q., TEODORO, M. L., REA, S., MECHTLER, K., KOWALSKI, J. A., HOMON, C. A., KELLY, T. A. & JENUWEIN, T. 2007. Reversal of H3K9me2 by a small-molecule inhibitor for the G9a histone methyltransferase. *Mol Cell,* 25**,** 473-81.

KUMARI, D. & USDIN, K. 2012. Is Friedreich ataxia an epigenetic disorder? *Clin Epigenetics,* 4**,** 2.

KUMARI, D. & USDIN, K. 2016. Sustained expression of FMR1 mRNA from reactivated fragile X syndrome alleles after treatment with small molecules that prevent trimethylation of H3K27. *Hum Mol Genet,* 25**,** 3689-3698.

KUPPERMAN, E., LEE, E. C., CAO, Y., BANNERMAN, B., FITZGERALD, M., BERGER, A., YU, J., YANG, Y., HALES, P., BRUZZESE, F., LIU, J., BLANK, J., GARCIA, K., TSU, C., DICK, L., FLEMING, P., YU, L., MANFREDI, M., ROLFE, M. & BOLEN, J. 2010. Evaluation of the proteasome inhibitor MLN9708 in preclinical models of human cancer. *Cancer Res,* 70**,** 1970-80.

LA SPADA, A. R. 1997. Trinucleotide repeat instability: genetic features and molecular mechanisms. *Brain Pathol,* 7**,** 943-63.

LABUDA, M., LABUDA, D., MIRANDA, C., POIRIER, J., SOONG, B. W., BARUCHA, N. E. & PANDOLFO, M. 2000. Unique origin and specific ethnic distribution of the Friedreich ataxia GAA expansion. *Neurology,* 54**,** 2322-4.

LAGEDROST, S. J., SUTTON, M. S., COHEN, M. S., SATOU, G. M., KAUFMAN, B. D., PERLMAN, S. L., RUMMEY, C., MEIER, T. & LYNCH, D. R. 2011. Idebenone in Friedreich ataxia cardiomyopathy-results from a 6-month phase III study (IONIA). *Am Heart J,* 161**,** 639-645.e1.

LAMARCHE, J. B., COTE, M. & LEMIEUX, B. 1980. The cardiomyopathy of Friedreich's ataxia morphological observations in 3 cases. *Can J Neurol Sci,* 7**,** 389-96.

LAVECCHIA, A., DI GIOVANNI, C., CERCHIA, C., RUSSO, A., RUSSO, G. & NOVELLINO, E. 2013. Discovery of a novel small molecule inhibitor targeting the frataxin/ubiquitin interaction via structure-based virtual screening and bioassays. *J Med Chem,* 56**,** 2861-73.

LAYER, G., OLLAGNIER-DE CHOUDENS, S., SANAKIS, Y. & FONTECAVE, M. 2006. Iron-sulfur cluster biosynthesis: characterization of Escherichia coli CYaY as an iron donor for the assembly of [2Fe-2S] clusters in the scaffold IscU. *J Biol Chem,* 281**,** 16256-63.

LECKER, S. H., GOLDBERG, A. L. & MITCH, W. E. 2006. Protein degradation by the ubiquitin-proteasome pathway in normal and disease states. *J Am Soc Nephrol,* 17**,** 1807-19.

LEE, K. K. & WORKMAN, J. L. 2007. Histone acetyltransferase complexes: one size doesn't fit all. *Nat Rev Mol Cell Biol,* 8**,** 284-95.

LEHNERTZ, B., NORTHROP, J. P., ANTIGNANO, F., BURROWS, K., HADIDI, S., MULLALY, S. C., ROSSI, F. M. & ZAPH, C. 2010. Activating and inhibitory functions for the histone lysine methyltransferase G9a in T helper cell differentiation and function. *J Exp Med,* 207**,** 915-22.

LI, K., BESSE, E. K., HA, D., KOVTUNOVYCH, G. & ROUAULT, T. A. 2008. Iron-dependent regulation of frataxin expression: implications for treatment of Friedreich ataxia. *Hum Mol Genet,* 17**,** 2265-73.

LI, Y., LU, Y., POLAK, U., LIN, K., SHEN, J., FARMER, J., SEYER, L., BHALLA, A. D., ROZWADOWSKA, N., LYNCH, D. R., BUTLER, J. S. & NAPIERALA, M. 2015. Expanded GAA repeats impede transcription elongation through the FXN gene and induce transcriptional silencing that is restricted to the FXN locus. *Hum Mol Genet,* 24**,** 6932-43.

LIBRI, V., YANDIM, C., ATHANASOPOULOS, S., LOYSE, N., NATISVILI, T., LAW, P. P., CHAN, P. K., MOHAMMAD, T., MAURI, M., TAM, K. T., LEIPER, J., PIPER, S., RAMESH, A., PARKINSON, M. H., HUSON, L., GIUNTI, P. & FESTENSTEIN, R. 2014. Epigenetic and neurological effects and safety of high-dose nicotinamide in patients with Friedreich's ataxia: an exploratory, open-label, dose-escalation study. *Lancet,* 384**,** 504-13.

LIU, J., VERMA, P. J., EVANS-GALEA, M. V., DELATYCKI, M. B., MICHALSKA, A., LEUNG, J., CROMBIE, D., SARSERO, J. P., WILLIAMSON, R., DOTTORI, M. & PEBAY, A. 2011. Generation of induced pluripotent stem cell lines from Friedreich ataxia patients. *Stem Cell Rev,* 7**,** 703-13.

LOCKE, J., KOTARSKI, M. A. & TARTOF, K. D. 1988. Dosage-dependent modifiers of position effect variegation in Drosophila and a mass action model that explains their effect. *Genetics,* 120**,** 181-98.

LODI, R., HART, P. E., RAJAGOPALAN, B., TAYLOR, D. J., CRILLEY, J. G., BRADLEY, J. L., BLAMIRE, A. M., MANNERS, D., STYLES, P., SCHAPIRA, A. H. & COOPER, J. M. 2001a. Antioxidant treatment improves in vivo cardiac and skeletal muscle bioenergetics in patients with Friedreich's ataxia. *Ann Neurol,* 49**,** 590-6.

LODI, R., TAYLOR, D. J. & SCHAPIRA, A. H. 2001b. Mitochondrial dysfunction in friedreich's ataxia. *Biol Signals Recept,* 10**,** 263-70.

LODI, R., TONON, C., CALABRESE, V. & SCHAPIRA, A. H. 2006. Friedreich's ataxia: from disease mechanisms to therapeutic interventions. *Antioxid Redox Signal,* 8**,** 438-43.

MADEIRA, C., FREITAS, M. E., VARGAS-LOPES, C., WOLOSKER, H. & PANIZZUTTI, R. 2008. Increased brain D-amino acid oxidase (DAAO) activity in schizophrenia. *Schizophr Res,* 101**,** 76-83.

MANI, A. & GELMANN, E. P. 2005. The ubiquitin-proteasome pathway and its role in cancer. *J Clin Oncol,* 23**,** 4776-89.

MARIAPPAN, S. V., CATASTI, P., SILKS, L. A., 3RD, BRADBURY, E. M. & GUPTA, G. 1999. The high-resolution structure of the triplex formed by the GAA/TTC triplet repeat associated with Friedreich's ataxia. *J Mol Biol,* 285**,** 2035-52.

MARIOTTI, C., NACHBAUER, W., PANZERI, M., POEWE, W., TARONI, F. & BOESCH, S. 2013. Erythropoietin in Friedreich ataxia. *J Neurochem,* 126 Suppl 1**,** 80-7.

MARTELLI, A., WATTENHOFER-DONZE, M., SCHMUCKER, S., BOUVET, S., REUTENAUER, L. & PUCCIO, H. 2007. Frataxin is essential for extramitochondrial Fe-S cluster proteins in mammalian tissues. *Hum Mol Genet,* 16**,** 2651-8.

MCCABE, M. T., OTT, H. M., GANJI, G., KORENCHUK, S., THOMPSON, C., VAN ALLER, G. S., LIU, Y., GRAVES, A. P., DELLA PIETRA, A., 3RD, DIAZ, E., LAFRANCE, L. V., MELLINGER, M., DUQUENNE, C., TIAN, X., KRUGER, R. G., MCHUGH, C. F., BRANDT, M., MILLER, W. H., DHANAK, D., VERMA, S. K., TUMMINO, P. J. & CREASY, C. L. 2012. EZH2 inhibition as a therapeutic strategy for lymphoma with EZH2-activating mutations. *Nature,* 492**,** 108-12.

MEIER, T. & BUYSE, G. 2009. Idebenone: an emerging therapy for Friedreich ataxia. *J Neurol,* 256 Suppl 1**,** 25-30.

MIRANDA, C. J., SANTOS, M. M., OHSHIMA, K., SMITH, J., LI, L., BUNTING, M., COSSEE, M., KOENIG, M., SEQUEIROS, J., KAPLAN, J. & PANDOLFO, M. 2002. Frataxin knockin mouse. *FEBS Lett,* 512**,** 291-7.

MIRKIN, S. M. 2007. Expandable DNA repeats and human disease. *Nature,* 447**,** 932-40.

MITOMA, H. & MANTO, M. 2016. The physiological basis of therapies for cerebellar ataxias. *Ther Adv Neurol Disord,* 9**,** 396-413.

MONROS, E., MOLTO, M. D., MARTINEZ, F., CANIZARES, J., BLANCA, J., VILCHEZ, J. J., PRIETO, F., DE FRUTOS, R. & PALAU, F. 1997. Phenotype correlation and intergenerational dynamics of the Friedreich ataxia GAA trinucleotide repeat. *Am J Hum Genet,* 61**,** 101-10.

MONTERMINI, L., ANDERMANN, E., LABUDA, M., RICHTER, A., PANDOLFO, M., CAVALCANTI, F., PIANESE, L., IODICE, L., FARINA, G., MONTICELLI, A., TURANO, M., FILLA, A., DE MICHELE, G. & COCOZZA, S. 1997a. The Friedreich ataxia GAA triplet repeat: premutation and normal alleles. *Hum Mol Genet,* 6**,** 1261-6.

MONTERMINI, L., KISH, S. J., JIRALERSPONG, S., LAMARCHE, J. B. & PANDOLFO, M. 1997b. Somatic mosaicism for Friedreich's ataxia GAA triplet repeat expansions in the central nervous system. *Neurology,* 49**,** 606-10.

MONTERMINI, L., RICHTER, A., MORGAN, K., JUSTICE, C. M., JULIEN, D., CASTELLOTTI, B., MERCIER, J., POIRIER, J., CAPOZZOLI, F., BOUCHARD, J. P., LEMIEUX, B., MATHIEU, J., VANASSE, M., SENI, M. H., GRAHAM, G., ANDERMANN, F., ANDERMANN, E., MELANCON, S. B., KEATS, B. J., DI DONATO, S. & PANDOLFO, M. 1997c. Phenotypic variability in Friedreich ataxia: role of the associated GAA triplet repeat expansion. *Ann Neurol,* 41**,** 675-82.

MORERA, L., LUBBERT, M. & JUNG, M. 2016. Targeting histone methyltransferases and demethylases in clinical trials for cancer therapy. *Clin Epigenetics,* 8**,** 57.

MOSCHNER, C., PERLMAN, S. & BALOH, R. W. 1994. Comparison of oculomotor findings in the progressive ataxia syndromes. *Brain,* 117 (Pt 1)**,** 15-25.

MOTHET, J. P., PARENT, A. T., WOLOSKER, H., BRADY, R. O., JR., LINDEN, D. J., FERRIS, C. D., ROGAWSKI, M. A. & SNYDER, S. H. 2000. D-serine is an endogenous ligand for the glycine site of the N-methyl-D-aspartate receptor. *Proc Natl Acad Sci U S A,* 97**,** 4926-31.

MOTHET, J. P., POLLEGIONI, L., OUANOUNOU, G., MARTINEAU, M., FOSSIER, P. & BAUX, G. 2005. Glutamate receptor activation triggers a calcium-dependent and SNARE protein-dependent release of the gliotransmitter D-serine. *Proc Natl Acad Sci U S A,* 102**,** 5606-11.

MURAYAMA, S., BOULDIN, T. W. & SUZUKI, K. 1992. Pathological study of corticospinal-tract degeneration in Friedreich's ataxia. *Neuropathol Appl Neurobiol,* 18**,** 81-6.

MUZ, B., GHAZARIAN, R. N., OU, M., LUDERER, M. J., KUSDONO, H. D. & AZAB, A. K. 2016. Spotlight on ixazomib: potential in the treatment of multiple myeloma. *Drug Des Devel Ther,* 10**,** 217-26.

NABHAN, J. F., GOOCH, R. L., PIATNITSKI CHEKLER, E. L., PIERCE, B. & BULAWA, C. E. 2015. Perturbation of cellular proteostasis networks identifies pathways that modulate precursor and intermediate but not mature levels of frataxin. *Sci Rep,* 5**,** 18251.

NACHBAUER, W., HERING, S., SEIFERT, M., STEINKELLNER, H., STURM, B., SCHEIBER-MOJDEHKAR, B., REINDL, M., STRASAK, A., POEWE, W., WEISS, G. & BOESCH, S. 2011. Effects of erythropoietin on frataxin levels and mitochondrial function in Friedreich ataxia--a dose-response trial. *Cerebellum,* 10**,** 763-9.

NAGESHWARAN, S. & FESTENSTEIN, R. 2015. Epigenetics and Triplet-Repeat Neurological Diseases. *Front Neurol,* 6**,** 262.

NAWAZ, Z. & O'MALLEY, B. W. 2004. Urban renewal in the nucleus: is protein turnover by proteasomes absolutely required for nuclear receptor-regulated transcription? *Mol Endocrinol,* 18**,** 493-9.

NICKELL, S., BECK, F., SCHERES, S. H., KORINEK, A., FORSTER, F., LASKER, K., MIHALACHE, O., SUN, N., NAGY, I., SALI, A., PLITZKO, J. M., CARAZO, J. M., MANN, M. & BAUMEISTER, W. 2009. Insights into the molecular architecture of the 26S proteasome. *Proc Natl Acad Sci U S A,* 106**,** 11943-7.

O'NEILL, H. A., GAKH, O. & ISAYA, G. 2005. Supramolecular assemblies of human frataxin are formed via subunit-subunit interactions mediated by a non-conserved amino-terminal region. *J Mol Biol,* 345**,** 433-9.

OBAIDAT, A., WEISS, J., WAHLGREN, B., MANAM, R. R., MACHERLA, V. R., MCARTHUR, K., CHAO, T. H., PALLADINO, M. A., LLOYD, G. K., POTTS, B. C., ENNA, S. J., NEUTEBOOM, S. T. & HAGENBUCH, B. 2011. Proteasome regulator marizomib (NPI-0052) exhibits prolonged inhibition, attenuated efflux, and greater cytotoxicity than its reversible analogs. *J Pharmacol Exp Ther,* 337**,** 479-86.

OGAWA, M., SHIGETO, H., YAMAMOTO, T., OYA, Y., WADA, K., NISHIKAWA, T. & KAWAI, M. 2003. D-cycloserine for the treatment of ataxia in spinocerebellar degeneration. *J Neurol Sci,* 210**,** 53-6.

OH, S. Y., SEOK, J. Y., CHOI, Y. S., LEE, S. H., BAE, J. S. & LEE, Y. M. 2015. The Histone Methyltransferase Inhibitor BIX01294 Inhibits HIF-1alpha Stability and Angiogenesis. *Mol Cells,* 38**,** 528-34.

OHSHIMA, K., SAKAMOTO, N., LABUDA, M., POIRIER, J., MOSELEY, M. L., MONTERMINI, L., RANUM, L. P., WELLS, R. D. & PANDOLFO, M. 1999. A nonpathogenic GAAGGA repeat in the Friedreich gene: implications for pathogenesis. *Neurology,* 53**,** 1854-7.

ORSUCCI, D., CALDARAZZO IENCO, E., MANCUSO, M. & SICILIANO, G. 2011. POLG1-related and other "mitochondrial Parkinsonisms": an overview. *J Mol Neurosci,* 44**,** 17-24.

OUELLET, D. L., CHERIF, K., ROUSSEAU, J. & TREMBLAY, J. P. 2017. Deletion of the GAA repeats from the human frataxin gene using the CRISPR-Cas9 system in YG8R-derived cells and mouse models of Friedreich ataxia. *Gene Ther,* 24**,** 265-274.

PANDOLFO, M. 1999. Molecular pathogenesis of Friedreich ataxia. *Arch Neurol,* 56**,** 1201-8.

PANDOLFO, M. 2002. The molecular basis of Friedreich ataxia. *Adv Exp Med Biol,* 516**,** 99-118.

PANDOLFO, M. 2008. Friedreich ataxia. *Arch Neurol,* 65**,** 1296-303.

PANDOLFO, M. & HAUSMANN, L. 2013. Deferiprone for the treatment of Friedreich's ataxia. *J Neurochem,* 126 Suppl 1**,** 142-6.

PANDOLFO, M. & MONTERMINI, L. 1998. Prenatal diagnosis of Friedreich ataxia. *Prenat Diagn,* 18**,** 831-3.

PARKINSON, M. H., SCHULZ, J. B. & GIUNTI, P. 2013. Co-enzyme Q10 and idebenone use in Friedreich's ataxia. *J Neurochem,* 126 Suppl 1**,** 125-41.

PEARSON, C. E., NICHOL EDAMURA, K. & CLEARY, J. D. 2005. Repeat instability: mechanisms of dynamic mutations. *Nat Rev Genet,* 6**,** 729-42.

PELLOM, S. T., JR. & SHANKER, A. 2012. Development of Proteasome Inhibitors as Therapeutic Drugs. *J Clin Cell Immunol,* S5**,** 5.

PERDOMINI, M., BELBELLAA, B., MONASSIER, L., REUTENAUER, L., MESSADDEQ, N., CARTIER, N., CRYSTAL, R. G., AUBOURG, P. & PUCCIO, H. 2014. Prevention and reversal of severe mitochondrial cardiomyopathy by gene therapy in a mouse model of Friedreich's ataxia. *Nat Med,* 20**,** 542-7.

PETERS, A. H., KUBICEK, S., MECHTLER, K., O'SULLIVAN, R. J., DERIJCK, A. A., PEREZ-BURGOS, L., KOHLMAIER, A., OPRAVIL, S., TACHIBANA, M., SHINKAI, Y., MARTENS, J. H. & JENUWEIN, T. 2003. Partitioning and plasticity of repressive histone methylation states in mammalian chromatin. *Mol Cell,* 12**,** 1577-89.

PIANESE, L., BUSINO, L., DE BIASE, I., DE CRISTOFARO, T., LO CASALE, M. S., GIULIANO, P., MONTICELLI, A., TURANO, M., CRISCUOLO, C., FILLA, A., VARRONE, S. & COCOZZA, S. 2002. Up-regulation of c-Jun N-terminal kinase pathway in Friedreich's ataxia cells. *Hum Mol Genet,* 11**,** 2989-96.

PIANESE, L., CAVALCANTI, F., DE MICHELE, G., FILLA, A., CAMPANELLA, G., CALABRESE, O., CASTALDO, I., MONTICELLI, A. & COCOZZA, S. 1997. The effect of parental gender on the GAA dynamic mutation in the FRDA gene. *Am J Hum Genet,* 60**,** 460-3.

PICKART, C. M. & EDDINS, M. J. 2004. Ubiquitin: structures, functions, mechanisms. *Biochim Biophys Acta,* 1695**,** 55-72.

PIZZI, C., DI MAIO, M., DANIELE, S., MASTRANZO, P., SPAGNOLETTI, I., LIMITE, G., PETTINATO, G., MONTICELLI, A., COCOZZA, S. & CONTEGIACOMO, A. 2007. Triplet repeat instability correlates with dinucleotide instability in primary breast cancer. *Oncol Rep,* 17**,** 193-9.

POLLEGIONI, L., PIUBELLI, L., SACCHI, S., PILONE, M. S. & MOLLA, G. 2007. Physiological functions of D-amino acid oxidases: from yeast to humans. *Cell Mol Life Sci,* 64**,** 1373-94.

POOK, M. A., AL-MAHDAWI, S., CARROLL, C. J., COSSEE, M., PUCCIO, H., LAWRENCE, L., CLARK, P., LOWRIE, M. B., BRADLEY, J. L., COOPER, J. M., KOENIG, M. & CHAMBERLAIN, S. 2001. Rescue of the Friedreich's ataxia knockout mouse by human YAC transgenesis. *Neurogenetics,* 3**,** 185-93.

PUCCIO, H., ANHEIM, M. & TRANCHANT, C. 2014. Pathophysiogical and therapeutic progress in Friedreich ataxia. *Rev Neurol (Paris),* 170**,** 355-65.

PUCCIO, H., SIMON, D., COSSEE, M., CRIQUI-FILIPE, P., TIZIANO, F., MELKI, J., HINDELANG, C., MATYAS, R., RUSTIN, P. & KOENIG, M. 2001. Mouse models for Friedreich ataxia exhibit cardiomyopathy, sensory nerve defect and Fe-S enzyme deficiency followed by intramitochondrial iron deposits. *Nat Genet,* 27**,** 181-6.

PUNGA, T. & BUHLER, M. 2010. Long intronic GAA repeats causing Friedreich ataxia impede transcription elongation. *EMBO Mol Med,* 2**,** 120-9.

QIN, J., MA, X., QI, H., SONG, B., WANG, Y., WEN, X., WANG, Q. M., SUN, S., LI, Y., ZHANG, R., LIU, X., HOU, H., GONG, G. & XU, Y. 2015. Transplantation of Induced Pluripotent Stem Cells Alleviates Cerebral Inflammation and Neural Damage in Hemorrhagic Stroke. *PLoS One,* 10**,** e0129881.

RADISKY, D. C., BABCOCK, M. C. & KAPLAN, J. 1999. The yeast frataxin homologue mediates mitochondrial iron efflux. Evidence for a mitochondrial iron cycle. *J Biol Chem,* 274**,** 4497-9.

RAI, M., SORAGNI, E., CHOU, C. J., BARNES, G., JONES, S., RUSCHE, J. R., GOTTESFELD, J. M. & PANDOLFO, M. 2010. Two new pimelic diphenylamide HDAC inhibitors induce sustained frataxin upregulation in cells from Friedreich's ataxia patients and in a mouse model. *PLoS One,* 5**,** e8825.

RAI, M., SORAGNI, E., JENSSEN, K., BURNETT, R., HERMAN, D., COPPOLA, G., GESCHWIND, D. H., GOTTESFELD, J. M. & PANDOLFO, M. 2008. HDAC inhibitors correct frataxin deficiency in a Friedreich ataxia mouse model. *PLoS One,* 3**,** e1958.

RENTSCH, A., LANDSBERG, D., BRODMANN, T., BULOW, L., GIRBIG, A. K. & KALESSE, M. 2013. Synthesis and pharmacology of proteasome inhibitors. *Angew Chem Int Ed Engl,* 52**,** 5450-88.

RICHARDSON, P. G., MITSIADES, C., HIDESHIMA, T. & ANDERSON, K. C. 2006. Bortezomib: proteasome inhibition as an effective anticancer therapy. *Annu Rev Med,* 57**,** 33-47.

RICHARDSON, P. G., SONNEVELD, P., SCHUSTER, M. W., STADTMAUER, E. A., FACON, T., HAROUSSEAU, J. L., BEN-YEHUDA, D., LONIAL, S., GOLDSCHMIDT, H., REECE, D., BLADE, J., BOCCADORO, M., CAVENAGH, J. D., BORAL, A. L., ESSELTINE, D. L., WEN, P. Y., AMATO, A. A., ANDERSON, K. C. & SAN MIGUEL, J. 2009. Reversibility of symptomatic peripheral neuropathy with bortezomib in the phase III APEX trial in relapsed multiple myeloma: impact of a dose-modification guideline. *Br J Haematol,* 144**,** 895-903.

RIZZUTO, N., MONACO, S., MORETTO, G., GALIAZZO-RIZZUTO, S., FIASCHI, A., FORTI, A. & DE MARIA, R. 1981. Friedreich's ataxia. A light- and electron microscopic study of peripheral nerve biopsies. *Acta Neuropathol Suppl,* 7**,** 344-7.

ROCCA, C. J., KREYMERMAN, A., UR, S. N., FRIZZI, K. E., NAPHADE, S., LAU, A., TRAN, T., CALCUTT, N. A., GOLDBERG, J. L. & CHERQUI, S. 2015. Treatment of Inherited Eye Defects by Systemic Hematopoietic Stem Cell Transplantation. *Invest Ophthalmol Vis Sci,* 56**,** 7214-23.

ROCK, K. L., GRAMM, C., ROTHSTEIN, L., CLARK, K., STEIN, R., DICK, L., HWANG, D. & GOLDBERG, A. L. 1994. Inhibitors of the proteasome block the degradation of most cell proteins and the generation of peptides presented on MHC class I molecules. *Cell,* 78**,** 761-71.

ROTHBART, S. B. & STRAHL, B. D. 2014. Interpreting the language of histone and DNA modifications. *Biochim Biophys Acta,* 1839**,** 627-43.

ROTIG, A., DE LONLAY, P., CHRETIEN, D., FOURY, F., KOENIG, M., SIDI, D., MUNNICH, A. & RUSTIN, P. 1997. Aconitase and mitochondrial iron-sulphur protein deficiency in Friedreich ataxia. *Nat Genet,* 17**,** 215-7.

ROZEN, S. & SKALETSKY, H. 2000. Primer3 on the WWW for general users and for biologist programmers. *Methods Mol Biol,* 132**,** 365-86.

RUFINI, A., CAVALLO, F., CONDO, I., FORTUNI, S., DE MARTINO, G., INCANI, O., DI VENERE, A., BENINI, M., MASSARO, D. S., ARCURI, G., SERIO, D., MALISAN, F. & TESTI, R. 2015. Highly specific ubiquitin-competing molecules effectively promote frataxin

accumulation and partially rescue the aconitase defect in Friedreich ataxia cells. *Neurobiol Dis,* 75**,** 91-9.

RUFINI, A., FORTUNI, S., ARCURI, G., CONDO, I., SERIO, D., INCANI, O., MALISAN, F., VENTURA, N. & TESTI, R. 2011. Preventing the ubiquitin-proteasome-dependent degradation of frataxin, the protein defective in Friedreich's ataxia. *Hum Mol Genet,* 20**,** 1253-61.

RUSTIN, P., VON KLEIST-RETZOW, J. C., CHANTREL-GROUSSARD, K., SIDI, D., MUNNICH, A. & ROTIG, A. 1999. Effect of idebenone on cardiomyopathy in Friedreich's ataxia: a preliminary study. *Lancet,* 354**,** 477-9.

SACCA, F., PIRO, R., DE MICHELE, G., ACQUAVIVA, F., ANTENORA, A., CARLOMAGNO, G., COCOZZA, S., DENARO, A., GUACCI, A., MARSILI, A., PERROTTA, G., PUORRO, G., CITTADINI, A. & FILLA, A. 2011. Epoetin alfa increases frataxin production in Friedreich's ataxia without affecting hematocrit. *Mov Disord,* 26**,** 739-42.

SACCHI, S. 2013. D-Serine metabolism: new insights into the modulation of D-amino acid oxidase activity. *Biochem Soc Trans,* 41**,** 1551-6.

SACCHI, S., BERNASCONI, M., MARTINEAU, M., MOTHET, J. P., RUZZENE, M., PILONE, M. S., POLLEGIONI, L. & MOLLA, G. 2008. pLG72 modulates intracellular D-serine levels through its interaction with D-amino acid oxidase: effect on schizophrenia susceptibility. *J Biol Chem,* 283**,** 22244-56.

SACCHI, S., ROSINI, E., POLLEGIONI, L. & MOLLA, G. 2013. D-amino acid oxidase inhibitors as a novel class of drugs for schizophrenia therapy. *Curr Pharm Des,* 19**,** 2499-511.

SAID, G., MARION, M. H., SELVA, J. & JAMET, C. 1986. Hypotrophic and dying-back nerve fibers in Friedreich's ataxia. *Neurology,* 36**,** 1292-9.

SAKAMOTO, N., CHASTAIN, P. D., PARNIEWSKI, P., OHSHIMA, K., PANDOLFO, M., GRIFFITH, J. D. & WELLS, R. D. 1999. Sticky DNA: self-association properties of long GAA.TTC repeats in R.R.Y triplex structures from Friedreich's ataxia. *Mol Cell,* 3**,** 465-75.

SAKAMOTO, N., LARSON, J. E., IYER, R. R., MONTERMINI, L., PANDOLFO, M. & WELLS, R. D. 2001. GGA*TCC-interrupted triplets in long GAA*TTC repeats inhibit the formation of triplex and sticky DNA structures, alleviate transcription inhibition, and reduce genetic instabilities. *J Biol Chem,* 276**,** 27178-87.

SANCHEZ-CASIS, G., COTE, M. & BARBEAU, A. 1976. Pathology of the heart in Friedreich's ataxia: review of the literature and report of one case. *Can J Neurol Sci,* 3**,** 349-54.

SANDI, C., AL-MAHDAWI, S. & POOK, M. A. 2013. Epigenetics in Friedreich's Ataxia: Challenges and Opportunities for Therapy. *Genet Res Int,* 2013**,** 852080.

SANDI, C., PINTO, R. M., AL-MAHDAWI, S., EZZATIZADEH, V., BARNES, G., JONES, S., RUSCHE, J. R., GOTTESFELD, J. M. & POOK, M. A. 2011. Prolonged treatment with pimelic o-aminobenzamide HDAC inhibitors ameliorates the disease phenotype of a Friedreich ataxia mouse model. *Neurobiol Dis,* 42**,** 496-505.

SANDI, C., SANDI, M., ANJOMANI VIRMOUNI, S., AL-MAHDAWI, S. & POOK, M. A. 2014. Epigenetic-based therapies for Friedreich ataxia. *Front Genet,* 5**,** 165.

SANTOS, R., LEFEVRE, S., SLIWA, D., SEGUIN, A., CAMADRO, J. M. & LESUISSE, E. 2010. Friedreich ataxia: molecular mechanisms, redox considerations, and therapeutic opportunities. *Antioxid Redox Signal,* 13**,** 651-90.

SATO, T., KANEDA, A., TSUJI, S., ISAGAWA, T., YAMAMOTO, S., FUJITA, T., YAMANAKA, R., TANAKA, Y., NUKIWA, T., MARQUEZ, V. E., ISHIKAWA, Y., ICHINOSE, M. & ABURATANI, H. 2013. PRC2 overexpression and PRC2-target gene repression relating to poorer prognosis in small cell lung cancer. *Sci Rep,* 3**,** 1911.

SAVELIEV, A., EVERETT, C., SHARPE, T., WEBSTER, Z. & FESTENSTEIN, R. 2003. DNA triplet repeats mediate heterochromatin-protein-1-sensitive variegated gene silencing. *Nature,* 422**,** 909-13.

SAVOURET, C., BRISSON, E., ESSERS, J., KANAAR, R., PASTINK, A., TE RIELE, H., JUNIEN, C. & GOURDON, G. 2003. CTG repeat instability and size variation timing in DNA repair-deficient mice. *Embo j,* 22**,** 2264-73.

SAZANOV, L. A. & HINCHLIFFE, P. 2006. Structure of the hydrophilic domain of respiratory complex I from Thermus thermophilus. *Science,* 311**,** 1430-6.

SCHMUCKER, S., ARGENTINI, M., CARELLE-CALMELS, N., MARTELLI, A. & PUCCIO, H. 2008. The in vivo mitochondrial two-step maturation of human frataxin. *Hum Mol Genet,* 17**,** 3521-31.

SCHNIEPP, R., WUEHR, M., ACKL, N., DANEK, A., BRANDT, T., STRUPP, M. & JAHN, K. 2011. 4-Aminopyridine improves gait variability in cerebellar ataxia due to CACNA 1A mutation. *J Neurol,* 258**,** 1708-11.

SCHNIEPP, R., WUEHR, M., NEUHAEUSSER, M., BENECKE, A. K., ADRION, C., BRANDT, T., STRUPP, M. & JAHN, K. 2012. 4-aminopyridine and cerebellar gait: a retrospective case series. *J Neurol,* 259**,** 2491-3.

SCHOENLE, E. J., BOLTSHAUSER, E. J., BAEKKESKOV, S., LANDIN OLSSON, M., TORRESANI, T. & VON FELTEN, A. 1989. Preclinical and manifest diabetes mellitus in young patients with Friedreich's ataxia: no evidence of immune process behind the islet cell destruction. *Diabetologia,* 32**,** 378-81.

SCHULZ, J. B., BOESCH, S., BURK, K., DURR, A., GIUNTI, P., MARIOTTI, C., POUSSET, F., SCHOLS, L., VANKAN, P. & PANDOLFO, M. 2009. Diagnosis and treatment of Friedreich ataxia: a European perspective. *Nat Rev Neurol,* 5**,** 222-34.

SCHULZ, J. B., DEHMER, T., SCHOLS, L., MENDE, H., HARDT, C., VORGERD, M., BURK, K., MATSON, W., DICHGANS, J., BEAL, M. F. & BOGDANOV, M. B. 2000. Oxidative stress in patients with Friedreich ataxia. *Neurology,* 55**,** 1719-21.

SHAN, B., XU, C., ZHANG, Y., XU, T., GOTTESFELD, J. M. & YATES, J. R., 3RD 2014. Quantitative proteomic analysis identifies targets and pathways of a 2-aminobenzamide HDAC inhibitor in Friedreich's ataxia patient iPSC-derived neural stem cells. *J Proteome Res,* 13**,** 4558-66.

SHARMA, R., BHATTI, S., GOMEZ, M., CLARK, R. M., MURRAY, C., ASHIZAWA, T. & BIDICHANDANI, S. I. 2002. The GAA triplet-repeat sequence in Friedreich ataxia shows a high level of somatic instability in vivo, with a significant predilection for large contractions. *Hum Mol Genet,* 11**,** 2175-87.

SHETTY, P., RAVINDRAN, G., SARANG, S., THAKUR, A. M., RAO, H. S. & VISWANATHAN, C. 2009. Clinical grade mesenchymal stem cells transdifferentiated under xenofree conditions alleviates motor deficiencies in a rat model of Parkinson's disease. *Cell Biol Int,* 33**,** 830-8.

SHI, Y., LAN, F., MATSON, C., MULLIGAN, P., WHETSTINE, J. R., COLE, P. A., CASERO, R. A. & SHI, Y. 2004. Histone demethylation mediated by the nuclear amine oxidase homolog LSD1. *Cell,* 119**,** 941-53.

SILVA, A. M., BROWN, J. M., BUCKLE, V. J., WADE-MARTINS, R. & LUFINO, M. M. 2015. Expanded GAA repeats impair FXN gene expression and reposition the FXN locus to the nuclear lamina in single cells. *Hum Mol Genet,* 24**,** 3457-71.

SIREN, A. L., FASSHAUER, T., BARTELS, C. & EHRENREICH, H. 2009. Therapeutic potential of erythropoietin and its structural or functional variants in the nervous system. *Neurotherapeutics,* 6**,** 108-27.

SMITH, S. M., USLANER, J. M. & HUTSON, P. H. 2010. The Therapeutic Potential of D-Amino Acid Oxidase (DAAO) Inhibitors. *Open Med Chem J,* 4**,** 3-9.

SON, L. S., BACOLLA, A. & WELLS, R. D. 2006. Sticky DNA: in vivo formation in E. coli and in vitro association of long GAA*TTC tracts to generate two independent supercoiled domains. *J Mol Biol,* 360**,** 267-84.

SORAGNI, E. & GOTTESFELD, J. M. 2016. Translating HDAC inhibitors in Friedreich's ataxia. *Expert Opin Orphan Drugs,* 4**,** 961-970.

SORAGNI, E., MIAO, W., IUDICELLO, M., JACOBY, D., DE MERCANTI, S., CLERICO, M., LONGO, F., PIGA, A., KU, S., CAMPAU, E., DU, J., PENALVER, P., RAI, M., MADARA, J. C., NAZOR, K., O'CONNOR, M., MAXIMOV, A., LORING, J. F., PANDOLFO, M., DURELLI, L., GOTTESFELD, J. M. & RUSCHE, J. R. 2014. Epigenetic therapy for Friedreich ataxia. *Ann Neurol,* 76**,** 489-508.

STRAWSER, C. J., SCHADT, K. A. & LYNCH, D. R. 2014. Therapeutic approaches for the treatment of Friedreich's ataxia. *Expert Rev Neurother,* 14**,** 949-57.

STRUPP, M., SCHULER, O., KRAFCZYK, S., JAHN, K., SCHAUTZER, F., BUTTNER, U. & BRANDT, T. 2003. Treatment of downbeat nystagmus with 3,4-diaminopyridine: a placebo-controlled study. *Neurology,* 61**,** 165-70.

STRUPP, M., TEUFEL, J., HABS, M., FEUERECKER, R., MUTH, C., VAN DE WARRENBURG, B. P., KLOPSTOCK, T. & FEIL, K. 2013. Effects of acetyl-DL-leucine in patients with cerebellar ataxia: a case series. *J Neurol,* 260**,** 2556-61.

STURM, B., STUPPHANN, D., KAUN, C., BOESCH, S., SCHRANZHOFER, M., WOJTA, J., GOLDENBERG, H. & SCHEIBER-MOJDEHKAR, B. 2005. Recombinant human erythropoietin: effects on frataxin expression in vitro. *Eur J Clin Invest,* 35**,** 711-7.

TACHIBANA, M., UEDA, J., FUKUDA, M., TAKEDA, N., OHTA, T., IWANARI, H., SAKIHAMA, T., KODAMA, T., HAMAKUBO, T. & SHINKAI, Y. 2005. Histone methyltransferases G9a and GLP form heteromeric complexes and are both crucial for methylation of euchromatin at H3-K9. *Genes Dev,* 19**,** 815-26.

TAJIRI, N., STAPLES, M., KANEKO, Y., KIM, S. U., ZESIEWICZ, T. A. & BORLONGAN, C. V. 2014. Autologous stem cell transplant with gene therapy for Friedreich ataxia. *Med Hypotheses,* 83**,** 296-8.

TAKAYASU, N., YOSHIKAWA, M., WATANABE, M., TSUKAMOTO, H., SUZUKI, T., KOBAYASHI, H. & NODA, S. 2008. The serine racemase mRNA is expressed in both neurons and glial cells of the rat retina. *Arch Histol Cytol,* 71**,** 123-9.

TAKESHIMA, H., WAKABAYASHI, M., HATTORI, N., YAMASHITA, S. & USHIJIMA, T. 2015. Identification of coexistence of DNA methylation and H3K27me3 specifically in cancer cells as a promising target for epigenetic therapy. *Carcinogenesis,* 36**,** 192-201.

TANII, Y., NISHIKAWA, T., HASHIMOTO, A. & TAKAHASHI, K. 1994. Stereoselective antagonism by enantiomers of alanine and serine of phencyclidine-induced hyperactivity, stereotypy and ataxia in the rat. *J Pharmacol Exp Ther,* 269**,** 1040-8.

TARTOF, K. D., BISHOP, C., JONES, M., HOBBS, C. A. & LOCKE, J. 1989. Towards an understanding of position effect variegation. *Dev Genet,* 10**,** 162-76.

TARTOF, K. D., HOBBS, C. & JONES, M. 1984. A structural basis for variegating position effects. *Cell,* 37**,** 869-78.

THOMAS, L. R., MIYASHITA, H., COBB, R. M., PIERCE, S., TACHIBANA, M., HOBEIKA, E., RETH, M., SHINKAI, Y. & OLTZ, E. M. 2008. Functional analysis of histone methyltransferase g9a in B and T lymphocytes. *J Immunol,* 181**,** 485-93.

TOZZI, G., NUCCETELLI, M., LO BELLO, M., BERNARDINI, S., BELLINCAMPI, L., BALLERINI, S., GAETA, L. M., CASALI, C., PASTORE, A., FEDERICI, G., BERTINI, E. & PIEMONTE, F. 2002. Antioxidant enzymes in blood of patients with Friedreich's ataxia. *Arch Dis Child,* 86**,** 376-9.

TSOU, A. Y., PAULSEN, E. K., LAGEDROST, S. J., PERLMAN, S. L., MATHEWS, K. D., WILMOT, G. R., RAVINA, B., KOEPPEN, A. H. & LYNCH, D. R. 2011. Mortality in Friedreich ataxia. *J Neurol Sci,* 307**,** 46-9.

USDIN, K. & GRABCZYK, E. 2000. DNA repeat expansions and human disease. *Cell Mol Life Sci,* 57**,** 914-31.

VANKAN, P. 2013. Prevalence gradients of Friedreich's ataxia and R1b haplotype in Europe co-localize, suggesting a common Palaeolithic origin in the Franco-Cantabrian ice age refuge. *J Neurochem,* 126 Suppl 1**,** 11-20.

VARIER, R. A. & TIMMERS, H. T. 2011. Histone lysine methylation and demethylation pathways in cancer. *Biochim Biophys Acta,* 1815**,** 75-89.

VERRALL, L., BURNET, P. W., BETTS, J. F. & HARRISON, P. J. 2010. The neurobiology of D-amino acid oxidase and its involvement in schizophrenia. *Mol Psychiatry,* 15**,** 122-37.

VERRALL, L., WALKER, M., RAWLINGS, N., BENZEL, I., KEW, J. N., HARRISON, P. J. & BURNET, P. W. 2007. d-Amino acid oxidase and serine racemase in human brain: normal distribution and altered expression in schizophrenia. *Eur J Neurosci,* 26**,** 1657-69.

VETCHER, A. A., NAPIERALA, M., IYER, R. R., CHASTAIN, P. D., GRIFFITH, J. D. & WELLS, R. D. 2002. Sticky DNA, a long GAA.GAA.TTC triplex that is formed intramolecularly, in the sequence of intron 1 of the frataxin gene. *J Biol Chem,* 277**,** 39217-27.

VINITSKY, A., MICHAUD, C., POWERS, J. C. & ORLOWSKI, M. 1992. Inhibition of the chymotrypsin-like activity of the pituitary multicatalytic proteinase complex. *Biochemistry,* 31**,** 9421-8.

VOLKEL, P. & ANGRAND, P. O. 2007. The control of histone lysine methylation in epigenetic regulation. *Biochimie,* 89**,** 1-20.

VYAS, P. M., TOMAMICHEL, W. J., PRIDE, P. M., BABBEY, C. M., WANG, Q., MERCIER, J., MARTIN, E. M. & PAYNE, R. M. 2012. A TAT-frataxin fusion protein increases lifespan and cardiac function in a conditional Friedreich's ataxia mouse model. *Hum Mol Genet,* 21**,** 1230-47.

VYKLICKY, V., KORINEK, M., SMEJKALOVA, T., BALIK, A., KRAUSOVA, B., KANIAKOVA, M., LICHNEROVA, K., CERNY, J., KRUSEK, J., DITTERT, I., HORAK, M. & VYKLICKY, L. 2014. Structure, function, and pharmacology of NMDA receptor channels. *Physiol Res,* 63 Suppl 1**,** S191-203.

WALDVOGEL, D., VAN GELDEREN, P. & HALLETT, M. 1999. Increased iron in the dentate nucleus of patients with Friedrich's ataxia. *Ann Neurol,* 46**,** 123-5.

WEIMANN, J. M., CHARLTON, C. A., BRAZELTON, T. R., HACKMAN, R. C. & BLAU, H. M. 2003. Contribution of transplanted bone marrow cells to Purkinje neurons in human adult brains. *Proc Natl Acad Sci U S A,* 100**,** 2088-93.

WILSON, R. B. 2003. Frataxin and frataxin deficiency in Friedreich's ataxia. *J Neurol Sci,* 207**,** 103-5.

WILSON, R. B. 2012. Therapeutic developments in Friedreich ataxia. *J Child Neurol,* 27**,** 1212-6.

WONG, A., YANG, J., CAVADINI, P., GELLERA, C., LONNERDAL, B., TARONI, F. & CORTOPASSI, G. 1999. The Friedreich's ataxia mutation confers cellular sensitivity to oxidant stress which is rescued by chelators of iron and calcium and inhibitors of apoptosis. *Hum Mol Genet,* 8**,** 425-30.

YANDIM, C., NATISVILI, T. & FESTENSTEIN, R. 2013. Gene regulation and epigenetics in Friedreich's ataxia. *J Neurochem,* 126 Suppl 1**,** 21-42.

YOON, T. & COWAN, J. A. 2003. Iron-sulfur cluster biosynthesis. Characterization of frataxin as an iron donor for assembly of [2Fe-2S] clusters in ISU-type proteins. *J Am Chem Soc,* 125**,** 6078-84.

YOON, T. & COWAN, J. A. 2004. Frataxin-mediated iron delivery to ferrochelatase in the final step of heme biosynthesis. *J Biol Chem,* 279**,** 25943-6.

YOON, T., DIZIN, E. & COWAN, J. A. 2007. N-terminal iron-mediated self-cleavage of human frataxin: regulation of iron binding and complex formation with target proteins. *J Biol Inorg Chem,* 12**,** 535-42.

ZENG, D., LIU, M. & PAN, J. 2017. Blocking EZH2 methylation transferase activity by GSK126 decreases stem cell-like myeloma cells. *Oncotarget,* 8**,** 3396-3411.

ZHANG, L., TANG, H., KOU, Y., LI, R., ZHENG, Y., WANG, Q., ZHOU, X. & JIN, L. 2013. MG132-mediated inhibition of the ubiquitin-proteasome pathway ameliorates cancer cachexia. *J Cancer Res Clin Oncol,* 139**,** 1105-15.

ZHENG, Q., HUANG, T., ZHANG, L., ZHOU, Y., LUO, H., XU, H. & WANG, X. 2016. Dysregulation of Ubiquitin-Proteasome System in Neurodegenerative Diseases. *Front Aging Neurosci,* 8**,** 303.

ZHOU, Q. & SHENG, M. 2013. NMDA receptors in nervous system diseases. *Neuropharmacology,* 74**,** 69-75.

ZUCKERKANDL, E. 1974. A possible role of "inert" heterochromatin in cell differentiation. Action of and competition for "locking" molecules. *Biochimie,* 56**,** 937-54.